Universidad de Valladolid

Escuela de Doctorado Universidad de Valladolid

PROGRAMA DE DOCTORADO EN INVESTIGACIÓN BIOMÉDICA

TESIS DOCTORAL:

METABOLIC REWIRING IS REQUIRED FOR INFLAMMATION, CALCIFICATION, AND OSTEOGENIC DIFFERENTIATION OF HUMAN AORTIC VALVE INTERSTITIAL CELLS EXPOSED TO AN INFLAMMATORY MILIEU, AND MIMICS THE METABOLIC PHENOTYPE IN CALCIFIED AORTIC VALVES

Presentada por Tania Sánchez-Bayuela Recio
para optar al grado de Doctor/a por la
Universidad de Valladolid

Dirigida por:
Dra. María del Carmen García Rodríguez

Universidad de Valladolid

Escuela de Doctorado Universidad de Valladolid

PROGRAMA DE DOCTORADO EN INVESTIGACIÓN BIOMÉDICA

TESIS DOCTORAL:

LA REPROGRAMACIÓN METABÓLICA ES NECESARIA PARA LOS PROCESOS DE INFLAMACIÓN, CALCIFICACIÓN Y DIFERENCIACIÓN OSTEOGÉNICA DE LAS CÉLULAS INTERSTICIALES DE LA VÁLVULA AÓRTICA EXPUESTAS A UN AMBIENTE INFLAMATORIO Y REFLEJAN EL FENOTIPO METABÓLICO DE LAS VÁLVULAS AÓRTICAS CALCIFICADAS

Presentada por Tania Sánchez-Bayuela Recio
para optar al grado de Doctor/a por la
Universidad de Valladolid

Dirigida por:
Dra. María del Carmen García Rodríguez

A mi familia,
por ser mi pilar fundamental.

FINANCIACIÓN/ FUNDING

Este trabajo de investigación ha sido posible gracias a la financiación concedida en convocatoria pública competitiva de los siguientes proyectos de investigación:

1) "El eje metabolismo/epigenoma en la polarización de la respuesta inmune". Ministerio de Economía y Competitividad, Plan Nacional I+D+i, SAF2017-83079-R (Retos). 2018-2020. Investigadores principales Mariano Sánchez Crespo y Mª del Carmen García Rodríguez.

2) "Evaluación de los interferones como nuevas dianas terapéuticas de la estenosis aórtica calcificada. Gerencia de Salud, Consejería de Sanidad, Junta de Castilla y León. GRS2205/A/2020. 2021. Investigador principal Javier López Diaz.

3) "El metabolismo energético del sistema inmune: una fuente para el desarrollo de nuevas terapéuticas" Ministerio de Economía y Competitividad, Plan Nacional I+D+i, PID2020-113751RB-I00 (Retos). 2021-2024. Investigadores principales: Mª Carmen García Rodríguez y Mariano Sánchez Crespo.

4) "Valvular and congenital heart disease". Instituto de Salud Carlos III, Centro de Investigación Biomédica en Red de enfermedades cardiovasculares (CIBERCV), CB16/11/00260. Investigador principal Alberto San Román Calvar.

Además, la realización de este trabajo ha recibido el apoyo económico de las siguientes instituciones:

-Universidad de Valladolid-Banco Santander. Contrato predoctoral 2018-2023.

- Short-Term Fellowship para la realización de la estancia en USA en 2022: Beca del Vicerrectorado de Investigación de Valladolid y beca de movilidad internacional ERASMUS+ de la oficina de Relaciones Internacionales de la Universidad de Valladolid.

AGRADECIMIENTOS/ ACKOWLEDGEMENTS

Sé que he bromeado muchas veces con este apartado de la tesis, pero creo que finalmente lo he superado satisfactoriamente. Puede que haya sido uno de los que más difíciles me han parecido de toda la tesis (¡ojito!).

Esta tesis va por todos los que la habéis vivido conmigo o, más bien, sufrido, porque así lo he sentido a veces y así creo que lo he transmitido. Quiero dar las gracias a todas las personas que han estado cada día, sufriéndome, en persona o en la distancia, todas las personas que han convertido los momentos malos en buenos, y las que me han apoyado en todo lo que he querido hacer, confiando en mí muchísimo más de lo que yo misma lo he hecho. Creo haberos dado mi mejor y mi peor parte, aunque espero que sintáis que la buena ha ganado. Yo me llevo todo lo bueno de cada uno de vosotros, me voy con el corazón inmensamente lleno.

- Gracias a quienes me han dado la oportunidad.
- Gracias a las personas que me han enseñado lo que sé, que han sido todas y cada una de las personas que forman el IBGM.
- Gracias a las personas que trabajan en el IBGM haciendo que sea un lugar bonito para trabajar desde primerita hora de la mañana.
- Gracias las personas que son y fueron E10, por permitirme sacar esta tesis adelante, concretamente a mis predecesores por enseñarme lo que sé y por seguir aguantando alguna que otra cosilla años después.
- Gracias a mi mami vallisoletana, MI Cris:
    - Por ser la persona que ha estado a pie de cañón en el 100% de los momentos.
    - Por aguantar los días en los que se me antojó diseñar experimentos para 5 personas siendo únicamente 2.
    - Por aguantarme en la cuarentena y darme mucho apoyo.
    - Por actuar como mi madre sabiendo que ella está lejos.
    - Por las cervezas y castañas cuando eran las 11 pm y seguíamos en el laboratorio.
    - Por estar ahí cuando tuvimos que vivir en el laboratorio de lunes a domingo.
    - Por apoyarme a lanzarme a la piscina ante cualquier idea descabellada.
    - Gracias a ti esta tesis puede ser lo que es.
- Gracias a todas las personas que forman la tercera planta por ser MI SECTA FAVORITA.
- Gracias a todo el E5 por ser unas máquinas con patitas y ayudarme SIEMPRE, SIEMPRE, SIEMPRE.

AGRADECIMIENTOS

- Gracias a todos los componentes de MSC, me faltan palabras para agradecer lo bien que me habéis hecho sentir desde mi llegada al IBGM.
- Gracias a todas las personas que han hecho del IBGM mi segunda casa.
- Gracias por formar los días internacionales de casas rurales, vacaciones, fiestas, y cervezas después de días o semanas eternas.
- Gracias a las personas que han pasado por el E10 camufladas de "personas que venían a aprender", y me han enseñado más de lo que nunca hubiese imaginado
- Gracias a las personas que fueron IBGM y ahora son indispensables en mi día a día, porque el vino y visilleo siga siempre a la cabeza.
- Gracias a las personas con las que he compartido prácticas en medicina, por ser una sonrisa asegurada, por transmitir calma, por perdonar mis pequeños despistes y dejarme participar activamente en la docencia.
- Gracias a todas mis compañeras de piso, que por circunstancias de la vida me han acabado dejando solita en Valladolid. Habéis sido una bonita familia y un bonito apoyo.
- Gracias a las personas que conocí y con las que compartí la estancia. Por convertiros en amigos y familia estando fuera de casa. Por los viajes, comidas, lluvia de ideas, enseñarme técnicas que no conocía, apoyarme en lo que quería conseguir, fiestas, y sobre todo por darme la oportunidad de irme. (I want to say thanks to all the people who I met during my internship in Cornell. For being my friends and my family while I was away from home. Thank you for the trips, meals, brainstorming, teaching me new techniques, being happy when achieving my aims, parties, and, giving me the opportunity to work with you, Butcher's lab).
- Gracias a las personas que conocí en el congreso HVS y que tanto me han ayudado en el final del proceso, convirtiéndose en mi futura y próxima familia.
- Gracias a todas mis chicas de Salamanca Cris, Eva y Ana, por aguantarme a diario, animarme, y por hacer que mi hogar se encuentre un poquito más cerca de mí. Ana, gracias por ser mi mitad desde antes, incluso de conocernos. Sin ti nada de esto habría sido lo mismo.
- Gracias a mis chicos y chicas de la carrera, sois pieza indispensable de este largo proceso.
- Gracias a mis amigas y amigos de Fuensalida, mi PTMC y mi casi PTMC, que desde la distancia han estado ahí apoyándome en el proceso más de lo que nunca hubiese imaginado y me han hecho el tiempo de la tesis más llevadero con visitas, cervezas, y viajes.
- Gracias a TODA mi familia, por entender que el proceso a veces no ha sido fácil, por aguantarme y por ser el hogar donde SIEMPRE, SIEMPRE, SIEMPRE, quiero volver.
- Gracias a mis padres y mi hermano por ser el mejor soporte que jamás haya podido imaginar. Sois el pilar que me sostiene. Sin vosotros nada de esto podría haber sido posible (ni nada de lo que venga).

INDEX

CONTENTS

INDEX

INDEX

ABBREVIATIONS

2-DG: 2-deoxy-D-glucose
3, 2-D: Three, two dimension
Ac-CoA: Acetyl-CoA
ACE: Angiotensin converting enzyme
ACLY: ATP citrate-lyase
ACO: Aconitase
Akt: Protein kinase B.
ALP: Alkaline phosphatase
AMPK: AMP-activated protein kinase
ARS: Alizarin red staining
AS: Aortic valve stenosis
ATGL: Adipose triglyceride lipase
ATP, ADP, AMP: adenosine tri, di, mono phosphate
AV: Aortic valve
aVIC: Activated valvular interstitial cells
BCA: Bicinchoninic acid assay
BCL2: B-cell lymphoma-2
BMP-2: Bone morphogenetic protein -2
BPTES: Bis-2-(5-phenylacetamido-1,2,4-thiadiazol-2-yl)ethyl sulfide
BSA: Bovine serum albumin
C.I, II, III, IV: Complex I, II, III, IV
CASP: Caspase
CAVD: Calcific aortic valve disease
CM: Control medium
COX: Cyclooxygenase
CS: Citrate synthase
CT: Computerized tomography
CTP, CMP: Cytidine tri, mono phosphate
Cyt c: Cytochrome C
Cyt: cytoplasm
DAMP: Damage-associated molecular patterns
DAPI: 4’,6-Diamidino-2-phenylindole dihydrochloride
DCA: Dichloroacetate
DCFH-DA: 2’-7’dichlorofluorescin diacetate
DEPC: Diethyl pyrocarbonate
DGAT1: Diglyceride acyltransferase
DHAP: Dihydroxyacetone phosphate
DMEM: Dulbecco's Modified Eagle Medium
DMM: Dimethyl malonate
DMSO: Dimethyl sulfoxide
DNA: Deoxyribonucleic acid
dNTP: Deoxynucleotide Triphosphates
dsRNA: Double-stranded RNA
DTT: Dithiothreitol
E4P: Erythrose-4-phosphate
ECAR: Extracellular acidification rate
ECM: Extracellular matrix
EDTA: Ethylenediaminetetraacetic acid
EGM-2: Endothelial growth medium-2
ELISA: Enzyme-Linked Immunosorbent Assay

ABBREVIATIONS

EndMT: Endothelial-to-mesenchymal transition
ER stress: Endoplasmic reticulum stress
ERK: Extracellular signal-regulated kinase
ETC: Electron transport chain
FA: Fatty acid
FAD^+, $FADH_2$: Flavin adenine dinucleotide oxidized/reduced
FAS: Fatty acid synthase
FBSi: Inactivated fetal bovine serum
FCCP: Carbonyl cyanide-p-trifluoromethoxyphenylhydrazone
FITC: Fluorescein isothiocyanate
FMN: Flavin mononucleotide
G3P: Glycerol-3-phosphate
G3PD: Glycerol-3-phosphate dehydrogenase
G6P: Glucose-6-phosphate
G6PDi: G6PD inhibitor
GAPDH: Glyceraldehyde phosphate dehydrogenase
GAPDH: Glyceraldehyde phosphate dehydrogenase
GAS: IFN-γ-activated sequences
GLS: Glutamine synthase
GLUT: Glucose transporter
GlycoATP: Glycolytic ATP
GPAT: Glycerol-3-phosphate acyltransferase
GPAT: Glycerol-3-phosphate acyltransferase
GSSG/GSH: Glutathione disulfide oxidized/ glutathione reduced
GTP, GMP: Guanosine tri, mono phosphate
GlycoPER: Glycolytic Proton Efflux Rate
HCR: Hybridization chain reaction
HDL: High density lipoprotein
HIF: Hypoxia inducible factor
HIF-1α: Hypoxia inducible factor 1α
HK: Hexokinase
HRP: Horseradish peroxidase
ICAM-1: Intercellular adhesion molecule 1
IDH: Isocitrate dehydrogenase
IFN: Interferons
IFNAR: Interferon α/β receptor
IFNGR: Interferon γ receptor
IL: Interleukin
IMP: Inosine monophosphate
IRF: Interferon regulatory factor
JAK: Janus kinases
JNK: c-Jun N terminal kinase 2
KDa: Kilodalton
LAC: Lactate
$LacNa^+$: Sodium lactate
LDH: Lactate dehydrogenase
LDL: Low density lipoproteins
Lp (a): Lipoprotein a
LPS: Lipopolysaccharide
M: Mass
MAPK: Mitogen-activated protein kinases

MCAD: Medium-chain acyl-coenzyme A dehydrogenase
MCT: Monocarboxylate transporter
MDH: Malate dehydrogenase
ME: Malic enzyme
MitoATP: Mitochondrial ATP
MMP: Matrix metalloproteinase
MPC: Monocarboxylate pyruvate carrier
mRNA: messenger ribonucleic acid
MyD88: Myeloid differentiation primary response protein 88
NAC: N-acetyl-L-cysteine
NAD^+/NADH: Nicotinamide adenine dinucleotide oxidized/ reduced
$NADP^+$/NADPH: Nicotinamide adenine dinucleotide phosphate oxidized/reduced
NADS: NAD^+ synthetase
NAM: nicotinamide mononucleotide
NAMN: nicotinic acid mononucleotide
NAMNPT: nicotinamide phosphoribosyltransferase
NF-κB: Nuclear factor kappa-light-chain-enhancer of activated B cells
NMNAT: nicotinamide mononucleotide adenyltransferase
NOX: NADPH oxidase
NS: non-significant
Nuc: Nuclei
OAA: Oxaloacetate
OCR: Oxygen consumption rate
OGM: Osteogenic medium
Ox-LDL: Oxidized LDL
OxPPP: Oxidative phase of pentose phosphate pathway
OXPHOS: Oxidative phosphorylation
PAMP: Pathogen-associated molecular patterns
PAVEC: Porcine aortic valve endothelial cell
PAVIC: Porcine aortic valve interstitial cell
PBS: Phosphate-buffered saline
PDC: Pyruvate dehydrogenase complex
PDK: Pyruvate dehydrogenase kinase
PDMS: poly-dimethylsiloxane
PFKFB3: 6-phosphofructo-2-kinase/fructose-2,6-bisphosphatase
PGE2: Prostaglandin E2
Pi: Inorganic phosphate
PI3K: Phosphatidylinositol 3 kinase
PI3K: Phosphoinositide 3-kinase
PKM: Pyruvate kinase
Poly (I:C): Polyinosinic:polycytidylic acid
PPARA: Peroxisome proliferator-activated receptor alpha
PPARG: Peroxisome proliferator-activated receptor gamma
PPP: Pentose Phosphate Pathway
PRPP: Phosphoribosyl pyrophosphate
PVDF: Polyvinylidene Fluoride
PYR: Pyruvate
qPCR: Quantitative polymerase chain reaction
qVIC: Quiescent valvular interstitial cells
R5P: Ribose-5-phosphate
Redox: Reduction-oxidation

ABBREVIATIONS

RNA: Ribonucleic acid
ROS: Reactive oxygen species
Rot/AA: Rotenone/antimycin A
RPMI: Roswell Park Memorial Institute medium
RT: Retrotranscriptase
Ru5P: Ribulose-5-phosphate
RUNX2: Runt-related transcription factor-2
Ruxo: Ruxolitinib
SD: Standard deviation
SDH: Succinate dehydrogenase
SDS-PAGE: sodium dodecyl sulfate–polyacrylamide gel electrophoresis
siRNA: Small interference RNAs
SIRT: Sirtuin
SOD: Superoxide dismutase
STAT: Signal transducer and activator of transcription
SVi: Stroke volume index
TCA: Tricarboxylic acid
TGF-β: Transforming growth factor-β
TIMP: Tissue inhibitor of matrix metalloproteases
TIRAP: TIR domain-containing adaptor protein
TLR: Toll-like receptor
TMRM: Tetramethylrhodamine methyl ester
TNF-α: Tumor-necrosis factor-α
TRAF: Tumor necrosis factor receptor (TNF-R)-associated factor. 3
TRAM: TRIF-related adaptor molecule
TRIF: TIR-domain-containing adapter-inducing interferon-β
UMP: uridine monophosphate
UPLC/MS: Ultra Performance Liquid Chromatography Mass Spectrometry
VCAM-1: Vascular cellular adhesion molecule
VEC: Valvular endothelial cells
VEGF: Vascular endothelial growth factor
VIC: Aortic valve interstitial cells
VSMC: Vascular smooth muscle cell
VSMC: Vascular smooth muscle cells
WB: Western blot
X5P: Xylulose-5-phosphate
α-KG: α-ketoglutarate
α-SMA: α-Smooth muscle actin

ABSTRACT

ABSTRACT

Introduction and objectives: Inflammation has been linked to metabolic reprogramming in several diseases, including cardiovascular pathogenesis. Calcific aortic valve disease (CAVD) is an increasingly prevalent valvulopathy, yet surgical replacement is the only available therapy. CAVD is characterized by a damaged endothelium, inflammation, exaggerated matrix remodeling, calcification, and metabolic changes. At the cellular level, recent evidence disclose the interplay between innate immunity/inflammatory pathways, i.e., Toll-like receptors (TLR)3/4 and interferon-γ receptor signaling, on the differentiation, calcification, and inflammation of valve interstitial cells (VIC) via stabilization of hypoxia-inducible factor (HIF)-1α. Given that this transcription factor is associated with metabolic reprogramming in several diseases, inflammation and metabolism may work in an interconnected manner in CAVD. Therefore, the main goal of this study was to investigate the metabolic reprogramming of VIC under inflammatory settings, and its contribution to the processes relevant to CAVD pathogenesis.

Material and methods: Human VIC from patients with no valve disease were used as a model. To mimic an inflammatory environment, cells were treated with pro-inflammatory cytokines and pathogen patterns recognized by TLRs. Metabolic analysis was performed by real-time metabolic analysis using Seahorse extracellular flux assays, and [U-^{13}C]-glucose tracing, by liquid chromatography/mass spectrometry. Metabolic gene profiles and metabolite production were evaluated by qPCR, Western blot, and commercial kits. Inflammation, calcification, and apoptosis were studied using Western blot, ELISA, qPCR, immunofluorescence, flow cytometry, gene silencing, and *in vitro* calcification assays. Validation of findings in human VIC was performed in quiescent VIC dedifferentiated from human VIC, in porcine 3D VIC-valve endothelial cell co-cultures, as well in valve leaflets and VIC explanted from patients with/without CAVD.

Results: The main finding of the study is that inflammatory stimuli drive a metabolic reprogramming of VIC to a hyperglycolytic phenotype that mimics the metabolic phenotype in calcified valves. It is characterized by enhanced glycolysis and glycolytic ATP production, impaired pentose phosphate pathway (PPP), as well as damaged mitochondrial function with uncoupling of electron transport chain (ETC) and oxidative phosphorylation (OXPHOS). Furthermore, metabolic dysregulation is associated with reactive oxygen species (ROS) production, as well as increased reliance on glucose uptake for energy production and metabolite accumulation. Pharmacological approaches to metabolic routes demonstrate the role of glycolysis upregulation in processes relevant to CAVD, such as VIC differentiation, calcification, and inflammation, and have further highlight the contribution of PPP and oxidative stress in these processes. Our findings further reveal the involvement of the Janus kinase (JAK)-STAT/HIF-1α and nuclear factor (NF)-kB pathways in the metabolic reprogramming. Finally, the shift in VIC, also found in 3D VIC-VEC co-cultures exposed to inflammatory stimuli, replicates the hyperglycolytic profile of calcified cells and valve leaflets.

Conclusion: Inflammation drives a metabolic shift in human VIC, mirroring the glycolytic phenotype in calcified valves, which is characterized by hyperglycolysis that is necessary to support inflammation,

calcification, and osteogenic differentiation of VIC. Additional reprogramming of complementary catabolic pathways, such as PPP, tricarboxylic acid cycle, and oxidative phosphorylation, generates redox homeostasis alterations that further contribute to pathological processes in VIC. Thus, inflammation-triggered changes in metabolic phenotypes may play a relevant pathogenic role in the initial stages of CAVD, and the identified metabolic routes may provide therapeutic clues for the disease.

ABSTRACT

Introducción y objetivos: La inflamación se ha relacionado con la reprogramación metabólica en varias enfermedades, incluyendo en el ámbito cardiovascular. La estenosis aórtica calcificada (CAVD) es una valvulopatía cada vez más prevalente, sin embargo, la sustitución quirúrgica es la única terapia disponible. La CAVD se caracteriza por el daño endotelial, una respuesta inflamatoria desregulada, la remodelación exagerada de la matriz extracelular, la calcificación y los cambios metabólicos. A nivel celular, estudios recientes han puesto de manifiesto la interacción entre la inmunidad innata y las vías inflamatorias, específicamente los receptores tipo Toll (TLR) 3/4 y la señalización del receptor de interferón-γ, en procesos de inflamación, calcificación y diferenciación de las células intersticiales de la válvula (VIC) a través de la estabilización del factor de transcripción dependiente de hipoxia (HIF)-1α. Dado que HIF-1α se ha asociado con la reprogramación metabólica en varias enfermedades, estas evidencias sugieren que la inflamación y el metabolismo pueden trabajar de manera interconectada en CAVD. Teniendo esto en cuenta, el objetivo principal de este estudio fue investigar la reprogramación metabólica de las VIC en entornos inflamatorios y su contribución a procesos relevantes en la patogénesis de CAVD.

Material y métodos: Se utilizaron VIC humanas de pacientes control para generar el modelo de la enfermedad. Para generar un entorno inflamatorio, las células se trataron con citoquinas proinflamatorias y patrones asociados a patógenos reconocidos por los TLRs. Para el análisis del metabolismo celular se utilizó el analizador metabólico en tiempo real *Seahorse* además de experimentos fluxómica y trazado de [U-^{13}C]-glucosa mediante cromatografía líquida/espectrometría de masas. Los perfiles de genes metabólicos y los metabolitos se evaluaron mediante qPCR, Western blot y kits comerciales. La inflamación, calcificación y apoptosis se estudiaron utilizando Western blot, ELISA, qPCR, inmunofluorescencia, citometría de flujo y ensayos de calcificación *in vitro*. Para la validación de los resultados obtenidos en VIC humanas, se utilizaron técnicas de desdiferenciación de células VIC a células con fenotipo quiescente y de co-cultivos de VIC-VEC en 3D. Además, los resultados también se validaron en válvulas y VIC explantadas de pacientes con o sin CAVD.

Resultados: El hallazgo principal es la reprogramación metabólica de las VIC hacia un fenotipo hiperglucolítico inducido por agentes inflamatorios. Se caracteriza por el aumento de la glucólisis y la producción de ATP glucolítico, la alteración de la ruta de la pentosa fosfato (PPP), así como el daño en la función mitocondrial con desacoplamiento de la cadena de transporte de electrones (ETC) y la fosforilación oxidativa (OXPHOS). Además, la desregulación metabólica está relacionada con la producción de especies reactivas de oxígeno (ROS) y con una mayor dependencia de la captación de glucosa para la producción de factores de energía y la acumulación de metabolitos. Aproximaciones farmacológicas de rutas metabólicas, demostraron el papel de la sobrerregulación de la glucólisis y de la producción de ROS, así como la desregulación de PPP en procesos relevantes para CAVD, como inflamación, calcificación y diferenciación de las VIC. Nuestros hallazgos también revelaron el papel de la PKM2 y de las vías del factor nuclear (NF)-κB y Janus kinase (JAK)-STAT/HIF-1α en la reprogramación metabólica. Finalmente, el cambio metabólico

ABSTRACT

caracterizado en VIC, también se encontró en los co-cultivos 3D expuestos a estímulos inflamatorios y replica el perfil hiperglucolítico de las células y válvulas de pacientes con CAVD.

Conclusión: El ambiente inflamatorio induce una reprogramación metabólica de VIC, que refleja el fenotipo glucolítico de las válvulas estenóticas. Esta reprogramación se caracteriza por el aumento de la glucólisis, necesario para mediar la inflamación, la calcificación y la diferenciación osteogénica de las VIC. La reprogramación adicional de vías catabólicas complementarias, como la vía de las pentosas fosfato, el ciclo de los ácidos tricarboxílicos y la fosforilación oxidativa, genera alteraciones en la homeostasis redox que también contribuyen a los procesos patológicos en VIC. Por lo tanto, las alteraciones metabólicas desencadenadas por un ambiente inflamatorio podrían desempeñar un papel patogénico relevante en las etapas tempranas de CAVD, y las rutas metabólicas identificadas pueden ser potenciales dianas terapéuticas para la enfermedad.

HYPOTHESIS AND OBJECTIVES

Based on (i) the link between Inflammation and metabolic reprogramming in health and disease (reviewed in Pearce et al., 2013 & Phadwal et al., 2021), (ii) the association between immune/inflammatory mediators and receptors to CAVD, i.e., the cytokine IFNγ released by activated T lymphocytes in aortic valves (Nagy et al., 2017), and the pathogen pattern sensors TLR3/4 (reviewed by García-Rodríguez et al., 2018); (iii) the reported interplay between TLR3/4 and IFNGR on immune non-hypoxic stabilization of HIF-1α and subsequent VIC calcification via JAK-STAT pathway (Parra-Izquierdo et al., 2019, 2021); (iv) the link between HIF-1α transcription factor and metabolic rewiring (reviewed in Semenza et al., 2011), we hypothesized that an inflammatory milieu could play a key role in the early phases of CAVD by promoting a metabolic reprogramming of human VIC thus contributing to processes relevant to CAVD pathogenesis like inflammation, differentiation, and calcification.

The main goal of this study was to characterize the basal metabolism of human VIC and to elucidate the metabolic reprogramming induced by an inflammatory milieu and the ensuing impact on VIC physiopathology. The specific objectives of this study are as follows:

1. To characterize the basal metabolic profile of human VIC and their reliance on different metabolic pathways for energy and biomass production.
2. To investigate the effect of an inflammatory environment generated by cytokines and pathogen patterns on the metabolic phenotype of VIC, particularly focusing on catabolic pathways such as glycolysis, PPP, TCA, and OXPHOS, leading to redox homeostasis dysregulation.
3. To elucidate the impact of the metabolic shift, intermediate metabolites, and oxidative stress on VIC physiopathology, particularly investigating processes related to CAVD, such as differentiation, calcification, and inflammation.
4. To identify the molecular mechanisms mediating the inflammatory stimuli-induced metabolic reprogramming of VIC.
5. To confirm the *in vitro* findings in the quiescent VIC and 3D VIC-VEC (swine) co-culture model, as well as in the valve tissue and VIC from patients with and without CAVD.

INTRODUCTION

I.1- The heart valves

The heart is a complex muscle composed by red muscle and it is responsible for circulating blood through the three segments of the circulatory system: the coronary system (supplying blood to the heart), the pulmonary system (involving the heart and lungs), and the systemic system (supplying blood to the body's organs and tissues). The heart is comprised of three distinct layers: the outermost layer, the epicardium; the middle layer, the myocardium; and the innermost, the endocardium (**Figure I**).

There is an atrium and a ventricle on each side of the heart. The right atrium receives deoxygenated blood from the heart and superior and inferior vena cava, which then moves through the right **atrioventricular valve** or **tricuspid valve**, which only opens in one direction to prevent the blood from flowing back. Once the right ventricle is filled, it pumps blood through the pulmonary arteries to the lungs, where it undergoes reoxygenation. Following its passage through the pulmonary arteries, the right **semilunar valves or pulmonary valves** shut to prevent any backward flow of blood into the right ventricle. Next, the left atrium receives oxygen-rich blood from the lungs via the pulmonary veins. The **left atrioventricular valve or mitral valve** separates the chambers on the left side of the heart. Once the blood passes through the bicuspid valve, it enters the left ventricle, where it is subsequently pumped through the aorta, carrying oxygenated blood to the body's muscles and organs. After the blood is ejected from the left ventricle into the aorta, the **aortic semilunar valve** or **aortic valve (AV)** closes, thus preventing any blood from flowing back into the left ventricle.

The heart functions as a pump through a combination of electrical and mechanical events, known as the cardiac cycle, which is based on pressure changes resulting in the movement of the blood through the different chambers of the heart and the body. The cardiac cycle is divided into two phases. During the diastolic phase, the atrioventricular valves open, permitting blood flow into the heart and ventricles. Once the ventricles are filled, the atrioventricular valves close, and the semilunar valves open. During this transition, electrochemical changes in the myocardium create pressure alterations, leading to the concentric contraction of cardiac muscle, resulting in the systolic or contraction phase. During systole, electrical impulses prompt the ventricles to contract, propelling blood into the pulmonary and aorta arteries. At this point, the valves are responsible for maintaining the direction of the blood, leading to the movement of the blood to the next chamber. Therefore, maintenance of the physiology and function of the four valves is crucial for heart function. However, infections, degeneration, and congenital disorders can cause valve malfunctions, thereby affecting the overall functionality of the heart (Pollock et al., 2023).

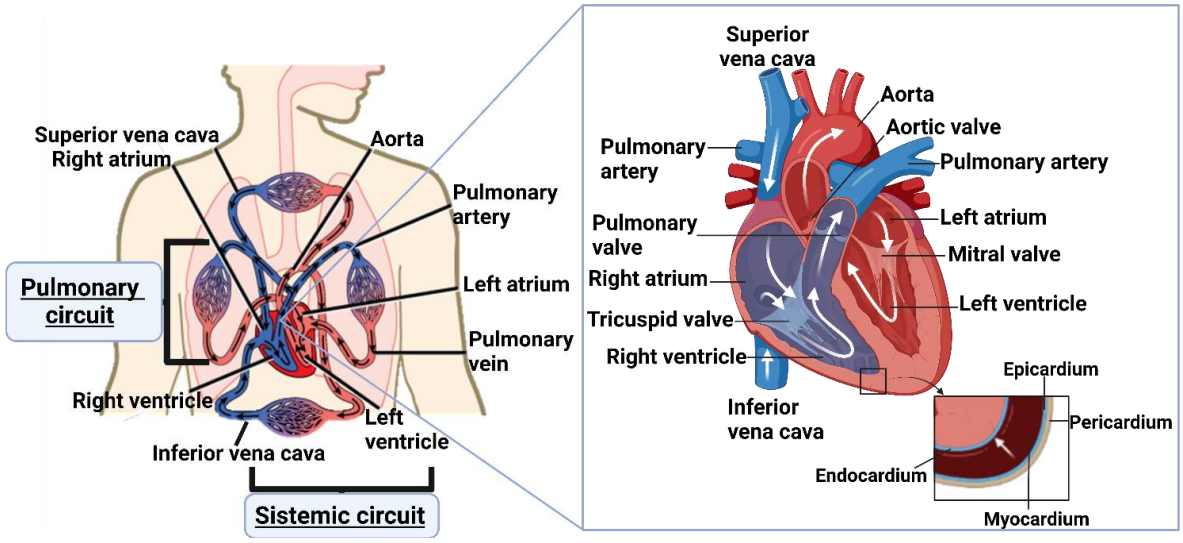

Figure I. Circulatory system circuits and representation of the human heart anatomy. The pulmonary system involving the heart and lungs. The systemic system supplying blood to the body's organs and tissues. Heart composition on the left and right sides and the layers composing the heart: endocardium, myocardium, epicardium, and pericardium. Created with BioRender.com.

I.1.1- Heart valve structure and cellular composition

I.1.1.1-Valve types and composition

There are two atrioventricular valves, as shown in **Figure II**: the right atrioventricular or tricuspid valve and the left atrioventricular or mitral valve. Each valve is a complex arranged by an orifice that is surrounded by a ring, two or three cusps that extend centrally to close the orifice, and supporting structures known as *the chordae tendineae* and papillary muscles. The term *chordae tendineae* or tendinous cords refers to collagen structures that function as bridges between the leaflets and papillary muscles. In contrast, papillary muscles are muscular extensions that participate in mechanical activity. Finally, a leaflet or cusp is a projection of the valve, whose function is to occlude the valve orifice when apposed with adjacent leaflets, preventing retrograde flow.

In contrast, there are two semilunar valves, as shown in **Figure II**; on the right, the pulmonary valve is at the root of the pulmonary artery. On the left side, the AV is found at the root of the ascending aorta. Each valve has a supporting fibrous skeleton and associated cusp, but they lack the typical *chordae tendineae* or papillary muscle attachments present in the atrioventricular valves. The pulmonary valve has three cusps, called anterior, right, and left, attached to the root of the pulmonary artery (Anderson et al., 2000). Conversely, the AV is larger than the pulmonary valve and consists of three cusps: right coronary, left coronary, and non-coronary cusps. In this case, the cusps are attached to the aorta via a fibrous annulus (Anderson, 2000). Specifically, in humans, the AV is an avascular tricuspid structure smaller and thicker than 1 mm; however, it is richly innervated by a highly preserved network of afferent and efferent nerves that contribute to valve structure and function (Gerald Litwack, 2018).

I.1.1.2- Valve structure

Valve functionality is accomplished by a complex and specialized organization of cells and extracellular matrix (ECM) layers, as shown in **Figure II**. Generally, the same composition and cell types were found in the four heart valves. Valve surfaces are covered by continuous endothelium, and the valve interstice is arranged by three layers of connective tissue. Semilunar valves are divided into (i) the ventricularis, which is oriented to the ventricle and is directly in contact with pulsatile blood. It is composed of elastin fibers oriented radially, allowing valve flexibility. (ii) Spongiosa, located between the ventricularis and fibrosa, is composed of glycosaminoglycans and proteoglycans, whose major function is to support and facilitate the movement of valve cups. Proteoglycans are highly hydrated and function as ‘‘shock absorbers’’ during different parts of the cardiac cycle. (iii) Fibrosa oriented to the major arteries. It is composed of dense connective tissue containing circumferentially oriented collagen fibers that support most of the hemodynamic challenges of the valve (reviewed in Rutkovskiy et al., 2017). The structure is the same in the case of atrioventricular valves, with the only difference being that in these valves, the ventricularis layer is called the atrialis because it is directed towards the atrium.

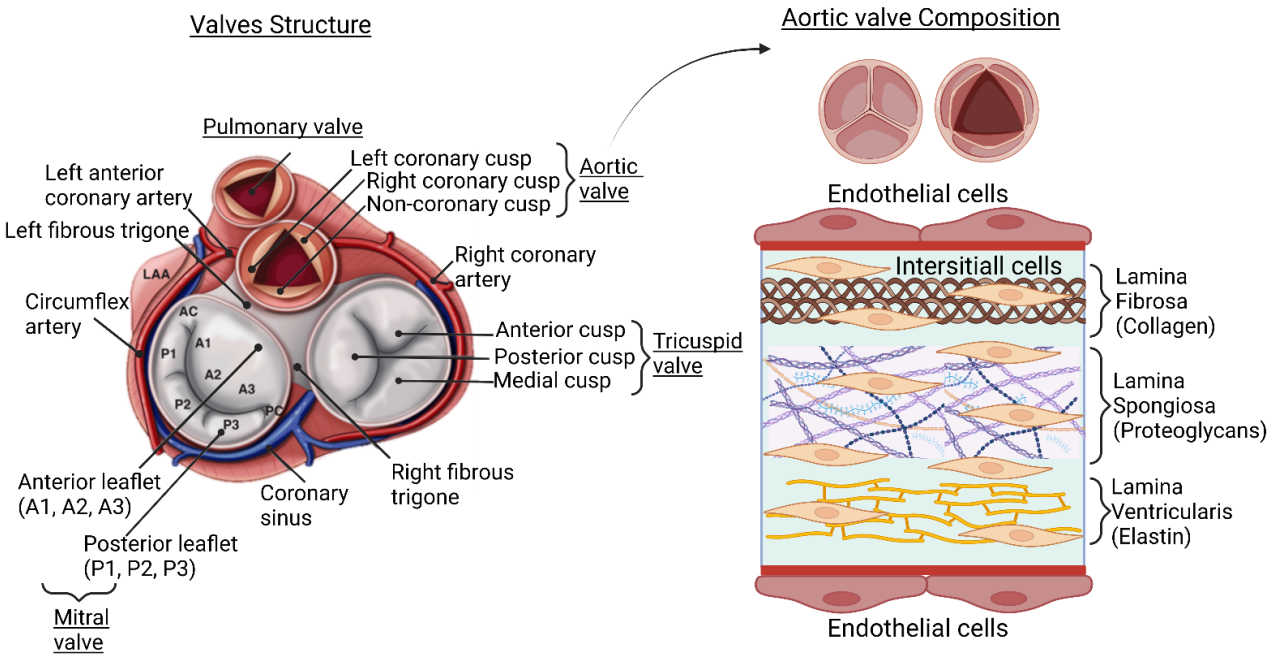

Figure II. **Structure of the four heart valves and layer composition of the AV.** Structure and location of the pulmonary, aortic, tricuspid, and mitral valves. Composition of the AV layers: (i) ventricularis, which is oriented to the ventricle and composed of elastin fibers. (ii) The spongiosa, located between the ventricularis and fibrosa, is composed of glycosaminoglycans and proteoglycans. (iii) Fibrosa, which is oriented to the major arteries or atrium and is composed of dense connective tissue containing collagen fibers. Created with BioRender.com.

I.1.1.3- Valve cellular composition

During development, AV is formed from endocardial cushions, which originate when endothelial cells migrate into the cardiac jelly, followed by the endothelial-to-mesenchymal transition (EndMT). This

process is the initial step in subsequent tri-layered AV formation. The migration, differentiation, and delamination of these cells is a tightly regulated sequence of events that is dependent on specific signaling molecules, such as NOTCH1, transforming growth factor β (TGF-β), and the WNT/β-catenin pathway, as well as hemodynamic cues (Y. Li et al., 2018). Most of the signals that are operational during morphogenesis continue to influence growth and adaptation in postnatal life as demonstrated by valvular endothelial cells (VEC) expressing α-smooth muscle actin (α-SMA) due to its EndMT, which could be helpful for valve repair and interstitial cell regeneration (reviewed in Y. Li et al., 2018).

- **Valvular endothelial cells (VEC)**

VEC define the endothelium as a continuous cell layer that covers the valve. For many years, aortic VEC have been thought to be passive structures with no relevant role in valve physiology, only responding to changes in transvalvular pressure. However, several studies have demonstrated that aortic VEC have homeostatic functions in nutrient exchange and ECM synthesis, play a role in inflammation, and maintain the VIC phenotype (reviewed in Driscoll et al., 2021).

Although valve endothelial cells share certain functions with vascular endothelial cells, such as the expression of Von Willebrand factor, nitric oxide synthesis, production of prostacyclin and ECM proteins, and presence of typical endothelial cellular junctions (Manduteanu et al., 1988), there are several differences between them. For example, whereas the vascular endothelium aligns itself with the long axis of the cell parallel to flow (except in areas of turbulent flow), VEC are oriented perpendicular to the direction of flow (Deck., 1986). Furthermore, a comparison of the transcriptional profiles of vascular and valvular endothelial cells revealed phenotypic differences in terms of inflammatory and osteogenic genes as well as a major influence of shear stress (Butcher et al., 2006). In addition, it has been recently reported that VEC lining the aortic and ventricular sides support different shear stresses and exhibit differences during disease. Histologically, AV calcification occurs exclusively on the aortic side of the valve; thus, VEC on the aortic side are less resistant to calcification (El-Hamamsy et al., 2010).

- **Valvular interstitial cells (VIC)**

VIC can originate in endothelial cells because of EndMT. VIC are distributed along the three layers of the valve, and they are reported to respond differently to cytokines in their environment depending on the cell location. For example, VIC located in fibrosa demonstrated greater *in vitro* calcification potential that the ones derived from ventricularis (Schlotter et al., 2018)

VIC are a heterogeneous population of different cell types, mainly fibroblasts, smooth muscle cells, and myofibroblasts, which are crucial for maintaining valve function. Under homeostatic conditions, most cells are quiescent fibroblasts (qVIC) that do not express α-SMA. They are mainly responsible for the generation, maintenance, and repair of the ECM owing to their secretory properties; however, they do not

have ECM remodeling or contracting properties. Additionally, smooth muscle cells exhibit both secretory and contractile properties (reviewed in Rutkovskiy et al., 2017). Intriguingly, there is a small part of qVIC, which have been partially activated and have acquired a myofibroblast-like phenotype and are called activated VIC (aVIC). aVIC are characterized by proliferative and contractile properties, and their function is to contract the ECM (reviewed in Rutkovskiy et al., 2017). These cells are α-SMA-positive and secrete growth factors, cytokines, and molecules related to matrix remodeling, such as matrix metalloproteinases (MMP) and their counterparts, tissue inhibitors of metalloproteinases (TIMP). In fact, myofibroblasts are believed to account for calcification nodules due to the formation of cell aggregates, which lead to the sedimentation of calcium salts, collagen type I and elastin chains, bone sialoprotein, apoptotic bodies, and others.

The proper function of the valve depends on the transition and equilibrium between the VIC phenotypes. VIC imbalance can trigger valve disease (reviewed in Bian et al., 2021). When valve homeostasis is disrupted, interstitial cells have been demonstrated to undergo a transition into an osteoblast-like phenotype, leading to valve calcification. Osteoblastic differentiation of VIC is similar to physiological osteogenesis and is largely orchestrated by Runt-related transcription factor 2 (Runx2) and bone morphogenetic proteins (BMPs). The osteoblastic pathway does not normally involve the activation of α-SMA or contraction of the ECM, although there is a certain degree of overlap (reviewed in Rutkovskiy et al., 2017).

For *in vitro* studies, the main source of cells with close anatomical similarity to humans is porcine AV. Other important animal models include sheep and cows. More recently, VIC have been successfully isolated and cultured from mice. The main disadvantage of using animal cells is that the experiments must be replicated using human cells before further clinical application. However, the use of human cells has several drawbacks, including patient age, sex, and concomitant diseases. The major variables that play a crucial role are the amount of calcium, the pressure gradient, and the valve anatomy. Human cells used as controls are mainly obtained from: (i) donor hearts that were considered unusable for transplantation, (ii) hearts removed from recipients of heart transplantation without a history of AV disease, (iii) non-calcified AV removed because of valve insufficiency, (iv) pediatric valves removed due to congenital abnormality, (v) valves extracted during surgery for aortic dissection, and (vi) non-calcified cusps (or portions of the cusp) of the calcified valve (reviewed in Rutkovskiy et al., 2017).

- **Stem cells**

Recently, a population of resident stem cells has been identified in advanced valvular lesions. Chen et al., 2009 found high frequencies of mesenchymal progenitors (48.0 ± 5.7%) and osteoprogenitors (44.1 ± 12.0%) in AV lesions. These cells seem to originate from hematopoietic-derived stem cells towards the

cardiac valves. Although they do not have an identified role in the valve, they are thought to contribute to valve repair and cell regeneration and participate in valve calcification in some disease stages.

- **Immune cells**

Immune cells have been detected not only in human stenotic valves but also in healthy ones (reviewed in Raddatz et al., 2019 & Bartoli-Leonard et al, 2021). Although the presence of immune cells is limited and highly regulated in healthy valves, it plays a key role in maintaining tissue integrity by keeping the balance between inflammation and tissue repair and preventing infection. Up to 15% of cells in the healthy valve are immune cells such as macrophages and T lymphocytes, and the number further increase in calcified valves (reviewed in Raddatz et al., 2019). Activation of resident immune cells could participate in the inflammation-induced mechanisms leading to calcification. Additionally, Coté et al. (2013) reported that chronic inflammatory cell types, such as $CD45^+$ leukocytes, $CD68^+$ macrophages, and scattered $CD3^+$ T cells, were present in the valve near the calcified areas. This inflammatory infiltrate in the valve has been associated with several indices of remodeling, suggesting that inflammation may participate in mineralization and fibrotic processes (Coté et al., 2013). The infiltrated immune cells can secrete a wide range of active inflammatory cytokines, such as tumor necrosis factor (TNF)-α or interleukins (IL), such as IL-6, IL-8, and IL-1β, as well as ECM remodeling molecules, such as MMP, that can be sensed by VIC and activate pathological responses.

I.1.2- Heart valve disease

The incidence of valve heart disease is growing so quickly that it causes a marked increase in cardiovascular morbidity and mortality in all geographical areas, including both developed and developing nations. In fact, a recent large-scale community echocardiographic screening revealed that half of the population over 65 years of age suffers from several types and grades of valvular diseases (Arcy et al., 2016). Therefore, valve heart diseases require a better understanding of the mechanisms that trigger and underlie them, as well as the development of novel treatments.

Healthy valve leaflets can fully open and close during the heartbeat; however, diseased valves may not be fully open and closed. Any valve in the heart can become diseased; however, the AV is the most affected. In general, the two main outcomes of valvular heart disease are stenosis and regurgitation. In both cases, the heart must work harder to overcome the problems and pump, which can lead to cardiac failure, ventricular hypertrophy, stroke, sudden cardiac arrest, and death.

(i) **Regurgitation (or leakage of the valve):** The valve cannot close completely during diastole, causing blood to flow backward through the valve.

(ii) **Stenosis (or narrowing of the valve)***:* The valve loses its homeostasis and generates exacerbated remodeling as well as calcific nodules. These processes lead to valve thickening and incomplete opening, thus leading to a limited blood flow through the aorta.

I.1.2.1- Valvulopathies

As mentioned, the four valves can experience stenosis or regurgitation, although aortic valve stenosis is the most common.

- **Mitral valve diseases**: Mitral valve stenosis has a low prevalence, affecting 0.2% of the population aged > 75 years. However, mitral valve regurgitation is one of the most common valvular diseases, with a prevalence of 9.3% in the population over 75 years old, affecting 24 million people worldwide. The final consequence of mitral regurgitation is cardiac muscle hypertrophy (reviewed in Coffey et al., 2021).

- **Tricuspid valve disease**: Tricuspid valve stenosis is a rare disease, which is often a consequence of tricuspid regurgitation and mitral stenosis. However, tricuspid regurgitation has a prevalence of 10% in all populations and its prevalence has increased in developed nations. It is also commonly associated with mitral regurgitation (reviewed in Coffey et al., 2021).

- **Pulmonary valve diseases**: The pulmonary valve rarely suffers from acquired valve disease; however, pulmonary stenosis accounts for approximately 8% of all congenital heart defects. Owing to the increase in pressure due to stenosis, subsequent tricuspid regurgitation can occur (reviewed in Coffey et al., 2021).

- **Aortic valve diseases:** AV frequently suffer from acquired valve disease in comparison to pulmonary valves, even though their structures are similar. AV stenosis leading to calcific aortic valve disease (CAVD) is the most common valvular pathology in developed nations. It affects 9 million people worldwide, and its prevalence has been increasing with population aging and an increase in atherosclerosis. It has been estimated that approximately 34% of the population over 65 years of age suffer from early and asymptomatic AV lesions called AV sclerosis, and it has been demonstrated that over time, 16% of AV sclerosis progresses into aortic stenosis. On the other hand, regurgitation is present in 2% of the population over 75 years of age in developed countries (reviewed in Coffey et al., 2021).

Due to the fact that AV is the most diseased valve and the lack of pharmacological treatment for CAVD, yet surgical replacement and transcatheter aortic valve implantation (TAVI) are the only available treatments, it is extremely important to understand the molecular processes underlying CAVD progression in order to identify new targets for the treatment and/or prevention of the disease.

I.2-Calcific aortic valve disease (CAVD)

Calcific aortic valve disease (CAVD) is the most prevalent valve heart disease in the elderly population of developed countries with projected disease burden expected to increase from 2.5 million in 2000 to 4.5 million in 2030 (Yutzey et al., 2014). CAVD was initially thought to be a passive process consequence of valve tissue degeneration. However, it is currently considered an active disease characterized by cell-mediated processes that lead to disease onset and progression (reviewed in Rajamannan et al., 2011). CAVD and atherosclerosis share some risk factors, including hypertension, advanced age, male sex, high cholesterol levels, smoking, renal failure, and low-density lipoproteins (LDL) (reviewed in Moncla et al., 2023).

The initial stages of CAVD that lead to valve sclerosis are similar to those of atherosclerosis, and endothelial damage, inflammation, and lipid deposition play key roles in the first stages of both diseases. However, later stages of stenosis involving structural changes and macrocalcification are more complex than atherosclerotic ones, which could be the reason why pharmacological approaches used for atherosclerosis treatment, i.e., statins, have not been efficient for the treatment of CAVD (reviewed in Alushi et al., 2020). A potential explanation for this failure could be the late intervention since lipids play a pathogenic roles in early but not in advanced stages of the disease.

Generally, the symptoms are minimal and appear at the end of the disease; therefore, the pressure overload generated due to AV stenosis can lead to progressive left ventricular hypertrophy, life-threatening symptoms (angina and syncope), and in the worst scenario, could lead to heart failure and, without intervention, death within months to a few years.

I.2.1-CAVD risk factors

Some Retrospective and prospective studies have revealed that age, male sex, hypertension, smoking, and some metabolism-related factors, such as diabetes mellitus, obesity, and elevated plasma lipoprotein (Lp)-a and low-density lipoprotein (LDL) cholesterol, are associated with the risk of CAVD (reviewed in Junco-Vicente et al., 2020).

- **Hypertension:** A high arterial pressure condition is considered when systolic blood pressure is higher than 140 mmHg and/or diastolic pressure is higher than 90 mmHg. Hypertension has been associated with faster progression of AV stenosis, as shown by the Helsinki Aging Study (Lehti et al., 2021) and the PROGRESSA study (Tastet et al., 2017). Additionally, the MESA study results showed that higher pressure and wave reflection promote abnormal hemodynamics, which leads to calcification and ECM remodeling (Owens et al., 2010).
- **Age:** This is the most important risk factor for CAVD, and it is an increasing risk factor with a two-fold increase every ten years. In fact, the rise in prevalence is related to an increase in life expectancy, as demonstrated by the Cardiovascular Health Study (CHS) (reviewed in Moncla et al., 2023).

- **Cigarette Smoking**: In general, it is associated with a decrease in life expectancy of up to 10 years. Additionally, several studies have associated smoking with a two-fold increase in the risk of developing cardiovascular diseases, especially CAVD, as reported by the MESA study (Owens et al., 2010).
- **Male sex:** Epidemiological studies such as the Framingham Offspring Study (FOS) and CHS have demonstrated a two-fold increase in the risk of CAVD in men compared to women (reviewed in Alushi et al., 2020)**.**
- **Obesity:** Several studies, such as the Cohort of Swedish Men and the Swedish Mammography Cohort, have demonstrated that overall and visceral obesity are associated with the incidence and progression of CAVD (Kaltoft et al., 2020). Visceral fat is associated with increased LDL and inflammatory cytokine production as well as reduced HDL and atherogenic adipokines. The oxidation of lipids and apolipoprotein B by free oxygen radicals generates oxidized LDL, which can stimulate the inflammation and differentiation of valve myofibroblasts (Peltier et al., 2003).
- **Congenital valve malformation:** an altered number of aortic valve cups, bicuspid or unicuspid, has been associated with CAVD risk (reviewed in Alushi et al., 2020 & Junco-Vicente et al., 2020). Bicuspid AV (BAV), which is three times more common in men than in women, is the most common congenital cardiac abnormality causing CAVD (Kong et al., 2020). The most common malformation of the bicuspid valve is the fusion of the left and right coronary cusps, which affects hemodynamic regulation, and wall shear stress supported by the tissue increases the predisposition to CAVD (Kong et al., 2020).
- **Lipids**: It is well known that the accumulation of LDL-cholesterol is associated with greater odds of developing aortic sclerosis and stenosis. Other lipids, such as Lp (a), a transporter of oxidized phospholipids, have been demonstrated to be risk factors for cardiovascular disease (Zheng et al., 2019). In fact, immunohistological studies have found the colocalization of apolipoprotein-(a) and apolipoprotein-(b) with calcium in stenotic lesions and has been associated with faster disease progression (Zheng et al., 2019).
- **Diabetes mellitus**: It was associated with a greater risk of CAVD and cardiovascular disease in the Cardiovascular Health in Ambulatory Care Research Team cohort (Tu et al., 2015). In fact, increased calcium content has been demonstrated in the AV of diabetic patients (Katz et al., 2006). A recent study in VIC demonstrated an upregulation of glycolysis and oxidative phosphorylation (OXPHOS) under high-level insulin or glucose treatment, leading to increased proliferation and collagen type I production, and decreased α-SMA. This suggests a potential role of diabetes in the early phases of AV degeneration (Selig et al., 2019).

- **Kidney dysfunction and mineral metabolism**: CAVD is prevalent in patients suffering from renal failure. In fact, kidney dysfunction has been associated with a faster and more severe progression of CAVD (Rattazzi et al., 2013). The cause of this association could be the elevated levels of some ions, such as calcium, phosphate, and calcium-phosphate molecules, at the end-stage of renal disease. In fact, high serum phosphate levels have been associated with a greater risk of AV calcification and sclerosis (Linefsky et al., 2011).

I.2.2-CAVD diagnosis, risk stratification and treatment

I.2.2.1- Diagnosis

The early detection of aortic stenosis initial stages has significant value in preventing future cardiovascular complications resulting from CAVD. The conventional diagnostic approach for CAVD was two-dimensional echocardiography; however, its limitations have prompted clinicians to explore novel and complementary techniques.

(i) **Echocardiography**: This non-invasive procedure uses sound waves to provide morphologic and hemodynamic evaluation of the valve, enabling the evaluation of blood flow through the heart and its valves. This method can identify weakened heart muscle and determine the severity of AV stenosis.

(ii) **Exercise or stress tests**: These tests involve monitoring the heart while the individual walks on a treadmill or rides a stationary bike to determine if symptoms of CAVD occur during physical activity.

(iii) **Cardiac computerized tomography scan**: It combines multiple X-ray images and provides detailed cross-sectional views of the heart. This procedure is mainly performed to assess the calcification burden of the valve and confirm the diagnosis obtained by echocardiography. This method can measure the size of the aorta and provide information regarding the condition of the AV.

(iv) **Cardiac magnetic resonance imaging** (MRI) scans using magnetic fields and radio waves provide detailed images of the heart. Although it is not recommended for diagnosis of AS, it can be sometimes useful in determining the size of the aorta and assessing the severity of AV stenosis.

(v) **Cardiac catheterization**: Cardiac catheterization: Crossing the calcified valve with the catheter is not currently recommended for the diagnosis of AV disease, except for very specific cases where all the other technics did not provide great evaluation.

I.2.2.2- Risk stratification

Risk stratification of CAVD-diagnosed patients is vital for providing personal treatment, predicting disease progression and complications, stabilizing the time of intervention, applying preventive therapies

such as cholesterol-lowering therapies, and allowing appropriate recruitment of people for studying different disease stages in clinical trials. Currently, prediction relies on traditional cardiovascular risk factors and established algorithms such as the Framingham Risk Score, Pooled Cohort Equations, and European SCORE Risk Charts (reviewed in Junco-Vicente et al., 2020). However, these predictive methods are not sufficiently accurate for assessing the disease severity.

Depending on the parameters determined by the diagnosis and risk score tests, four different grades of CAVD severity can be defined (Vahanian et al., 2022). (i) High-gradient aortic stenosis is characterized by a valve area of 1 cm^2 or less and a mean gradient of > 40 mmHg. (ii) Low-flow, low-gradient aortic stenosis with reduced ejection fraction: valve area ≤ 1 cm^2, mean gradient < 40 mmHg, ejection fraction < 50%, and stroke volume index (SVi) ≤ 35 mL/m^2. (iii) For low-flow, low-gradient aortic stenosis with preserved ejection fraction: valve area of 1 cm^2 or less, mean gradient below 40 mmHg, ejection fraction of 50% or higher, and SVi of 35 mL/m^2 or less. (iv) normal-flow, low-gradient aortic stenosis with preserved ejection fraction: valve area of 1 cm^2 or less, mean gradient below 40 mmHg, ejection fraction of 50% or higher, and SVi greater than 35 mL/m^2.

I.2.2.3- Treatment

Currently, the only available therapies are surgical valve replacement and transcatheter AV implantation. Additionally, as recently reviewed by the European Society of Cardiology (ESC) and the European Association for Cardio-Thoracic Surgery (EACTS), no medical treatment has been approved or recommended for directly addressing CAVD, and surgery remains the only recommended option (Vahanian et al., 2022):

(i) **Valve Repair**: It has been used since 1920 and applied in the case of a bicuspid aortic valve. It is based on remodeling of the valve cusps to obtain an appropriate way of opening and closing. The main advantage of this method is the low mortality risk and the lack of complications such as infection. However, it has been replaced by modern practices (reviewed in Moncla et al., 2023).

(ii) **Balloon aortic valvuloplasty**: The objective of this method is to dilate the narrowed opening of the valve by introducing a balloon directly into the stenosed valve, which can cause complications, such as coronary occlusion, myocardial ischemia, and ventricular dysfunction. Additionally, it does not provide long-term results, as the dilated valve can be restenosed in adults (reviewed in Moncla et al., 2023).

(iii) **Surgical aortic valve replacement:** It is the most common treatment for severe CAVD. It consists of surgery to replace the stenotic valve with a new one, which is inserted directly into the aortic root. This treatment has advantages related to survival improvement but also some risks of thrombosis, stroke,

or heart attack. Additionally, the new valve can be calcified over time (reviewed in Boskovsky et al., 2021). Two main kinds of valves are used for valve replacement.

- Mechanical valves: They are composed of pyrolytic carbon, metal, or plastic, and can open pivotally. The main advantage is their durability of up to 25 years, but they have an elevated risk of thrombosis as they are more sensitive to shear stress owing to their mechanical structure. These valves have rigid leaflets that can create high-velocity jets of blood flow when they open, leading to areas of increased shear stress in the surroundings, which can result in valve damage and activation of platelets. Additionally, the mechanical movement of the valve leaflets can disrupt the smooth laminar flow of blood, leading to turbulent flow patterns near the valve orifice. Turbulent flow generates higher shear forces and increases the risk of platelet activation and blood clot formation. For these reasons, patients who have been replaced with a mechanical valve must be treated in parallel with anticoagulants, which increase the risk of bleeding, stroke, cardiac tamponade, and death (reviewed in Boskovsky et al., 2021).

- Bioprosthetic heart valves: These are made from animal tissue, mostly porcine or bovine pericardium, but sometimes human donors can be used. The main limitation of these valves is their short durability (close to 15 years) due to deterioration or new calcification. The main advantage is that patients only need to be treated with anticoagulants for a short period of time after surgery since during the manufacturing process, before the replacement, the bioprosthetic valve is treated with anti-coagulants and anti-mineralization agents. In recent years, attempts have been made to solve the durability problem by treating patients with anti-calcification and anti-mineralization drugs after surgery (reviewed in Boskovsky et al., 2021).

(iv) **Transcatheter aortic valve implantation**: This is a less invasive technology that is used in older patients who are at risk of undergoing surgery. The process is like arterial stent collocation, as it consists of a stented valve that is delivered to the location of the stenotic one. It is delivered through a catheter, and once it reaches its destination, it is expanded to replace the damaged valve (reviewed in Moncla et al., 2023).

Several pharmacological approaches are currently under investigation. A review by Myasoedova et al. (2018) presented oxidized LDL, oxidized phospholipids, lipoproteins associated with phospholipase A2, Lp (a), and other factors related to lipid metabolism as targetable components for the prevention and treatment of aortic stenosis in humans. However, as reviewed by Moncla et al. (2023), randomized clinical trials evaluating the reduction of LDL cholesterol levels with the use of statins did not show a benefit on the progression of CAVD. Additionally, there are ongoing trials testing novel antisense oligonucleotides and small interfering ribonucleic acid (RNA) targeting the production of Lp (a) by the liver. These trials have shown promising results, with an 80% reduction in plasma Lp (a) levels (reviewed in Moncla et al., 2023). On the

other hand, mineral turnover was proposed as a potential target. However, a small-scale randomized clinical trial evaluating the effects of denosumab, an antibody to TNFSF11, and alendronic acid, a bisphosphonate, on the progression of CAVD, did not show any effect (reviewed in Moncla et al., 2023). Furthermore, other metabolism-related targets are druggable, have been proposed to be targetable such as insulin-like growth factor LysoPA, leukotrienes, platelet activation, RAAS, cadherin 11, and NADPH-oxidase (NOX)-2 (reviewed in Moncla et al., 2023). Finally, β-blockers and angiotensin-converting enzyme inhibitors (ACE inhibitors) are used in patients with CAVD to manage symptoms such as hypertension (high blood pressure) and to control heart rate, but not to treat the valve disease (reviewed in Moncla et al., 2023).

I.3- Calcific aortic valve disease pathogenesis

At first, CAVD was considered a passive degenerative process related to aging. However, accumulating evidence has shown that CAVD is an active inflammatory disease triggered by several factors (reviewed in Aikawa et al., 2012 & Rajamannan et al., 2011). The paradigm change is based on studies identifying the role of chronic inflammation, lipoproteins, renin-angiotensin, and molecular mediators on calcification in stenotic valves. Additionally, this evidence is supported by the identification of signaling pathways and genetic factors mediating valve pathogenesis. Thus, the new paradigm points to several etiologies of the disease: infective, degenerative, or only congenital (reviewed in Miller et al., 2011).

The pathological mechanisms underlying the progression of CAVD include endothelial injury, inflammatory reactions, and oxidative stress. When the endothelium is disrupted, damage can be repaired to maintain valve homeostasis (reviewed in Pawade et al., 2015). However, sometimes endothelium damage cannot be repaired or over-repaired, thus leading to subsequent processes such as altered cell composition and valve remodeling, causing valve thickening and calcification nodule formation. Together, these alterations result in diseased nonfunctional valves and hemodynamic changes. The disease occurs in three stages, as shown in **Figure III** (Aikawa et al., 2012). The first stage is aortic valve sclerosis, characterized by endothelial damage, ECM secretion, and infiltration of inflammatory cells, leading to an inflammatory state (reviewed in Rajamannan et al., 2011). Later, during the progression phase, these processes trigger partial activation of VIC to a myofibroblast lineage and later lead to the formation of emerging small calcification nodules (reviewed in Pawade et al., 2015). Finally, the calcification phase is the formation of huge calcium deposits, causing the valve leaflet to stiffen and deform, generating an altered hemodynamic. Additionally, the number of VIC in the valve is reduced because they undergo osteogenic transformation upon lipid infiltration and oxidation (Aikawa et al., 2012).

I.3.1-Initiation phase: endothelial disruption and inflammation

I.3.1.1-Endothelial cell dysfunction

Endothelial damage and cell dysfunction are mainly caused by mechanical forces, bacterial and viral infections, and molecular mediators. Endothelial cells are sensitive to hemodynamics forces thanks to "environmental sensors" like ion channels, integrins, intercellular junction proteins, caveolae, the glycocalyx, G protein-coupled receptors and tyrosine kinase receptors. These sensors convert mechanical stimuli into biomechanical signals to elicit biological responses (Tarbell et al., 2014). Among the VEC responses, the first event that occurs during CAVD initiation is the production of reactive oxidative stress. Experiments using an inhibitor of endothelial nitric oxide synthase significantly reduced oxidative stress in calcified valves, demonstrating that the endothelium is the major source of oxidative stress (Miller et al., 2008).

Under physiological conditions, most of the pressure received by VEC is laminar shear force, although to a lesser extent, they are also exposed to oscillatory shear stress. However, under pathological conditions, such as a long-term increase in arterial blood pressure or enhancement in cardiac load, oscillatory shear stress is highly increased on endothelial cells. When VEC are exposed to continuously disturbed blood flow, the valve endothelium is altered, leading to damage in the basement membrane and protective barrier. At the cellular level, disturbed flow can activate not only the VEC layer, but also VIC from the fibrosa layer, thereby contributing to the progression of the first stages of the disease. VEC respond by changing their morphology, gene regulation, protein expression, transendothelial transport, alignment, and release of molecules and proteins from the surface (Deb et al., 2022 & Driscoll et al., 2021).

In addition to hemodynamic alterations, other factors that induce endothelial dysfunction include pro-inflammatory cytokines. Specifically, TNF-α can be secreted not only by immune-infiltrated cells but also by endothelial cells under stress conditions and can alter the ECM (Dahal et al., 2017 & Mahler et al., 2008), leading to EndMT, which can function as a source of osteogenic cells. Therefore, an interplay between hemodynamics and other factors, such as infection or increased serum levels of inflammatory mediators, may play a key role in CAVD initiation (Arjunon et al., 2017).

I.3.1.2- Inflammation

Inflammation is a hallmark of CAVD. Both innate and adaptive immunity play important roles in disease initiation and propagation, as supported by clinical and cellular studies (reviewed in Bartoli-Leonard et al., 2021 & Raddatz et al., 2019). Interestingly, recent studies have described the interconnectivity between the immune system and resident valve cells (Schlotter et al., 2018).

Inflammation is the primary response of innate immunity and occurs after endothelial dysfunction, immune cell infiltration, and lipid deposition. Both cellular and humoral innate immune responses are implicated in this process. The role of innate immunity is to overcome inflammatory stimuli and repair

damage. However, if the insult persists, inflammation progresses over time (reviewed in Bartoli-Leonard et al., 2021). In fact, the innate immunity response pathway plays an important role in signal integration in both VEC and VIC and can be activated by different extracellular signals, such as angiotensin II, ox-LDL, CD40 ligand, advanced glycation end-products, and cytokines via toll-like receptors (TLR) and the nuclear factor-κB (NF-κB) pathway (reviewed in Bartoli-Leonard et al., 2021; García-Rodríguez et al., 2018). The NF-κB pathway leads to the expression of adhesion molecules, mainly intercellular adhesion molecule (ICAM)-1 and vascular endothelial molecule (VCAM)-1, after endothelial injury, which facilitates subsequent infiltration of immune cells (reviewed in Raddatz et al., 2019). Additionally, VIC also participate actively in the regulation of inflammation by producing cytokines via NF-κB activation such as IL6, which has been found to be highly expresses in severe CAVD and to be a strong inducer of *in vitro* calcification (reviewed in Raddatz et al., 2019).

- Immune cell infiltration and cytokine secretion

As a consequence of the valve endothelium disruption, immune cells can infiltrate the valve. Over time, several studies have detected increased T lymphocytes, monocytes, and antigen-presenting cells, such as macrophages, leukocytes, and B cells, in stenotic valves (reviewed in Raddatz et al., 2019). In fact, the population of leukocytes (10-15%) was arranged by bone marrow-derived progenitor cells and molecular histocompatibility complex II dendritic cells or antigen-presenting cells. Thus, antigen presentation has been described to promote lymphocyte T activation, leading to the first step of adaptive immunity and interferon (IFN)-γ secretion. IFN-γ, in combination with lipopolysaccharide (LPS), has been shown to stimulate macrophage polarization through an inflammatory state M1, in which they can release inflammatory interleukins such as IL-12 and TNF-α. Additionally, IFN-γ-activated macrophages cooperate with osteogenic progenitor cells found in calcified regions to promote skeletal bone formation in diseases involving heterotopic ossification (reviewed in Raddatz et al., 2019).

Additionally, other cytokines have been found to be upregulated in calcified valves, such as IL-1β, which has been found in valves with more severe remodeling as it can enhance the expression of MMP, exacerbating the process of valvular stenosis via NF-κB (Isoda et al., 2010). Supporting this finding, IL-1R, which opposes the effect of IL-1β was found to be downregulated in stenotic valves (reviewed in Raddatz et al., 2019). On the other hand, IL-6 is also upregulated in stenotic valves and can be sensed not only by T-cells leading to their maturation but also by other valve resident cells. Furthermore, TGF-β, which can be secreted by immune cells and fibroblasts, has been demonstrated to be present in stenotic valves and is associated with osteogenic, fibrotic, and apoptotic activity (reviewed in Raddatz et al., 2019). These inflammatory cytokines have been described to increase the expression of bone morphogenetic protein 2 (BMP2) and alkaline phosphatase enzyme, leading to osteoblast-like phenotype transformation and CAVD initiation (Zeng et al., 2016).

- Lipids deposition

It has been detected the presence of lipids deposited in the valve cusps upon endothelial injury. These lipid droplets include ox-LDL, lp (a), apolipoproteins B and E, and renin-angiotensin converting enzyme (ACE), which can trigger a chronic inflammatory response by attracting immune cells (reviewed in Towler, 2013).

- OxLDL: LDL are infiltrated and deposited within the valve and are oxidized during the process (oxLDL) because of the cell oxidative status. In fact, Ox-LDL are highly cytotoxic and stimulate inflammation and ossification in the later stages of CAVD. Strikingly, oxLDL, inflammatory cells, and TNF-α expression have been reported to colocalize in calcified valves (reviewed in Nsaibia et al., 2022).

- Lp-(a): It carries a high content of lysophosphatidylcholine, which is related to inflammation, mineralization, and calcification of the AV (Zheng et al., 2019).

- Arachidonic acid route: Arachidonic acid is the precursor of lipid mediators, such as leukotrienes and prostaglandins. The enzyme involved in leukotriene synthesis, which is overexpressed in CAVD, is 5-lipoxygenase and plays a role in inflammation (Nagy et al., 2011). Additionally, the inducible enzyme cyclooxygenase 2 (COX-2), normally has a low activity in normal tissue/cells. However, it is induced over 10-80 times in VIC isolated from stenotic valves, increasing the contents of PGE2, PGI1, and PGE1 (Wirrig et al., 2015).

- Renin-angiotensin system activation

The renin-angiotensin-converting enzyme (ACE) and its product angiotensin II can be detected in calcification lesions usually associated with apolipoprotein B and LDL. The role of ACE in inflammation development and CAVD progression has been reported since the receptor type I of angiotensin II, was found to be expressed by fibroblasts of diseased valves. Further studies in mice have associated angiotensin II with leaflet thickening in the early phase of aortic stenosis (reviewed in Bian et al., 2021).

- Pathogen-derived molecules

Infections can also trigger immune response once endothelium has been damaged. Several studies have demonstrated the presence of some bacteria (*Chlamydia pneumoniae, Helicobacter pylori*) and viruses (Cytomegalovirus, Epstein-Barr virus, and Herpes simplex) associated with immune cells in inflamed areas of calcified valves (Nakano et al., 2006). Pathogen molecular patterns or PAMP from viral and/or bacterial infections can be recognized by the Toll-like receptor (TLR), innate receptors found upregulated in stenotic valves and associated with inflammation-induced calcification, as reviewed by García-Rodríguez et al., 2018 and addressed in the section 1.4.1.

I.3.1.3- Valve cell differentiation and microcalcification

Several studies have pointed to calcification as an active cellular-mediated process involving a phenotypic shift of resident valve cells (Zhu et al., 2015). Although both cells in the valve have been shown to play a role in calcification formation, VIC is the most important regulator, as reviewed by Rutkovskiy et al. (2017). The way in which VIC trigger calcification is by sensing the pro-inflammatory environment around them through TLR and cytokine receptors (Meng et al., 2008). However, VIC are also sensitive to shear stress in a more indirect way than VEC since they do not possess the same sensory and signaling mechanisms but they can indirectly sense mechanical forces, including shear stress, through mechanotransduction by converting mechanical forces into biochemical signals. Taken together, evidence shows a strong involvement of inflammation in the initiation phase of the disease, a role that loses relevance in the propagation and late-stage phases, where calcification and fibrosis-related pathways play a key role (Aikawa et al., 2012).

In healthy conditions, most cells in the valve interstice are quiescent (qVIC), and only 5% are activated (aVIC) and exhibit a myofibroblast phenotype. However, under pathological conditions, this balance is disrupted and the percentage of myofibroblasts increases. When this situation is not reversed in a brief period and a high percentage of myofibroblasts is prolonged, CAVD development is promoted (reviewed in Rutkovskiy et al., 2017). Three mechanisms have been described for calcification of VIC:

(i) First, dystrophic calcification is the most common method of VIC calcification (Aikawa et al., 2007). At first, it was considered a passive process in the degeneration of connective tissues. Currently, this mechanism is known to be based on the formation of calcified nodules by matrix vesicles contain several enzymes and ions. These vesicles originate from cellular necrotic and apoptotic bodies containing calcium and inorganic phosphate (Pi) ions, promoting the formation of hydroxyapatite crystals, which play a fundamental role in calcific lesion formation (Bertazzo et al., 2013).

(ii) The second mechanism of VIC calcification is called osteogenic calcification or heterotopic ossification. It is considered an active process in abnormal tissue repair. It is based on the formation of true mature lamellar bone structures, as suggested by a previous analysis showing osteoid cells, collagen scaffold, multinucleated osteoclast-like, and fatty marrow pockets in stenotic valves (Torre et al., 2016).

(iii) A third mechanism has been proposed to resolve the discordance between the low amount of true bone formation in calcified valves and high prevalence of osteogenic marker expression (Aikawa et al., 2007). Some VIC have been proposed to present an osteogenic-like phenotype that differs from the true bone formation (reviewed in Miller et al., 2011). Additionally, endothelial cells have been described to suffer an inflammatory-induced differentiation into osteogenic cells via EndMT leading to an altered ECM (Mahler et al., 2008).

I.3.2-Propagation phase: fibrosis, osteogenesis, and angiogenesis

ECM remodeling is a pivotal process in maintaining valve homeostasis, and ECM alteration is an early event in the progression of CAVD. The key point for maintaining ECM homeostasis under normal conditions is the balance between MMP and its agonist, TIMP, which is tightly regulated. In patients with CAVD, the expression of MMP and cathepsins has been found to be upregulated, i.e., MMP-1, 2,3 and 9 altering the MMP/TIMP balance thus promoting fibrosis in the valve (reviewed in Raddatz et al., 2019). This abnormal matrix remodeling, which includes collagen degradation and the expression of some proteoglycans, leads to increased stiffness, which further promotes VIC activation and calcification (Yip et al., 2009). In fact, the expression of proteoglycans, such as biglycan, decorin, and versican, has been reported to be increased in valves from patients with CAVD compared to control valves. It has been proposed that this overexpression could act as an endogenous danger signal by promoting inflammation and later mineralization via TLR2 (reviewed in García-Rodríguez et al., 2018). An interesting feature of CAVD is that calcified valves exhibit sex-specific differences in the degree of fibrosis and mineralization.

I.3.2.2- Osteogenesis process

Human valves exhibit high plasticity, and VIC can transdifferentiate into activated myofibroblasts, osteoblast-like cells, or adipocytes. In fact, human calcified valves exhibit overexpression of several osteogenic genes and transcription factors compared to healthy valves (Bossé et al., 2009). A recent report has identified a subpopulation of VIC that expresses elevated levels of CD44 and co-markers ($CD29^{+}$ $CD95^{+}$ $CD37^{+}$ $CD45^{low}$) as a disease-driver cell population with multilineage potential and osteogenic activity (Decano et al., 2022). The interaction between CD44 and its ligands osteopontin and hyaluronan, which are glycosaminoglycans present in the valve, promotes mineralization in VIC *in vitro* (reviewed in Rutkovskiy et al., 2017). Furthermore, stenotic valve tissue expresses markers and transcription factors associated with mineralization and osteogenic processes. For example, *RUNX2* has been proposed to be the most important gene mediating osteogenic processes in CAVD. Indeed, RUNX2 promotes the expression of alkaline phosphatase, an ectonucleotidase crucial in mineralization regulation (Rajamannan et al., 2014). Other ectonucleotidases, such as ectonucleotide pyrophosphate-phophodiesterase family member 1 and 5'-nucleotidase, are dysregulated in CAVD because they are important to produce nucleotide derivatives and inorganic phosphate production, which promotes calcification in the valve (Côté et al., 2012 & Zheng et al., 2019). Additionally, some other transcription factors such as osterix and homeobox protein MSX-2 are upregulated in diseased valves and can contribute to osteogenesis (Boström et al.,2011).

Another family related to osteogenic signaling are morphogens, which have been found to be upregulated in calcified valves. Particularly, BMP-2, which is a potent osteogenic differentiation factor belonging to TGF-β signaling (Rajamannan et al., 2014). Several *in vitro* studies have shown that BMP2

induces VIC mineralization (reviewed in Rutkovskiy et al., 2017). Additionally, BMP2 has been described to function as a downstream mediator of TLR-induced osteogenesis by triggering the expression of RUNX2 and other differentiation mediators such as osteopontin, osteocalcin, and bone sialoprotein (reviewed in Rutkovskiy et al., 2017).

Some evidence emphasizes the role of some pathways involved in development, WNT, and NOTCH in the VIC transition to osteoblast-like cells (Bossé et al., 2009). In this context, NOTCH1 has been identified as a negative regulator of RUNX2 and BMP2 expression (Bossé et al., 2009). Finally, remodeling factors of osteogenic metabolism have been identified to promote VIC calcification, such as receptor activator of NF-κB (RANK) and its ligand RANKL (reviewed in Pawade et al., 2015). During CAVD, RANKL is overexpressed, and one possible explanation could be through IL-6 pathway activation, which subsequently produces ECM and calcification (Wada et al.,2006). Remarkably, while in the bone, the binding of RANKL to RANK promotes osteoclast activity and osteoporosis, in vascular and valvular cells, it has the opposite effects (Hjortnaes et al., 2010).

I.3.2.3- Neovascularization process

Healthy mature valves are normally avascular, while diseased valves have been reported to have a pathological formation of new vascular vessels, due to an imbalance between pro-angiogenic and anti-angiogenic factors, suggesting the importance of angiogenesis in the propagation phase of the disease (reviewed in Rajamannan et al., 2011). In healthy valves, chondromodulin-1, an anti-angiogenic factor, is highly expressed, but it is downregulated in diseased valves, thus leading to the upregulation of vascular endothelial growth factor (VEGF)-A, an angiogenic factor. In late lesions, histopathological experiments show new vessels in calcified areas associated with the expression of angiogenic factors, such as VEGF, endothelial nitric oxide synthase, and a member of the hypoxia-inducible factor (HIF) family, HIF-2α, suggesting a role for the HIF/VEGF-A axis in controlling the development of new vessels (Akahori et al., 2014). Finally, some authors have proposed that the endothelium surface, circulating endothelial progenitor cells, and/or resident VIC are the source of endothelial cells forming vessels (reviewed in Bian et al., 2021).

I.3.3-Last phase

In the last step of CAVD development, valve leaflets are completely thickened and vascularized, and calcification change from microcalcifications to macrocalcifications, which are widespread (**Figure III**). The importance of inflammation at the initial stages, loss importance in this phase, and processes totally differ from atherosclerosis (Aikawa et al., 2012). At this point, valve degeneration occurs and could later lead to additional cardiac problems such as left ventricular hypertrophy. Finally, when the valve is highly calcified, the area of the valve is significantly reduced, and aortic regurgitation can sometimes occur. At this point, valve replacement is necessary within two years.

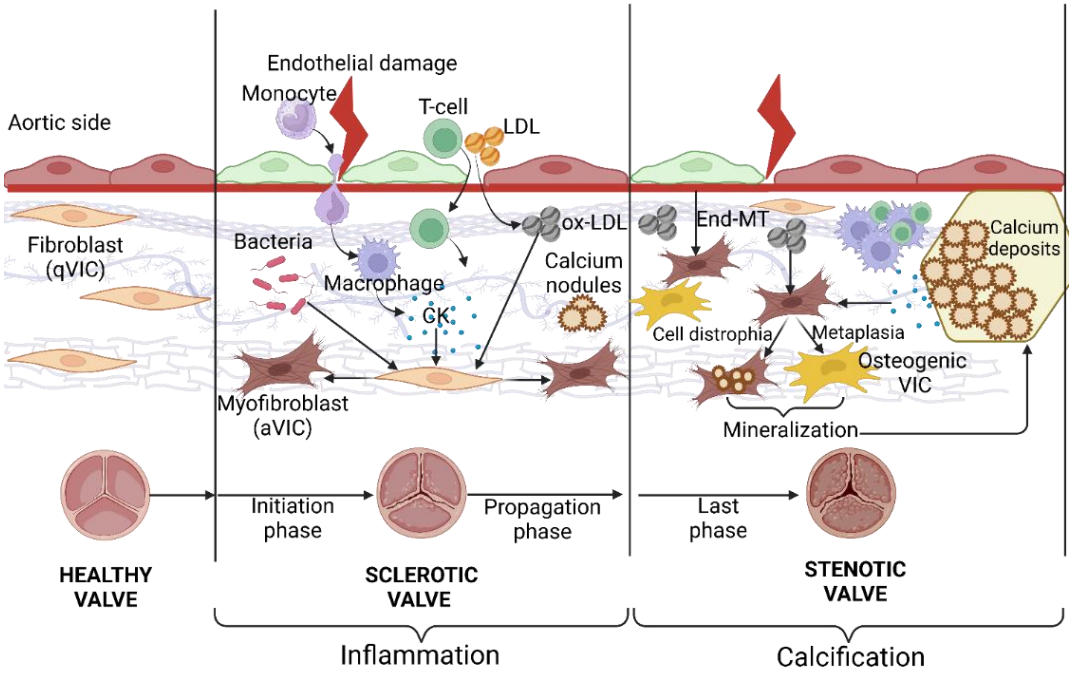

Figure III. Scheme of the three stages of the disease. The scheme represents the three distinct stages of the disease, and the different cellular types and processes that occur. aVIC indicates partially active myofibroblast; End-MT, endothelial-mesenchymal transition; LDL, low-density lipoproteins; qVIC, quiescent valve interstitial cells. Created with BioRender.com.

I.4- Inflammation as an initiator of CAVD

I.4.1 Cytokines and CAVD

Cytokines and their signaling pathways have been associated with CAVD. TGF-β has been demonstrated to be present in the aortic valve and increases upon disease, and it is associated with osteogenic, fibrotic, and apoptotic activity (reviewed in Raddatz et al., 2019). TGF-β has also been shown to be induced by shear stress in VIC (X. Wang et al., 2017). Additionally, TNF-α has been associated with processes underlying CAVD and is a key communicator between endothelial and interstitial cells in valves (Driscoll et al., 2021 & Parra-Izquierdo et al., 2021). However, in mitral valve interstitial cells, TNF-α and IL-1β have been reported to suppress myofibroblast activation in 3D-cultures (Zhu et al., 2021). Furthermore, IL-6 has been found to be upregulated in stenotic lesions and has been described as an osteogenic-differentiation inductor of VIC (reviewed in Bian et al., 2021). Remarkably, interferons (IFN) have been associated with atherosclerotic and aortic valve lesions (Boshuizen et al., 2015). This section focuses on IFN types, signaling pathways, and their role on CAVD pathogenesis.

I.4.1.1-Interferons (IFN)

IFN are soluble glycoproteins which have a role in innate and adaptive immune responses (reviewed in Ivashkiv, 2014;2018). The IFN family is divided into three groups, type I, II and III, being type I and II are the best characterized. This classification is based on specific receptors and the cellular types that produce them.

Type I IFN are pleiotropic cytokines secreted by most cell types in response to viral infections. The family of type I IFN includes protein isoforms: IFN-α, β, κ, δ, ε, τ, ω, and ζ. IFN-α and IFN-β are primarily produced because they can inhibit viral replication and induce the expression of major histocompatibility complex type I in virus-infected cells, thus inducing an adaptive T cell response (reviewed in Ivashkiv et al., 2014). All type I interferons are recognized by receptors composed of two subunits, IFN-α/β receptor (IFNAR)-1 and 2, which signal through the JAK-STAT pathway. Currently, it is known that type I IFNs also contribute to the antibacterial response, as they are produced in response to the activation of TLR4 and TLR3. In addition, type I IFN can also be induced by other endogenous pro-inflammatory mediators such as TNF-α (reviewed in Ivashkiv et al., 2014).

The only member of **the type II IFN** group is IFN-γ, which is secreted mainly by innate immune cells, such as lymphocytes, activated macrophages, and natural killer cells. Additionally, IFN-γ can also be produced by adaptive immune cells, such as T helper lymphocytes and cytotoxic lymphocytes CD8+. However, it has been described that endothelial cells, and vascular smooth muscle cells (VSMC) can produce IFN-γ. In fact, it has been narrowly associated with atherogenesis (Boshuizen et al. 2015). IFN-γ is produced in response to viruses and mediates a wide variety of immune responses. When an infection starts, helper T lymphocytes secrete IFN-γ, thus activating macrophages and resulting in the secretion of inflammatory mediators such as IL-12 and IL-18 to overcome the infection. Under the influence of IFN-γ, antigen presentation is increased because major histocompatibility complexes are upregulated on activated macrophages, thus resulting in a second wave of T cell activation, joining innate and adaptive immunity (reviewed in Ivashkiv, 2018).

Type III IFN have been described primarily as three isoforms of IFN-λ (IFN-λ1, IFN-λ2, and IFN-λ3), also known as IL-29, IL-28, and IL-28B. Their biological activity is similar to that of type I interferons. They are secreted by almost all cell types, but their receptors are primarily expressed in epithelial cells (Kotenko et al., 2017).

I.4.1.2-IFN receptors and Janus Kinase (JAK)-STAT signaling pathway

IFN receptors are structurally different cell surface receptors that signal through different factors, depending on the sensed IFN type:

- IFN-α/β receptor (IFNAR): These receptors are heterodimeric cell surface receptors (IFNAR1 and IFNAR2) that recognize type I IFN (**Figure IV**). After type I IFN binds to its receptor, heterodimerization occurs, leading to the activation of the kinases JAK1 and TYK2, which directly phosphorylate primarily the transcription factors STAT1-STAT2 that heterodimerize and associate with interferon related factor (IRF)-9 for their function. This complex, known as IFN-stimulated gene factor 3, binds to IFN response elements to initiate transcription of type I IFN-induced genes

(reviewed in Ivashkiv et al., 2014). However, type I IFN can also activate other members of the STAT family, such as STAT3, 4, 5, and 6, in various cell types, leading to the assembly of many other homodimers or heterodimers, depending on the cell type (reviewed in Ivashkiv et al., 2014). For example, type I IFN have been demonstrated to stimulate the homodimerization of STAT1, leading to the transcription of IFN-γ-activated genes.

- IFN-γ receptor (IFNGR): These heterodimeric membrane receptors IFNGR1 and IFNGR2 sense type II IFN-γ (**Figure IV**). When IFN-γ binds to its receptor, heterodimerization of the two subunits occurs, leading to activation of JAK1 and JAK2 kinases, which phosphorylate their substrate STAT1. STAT1 can homodimerize and bind to IFN-γ-activated sequences (GAS), thereby activating the transcription of genes controlled by these sequences (reviewed in Ivashkiv, 2018).

In some cases, type I and type II interferons can be secreted in parallel during the same immune response, and current evidence suggests the possibility of crosstalk between type I and type II IFN signaling. In fact, it is known that both signaling pathways are interconnected at several levels. For example, IFN-γ can induce the formation of the IRF-3 complex, thereby activating the expression of genes related to type I IFNs (reviewed in Ivashkiv et al., 2014). Additionally, it has also been observed that IFNAR1 can interact with IFNGR2, inducing the expression and activation of STAT1, which promotes the homodimerization of STAT1, which is characteristic of IFN-γ signaling, resulting in an enhanced response to IFN-γ (Gough et al., 2010).

The JAK-STAT pathway not only transduces IFN signals (**Figure IV**) but is also the master regulatory pathway involved in the sensing of more than 50 different cytokines. The JAK-STAT family is composed of three groups of proteins. On the one hand, receptors are necessary for sensing cytokines and growth factors. These receptors have multiple transmembrane polypeptides associated with the next most important effector, JAK tyrosine kinases, which are important for activating the signaling cascade (reviewed in Ivashkiv et al., 2014; 2018). Once the ligand binds to the receptor, the receptor dimerizes, and JAK proteins get closer and are auto-activated through tyrosine residue trans-phosphorylation. Finally, STAT are the final effectors of the pathway, which are recruited to JAK docking sites by their Src-homology 2 (SH_2) domains where they are phosphorylated. This phosphorylation allows STAT to dimerize and translocate to the nucleus, where they function as transcription factors (reviewed in Ivashkiv et al., 2014; 2018). There are several STAT factors namely STAT 1, 2, 3, 5, and 6, which are recruited differently depending on the sensed stimuli.

Alternatively, IFN can also signal through alternative signaling pathways in addition to JAK/STAT. For example, IFN can activate the PI3K-AKT-NF-kB and ERK-AP-1, which can cooperate with the JAK/STAT pathway. IFN-activated pathways are cell type- and IFN-type-specific (Boxel-Dezaire et al., 2006).

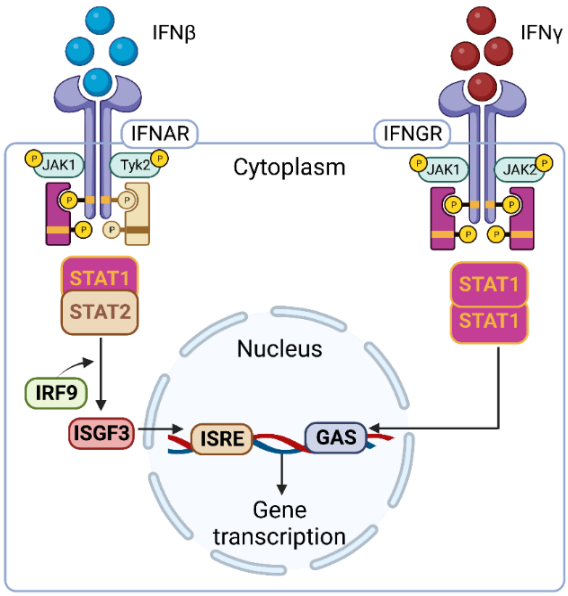

Figure IV. Schematic representation of canonical type I and II IFN signaling pathways GAS indicates IFN-γ-activated sequences; ISRE, IFN-sensitive response elements; IRF9, interferon response factor 9; ISGF3, interferon-stimulated gene factor 3. Created with BioRender.com.

I.4.1.3-IFN signaling and JAK-STAT in CAVD

Both IFN types have been associated with CAVD as they trigger human VIC calcification, as they have been demonstrated to play a key role in apoptosis, resulting in the formation of an inflammatory necrotic core, which later leads to mineralization of nodules in CAVD pathogenesis (Tabas et al., 2010).

On the one hand, type I IFN has been associated with AV calcification. The first evidence of the relationship between enhanced type I IFN and early onset of calcification in non-skeletal tissues, such as the aortic valve, comes from a rare autosomal dominant disease, Singleton-Merten syndrome (Singleton et al., 1973). Other evidence supporting the association between type I interferons and CAVD is that IFN-inducible cytokines are increased in stenotic aortic valves. Additionally, in *vitro* studies on human VIC have recently demonstrated that type I IFN promotes inflammation, differentiation, and calcification in VIC (Parra-Izquierdo et al., 2018). Surprisingly, our group also demonstrated an association between TLR3 activation and type I IFN production as well as IFN-inducible cytokines (Parra-Izquierdo et al., 2021).

On the other hand, type II IFN-γ is reported to play a key role in atherosclerosis, particularly in vascular cell proliferation and tissue remodeling, as well as in obesity, neural cells, and metabolic syndrome (reviewed in Ivashkiv., 2018). The role of IFN-γ in non-immune cells is due to the fact that IFNGR is ubiquitously expressed. Thus, non-immune cells can induce an IFNGR-induced response by producing chemokines that promote immune cell recruitment and suppress cell proliferation and survival (reviewed in Ivashkiv, 2018). Recent *in vitro* evidence supports the relationship between IFN-γ and CAVD. The first evidence of a causal relationship between IFN-γ and increased calcification was demonstrated by Nagy et al.

(2017), who showed the presence of $CD8^+$ T lymphocytes, which release IFN-γ, in calcified areas of the valve. They also demonstrated that IFN-γ could disrupt the calcium resorption potential of osteoclasts, thus contributing to increased calcification. Additionally, T lymphocytes present in valve lesions can secrete other cytokines, such as IL-6, which can also activate JAK-STAT signaling in VIC and promote calcification. Later, some recent *in vitro* studies in valve cells support the association between IFN-γ and VIC differentiation, inflammation, and calcification as well as the adhesion of VEC to monocytes, suggesting a link between IFN-γ and CAVD (Parra-Izquierdo et al., 2019; 2021a; 2021b).

JAK-STAT signaling is known to play a role in several disorders, including cardiovascular diseases (reviewed in Baldini et al., 2021). In fact, the role of JAK-STAT alterations can vary depending on the context. For example, while STAT3 has been identified as a protective transcription factor in hypertrophy, the activation of STAT1 in the heart has been linked to cell death and the progression of ischemic diseases (reviewed in Baldini et al., 2021). In addition, in the cardiovascular system, some effects of IFN-JAK/STAT signaling are potentiated by crosstalk with TLR signaling pathways (Niessner et al., 2007).

I.4.2- Innate immune receptor TLR and CAVD

The receptors of the innate immune system called Toll-like receptors (TLR) are specialized in recognizing conserved motifs present in pathogens, known as pathogen-associated molecular patterns (PAMP), and endogenous molecules released as a result of tissue damage, known as damage-associated molecular patterns (DAMP). TLR are type I transmembrane proteins characterized by an ectodomain that recognizes PAMP and a cytoplasmic domain known as the Toll/interleukin-1 receptor (TIR) domain, which is necessary for intracellular signaling (reviewed in Kawasaki et al., 2014). Each member of the TLR family recognizes a specific set of molecular patterns derived from various microorganisms, including bacteria, viruses, protozoa, and fungi (reviewed in Akira et al., 2006). In total, 10 TLRs have been identified in humans, and they can be classified based on the PAMP they recognize or based on their subcellular localization. While TLR1, 2, 4, 5, and 6 are located on the plasma membrane, TLR3, 7, 8, and 9 are located in intracellular compartments such as endosomes (reviewed in Akira et al., 2006).

I.4.2.1- TLR pattern recognition and signaling

The first TLR to be described was TLR4, which, together with its co-receptors, recognizes lipopolysaccharide (LPS), an endotoxin produced by gram-negative bacteria. On the other hand, TLR2, together with its cofactors TLR1 and TLR6, is capable of detecting peptidoglycans, lipoproteins, and lipopeptides from gram-positive bacteria, mycoplasma, and fungi (reviewed in Akira et al., 2006). Additionally, TLR2/4 are also sensitive to DAMP, heat shock proteins, reactive oxygen intermediates, and products resulting from ECM breakdown (reviewed in García-Rodríguez et al., 2018). On the other hand, TLR10 is believed to dimerize with TLR2 and TLR1, although its ligands are still unknown. Meanwhile, TLR5 is

highly expressed in intestinal epithelial cells where it recognizes flagellin. Finally, molecules derived from viruses and host-derived nucleic acids are sensed by intracellular-nucleic acid-sensing TLRs, such as TLR3 and TLR7-9 (reviewed in Akira et al., 2006).

Once the ligand is recognized by the receptor, dimerization of the receptor and a common signaling pathway occur. The intracellular signaling is mediated by myeloid differentiation primary response gene 88 (MyD88), except for TLR3, which uses a different adaptor called the TIR domain-containing adaptor inducing IFN-β (TRIF). In addition, some other adaptors have been identified, such as TIR domain-containing adaptor protein 43 (TIRAP), TRIF-related adaptor molecule (TRAM), and sterile α and heat-armadillo motif-containing protein (SARM). Since MyD88 is the most common TLR adaptor, TLR-mediated signaling is classified as follows:

(i) **MyD88-dependent pathway:** All TLR, except TLR3, can signal via this pathway.

(ii) **TRIF-dependent pathway**: This pathway is activated by TLR3 in response to ds-RNA and requires another adaptor protein, TRIF. TLR4 can also signal through a TRIF-dependent pathway via recruitment of a different adaptor, TRAM.

Both TLR-activated pathways can signal through the NF-κB and mitogen-activated protein kinases (MAPK) pathways. NF-κB transcription factor regulate the expression of some pro-inflammatory genes, such as TNF-α, IL-1β, ICAM-1, VCAM-1, and COX-2, as well as genes related to cell survival, differentiation, and proliferation (reviewed in García-Rodríguez et al., 2018). On the other hand, the MAPK pathway is formed by a family of serine-threonine protein kinases whose role is connecting cell-surface receptors to regulatory targets inside the cell. In response to TLR, MAPK activation is based on the phosphorylation of three main MAPK: extracellular signal-regulated kinase (ERK), p38, and c-Jun N-terminal kinases (JNK). The MAPK pathway finally activates several transcription factors involved in inflammation, cell proliferation, and survival (Gu et al., 2009). However, the TRIF-dependent pathway can specifically activate interferon-related factor (IRF)-3, which subsequently induces type I IFN transcription (Zhang et al., 2015).

I.4.2.2- TLR 2/3/4 pathways and CAVD

Numerous studies have linked TLR to various diseases, such as sepsis, asthma, and autoimmune diseases, as well as cardiovascular diseases, such as atherosclerosis, ischemic injury, and CAVD (reviewed in García-Rodríguez et al., 2018). The presence of pathogenic *Chlamydia pneumoniae* and bacteria associated with chronic periodontal infection in the fibrous layer of stenotic valves has led researchers to investigate the potential role of TLRs in CAVD, demonstrating a direct relationship between oral bacteria and valve calcification (Nakano et al., 2006).

INTRODUCTION

Several conserved motifs in pathogens have been associated with inflammation and osteogenesis in the aortic valve through TLR signaling, such as TLR2, TLR3, and TLR4 (reviewed in García-Rodríguez et al., 2018). This evidence underlies the possible role of TLR4/2/3-NF-κB in osteogenesis and supports the existence of inflammation-driven calcification (**Figure V**). *In vitro* evidence demonstrates that the TLR4 agonist LPS, present in gram-negative bacteria, acts as a pro-inflammatory factor via NF-κB signaling in VIC derived from healthy valves (Babu et al., 2008; Meng et al., 2008), an effect potentiated in VIC from patients with CAVD (Fernández-Pisonero et al., 2014 & Rutkovskiy et al., 2017). Notably, TLR4/2 ligands are pro-calcific factors that upregulate BMP2, RUNX2, and alkaline phosphatase and promote *in vitro* calcification in studies using β-glycerophosphate or elevated levels of inorganic phosphate (Babu et al., 2008 & Meng et al., 2008). TLR2 agonists, such as peptidoglycan, present in the membrane of gram-positive bacteria, and synthetic peptides, such as Pam3, can also promote a pro-calcific phenotype in VICs (López et al., 2012 & Rutkovsky et al., 2017). Finally, TLR3, through its activation by poly (I:C), a double-stranded (ds)RNA, has been associated with calcification, inflammation, and cellular differentiation in VIC (López et al., 2012 & Zhan et al., 2015). Notably, an interplay between TLR4/TLR3 and cytokines like IFN-γ has been described to potentiate pathological processes in VIC (Parra-Izquierdo et al., 2018; 2019; 2021).

On the other hand, DAMP have also recently been associated with the pathogenesis of CAVD through their effects on TLR (**Figure V**). For example, biglycan is dysregulated in CAVD pathology, and *in vitro* studies have demonstrated its pro-inflammatory and pro-osteogenic role in VICs via the MAPK pathway and the induction of BMP2 and TGF-β (reviewed in García-Rodríguez et al., 2018). Additionally, elevated levels of HMGB1, a TLR4 ligand, have been associated with CAVD. In fact, *in vitro* studies have demonstrated its role as a pro-inflammatory cytokine, leading to increased osteogenic markers and calcium deposition in human VIC (Shen et al., 2017). Other DAMP associated with the disease include matrilin-2, galectin-3, and heat shock proteins, which have been found accumulated in calcification nodules in human valves (reviewed in García-Rodríguez et al., 2018).

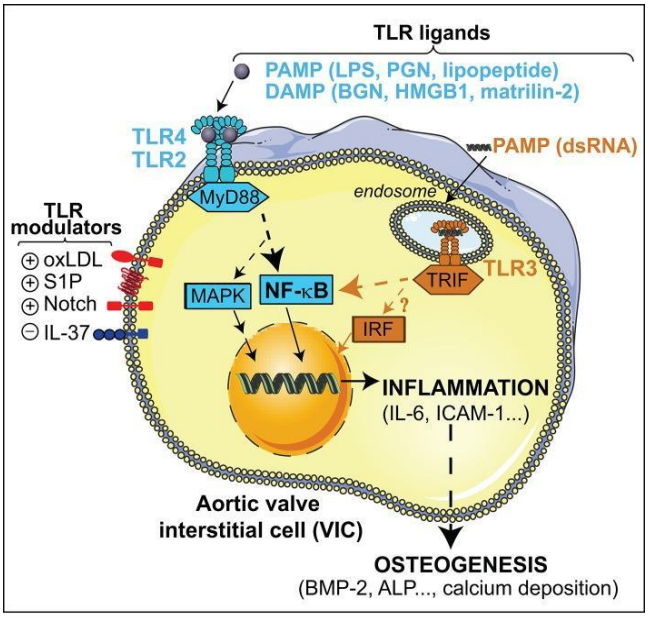

Figure V. Overview of TLR signaling pathways triggered by PAMPs and DAMPs in VIC. TLR2/4-MyD88 stimulation leads to NF-κB and MAP kinases activation and the subsequent induction of inflammatory mediators that promote the osteogenic reprogramming of VIC. Endosomal TLR3-TRIF stimulation triggers non-canonical NF-κB signaling, and IRF activation most likely promotes upregulation of inflammatory and osteogenic mediators. ALP, alkaline phosphatase; ICAM-1, Intercellular Adhesion Molecule 1; PGN, peptidoglycan. With permission from Garcia-Rodriguez et al. (2018)

I.4.3- Interplay between TLR and cytokine receptors in CAVD

Evidence in the cardiovascular system, specifically in atherogenesis, suggests that the potentiation of some effects of IFN-JAK/STAT signaling occur via crosstalk with TLR signaling pathways (Niessner et al., 2007). As mentioned, these pathways have been independently associated with CAVD, and more recently, cooperation between them on inflammation and calcification of human VIC has been described. Remarkably, the interplay between IFNGR and TLR4/3 has been associated with the non-hypoxic immune stabilization of HIF-1α, which is IFN-γ-specific and mediated via JAK/STAT signaling (Parra-Izquierdo et al., 2019; 2021). Notably, IFNGR-TLR4/3 interplay triggers a potent cellular response, including inflammation, differentiation, and calcification of VIC, as well as the upregulation of pro-angiogenic factors (**Figure VI**) (Parra-Izquierdo et al., 2019; 2021) like VEGF, detected in stenotic human valves (Perrotta et al., 2015). Additionally, Parra-Izquierdo et al. (2021) described an association between TLR3 activation and type I IFN production as well as IFN-inducible cytokines.

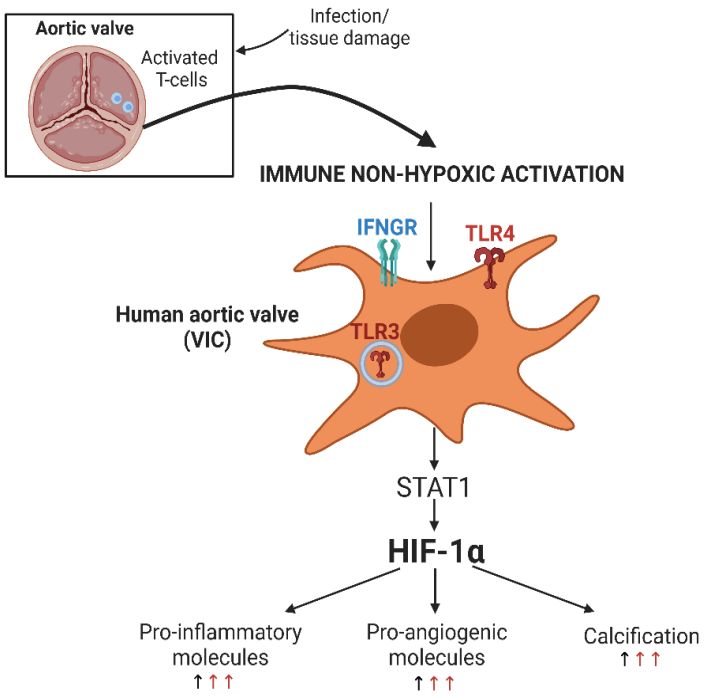

Figure VI. Interplay between TLR3/4 and IFNGR in the immune non-hypoxic activation of HIF-1α. Co-stimulation of VIC with IFNGR and TLR3/TLR4 ligands leads to JAK-SAT/HIF-1α activation and the subsequent induction of pro-inflammatory and pro-angiogenic molecules and calcification. Modified from Parra-Izquierdo et al. (2019).

I.5-Metabolic reprogramming in disease

In recent years, the role of metabolic reprogramming in several cell types has allowed us to consider immunometabolism as an emerging field of research that is susceptible to application in the search for therapeutic targets.

I.5.1- Metabolic rewiring in health and disease

The first evidence of metabolic rewiring in disease was found in the last century by Otto Warburg et al. (1926) in tumor cells. This metabolic rewiring is called the Warburg effect and consists of an increased uptake of glucose, glycolytic flux, and lactate production, even in the presence of oxygen. This phenomenon was described to be mediated by transcription factor HIF-1α and was called aerobic glycolysis. Notably, the production of ATP from glycolysis in the cytosol, despite being less efficient than OXPHOS, is approximately 100 times faster than that in the mitochondria, thus allowing cells to compete more effectively for limited fuel sources, giving them a survival advantage (reviewed in Vaupel et al., 2019). For decades, the Warburg effect has been described as a consequence of mitochondrial damage. However, more recently, it has been demonstrated that not only non-defective OXPHOS can occur during aerobic glycolysis but also an increase, as described in many contexts (reviewed in Vaupel et al., 2019). Nowadays it has been elucidated that metabolic reprogramming is different according to cell type, stimuli, time of stimulation or the availability of nutrients in the environment (Pearce et al., 2013). In fact, several recent metabolic studies have

demonstrated that proliferating cells that exhibit increased glucose consumption and lactate release also exhibit increased oxygen consumption and mitochondrial coupling efficiency (reviewed in Yao et al., 2019).

More recently, the term immunometabolism has been used to describe metabolic rewiring induced by immune signals in the immune system based on the Warburg effect. Although the term has been recently used, the first discovery in this field was in 1976, when Michl et al. demonstrated that macrophages increased glycolytic flux in response to inflammatory stimuli, leading to a pro-inflammatory response (Michl et al., 1976). Furthermore, in dendritic cells, a glycolytic reprogramming mediated by TLR has been described to be necessary for their activation (Everts et al., 2014). In fact, recent evidence in the immune context indicates that the activation of PAMP receptors involves a necessary metabolic reprogramming to carry out immune functions such as cytokine production and the polarization of the T lymphocyte response (Wolf et al., 2017).

Beyond the immune system, there is evidence of immune signals promoting cellular metabolic rewiring in non-immune cells. For example, TGF-β-induced metabolic reprogramming has been observed in lung myofibroblasts, leading to pulmonary fibrosis (Bernard et al., 2015). Furthermore, in endothelial cells, inflammatory mediators have been shown to modulate glycolysis, OXPHOS, and the pentose phosphate pathway (PPP), thus promoting inflammation and playing a role in cardiovascular pathogenesis (Xiao et al., 2021).

I.5.2-HIF-1α as a transcriptional regulator driving metabolic reprogramming

HIF-1α is a nuclear transcription factor that was initially identified as a hypoxia-inducible factor. Under normoxic conditions, it is constitutively degraded through its hydroxylation by prolyl hydroxylase. While, under hypoxia, HIF-α is not hydroxylated thus leading to its stabilization (reviewed in Masoud et al., 2015). However, its non-hypoxic stabilization and its role in metabolic reprogramming have been described in several contexts such as immune cells (reviewed in Semenza et al., 2011). In fact, in certain contexts such as cancer, its direct stabilization has been described due to the accumulation of certain metabolites, mainly fumarate, succinate and hydroxyglutarate, which operate by inhibiting 2-oxoglutarate-dependent enzyme reactions that regulate gene expression and the response to hypoxia. Other metabolites, such as lactate, kynurenine, methylglyoxal, sarcosine, glycine, hypotaurine, and (2R,3S)-dihydroxybutanoate, are also involved in HIF-1α stabilization. The accumulation of these metabolites plays a role in assisting cell proliferation and malignancy progression (reviewed by Beyoğlu et al., 2021). In the context of CAVD, recent evidence in human VIC disclosed HIF-1α stabilization by inflammatory and immune insults, and its association with VIC calcification. These findings may be relevant to initial stages of CAVD (Parra-Izquierdo et al., 2019 & Parra-Izquierdo et al., 2021).

HIF-1α is a transcriptional regulator of metabolic genes, mainly those regulating glycolysis, such as glucose transporter 1 (*GLUT1*), hexokinase II (*HKII*), fructose-2,6-biphosphatase 3 (*PFKFB3*), Pyruvate Kinase 2 (*PKM2*), and Lactate Dehydrogenase A *(LDHA*) (Gordan et al., 2008). Other studies in the immune context also demonstrated that HIF-1α can modulate the expression of cytochrome C oxidase (*COX7A1*), complex IV of the mitochondrial respiration chain (reviewed in Semenza et al., 2011). Additionally, direct regulation of the pentose phosphate pathway by HIF-1α has been shown to play a role in ribose-5-phosphate generation for subsequent nucleotide synthesis (Tong et al., 2009).

I.6- Energetic cellular metabolism

Metabolic pathways generally fulfill three main functions: i) energy generation, ii) production of "building blocks" necessary for cellular maintenance and proliferation, and iii) modulation of cellular responses.

I.6.1- Glycolysis

The glycolysis pathway takes place in the cytoplasm after glucose is taken up by glucose transporter type 1 (GLUT1) and metabolized into pyruvate, which involves the transformation of a six-carbon molecule into two three-carbon molecules. The fate of pyruvate can be its entry into the mitochondria for oxidation by the pyruvate dehydrogenase complex (PDC) or its reduction to lactate by lactate dehydrogenase A (LDHA) (**Figure VII**). Glycolysis occurs in both the aerobic and anaerobic states. In the presence of O_2, pyruvate enters the mitochondria for complete oxidation to CO_2 and H_2O in the tricarboxylic acid (TCA) cycle and electron transport chain (ETC), whereas in the absence of oxygen, pyruvate is reduced to lactate. Additionally, it has been described the use of aerobic glycolysis in the presence of O_2 in many cellular models other than cancer (Palsson-Mcdermott et al., 2013). Glycolysis is an energetically inefficient pathway as it generates a net total of two adenosine triphosphate (ATP) molecules per glucose molecule but provides a faster source of energy than other pathways, as well as the production of important metabolic intermediates, such as ribose-5-phosphate (R5P) for nucleotide synthesis, serine for purine synthesis and other amino acids, pyruvate for fatty acid synthesis through citrate formed in the TCA cycle, and reduction equivalents in the form of nicotinamide adenine dinucleotide (NADH). The main regulators of glycolytic pathways are listed below.

Hexokinase (HK) is a tissue-specific enzyme that phosphorylates glucose to glucose-6-phosphate (G6P), which is the first step in glycolysis and the starting point of PPP. Four isoforms of HK have been identified in mammals. HK- II has two hexokinase domains (N-terminal and C-terminal) and a high affinity for glucose, even at low concentrations (below 1 mM), and it is inhibited by its reaction product G6P. HK-II is considered the inducible form of HK, as its expression can increase approximately 100-fold in Th17 cells, and its inhibition with 2-deoxy-D-glucose (2-DG) suppresses Th17 cell differentiation (Semenza et al., 2011).

Pyruvate kinase (PKM) catalyzes the final irreversible step of glycolysis, which converts phosphoenolpyruvate to pyruvate by transferring a phosphate group to adenosine diphosphate (ADP), thus generating ATP. In mammals, there are four isoforms of pyruvate kinase encoded by two genes, PKLR and PKM, whose expression is regulated by tissue-specific factors and alternative splicing (reviewed in Vaupel et al., 2019). There are two main isoforms of PKM: PKM1 and PKM2. While PKM1 is upregulated in healthy tissues that demand a massive supply of energy, such as the heart, PKM2 is expressed in proliferating cells, especially in tumors. It has been reported that during immune and cancer cell metabolic reprogramming, PKM1 expression decreases in favor of PKM2 expression. It is an active enzyme whose activity depends on complex allosteric regulation. In the cytosol, PKM2 exhibits two main conformations: (i) high-activity tetramers, which increase lactate production and diminish pyruvate flux, probably due to the formation of a supramolecular complex with LDH (Mazurek et al., 2001); and (ii) low-activity dimers favored by Tyr105 phosphorylation, which can act as transcriptional cofactors favoring gene expression (reviewed in Puckett et al., 2021).

6-phosphofructo-1-kinase (PFK-1) controls the conversion of fructose-6-phosphate (F6P) to fructose-1,6-bisphosphate (F1,6P2). This step is considered the rate-limiting step of glycolysis (reviewed in Vaupel et al., 2019). PFK-1 is activated by fructose 2,6-bisphosphate (F2,6P2), an allosteric regulator that is the product of 6-phosphofructo-2-kinase (PFKFB3). PFKFB3 is a protein that plays a role in glycolysis by increasing the affinity of PFK-1 for F6P, overriding the inhibitory effect of ATP on PFK-1 (Judge et al., 2020). PFKFB3 is expressed in various tissues, particularly proliferating tissues, transformed cells, solid tumors, and leukemia cells. Its expression can be induced by factors such as hypoxia, progestin, and estradiol through the interaction of specific transcription factors such as HIF-1α, progesterone receptor, and estrogen receptor with response elements in the *PFKFB3* promoter (reviewed in Beyoğlu et al.,2021). Additionally, recent studies have revealed that PFKFB3 can localize to the nucleus in several cell lines stimulating cellular proliferation without affecting glucose metabolism (reviewed in Beyoğlu et al.,2021).

Lactate dehydrogenase A (LDHA), a key player in glycolysis, converts pyruvate into lactate, which plays an important role in aerobic glycolysis. Elevated expression of LDHA is commonly observed in rapidly proliferating cells, and blunted LDHA expression has been shown to inhibit tumor cell growth and vascularization (Khurshed et al., 2017). In addition to an increased lactate production, under hypoxic conditions, the expression of monocarboxylate transporter (MCT) 4 has been reported to increase, thus leading to a raise in lactate secretion, while the expression of MCT1 and MCT2 remained unchanged (Yetkin-Arik et al., 2019). Nowadays it has been widely described that lactate is not only a product of anaerobic metabolism but can also function as a signaling molecule via specific receptor G protein-coupled receptor 81 or monocarboxylate transporters (reviewed in Li et al., 2022).

Beyond its role in glycolysis, LDHA activity has been related to NAD^+ level replenishment since during glycolysis, NADH levels are increased while NAD^+ decreased. First, glyceraldehyde 3-phosphate (G3P) is oxidized to 1,3-bisphosphoglycerate by enzyme glyceraldehyde 3-phosphate dehydrogenase (GAPDH). This transformation is coupled with the reduction of cytosolic NAD^+ to NADH. There are three distinct mechanisms for oxidizing NADH in the cytosol and regenerating NAD^+. The first two mechanisms depend on the cytosolic enzyme malate dehydrogenase 1 and glycerol 3-phosphate dehydrogenase 1, which are components of malate-aspartate and glycerol-3-phosphate shuttles, respectively. The third mechanism for oxidizing NADH involves the reduction of pyruvate to lactate by LDH. Additionally, during its role in NAD^+ generation, LDH has been related to hydrogen peroxide (H_2O_2) production (reviewed in Corkey et al., 2020).

I.6.1.1- Glycolytic offshoots pathways

(i) Pentose phosphate pathway (PPP)

The PPP is an important part of glucose metabolism that takes place in the cytosol and supplies nicotinamide adenine diphosphate (NADPH) and ribose-5-phosphate (R5P). As mentioned earlier, the second metabolite generated during glycolysis is G6P, which results from the phosphorylation of glucose by HK. Instead of continuing its pathway in glycolysis towards pyruvate production, alternatively G6P can enter the PPP. This pathway is divided into two phases.

- The oxidative phase of PPP (oxPPP): The main objective is generating reducing power in the form of NADPH, which is subsequently needed for anabolic pathways to be used as a substrate of lipid synthesis and NADPH oxidases. The latter enzymes participate in pathogen elimination (reviewed in Piacenza et al.,2019), and the production of reduced glutathione (GSH) to control reactive oxygen species and oxidative damage (Krüger et al., 2011) (**Figure VII**). In the oxPPP, G6P is metabolized by the rate-limiting glucose-6-phosphate dehydrogenase (G6PD), which dehydrogenates G6P and catalyzes the first reaction of $NADP^+$ reduction to NADPH. Subsequently, another reduction reaction generates one more NADPH molecule, and the final product of this phase, ribulose-5-phosphate (Ru5P), in a reaction releasing an H^+ ion and one molecule of CO_2 (Stincone et al., 2015).
- Non-oxidative phase of PPP non-oxPPP: The main objective of this phase is generating ribose-5-phosphate (R5P), which serves as a precursor for nucleotides and coenzymes such as ATP, NAD, flavin adenine dinucleotide (FAD), and coenzyme A (reviewed in Tong et al., 2009). Another important carbohydrate generated by this pathway is erythrose-4-phosphate, which is necessary for the synthesis of aromatic amino acids (**Figure VII**). R5P can be generated through different reversible reactions. First, it can be generated by the isomerization of Ru5P by pentose-5-phosphate isomerase. Additionally, the direct incorporation of glycolytic metabolites, such as fructose-6-phosphate (F6P) and G3P, in the non-oxPPP has been described. These metabolites, through reversible reactions catalyzed by transketolases

and transaldolases, can generate R5P. Because these are reversible reactions, ribose-5-phosphate can also be converted back to glycolytic intermediates to feed glycolysis according to cellular needs. Therefore, this phase of the pathway connects the metabolic processes that generate NADPH with those that produce macromolecule synthesis, i.e., NADH and ATP (Stincone et al., 2015).

(ii) Synthesis of non-essential amino acid

Different intermediate metabolites from glycolysis can serve as precursors for the synthesis of non-essential amino acids, such as alanine, arginine, asparagine, aspartic acid, cysteine, glutamic acid, glutamine, glycine, proline, serine, and tyrosine. Alanine is derived from the direct condensation of **pyruvate** with glutamate to release α-ketoglutarate (**Figure VII**). Tyrosine is formed by a condensation reaction between glycolytic **phosphoenolpyruvate** and erythrose-4-phosphate from the PPP (**Figure VII**). Additionally, **3-phosphoglycerate** is used for the synthesis of serine, glycine, and cysteine. Serine is generated through reduction and transamination reactions with glutamate. Glycine is synthesized from serine by removing a carbon atom using the tetrahydrofolate carrier. Cysteine synthesis requires serine as the carbon backbone and methionine for the sulfur atom (Litwack, 2018). This metabolic pathway has been targeted in diseases such as lymphoblastic leukemia by inhibiting the carbon transfer to tetrahydrofolate (Gerald Litwack, 2018).

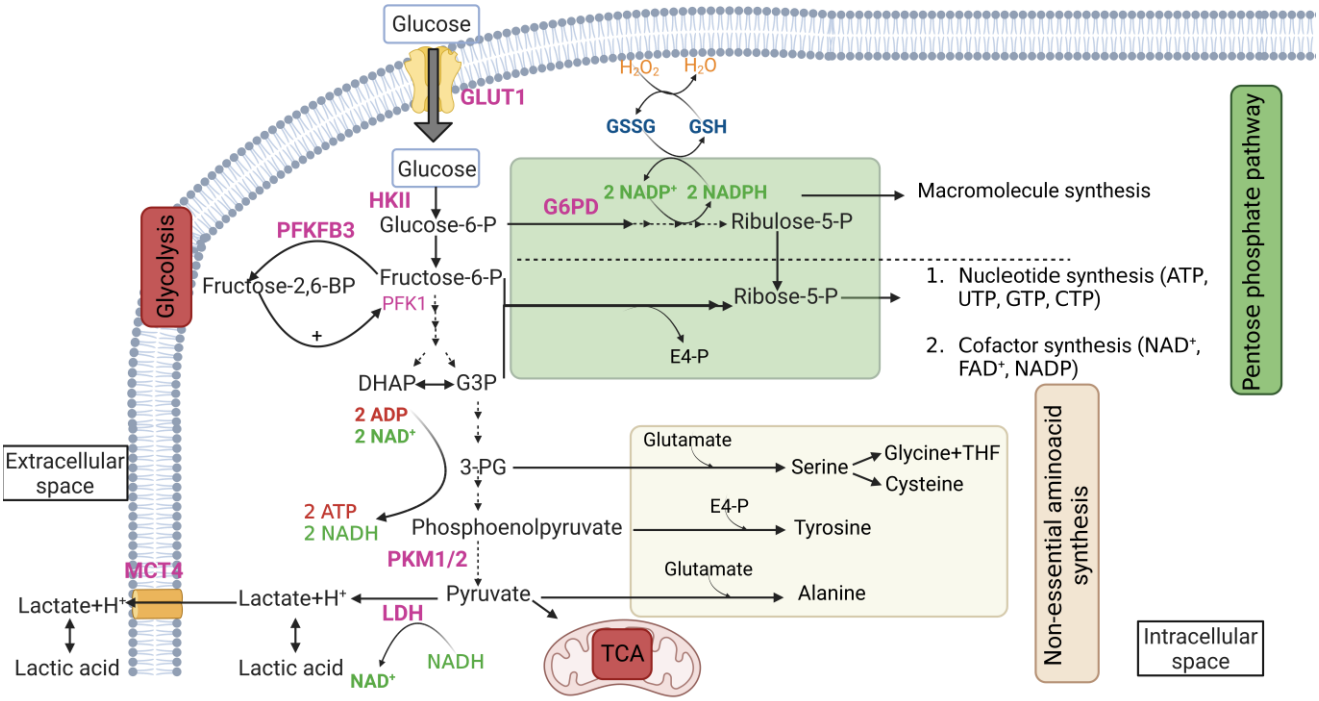

Figure VII. Schema of glucose uptake, canonical glycolysis, and pathways offshoot of glycolysis: pentose phosphate pathway and non-essential amino acid synthesis. ADP, adenosine monophosphate; ATP, adenosine triphosphate; CTP, cytosine triphosphate; DHAP, dihydroxyacetone phosphate; E4-P, erythrose-4-phosphate; FAD, flavin adenine dinucleotide; GLUT1, glucose transporter 1; GSSG, glutathione disulfide; GTP, guanidine triphosphate ; G3P, glyceraldehyde-3-phosphate; G6PD, glucose-6-phosphate dehydrogenase; HKII, hexokinase II; LDH, lactate dehydrogenase; NAD/NADH, nicotinamide adenine dinucleotide; NADPH, nicotinamide adenine dinucleotide phosphate; PFKFB3, 6-phosphofructo-2-kinase; UTP, uridine triphosphate; 3PG, 3-phosphoglycerate. Created with BioRender.com.

I.6.2- Tricarboxylic acid cycle (TCA)

The tricarboxylic acid cycle (TCA) or citric acid cycle, also known as the Krebs cycle, serves as the mitochondrial hub for the last steps in carbohydrate catabolism. The main functions of the citric acid cycle are: (i) to produce metabolites that can act as HIF-1α inductors or in nucleotide and amino acid synthesis (Tannahill et al., 2013); (ii) to capture the electrons that are released from molecules oxidation for later transference to ETC; and (iii) it has been recently described to have a role in NADPH mitochondrial production (reviewed in Bradshaw, 2019).

Under aerobic conditions, pyruvate generated by glycolysis passes through the pores of the outer mitochondrial membrane and is transported across the inner mitochondrial membrane by the mitochondrial pyruvate carrier (MPC). In the mitochondrial matrix, pyruvate is converted to acetyl-CoA and CO_2 in an irreversible reaction by the pyruvate dehydrogenase complex (PDC). The NADH formed in this reaction donates a hydride ion to complex I of the ETC. PDC, a hub between cytosolic and mitochondrial metabolism, is composed of three subunits and requires some cofactors for its function: thiamine pyrophosphate, lipoic acid, FADH2, and NADH. The complex is highly regulated primarily by covalent modifications; it can be allosterically activated by pyruvate and NAD^+, and inhibited by acetyl-CoA and NADH. The phosphorylation of PDC, conducted by pyruvate dehydrogenase kinase (PDK), decreases enzyme activity, and PDC can be dephosphorylated by a calcium-mediated phosphatase (**Figure VIII**).

The oxidation of acetyl-CoA, derived from glucose or fatty acids, takes place in the TCA cycle. The TCA cycle is composed of eight enzymes located in the mitochondrial matrix, except for succinate dehydrogenase (SDH), which is located in the inner mitochondrial membrane. Four of the eight chemical reactions conforming TCA are oxidation reactions, in which the oxidation energy is efficiently preserved in the form of reduced coenzymes NADH and $FADH_2$, which are directly transported to the mitochondrial ETC. To initiate a cycle, acetyl-CoA donates its acetyl group to the four-carbon compound oxaloacetate (OAA), so that citrate synthase assembles the six carbons of citrate. The resulting mitochondrial citrate can exit the mitochondria through the SLC25A1 transporter, which exchanges mitochondrial citrate for cytosolic malate, or it can continue in the citric acid cycle by converting it to isocitrate through the action of aconitase. The overall citric acid cycle is connected to the ETC, and one of the enzymes in the cycle, succinate dehydrogenase, which converts succinate to fumarate by oxidation, has the unique property of being part of the cycle, while also being complex II of the ETC.

Beyond the TCA function in energy production, different metabolites from the TCA cycle can serve as precursors for non-essential amino acid synthesis. In most amino acid synthesis pathways, the required amino group is derived from glutamate through a transamination reaction. Therefore, the direct synthesis of glutamate from **α-ketoglutarate** of TCA and NH_4 is essential. This direct amination is conducted by NADPH-

dependent glutamate dehydrogenase, located in the mitochondrial matrix. Once glutamate is synthesized, other amino acids can be produced, such as glutamine, which is derived from glutamate amination by glutamine synthetase, arginine, and proline. Glutamate can also be used for glutathione (γ-L-glutamyl-L-cysteinylglycine) synthesis, which is a tripeptide present in the body that is important for antioxidant processes and drug metabolism, acting as an enzyme substrate of glutathione peroxidase, glutathione S-transferase, and thiol transferase. Glutathione is usually present in its reduced form, GSH, which is maintained at the expense of NADPH, but GSH can be oxidized into GSSG under oxidative stress conditions. GSSG is a disulfide derivative derived from two glutathione molecules connected by a disulfide bond. Another TCA metabolite used for the direct synthesis of non-essential amino acids is **oxaloacetate**, which captures the amino group from glutamate, generating aspartate and α-ketoglutarate. This aspartate then captures another amino group from glutamine in an ATP-dependent reaction to generate asparagine and glutamate (Gerald Litwack, 2018) (**Figure VIII**).

I.6.2.1- TCA alternative pathways

Mitochondrial citrate can have different destinations depending on cellular conditions and needs. It can continue in the TCA cycle or exit the cytosol through the SLC25A1 transporter. In the cytosol, citrate is metabolized by ATP citrate lyase (ACLY) to form acetyl-CoA and OAA. The generated OAA can be converted to malate in the cytosol by cytosolic malate dehydrogenase (MDH), regenerating NAD^+. Malate can then reenter the mitochondria through the SLC25A1 transporter and be reincorporated into TCA, or it can be converted to pyruvate in the cytosol by malic enzyme 1 (ME1), generating NADPH in the process. If pyruvate is produced, it can go through different pathways (**Figure VIII**): (i) it can be converted to lactate by LDH in the cytosol; (ii) it can enter the mitochondria, where it can be metabolized by PDH to generate acetyl-CoA; or (iii) it can be directly transformed into malate in the mitochondria by malic enzyme 2 (ME2), which is called the citrate-pyruvate shuttle. Therefore, mitochondrial citrate has different fates, providing metabolic flexibility and adaptation to cellular needs (Arnold et al., 2022).

In contrast, cytosolic acetyl-CoA may have several destinations.

(i) <u>Acetylation</u>

Acetyl-CoA can play a key role in chromatin remodeling by modifying histone acetylation facilitating the transcription of genes (**Figure VIII**). The accessibility of transcription factors to deoxyribonucleic acid (DNA) depends on histone modifications such as methylation, acetylation, phosphorylation, and sumoylation (reviewed in Judge et al., 2020). When histones are acetylated in the amino group (by acetylase enzymes), their positive charge is reduced, decreasing their interaction with DNA, relaxing chromatin condensation, and allowing the access of transcription factors. Histone deacetylation, conducted by NAD^+-dependent deacetylases called sirtuins, has the opposite effect, silencing gene transcription. The regulation of histone

acetylation depends not only on the balance between acetylase and deacetylase enzymes, but also on nutrient availability and acetyl-CoA levels (reviewed in Boukouris et al., 2016). In the context of aortic valve and CAVD, the reduction of histone deacetylase 6, which promotes aortic valve calcification via the ER stress-mediated osteogenic pathway, has been recently reported (Fu et al., 2019).

(ii) Lipid synthesis

Acetyl-CoA can serve as a substrate for lipid synthesis in several steps of NADPH-dependent reactions (**Figure VIII**). Excess of lipids can be conjugated with proteins and secreted into the circulation or accumulate in cells in the form of lipid droplets. In the aortic valve and CAVD context, circulating lipids and lipid deposition have been associated with early CAVD onset.

I.6.3- Glutaminolysis

Glutaminolysis is a catabolic pathway that converts the amino acid glutamine into α-ketoglutarate in two steps. Glutamine is highly present in the blood and is considered a key anaplerotic substrate used by cells to replenish the TCA cycle and participate in ATP synthesis (Judge et al., 2020). The first step in glutaminolysis is the hydrolysis of the amino group of glutamine, catalyzed by glutaminase (GLS1), a mitochondrial enzyme that generates glutamate and ammonia (NH_3). Both reaction products can be later used for nucleotide synthesis but can also be transferred to a ketoacid, leading to the synthesis of non-essential amino acids. The glutamate generated can be secreted or transformed into α-ketoglutarate to fuel the TCA cycle. The conversion of glutamate to α-ketoglutarate can occur through three enzymes: glutamate dehydrogenase, alanine transaminase, and aspartate transaminase, the latter being part of the malate-aspartate shuttle. In these reactions, aspartate, CO_2, and ammonia are also generated (Judge et al., 2020) (**Figure VIII**).

Glutaminolysis occurs in proliferative cells, such as lymphocytes, and especially in tumor cells (Judge et al., 2020). In some tumor cells, the TCA is truncated by aconitase, an enzyme catalyzing the conversion of citrate to isocitrate, which is damaged by high concentrations of reactive oxygen species (Raineri et al., 1995). Furthermore, tumor cells overexpress glutaminase and malate decarboxylase or malic enzymes to generate alternative pathways for energy production from α-ketoglutarate. In summary, glutaminolysis is another fundamental pillar for energy production in malignant cells because, apart from being unaffected by ROS production, it provides the cell with significant energy (reviewed in Kodama et al., 2020).

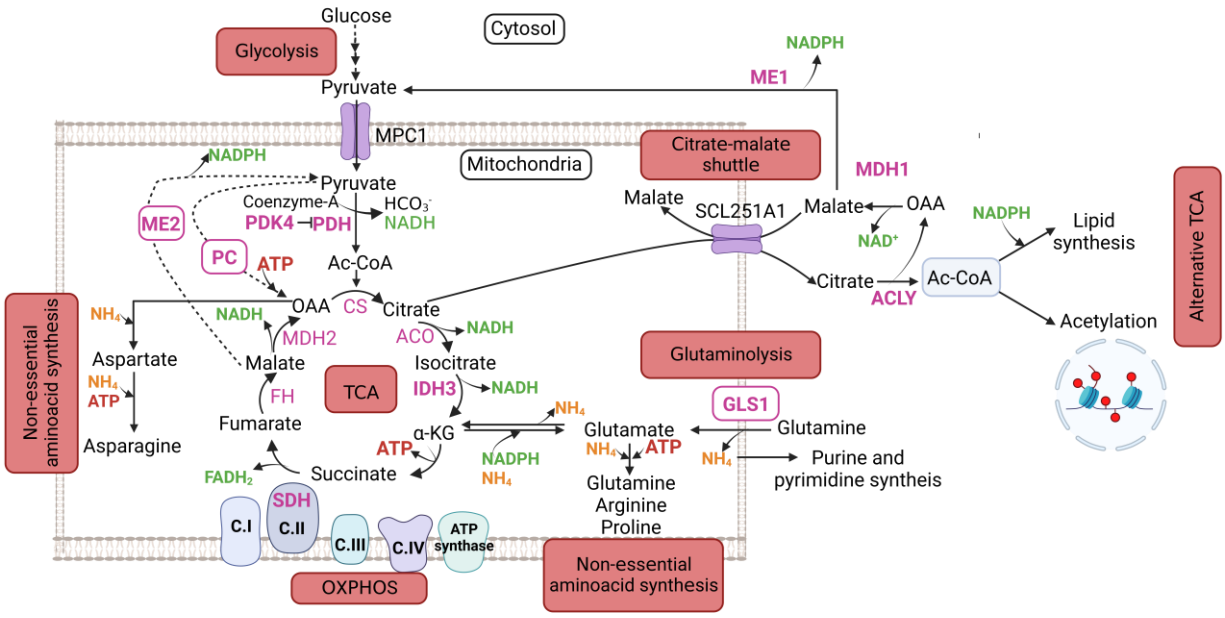

Figure VIII. Schema of the lower part of glucose metabolism: tricarboxylic acid cycle and its alternative pathways and glutaminolysis. ACLY, indicates acetyl-CoA citrate lyase; ACO, aconitase; ATP, adenosine triphosphate; CS, citrate synthase; FH, fumarate dehydrogenase; GLS1, glutamine synthase 1; IDH3, isocitrate dehydrogenase 3; MDH1, malate dehydrogenase 1; MDH2, malate dehydrogenase 2; ME1, malic enzyme 1; ME2, malic enzyme 2; MPC1, mitochondrial pyruvate carrier 1; NADH, nicotinamide adenine dinucleotide; NADPH, nicotinamide adenine dinucleotide phosphate; PC, pyruvate carboxylase; PDH, pyruvate dehydrogenase complex; PDK4, pyruvate dehydrogenase kinase 4**;** SDH, succinate dehydrogenase. Created with BioRender.com.

I.6.4- Mitochondrial electron transport chain (ETC) and oxidative phosphorylation (OXPHOS)

The main goal of the oxidation of carbohydrates, fatty acids, and amino acids is to generate energy in the form of ATP via OXPHOS through reactions that involve the transfer of electrons from NADH and $FADH_2$ to O_2, taking place in the ETC (**Figure IX**). ATP is the molecule that carries energy within cells, in addition to other functions, such as signaling and transducer molecule, as well as DNA synthesis. In fact, a significant role of ATP and adenosine as endogenous signaling molecules in immunity and inflammation has been reported (Bours et al., 2006).

The objective of the last stage of cellular respiration through the ETC is to transfer energy from electron carriers to ATP molecules in a reaction called OXPHOS. The ETC is composed of five transmembrane protein complexes that function as dehydrogenase enzymes capable of accepting and donating electrons: complexes I, II, III, IV, and V, also called ATP synthase. The electrons transported by ETC come from the reduction equivalents from the upper catabolic pathways, glycolysis, and the TCA cycle, in the form of reduced nicotinamide (NADH or NADPH) and flavin nucleotides (FMN or $FADH_2$). The ETC begins with complex I capturing electrons from NADH, and complex II or SDH (consisting of four subunits, A, B, C, and D) capturing electrons from succinate and $FADH_2$. The electrons captured by both complexes are transported by ubiquinone to the next complex. Complex III transports electrons from ubiquinone to cytochrome C (cyt C), allowing electrons to reach complex IV, which transfers electrons from cytochrome C to the final electron

acceptor, O_2. In healthy mitochondria, the ETC is coupled to ATP synthesis. When electrons pass from one carrier to another, the energy they lose is used to pump hydrogen ions from the mitochondrial matrix to the intermembrane space, creating an electrochemical gradient and a proton-motive force. Through the ATP synthase complex, this force drives the protons back into the mitochondrial matrix, generating the energy necessary for ATP synthesis from ADP and inorganic phosphate (reviewed in Yin et al., 2021) (**Figure IX**).

In the case of the TCA cycle, the reduction equivalents reach the transport chain directly, whereas the NADH generated in glycolysis must cross the mitochondrial membrane, which is relatively impermeable. Therefore, they require shuttle systems that are necessary not only for transport but also for the more efficient regeneration of cytosolic NAD^+ (reviewed in Yin et al., 2021). The shuttle systems are detailed below: (i) **Malate-aspartate shuttle**: Transfers the reduction equivalents from cytosolic NADH to cytosolic OAA to generate malate through cytosolic MDH. Malate then enters the mitochondria through the malate-aspartate shuttle. In mitochondria, malate is converted back to OAA by mitochondrial MDH, generating NADH (Judge et al., 2020) (**Figure IX**). (ii) **Glycerol-3-phosphate shuttle**: The reduction equivalents are transferred from cytosolic NADH to dihydroxyacetone phosphate by cytosolic glycerol-3-phosphate dehydrogenase to generate glycerol-3-phosphate. Subsequently, the electrons pass directly from G3P to ubiquinone, which is part of the ETC (Langston et al., 2019) (**Figure IX**).

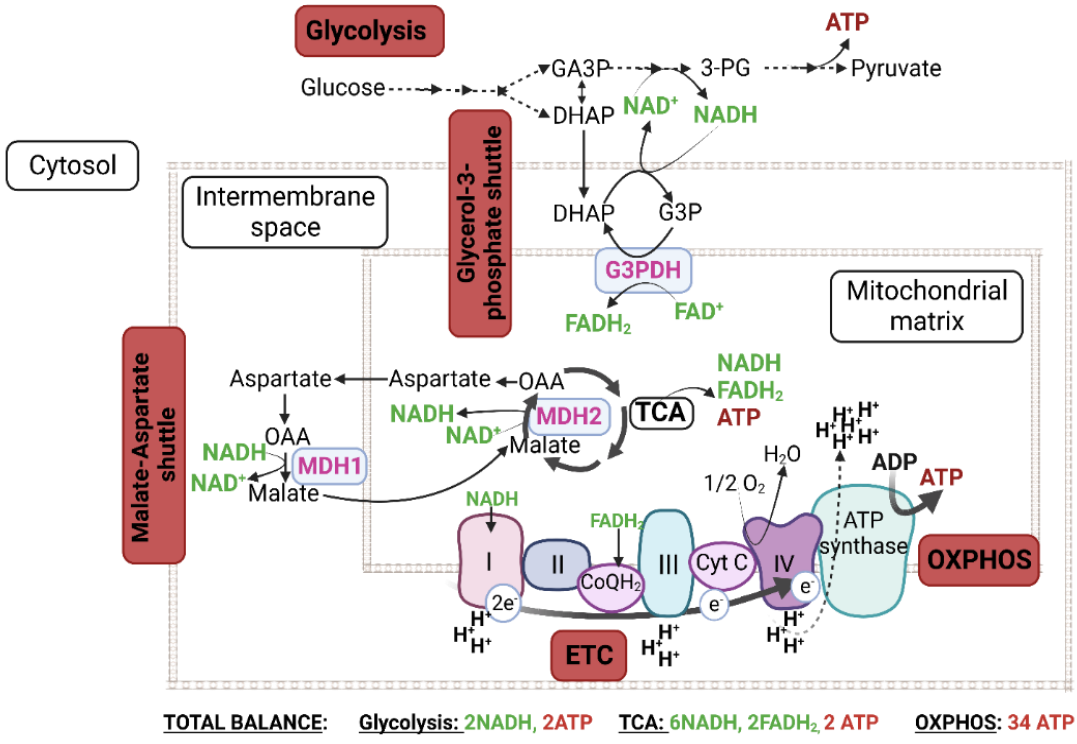

Figure IX. Schema of mitochondrial shuttles, electron transport chain and oxidative phosphorylation. ATP, adenosine triphosphate; $CoQH_2$, coenzyme Q; CytC, Cytochrome C; DHAP, dihydroxyacetone phosphate; ETC, electron transport chain; FAD/$FADH_2$ flavin adenine dinucleotide; GA3P, glyceraldehyde-3-phosphate; G3P, glycerol-3-phosphate; G3PDH, glycerol-3-phosphate dehydrogenase; NAD/NADH, nicotinamide adenine dinucleotide; NADPH, nicotinamide adenine dinucleotide phosphate; MDH1, malate dehydrogenase 1; MDH2, malate dehydrogenase 2; 3PG, 3-phosphoglycerate**;** OAA, oxaloacetate. Created with BioRender.com.

I.7- Other metabolic pathways

I.7.1- Synthesis of nucleotides

The nucleotide synthesis pathway is important due their multiple cellular functions. Nucleotides have a structural role, since 5'-monophosphate nucleotides, ribonucleotides, and deoxyribonucleotides are the monomers for building up cellular DNA and RNA. Additionally, they play a role in storing and providing chemical energy, primarily through adenosine phosphates, owing to the phosphoester bond between adenine and phosphoric acid molecules, thereby generating AMP, ADP, or ATP. Other molecules analogous to ATP are guanosine triphosphate (GTP), cytidine triphosphate (CTP), and uridine triphosphate (UTP); however, they have a more limited role as energy sources. Additionally, nucleotides are also components of cofactors such as NAD, NADP, FAD, and coenzyme A. Finally, some nucleotides can function as chemical intracellular messengers. For example, cyclic adenosine monophosphate (cAMP) is formed in cells from ATP and can function as a mediator of many hormonal processes by transducing and amplifying signals.

The de novo synthesis of nucleotides requires R5P generated in PPP, which needs to be activated to phosphoribosyl-1-pyrophosphate (PRPP) through the enzyme PRPP synthase, an ATP-dependent reaction. This pathway also requires amino acids, such as glycine, glutamine, and aspartate, derived from the synthesis of non-essential amino acids, CO_2, tetrahydrofolate, and NH_3. Although the metabolites required for nucleotide synthesis are the same, metabolic pathways differ between the synthesis of purine bases (adenine and guanine) or pyrimidine bases (thymine, cytosine, and uracil) (reviewed in Huang et al., 2021).

On the one hand, purines are composed of a bicyclic structure and the first step is the transfer of an amino group from glutamine to PRPP, catalyzed by the enzyme glutamine phosphoribosylpyrophosphate amidotransferase (GPAT), the most critical in purine synthesis. The synthesis continues in nine additional steps, culminating in the synthesis of inosine monophosphate (IMP), which is later transformed into AMP and GMP. The conversion of IMP to AMP or GMP requires energy in the form of GTP or ATP, respectively. The generated monophosphate nucleotides can be further converted into di- or triphosphate forms (reviewed in Huang et al., 2021) (**Figure X**).

On the other hand, the synthesis of pyrimidine bases does not involve PRPP in the first step but later. The initial step of the pathway starts with the synthesis of carbamoyl phosphate from glutamine, CO_2, and two ATP molecules in a reaction catalyzed by carbamoyl phosphate synthetase II. Following this, five reactions requiring aspartate in the second step and PRPP in the fifth step led to the synthesis of uridine monophosphate (UMP). Like IMP, UMP serves as an intermediate for the synthesis of other pyrimidines that can be phosphorylated later (reviewed in Huang et al., 2021) (**Figure X**).

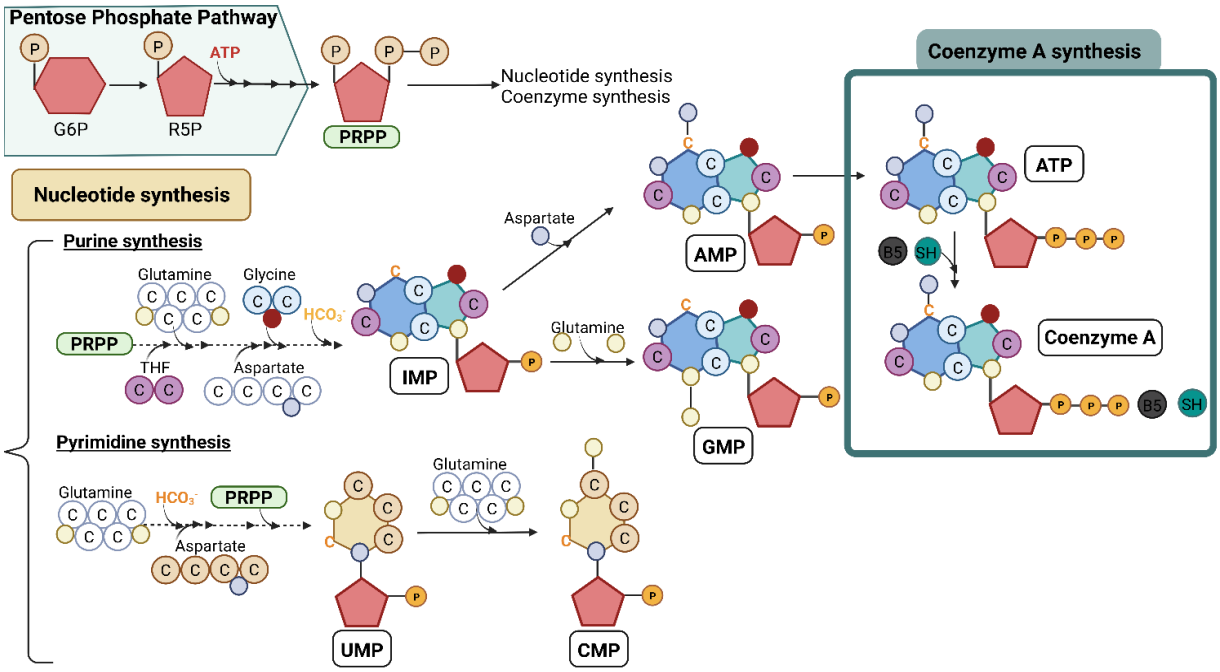

Figure X. Schema of nucleotide and coenzyme synthesis using PRPP derived from PPP-generated R5P. In this scheme, carbons are represented as circles labeled with C of different colors, depending on their precedence. NH3 groups are represented as small circles of different colors depending on the amino acid they originate from. AMP, indicates adenosine monophosphate; ATP, adenosine triphosphate; CMP, cytidine monophosphate; GMP, guanosine monophosphate; IMP, inosine monophosphate; PRPP, phosphoribosyl pyrophosphate; THF, tetrahydrofolate; UMP, uridine monophosphate. Created with BioRender.com.

I.7.1.1- Synthesis of cofactors from nucleotides

Coenzymes are organic, non-protein cofactors that do not have a specific substrate but are necessary as support for the function of other enzymes that act specifically. These enzymes catalyze oxidation and reduction reactions in the cell, and coenzymes help them by transferring electrons. Therefore, coenzymes typically exist in two forms, oxidized, and reduced. They function as carriers of functional groups, electron donors or acceptors, or carriers of specific chemical groups during enzymatic reactions. Examples of coenzymes include NAD^+, $NADP^+$, FAD, and coenzyme A.

In mammals, NAD^+ is synthesized by three pathways, both of which require PRPP (**Figure XI**): *de novo* synthesis from tryptophan, the Preiss-Handle, and the salvage pathway. In the de novo and Preiss-Handle, tryptophan, and nicotinic acid, respectively, are condensed with PRPP to generate nicotinic acid mononucleotide (NAMN). NAMN is subsequently condensed with ATP by nicotinamide mononucleotide adenyltransferase (*NMNAT*). Finally, the conversion of the nicotinic acid moiety to nicotinamide by glutamine-dependent NAD^+ synthetase (NADS) generates NAD^+. In the salvage process, precursors such as vitamin B3 compounds nicotinamide (NAM) or nicotinamide ribose (NR) generate nicotinamide mononucleotide (NMN) by nicotinamide phosphoribosyltransferase (*NAMPT*) or nicotinamide riboside kinase (*NRK*). Finally, NMN is condensed with ATP by the NMNAT enzymes to synthesize cellular NAD^+. On

the other hand, $NADP^+$ has the same formulation as NAD^+, but it has a phosphate group linked to carbon 2' of adenine, which is transferred to NAD^+ by NAD kinase (reviewed in Audrito et al., 2020).

The NAD^+/NADH balance is crucial, as NAD^+ is required for the proper functioning of many metabolic enzymes and NADH is necessary for driving ATP synthesis in the electron chain. Additionally, NAD^+ plays a significant role in signaling pathways, post-translational modifications, and epigenetic changes owing to its role as a cofactor for poly(ADP-ribose) polymerase 1 and NAD-dependent deacetylases (sirtuins) (reviewed in Chini et al., 2021). On the other hand, $NADP^+$ is essential in both anabolic and catabolic reactions. Catabolic pathways provide energy, among other things, in the form of NADPH, which acts as a cofactor for many enzymatic reactions. Subsequently, NADPH is used in anabolic processes, where it serves as a cofactor for reductases, providing the energy necessary for the synthesis of macromolecules from small molecules. As previously mentioned, the major source of NADPH in humans is the oxPPP, which supplies 60% of the cell requirements (Krüger et al., 2011).

Another group of cofactors belongs to the flavin nucleotide family, which is a derivative of riboflavin (vitamin B2), a nucleoside composed of a flavin nitrogenous base and ribitol pentose, derived from R5P. Two oxidized forms are primarily found, flavin mononucleotide (FMN), which is a phosphoric acid molecule attached to riboflavin and, the most common form, flavin adenine dinucleotide (FAD), which has the same structure than FMN but is attached to an adenine nucleotide. These cofactors also function as electron carriers in redox reactions, although the most common form in metabolic reactions is $FADH_2$. However, the main difference with nicotinamide coenzymes is that flavin coenzymes are tightly bound to enzymes; therefore, they are considered prosthetic groups.

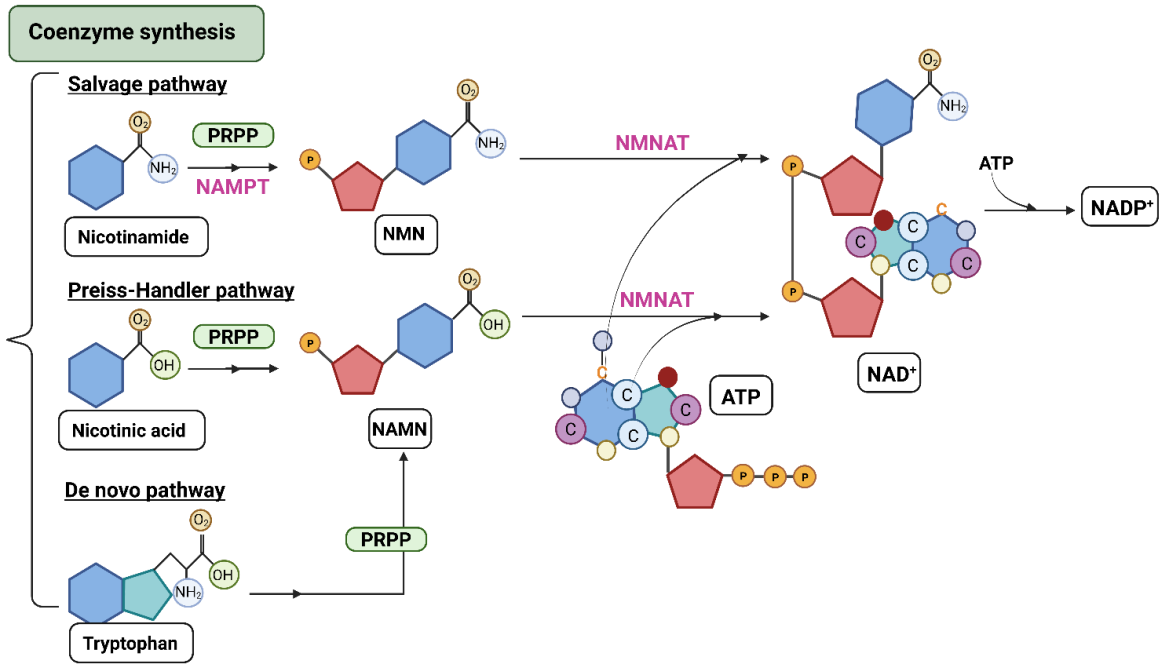

Figure XI. Schematic of cofactor synthesis using PRPP derived from PPP-generated R5P. ATP, adenosine triphosphate; NAD^+, nicotinamide adenine dinucleotide; $NADP^+$, nicotinamide adenine dinucleotide phosphate; NAMN, acid mononucleotide; NAMPT, nicotinamide phosphoribosyltransferase; NMN, nicotinamide mononucleotide; NMNAT, nicotinamide mononucleotide adenyltransferase; PRPP, phosphoribosyl pyrophosphate. Created with BioRender.com.

I.8- Metabolism and CAVD

Evidence from previous studies has highlighted the importance of metabolism in the development of CAVD. The first evidence was in 1995, when a metabolic aspect, such as the increased serum levels of Lp (a) were associated with AV sclerosis (Gotoh et al., 1995). Years later, other lipidic component such as LDL-cholesterol, was found in valve areas developing sclerosis and stenosis (Mothy et al., 2008 & Nkomo et al., 2006). From that point until the present, several studies have associated other lipids such as apolipoprotein-(a) and (b) with calcium in stenotic lesions and faster disease progression (Zheng et al., 2019). As a consequence of these discoveries, several other studies have been performed to understand the mechanisms implied in this association as well as lipid-lowering therapies (reviewed in Nsaibia et al., 2022). More recently, Surendran et al., 2020, in a metabolic analysis of the signature of aortic stenosis, discovered 19 metabolites that were differentially expressed in healthy versus stenotic valves, according to the AV calcification score (C-Score). The three most significantly altered pathways were involved in lipid metabolism and biosynthesis: glycerophospholipid metabolism, linoleic acid metabolism, and bile acid biosynthesis. In line with this altered lipid metabolism, a recent *in vitro* study using the VIC model in Garaikoetxea et al., 2022 showed that fatty acid-binding protein 4 (FABP4) expression and secretion are upregulated in VIC exposed to osteogenic media along with enhancement of inflammatory, pro-apoptotic, and osteogenic markers. FABP4 is a chaperone that plays a role in metabolism by regulating lipolysis, leading to cholesterol

ester accumulation, foam cell formation, and endothelial damage. Additionally, the secreted form can act as an adipokine that plays a role in the regulation of metabolism and inflammation (Li et al., 2021).

The first evidence related to glucose metabolism was published in Heather et al. (2011), who demonstrated a downregulation of genes regulating fatty acid and oxidative metabolism, accompanied by the upregulation of glucose transporters in heart biopsies of patients with hypertrophy and aortic valve impairment. Interestingly, some of these genes are known to be transcriptionally regulated by HIF-1α factor, which has also found to be present in stenotic valves (Perrotta et al., 2015). Moreover, other studies from 2015 started to associate glucose uptake with *RUNX2* expression, since glucose inhibits the AMPK-dependent proteasomal degradation of Runx2, thus leading to osteoblast differentiation (Wei et al., 2015). In the context of glucose metabolism, other studies on VIC derived from sheep and exposed to diabetic conditions, have demonstrated an upregulation of glycolysis, mitochondrial metabolism and OXPHOS under high-level insulin or glucose treatment, leading to increased collagen type I production while decreasing α-SMA but no morphological or mineralization changes, suggesting a potential role of diabetes in the early phases of aortic valve degeneration (Selig et al., 2019). Additionally, it has been described that pressure overload in AS triggers not only structural but also metabolic remodeling, increasing the risk of decompensation into heart failure going through left ventricular hypertrophy. The most common metabolic reprogramming occurring in AS is an abnormal cardiac substrate use going through the downregulation of fatty acid oxidation with the increased reliance on glucose metabolism and subsequent lipid accumulation on the myocardium (reviewed in Monga et al., 2022). Very recent evidence revealing new insights into the metabolic aspects of CAVD by Fu et al. (2022), S. Wang et al. (2022), Liu et al. (2023) and Zhong et al. (2023) will be discussed in the Discussion section.

Metabolic changes in many cellular models have been linked to alterations in cellular homeostasis and ROS generation of reactive oxygen species. Metabolic rewiring has been associated with changes in NAD^+/NADH, $NADP^+$/NADPH, and GSSG/GSH ratios, as well as the production of superoxide anion (O_2^-) and H_2O_2. In CAVD, H_2O_2 and the absence of antioxidant enzymes have been found to be significantly increased in valves of stenotic patients, particularly in areas close to calcified regions (Miller et al., 2008 & Hilaire et al., 2022). Moreover, the potential role of ROS in initiating CAVD has been described, as ROS has also been observed in patients with sclerosis before stenosis occurs (Branchetti et al., 2013). A direct role for ROS in the calcification of porcine aortic interstitial cells via the MAPK cascade has been reported (Das et al., 2013).

In conclusion, the association between inflammation and metabolism in CAVD pathogenesis is poorly understood, and the scrutiny of the metabolic pathways will shed light into the initial stages of the disease, and it might disclose novel therapeutic alternatives to end-stage valve replacement.

MATERIAL AND METHODS

M.1-Valve samples

M.1.1- Human aortic valve samples

Human aortic valve samples were obtained from patients undergoing cardiac surgery in the Hospital Clínico Universitario of Valladolid. Diagnostic protocols and surgical procedures for heart transplantation and valve replacement followed the current European guidelines for heart transplantation. Moreover, the study was conducted in accordance with the Helsinki Declaration and approved by the Review Board and Ethics committee of the Hospital Clínico Universitario of Valladolid (IRB protocol number PI 15-263). All patients were informed and provided written consent.

This study used a total of 45 control aortic valves (34 male/11 female patients), and 20 calcified aortic valves (12 male/8 female patients) (**Figure XII**). Details of the donor clinical characteristics are shown in **Table I.** Control non-mineralized valves were from recipients of heart transplantation with valve disease excluded by echocardiography. Calcified valves were obtained from patients with non-rheumatic severe aortic valve stenosis. Non-mineralized valves, used as control, were obtained from recipients of heart transplantation with no valve disease, confirmed by echocardiography. Patients' age ranges from 55 to 76 years old and were not biased for gender (**Table I**). Criteria for the inclusion of calcified valves in the study include having an aortic valve area of 0.7 ± 0.2 cm^2, a hemodynamic peak gradient of 88 ± 22 mmHg and a mean gradient of 56 ± 15 mmHg. Representative pictures of control and calcified valves are shown in **Figure XII**. After surgery, a small part of the valves was stored at -80^{o}C for later RNA extraction while the rest of the valve was used for valve cell isolation and culture. It is important to highlight that throughout this study, N indicates the number of VIC isolates from independent valve donors.

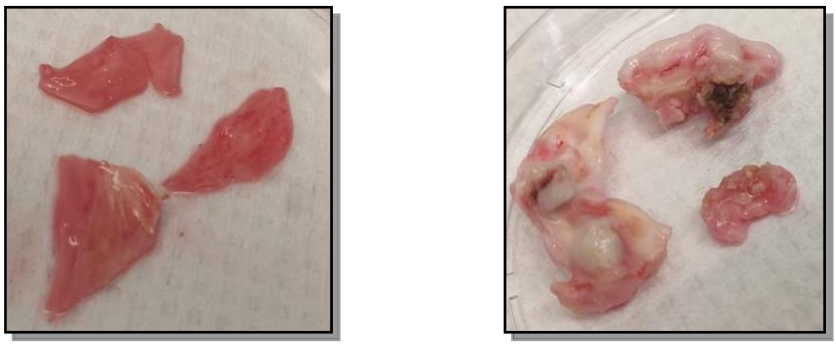

Figure XII. Photographs of a control (left) and a calcified (right) aortic valve included in this study.

Table I. Clinical characteristics of the valve donors in the study. All patients were Caucasian. Data are expressed as mean average ± SD for continuous variables or percentage of patients (%) for categorical variables. P-value was calculated using the Student´s t test (categorical variables), Fisher´s exact (frequency under 5) or chi-square tests (continuous variables). Characteristics and comorbidities were not significantly different between male and female groups.

	Control valves			**Calcified valves**		
	Male (N=34)	**Female (N=11)**	**p-value**	**Male (N=12)**	**Female (N=8)**	**p-value**
Age	56.51±10.78 (17-71)	58.27±7.86 (47-70)	0.623	77.38±5.61 (63-84)	78.38±4.41 (75-82)	0.676
Hypertension	6 (17.65%)	1 (9.10%)	0.663	4 (33.33%)	6 (75%)	0.169
Hypercholesterolemia	8 (23.53%)	2 (18.18%)	>0.99	6 (50%)	4 (50%)	0.373
Diabetes mellitus	11 (32.35%)	3 (27,27%)	>0.99	3 (25%)	2 (25%)	>0.99
Smoking	10 (29.41%)	1 (9.10%)	0.246	4 (33.33%)	0 (0%)	0.117
Renal failure	2 (5.88%)	0 (0%)	>0.99	1 (8.33%)	0 (0%)	>0.99
Etiology of heart failure	-Ischemic 18 (52.94%) -Idiopathic 10 (29.41%) -Sarcoidosis 1 (2.94%) -Cardiomyopathic hypertrophy 2 (5.88%) -Non-compaction cardiomyopathy 2 (5.88 %) -Valvular 1 (2.94%)	-Ischemic 4 (36.36%) -Idiopathic 6 (54.55%) -Cardiomyopathic hypertrophy 2 (5.88%)	0.643	-	-	-
Aortic valve area (cm2)				0.78±0.12	0.76±0.17	0.851
Peak gradient (mmHg)				66.91±14.93	78.2±14.94	0.169
Mean gradient (mmHg)				44.31±12.93	46±11.34	0.863
Statins				5 (41.67%)	5 (62.5%)	0.649

M.1.2-Porcine aortic valve samples

Porcine valves, widely used as analogue for endothelial and interstitial adult human valve cells, were used to validate alterations in metabolic gene profile in human valve cells. Porcine cells were used under supervision of Dr Butcher during a short-term stay in Cornell University, Ithaca. Non-mineralized porcine valves were used to isolate Porcine Aortic Valvular Endothelial Cells (PAVEC) and Porcine Aortic Valvular Interstitial Cells (PAVIC). These valves were kindly provided by Shirk Meats, Dundee, NY.

M.2- Human VIC and porcine VIC and VEC isolation and culture

M.2.1- Cell isolation and culture of human VIC and porcine VIC and VEC

Human VIC were isolated from human tricuspid aortic valve following protocols previously described (Meng et al., 2008 & López et al., 2012). First, valve cusps were rinsed with M199 medium (Corning Life Science, Tewksbury, MA) and then digested with 2.5 mg/mL type II collagenase (Invitrogen, Carlsbad, CA) also in M199 medium for 30 minutes at 37ºC in a shaking bath. Next, samples were quickly vortexed to remove endothelial valve cells. VIC populations were obtained by an additional digestion of valve leaflets with a 0.8 mg/mL collagenase solution for 3h at 37ºC in a shaking bath. The cell suspension was then quickly vortexed and centrifuged at 500 x g for 8 minutes at 4ºC. The supernatant was spun again at 1100xg for 8 min at 4 ºC. The cells were resuspended in M199, seeded into 75 cm^2 flask and cultured as indicated in the section M.2.2.

PAVIC and PAVEC were isolated from porcine tricuspid valves also using a collagenase digestion procedure (Butcher et al., 2004). First, valve cusps were rinsed with PBS and digested in collagenase type II (600 U/mL in DMEM) for 10 minutes and 37ºC in a sterile incubation at 5% CO_2. The leaflets were then softly swabbed to remove the endothelial layer without disrupting the interstitium. Later, the cell suspension containing PAVEC was centrifuged at 300 x g for 5 min twice to gently collect all the endothelial cells, which were later resuspended in DMEM. Cells were seeded in 1% gelatin coated 25 cm^2 flasks. The remaining tissue was further incubated with 600 U/mL collagenase at 37ºC for 12-18 hours to isolate interstitial cells. After incubation, the cell suspension containing PAVIC was centrifuged at 300 x g for 5 min and PAVIC were collected, rinsed, and then seeded in DMEM in 25 cm^2 flasks.

M.2.2- Valve cell culture

Human VIC were cultured in M199 growth media (Corning Life Science, Tewksbury, MA) supplemented with 10% heat-inactivated fetal bovine serum (FBSi) (Hyclone, Carlsbad, CA) and 1% antibiotic-antimycotic solution (100 units penicillin, 100 µg/mL streptomycin, 0.25 µg/mL amphotericin) (Gibco Invitrogen, Carlsbad, CA). Human VIC were later cultured in a 5% CO_2 incubator at 37ºC under humid atmosphere. Media was replaced twice a week. Cells were grown to 85-90% confluence and detached using trypsin-ethylenediaminetetraacetic (EDTA) solution, and then passed 1:3 or 1:4. For experimental purposes, only cells between passages 3 to 7 were used. For long-term storage in liquid nitrogen only passages 1 to 4 were processed. Cells were first frozen in FBSi supplemented with 10% of dimethyl sulfoxide (DMSO) at -80ºC and then transferred after 24h to liquid nitrogen containers.

PAVIC and PAVEC were screened for phenotype characterization by RT-qPCR, immunofluorescence, and Western blot techniques (Gould et al., 2010). Only VEC cultures with consistent CD31 and VE-Cadherin

positive expression, cobblestone morphology, and non-detectable α-SMA markers were used for further experiments. PAVIC were cultured in tissue-culture treated flasks at 37°C and 5% CO_2 in DMEM supplemented with 10% FBS (Invitrogen, Carlsbad, CA), 1% penicillin-streptomycin (P/S) (Invitrogen, Carlsbad, CA). PAVEC were cultured in flasks coated with 50 µg/ml rat-tail collagen I (BD Biosciences, San Jose, CA) at 37°C and 5% CO_2 in DMEM supplemented with 10% FBS 1% penicillin-streptomycin. PAVIC were used at passages 3 to 6, while PAVEC were used at passages 3 to 5.

M.2.3- Porcine 3D VIC-VEC co-cultures

Collagen hydrogels were prepared as previously described (Butcher et al., 2006), consisting in constrained 3D-culture platforms made with polycarbonate negative molds to form circular wells from cast SylGard 184® poly-dimethylsiloxane (PDMS) (Dow Corning, Midland, MI, USA) (**Figure XIII**). Beveled edges were machined into the geometry to secure a Type 310 stainless steel compression spring (Lee Spring, Brooklyn, NY, USA). This configuration provides an equi-biaxial mechanical constraint of casted cellularized collagen hydrogels (**Figure XIII**). Type I rat tail collagen (Ibidi, Madison, WI, USA) hydrogels containing PAVIC were prepared as previously described (Butcher et al., 2006). Briefly, PAVIC cells were encapsulated within the collagen gel suspension (2 mg/mL) at 400,000 cells/mL density and seeded into the poly-dimethylsiloxane scaffold. Hydrogels were then allowed to cast for 1h at 4°C, 1h at room temperature, and for 1h at 37°C. Later, PAVEC were topically seeded at 50,000 cells/cm^2 density. Hydrogels were kept in general media (DMEM, supplemented with 10% FBS and 1% penicillin-streptomycin) for 24h prior to activation with inflammatory stimuli.

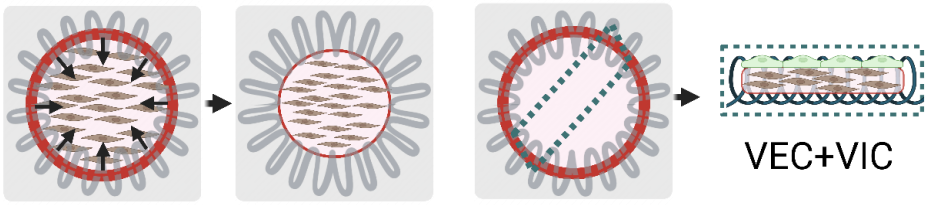

Figure XIII. **Schematic representation of *in vitro* 3D co-culture**. Remodeling of collagen hydrogels containing encapsulated VIC over time. Hydrogels are contained by custom PDMS culture wells with inset stainless steel compression spring. Black arrows (left schematic) indicate inward gel compaction. On the right image, primary cell culture configurations for valve endothelial cells (VEC), valve interstitial cells (VIC) and co-culture of VEC + VIC. Modified from Gee et al., 2021.

M.3- Protocol for cell activation

Prior to activation, human VIC were cultured for at least 6 hours with activation media (M199 supplemented with 2% FBSi and 1% antibiotic-antimycotic solution) and then treated with the indicated stimulus for the specified times in a final volume of 1 mL/well. When indicated, inhibitors, agonists, and drugs modulating metabolic routes were incubated for 1 prior to cell activation. A list of inflammatory stimuli, cytokines, TLR ligands and other metabolic activators, as well as working concentrations are shown

in **Table II** while a list of signaling and metabolic inhibitors with their corresponding working concentrations are listed in **Table III**.

PAVIC and PAVEC hydrogels were kept in general media (DMEM, supplemented with 10% FBS and 1% penicillin-streptomycin) for 24h prior to activation with inflammatory stimuli LPS (100 ng/mL) + IFN-γ (5 ng/mL), optimized to minimize cell death. Alternatively, hydrogels were exposed to osteogenic media (DMEM, supplemented with 10% FBS, 1% penicillin-streptomycin, 10 mM β-glycerophosphate, 50 µg/mL ascorbic acid and 100 ng/mL dexamethasone) to induce VIC differentiation into an osteoblast-like phenotype. Treatments were renewed every other day for 7 days. Microscopy images were taken along the experiment as control purposes. Hydrogels were processed either for protein or RNA extraction and FISH experiments, as detailed in following sections.

Table II. Stimuli used in this study.

Stimuli	Target	Working concentration	Vendor
Diethyl succinate	GPR91	5-10 mM	Sigma Aldrich, St Louis, MO
IFN-α (human recombinant)	IFNAR 1/2	100 ng/mL	Peprotech Inc, London, UK
IFN-γ (human recombinant)	IFNGR 1/2	100 ng/mL	Peprotech Inc, London, UK
IFN-γ (porcine recombinant)	IFNGR 1/2	5 ng/mL	R&D systems, Minneapolis, MI
TGF-β (human recombinant)	TGFR-β	10 ng/mL	Peprotech Inc, London, UK
TNF-α (human recombinant)	TNFR	5 ng/mL	Cell Biolabs, Rocky Hill
LPS from E. Coli O111B4	TLR4	1 µg/mL in human cell cultures 100 ng/mL in porcine 3D cultures	Sigma-Aldrich, St. Louis, MO
Poly (I:C) (HMW)	TLR3	1 µg/mL	Invivogen, San Diego, CA
Sodium citrate	SLC13A5	5 mM	Sigma-Aldrich, St. Louis, MO
Sodium lactate	GPR81	15 mM	Sigma-Aldrich, St. Louis, MO

Table III. Pharmacological inhibitors, agonists and antagonists used in this study.

Inhibitor	Target	Working concentration	Vendor
Antimycin A	Mitochondrial complex III inhibitor	0.5 µM	Sigma Aldrich, St Louis, MO
BPTES	Glutamine synthase I inhibitor	3 µM	Sigma Aldrich, St Louis, MO
Dimethyl malonate	Succinate dehydrogenase A inhibitor	5 mM	Sigma Aldrich, St Louis, MO
FCCP	Oxidative phosphorylation uncoupler	10 µM	Sigma Aldrich, St Louis, MO
G6PDi	Glucose-6-phosphate dehydrogenase	10 µM	Sigma Aldrich, St Louis, MO
Metformin	Mitochondrial Complex I inhibitor Mitochondrial glycerol-3-phosphate dehydrogenase inhibitor AMPK agonist	5 mM	Sigma Aldrich, St Louis, MO
N-acetyl-L-cysteine	GSH production enhancer ROS inhibitor	10 mM	Sigma Aldrich, St Louis, MO
NF-κB SN50	NF-κB translocation inhibitor	50 µg/mL	Calbiochem, Darmstad, Germany
Oligomycin	ATP synthase inhibitor	1.5 µM	Sigma Aldrich, St Louis, MO
PX-478	HIF-1α inhibitor	40 µM	MedChem Express, Monmouth Junction, NJ
Rotenone	Mitochondrial complex I inhibitor	1 µM	Sigma Aldrich, St Louis, MO
Ruxolitinib	JAK1/JAK2 inhibitor	6 µM	InvivoGen, San Diego, CA
Sodium	Pyruvate dehydrogenase kinase	5 mM	Sigma Aldrich, St Louis, MO

dichloroacetate	inhibitor		
Sodium oxamate	Monocarboxylate transporter-4 inhibitor	10 mM	Sigma Aldrich, St Louis, MO
Tunicamycin	N-linked glycosylation inhibitor	10 µM	Calbiochem, Germany
TEPP-46	Pyruvate kinase M2 activator	50 µM	Sigma Aldrich, St Louis, MO
UK-5099	Mitochondrial Pyruvate Carrier Inhibitor	50 µM	Sigma Aldrich, St Louis, MO
2-Deoxy-D-glucose	Hexokinase II inhibitor	10 mM	Sigma Aldrich, St Louis, MO

M.4- Quantitative reverse transcription polymerase chain reaction (RT-qPCR)

RT-qPCR is a method used for quantification of specific gene expression. First, complementary DNA (cDNA) is generated from total RNA using a reverse transcriptase. cDNA is later used as a template for q-PCR reaction based on the measurement of fluorophore incorporation within DNA in each amplification cycle.

M.4.1- RNA extraction

For the analysis of human VIC, total RNA was extracted using Tri Reagent® (Invitrogen, Carlsbad, CA) following the manufacturer´s protocol. Typically, 1 mL of reagent was used per 100,000 cells. Then, chloroform extraction was performed by adding 200 µL per 1mL of Tri Reagent. Samples were mixed thoroughly and centrifuged at 12,000 x g for 10 min at 4°C. The RNA-containing aqueous phase was collected and 500 µL of isopropanol were added. After mixing and incubating for 10 min at room temperature, samples were centrifuged at 12,000 x g for 10 min at 4°C. Supernatant was discarded and pellet was washed with 75% ethanol, air-dried, and resuspended in 15 µL of diethyl pyrocarbonate (DEPC)-treated water. Total RNA was measured by spectrophotometry using Nanodrop 1000 (Thermo Scientific, Waltham, MA).

For the analysis of human valve leaflets, 35-50 mg of tissue from non-stenotic and stenotic valves from patients, stored at -80°C, were homogenized in 1mL of TRI Reagent® using mechanical disintegration with an Omni tissue homogenizer (Omni International, Atlanta, GA). Samples were then centrifuged at 12000 rpm for 10 min at 4°C and supernatants were collected for RNA extraction, as described above for human VIC.

For the analysis of 3D porcine VIC-VEC co-culture model before RNA extraction cells were extracted from the hydrogel using collagenase digestion. 3D cultures were washed with PBS and digested with collagenase type II (600 U/mL) for 15 min at 37°C. Cells were then collected with Leibowitz media (Thermo Scientific, Carlsbad, MA) and wells were washed with Hank's Balanced Salt Solution (HBSS) before a second digestion with collagenase in the same conditions. Finally, cells were collected with Leibowitz media and centrifuged at 500 x g for 5 min. Cellular pellet was used for RNA extraction using E.Z.N.A. ® MicroElute® Total RNA kit (Omega, Bio-tek, Norcross, GA, USA) as described by the manufacturer. Total RNA was quantified using Nanodrop 1000 (Thermo Scientific, Waltham, MA).

M.4.2- Retrotranscriptase reaction to generate cDNA

For the analysis of human VIC and valve leaflets, 1500 ng of total RNA was used to generate complementary DNA by retrotranscriptase reaction. First, RNA was mixed with 300 ng of random primers (Invitrogen, Carlsbad, CA), 1 µL of 10 nM triphosphate deoxyribonucleotides mix (dNTPs) (Amersham Biosciences, London, UK) and distilled water up to 12.5 µL. Samples were incubated for 5 min at 65°C. Then, 4 µL of 5x First Strand Buffer (Invitrogen, Carlsbad, CA), 2 µL of 2 mM dithiothreitol (DTT) (Invitrogen, Carlsbad, CA) and 0.5 µL of ribonucleases inhibitor (RNAsin®) (Promega, Madison, WI) were added. Mixture was incubated for 2 min at 37°C. Finally, 1 µL of 200 U/ µL Moloney Murine Leukemia Virus retro-transcriptase (M-MLV) (Invitrogen, Carlsbad, CA) was added. Samples were incubated at 25°C for 10 min, then at 37°C for 50 min and finally, at 70°C for 15 min.

For the analysis of 3D porcine cells co-culture model, 1000 ng of total RNA were used to generate cDNA using a q-Script cDNA synthesis kit (Quantabio, Beverly, MA, USA), which is a mixture of an engineered M-MLV RT and a ribonuclease inhibitor protein. The protocol was performed as described by the manufacturer: 1 µL of M-MLV, 4 µL of 5x q-Script reaction buffer and distilled water up to 20 µL. Conditions used for retro-transcription reaction were: 5 min at 25°C, 30 min at 42°C and 5 min at 85°C.

M.4.3- Quantitative PCR

For the analysis of human VIC, 20 ng of cDNA were mixed with 0.4 µL of 10 µM of each primer for target genes, KAPA SYBR FAST ® master mix kit (Sigma Aldrich, St Louis, MO) and purified water was added to a final volume of 20 µL. Primers of human genes of interest used in the study are listed in **Table IV**, were obtained from previous reports and tested for 100% of complementarity with the target gene in the bioinformatics tool (https://www.ncbi.nlm.nih.gov/tools/primer-blast/). The qPCR was performed in a LightCycler480® (Roche Diagnostics, Rotkreuz, Switzerland) using the following conditions: (i) 5 min of denaturalization at 95°C, (ii) 45 cycles of 15 seconds at 95°C, 20 seconds at 60°C and 5 seconds at 72°, (iii) last cycle of 5 seconds 95°C, 1 min at 55°C and 10 seconds at 4°C. Transcription levels of each gene were normalized to GAPDH expression, a housekeeping gene used as an endogenous control. Data were expressed as $2^{-\Delta Ct}$ (Ct=cycle threshold; ΔCt=Ct of gene-Ct of GAPDH). Samples amplifying at >37 cycles were considered non-detectable.

For the analysis of swine 3D VIC-VEC co-cultures, 25 ng of cDNA were used. cDNA was mixed with 1 µL of 10 µM of each primer for the indicated target genes and 1X SYBR Green PCR master mix (Applied Biosystems, Foster City, Canada), and purified water was added up to 20 µL of final volume. The qPCR was conducted in a MiniOpticon Real-Time PCR Detection System (Bio-Rad, Hercules, Canada). The protocol included a total of 40 cycles, each of them consisting of 30 seconds at 95°C, 5 seconds at 95°C and 30

seconds at 60°C for PCR reaction followed by 10 seconds at 95°C, 5 seconds at 60°C and 5 seconds at 95°C for melting curve. Primers used are listed in **Table IV** and indicated with "p" which means they are porcine.

Table IV. Sequences of primers used in the study. (h) indicates human, (p) porcine.

Gene name	Forward primer sequence (5'-3')	Reverse primer sequence (5'-3')
ACTA2 (h) (α-SMA)	CCGACCGAATGCCAGAAGGA	ACAGAGTATTTGCGCTCCGAA
BAX (h)	CCCACCAGCTCTGAACAGTTC	CCAGCCACAAAGATGGTCAC
BCL2 (h)	GGTGGGGTCATGTGTGTGG	CGGTTCAGGTACTCAGTCATCC
BMP2 (h)	ACCCGCTGTCTTCTAGCGT	CTCAGGACCTCGTCAGAGGG
BMP2 (p)	AGCTTCCACCACGAAGAATC	CTCCCGAAAGACCTGAAGTT
BNIP3 (h)	GCCATCGGATTGGGGATCTAT	GCCACCCCAGGATCTAACAG
COX7A1 (h)	TGACATCCCGTTGTACCTGAA	AAGGAGGCCCAGCCAAG
COX7A1 (p)	CACCTACTGGACGAATCC	AGGTCCCGAGGTATTACAG
FAS (h)	TGGGCTTGCATGTATTCAAA	AGATGGCTTCAAGGAGCAAG
GAPDH (h)	TGCCAAATATGATGACATCAAGAA	GGAGTGGGTGTCGCTGTTG
GLS1 (h)	CTGGAAGCCTGCAAAGTAAAC	TGAGGTGTGTACTGGACTTGG
G6PD (h)	TGACCTGGCCAAGAAGAAGA	CAAAGAAGTCCTCCAGCTTG
G6PD (p)	GGCAACAGATACAAGAACGTGAAG	GCAGAAGACGTCCAGGATGAG
HIF1A (h)	AGTGTACCCTAACTAGCCGA	GTGCAGTGCAATACCTTCC
HKII (h)	TCACGGAGCTCAACCATGAC	GCTCCAAGCCCTTTCTCCAT
HKII (p)	GTTCCTGGCTCTGGATCTTGG	GGGATGGCGTAGATCTGGTTC
IDH3 (h)	ATCGGAGGTCTCGGTGTG	AGGAGGGCTGTGGGATTC
IL6 (h)	CACCTCTTCAGAACGAATTG	CTAGGTATACCTCAAACTCC
IL8 (h)	ATGACTTCCAAGCTGGCCCGT	TCCTTGCAAAACTGCACCT
MCT4 (h)	CTCGTGGTCTTCTGCATCTT	AAAATCAGGGAGGAGGTGAG
MCT4 (p)	CCCGTGTTCGTGGTGAGCTA	TGAAGAGGTAGACGGAGTAA
MDH2 (h)	TCGGCCCAGAACAATGCTAAA	GCGGCTTTGGTCTCGATG
ME1 (h)	ACCCTGGAAGAGAGACAGCA	CCAATTTACCCACAGGGATG
ME2 (h)	AGAGCTAGCCCAAGGGAGAC	TCAACACGTCTACCCCAACA
MMP1 (h)	CTGCTTACGAAATTTGCCGACAGA	GTTCTAGGGAAGCCAAAGGAGCTG
NAMPT (h)	ATCCTGTTCCAGGCTATTCTGT	CCCCATATTTTCTCACACGCAT
NMNAT1 (h)	TCATCATGGCAGAACTTGCT	TGGCACAGCTTTTGTTTTTG
NMNAT2 (h)	GGCACCGTCTCATCATGTGTCAG	CCCAAGATCTTGGCTGCAGTG
NMNAT3 (h)	CCCTGCAAATAGCAGCTACC	TGAGAAGCTGCGAGGTCTTT
NOX5 (h)	ACTATCTGGCTGCACATTCG	ACACTCCTCGACAGCCTCTT
NOX2 (h)	TGTTCAGCTATGAGGTGGTGA	TCAGATTGGTGGCGTTATTG
NOX4 (h)	AACCGAACCAGCTCTCAGAA	CCCAAATGTTGCTTTGGTTT
PDK4 (h)	CCCGCTGTCCATGAAGCAGC	CCAATGTGGCTTGGGTTTCC
PFKBF3 (h)	CCGTTGGAACTGACGCAGA	CACAGGATCTGGGCAACGAG
PFKBF3 (p)	GACCCGCTACCTCAACTGG	TGGCATCAAAAACCGCAAT
PKM1 (h)	GCATCATGCTGTCTGGAGAA	AACTATCAAAGCTGCTGCTA
PKM2 (h)	CTATCCTCTGGAGGCTGTGC	ACGATTATGGCCCCACTGCS
PKM2 (p)	GGAGGGTGGAGTGTTTGTCT	CTTAGCCTCCCTCACTCCC
PTGS2 (h) (COX2)	TTCAAAGATTGTGGGAA	AGATCATCTCTGCCTGAGTA
PTGS2 (p)	GGAGAGACAGCATAAACTGC	GTGTGTTAAACTCAGCAGCA
SDHA (h)	CAGCATGTGTTACCAAGCT	GGTGTCGTAGAAATGCCAC
SDHB (h)	GACACCAACCTCAATAAGGTCTC	GGCTCAATGGATTTGTACTGTGC
SLC25A1 (h) (GLUT1)	CTGCTCATCAACCGCAAC	CTTCTTCTCCCGCATCATCT
SLC25A1 (p)	GATGAAGGAGGAGTGCCG	CAGCACCACGGCGATGAGGAT
XBP1 (h)	TAAGACAGCGCTTGGGGATGGA	ATACCGCCAGAATCCATGGGGA
18S (p)	AAGGTCGGAGTGAACGGATT	CATTTGATGTTGGCGGGAT

M.5- Protein immunodetection by Western Blot

Western blot analysis was performed for the identification and semi-quantitation of target proteins in whole cell extracts. Proteins were separated by size in a polyacrylamide gel using electrophoresis, using the original sodium dodecyl sulphate (SDS-PAGE) method and denaturing conditions described by Laemmli method (Laemmli, 1970), followed by the transfer to a membrane and immunological detection.

M.5.1- Protein extraction and quantitation by the bicinchoninic acid assay (BCA)

Cells were grown to 80% confluence in 6-well plates and activated as previously described. For the isolation of whole cell extracts, cells were lysed with 75 µL/well of lysis buffer TNE (20 mM Tris–HCl pH 7.4, 150 mM NaCl, 5 mM EDTA) with phosphatase inhibitors (1 mM Na_3VO_4, 5 mM NaF) and protease inhibitors (10 µg/mL aprotinin, 10 µg/mL leupeptin, 1 mM phenylmethylsulfonyl fluoride (PMSF)). Then, cells were scraped and collected in an Eppendorf tube and later centrifuged at 7000 x g for 20 min at 4^{o}C. Supernatants containing proteins were collected in a new tube. For the isolation of cytoplasmic and nuclear extracts, cells were lysed using the Active Motif Nuclear and cytoplasmic extract kit (Active Motif, Rixensart, Belgium) following manufacturer's protocol.

Total protein concentration in cell lysates was measured using the BCA method, based on the ability of proteins to reduce Cu^{2+} to Cu^{+} in an alkaline environment. In this case, Pierce™ BCA protein assay kit (Thermo Scientific, Carlsbad, MA) was used. Briefly, 5 µL of the total protein extract was mixed with 100 µL of BCA reagent in a 96-well plate. BCA reagent was prepared with 50 parts of reagent A containing bicinchoninic acid in alkaline buffer and 1 part of reagent B containing cupric sulfate. The mixture was incubated for 30 min at 37^{o}C, and the absorbance was measured at 570 nm in Versamax microplate reader (Molecular Devices, Sunnyvale, Canada). The protein concentration was calculated by interpolating the absorbance results in a standard curve made with known concentrations of BSA.

M.5.2. Western blot procedure: SDS-PAGE and transfer

First, 30 µg of protein lysates were prepared in a final volume of 75 µL and then mixed with 17.5 µL Laemmli buffer 5X (325 mM Tris-HCl pH 7.5, 50% glycerol, 10% (w/v) SDS, 10% β-mercaptoethanol, and 0,01 mg/mL bromophenol blue). Samples were then heated at 100^{o}C for 5 min. Proteins were separated by electrophoresis using denaturing conditions in an 8-10% polyacrylamide gel in electrophoresis buffer (25 mM Tris hydroxymethyl aminomethane, 192 mM glycine and 0.1% (w/v) SDS, pH 8.3). Electrophoresis was set at constant 25 mA for each gel and 200 V. A molecular weight protein ladder was run in parallel as size standard (Bio-Rad). Later, proteins were transferred to a hybond polyvinylidene difluoride (PVDF) membrane using a wet-transfer system (Bio-Rad, Hercules, CA) set at 400 mA for 2h. PVDF membranes were previously activated in methanol for 1 min and washed with distilled water for 2 min.

M.5.3- Protein immunodetection and visualization by chemiluminescence

Prior to immunodetection, to eliminate non-specific bindings, membranes were first blocked for 1h at room temperature using blocking buffer (TBS-0.5% Tween buffer (TTBS) and 5% non-fat powdered milk) on a rocker platform. Then, incubation with the corresponding primary antibody was performed overnight at 4ºC. Primary antibodies were prepared as recommended by the manufacturer, usually in 5% non-fat milk or 5% BSA in TTBS with 0.02% sodium azide, as indicated in **Table V**. Next, membranes were washed 3 times with TTBS for 10 min at room temperature, and later incubated for 1h at room temperature with the corresponding secondary antibody conjugated to horseradish peroxidase (HRP) in 3% milk-in TTBS. Membranes were washed again as described, and then incubated with HRP blotting substrate ECL. The chemiluminescence was detected by exposing membranes to autoradiography films. Protein bands were scanned with a densitometer GS-800 (Bio-Rad) and quantified using Quantity One software (Bio-Rad). Anti-β-Tubulin antibody was used as a loading control. Results were expressed as arbitrary units (au) normalized to the loading control and referred to basal conditions. A list of antibodies used in this study is shown in **Table V**.

Table V. Primary and secondary antibodies used in this study.

Target protein	Molecular weight	Primary antibodies Working dilution/Secondary antibody	Vendor
HIF-1α	120/110	1:1000 (TTBS-5% milk)/Rabbit	Novus Biologicals, Madrid, Spain
ICAM-1	100	1:1000 (TTBS-5% milk)/Rabbit	Santa Cruz Biotech Inc, Santa Cruz, CA
p-p44/42 MAPK (Erk1/2) (Thr202/Tyr204)	44/42	1:1000 (TTBS-5% BSA)/Rabbit	Cell Signaling, Danvers, MA
p-STAT1 (Tyr701)	95	1:1000 (TTBS-5% BSA)/Rabbit	Cell Signaling, Danvers, MA
p-PKM2 (Tyr105)	42	1:1000 (TTBS-5% BSA)/Rabbit	Cell Signaling, Danvers, MA
p-AMPK (Thr172)	46	1:1000 (TTBS-5% BSA)/Rabbit	Cell Signaling, Danvers, MA
p-Acly (Ser455)	120	1:1000 (TTBS-5% BSA)//Rabbit	Cell Signaling, Danvers, MA
VCAM-1	110	1:200 (TTBS-5% milk)// Mouse	Santa Cruz Biotech Inc, Santa Cruz, CA
β-tubulin	55	1:20000 (TTBS-5% milk)// Mouse	Sigma-Aldrich. St. Louis, MO
SOD-2	27	1:1000 (TTBS-5% milk)//Mouse	Abcam, Cambridge, UK
Secondary antibodies (HRP-conjugated)			
Goat-anti-mouse IgG	1:3000 (TTBS-3%milk)		Bio-Rad, Hercules, CA
Goat-anti-rabbit IgG	1:2000 (TTBS-3% milk)		Agilent Technologies, Sta Clara, CA

M.6- Enzyme linked immunosorbent assay (ELISA)

ELISA is an antibody-based technique that allows the detection of secreted proteins based on their binding to a specific antibody attached to a solid surface, and then complexed to a second antibody conjugated to an enzyme, typically HRP. Detection is done by measuring the conjugated enzyme activity by oxidation of chromogenic reagents by a peroxidase like the HRP chromogenic substrate (3,3',5,5',tetramethylbenzidine) producing a detectable color change.

Protein secretion was measured in the supernatants of human valve cells activated for 24h or for 7 days in 3D VIC-VEC co-culture models. The volume of activation medium was 1mL in both cases. Supernatants were collected and stored -80^{o}C until use. Before performing the ELISA, supernatants were centrifuged at 1000 x g for 10 min to discard cellular debris and diluted as indicated in **Table VI**. Protein concentration was quantified using commercial ELISA kits following manufacturer's protocol. Absorbance was measured at 450 nm using a Versamax microplate reader (Molecular Devices, Sunnyvale, CA). Protein concentration was calculated by extrapolating data in a standard curve of the corresponding target protein. Values were normalized to total cell protein content, which was quantified as in M.6.1 section.

Table VI. Commercial ELISA kits and dilutions used in this study.

Target protein	Supernatant dilution	Vendor
IL-6 (Human)	Untreated and inhibited: 1/20 Stimulated: 1/100 Stimulated upon inhibition: 1/50	Diaclone, San Diego, CA
IL-6 (Swine)	Untreated: 1/20 Stimulated: 1/50	Invitrogen, Carlsbad, CA
IL-8 (Human)	Untreated and inhibited: No dilution. Stimulated: 1/40 Stimulated upon inhibition: 1/10	Diaclone, San Diego, CA
PGE_2 (Human)	None	Arbor assays

M.7- *In vitro* calcification assays

Calcification assays were performed using high inorganic phosphate and low serum conditions as previously described (Villa-Bellosta et al., 2015). Human VIC were cultured until 90% confluence in 6-well plates. Cells were then treated with the corresponding stimuli in calcification media (M199 media, 1% FBSi, 2.6 mM Pi and 1% antibiotic-antimycotic solution) for 7 days. Media and stimuli were renewed every two days for 7 days. Then, two different quantification methods were used to quantify mineralization and calcium.

M.7.1-Alizarin Red Staining (ARS) for detection of mineralization

This method allows the visualization and a semi-quantitation of mineralization based on the use of an anthraquinone derivative, Alizarin Red (Sigma-Aldrich, St. Louis, MO). Briefly, cells were washed with PBS and stained with a dye solution (1.4% Alizarin Red in water, pH 4.2) for 30 min. Cells were washed 3-5 times with PBS and images were taken using a phase-contrast microscope (Nikon Eclipse TS100) connected to a digital camera. Alizarin Red dye was later extracted with 10% acetic acid for 30 min as previously reported by (Gregory et al., 2004). Briefly, cells were incubated in 10% acetic acid for 2 h at room temperature and then harvested by scraping. The solution was then heated at 85 ºC for 15 min, followed by cooling on ice for 10 min. After centrifugation, the aqueous phase containing ARS was neutralized with NH_4OH and absorbance was measured at 450 nm using a Versamax microplate reader (Molecular Devices, Sunnyvale, CA). Data were expressed as fold increase referred to basal conditions.

M.7.2-Calcium deposits quantification

Ca^{2+} deposits were quantified using colorimetric methods, specifically, Calcium Quantichrom™ kit (Bioassay Systems, Hayward, CA), a method based on the binding of phenolsulfonephthalein dye to free calcium generating a stable and blue colored complex. For this purpose, cells were washed with PBS and then incubated with 0.6N HCl for 24h at 4ºC. Supernatants were then collected and 5 µL were used to measure calcium deposits as described by the manufacturer, by quantifying absorbance at 612 nm. In parallel, protein extracts were obtained by lysing cells with 0.1N NaOH and 0.1% SDS, and protein concentration was determined by the BCA method. Data were expressed as mg/dL of calcium and normalized to total protein content.

M.8- *In vitro* VIC differentiation and dedifferentiation

Cultured VIC were treated with the indicated agents for 14 days and cell morphology was evaluated by microphotography during the process.

M.8.1- VIC differentiation assays

Human VIC with myofibroblastic phenotype, were cultured up to 80-90% confluence. Osteogenic differentiation experiments were conducted in growth media, M199 medium with 10% FBSi and 1% antibiotic-antimycotic, for 21 days. Cells were activated with the specified inflammatory stimuli, and, when indicated, preincubated with the corresponding inhibitor for 1 h. Medium and stimuli were changed every two days. Microphotography was performed using a phase-contrast microscope (Nikon Eclipse TS100) connected to a digital camera. Additionally, to confirm the differentiation process, the levels of the myofibroblastic marker *ACTA2* and the osteogenic marker *BMP2* were measured by qPCR, as previously detailed.

M.8.2- *In vitro* dedifferentiation of VIC to qVIC

To dedifferentiate VIC (myofibroblast) to quiescent VIC (fibroblast), we used a method reported by Latif et al., 2015 that is based on the treatment with a fibroblast formulation media (FIB). Human VIC were cultured up to 80-90% confluence. Dedifferentiation experiments to generate fibroblast phenotype were performed using either control media (M199, 10% FBSi and 2mM L-Glutamine) or FIB (M199, 2% FBSi, 50 ng/mL insulin, 10 ng/mL fibroblast growth factor-2, and 2mM L-Glutamine) for 14 days as previously described (Latif et al., 2015). Media was changed every two days and microphotography was used to evaluate morphological changes (**Figure XIV**). After 14 days of treatment, the dedifferentiation process was confirmed by the spindle-shape cell morphology and by the downregulation of markers *ACTA2* and *COL3A1* (**Figure XIV**) as performed by Latif et al., 2015. These fibroblast-like cells were used for the analysis of RNA, protein, RNA, and metabolism.

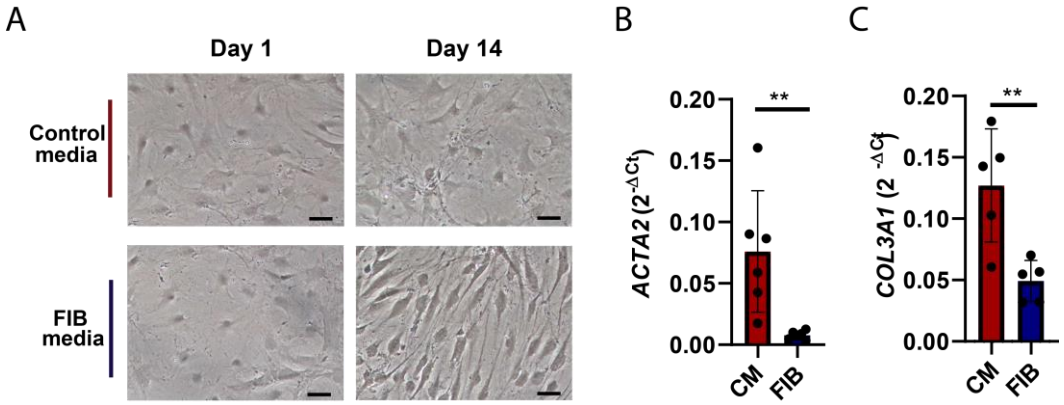

Figure XIV. **Analysis of dedifferentiation of VIC to qVIC.** Human VIC were cultured either on control media of FIB media for 14 d. A) Microphotographs of VIC in control media (above) and FIB media (below). (B) Expression levels of *ACTA2*. (C) Expression levels of *COL3A1*. (N=6). Black line indicates 50 µm; **, p<0.005.

M.9- Quantification of total Reactive Oxygen Species (ROS)

The production of ROS was measured using a cell-membrane permeable probe called 2',7'-dichlorodihydrofluorescein diacetate (DCFH-DA) (Sigma-Aldrich, St. Louis, MO), which is deacetylated by cellular esterases to form 2',7'-dichlorodihydrofluorescein (H_2DCF). In the presence of ROS, H_2DCF is quickly oxidized to 2',7'dichlorofluorescein (DCF), a green, fluorescent probe.

First, 30,000 cells were seeded in black 96-well plates with transparent bottom. Cells were allowed to attach for 24h and then activated with the indicated inflammatory stimuli for 24h and cultured in the conditions described in M.2.2. Then, media was removed, and cells were washed with PBS and incubated with 5 µM DCFH-DA in PBS for 30 min at 37°C in darkness. Finally, cells were washed with PBS and fluorescence was measured in a Cytation 5 microplate reader (Biotek/Agilent, Santa Clara, CA), using 488 nm excitation and 525 nm emission wavelength. Data were expressed as arbitrary units and referred to basal conditions.

M.10- Live-cell Metabolic Analysis

Real-time metabolic analysis was performed using the Agilent Seahorse XFe24 (Agilent, Sta Clara, CA). This equipment can measure the two main metabolic pathways: mitochondrial respiration and glycolysis by evaluating the oxygen consumption rate (OCR) and extracellular acidification rate (ECAR) of live cells in a multi-well plate. This method uses fluorescent probes that detect free O_2 and H^+. Briefly, the Seahorse metabolic analyzer measures basal OCR and ECAR rates before adding metabolic inhibitors. OCR is reported in units of pmol/minute and ECAR in mpH/minute. Inhibitors that have been preloaded into the drug delivery ports of the cartridge are then injected sequentially into the cells, thus allowing to calculate different metabolic parameters. Several assays can be performed by using a combination of different metabolic inhibitors. Later, an offline analysis of data is performed using the Seahorse Analytics software.

M.10.1- Cell seeding and activation and cartridge preparation

Prior to the metabolic analysis, both cells and cartridge required some preparations. 48h before the experiment, human VIC were seeded at a concentration of 30,000 cells/well in a Seahorse XF24 Cell Culture and allowed to attach overnight. The following day, cells were activated with the indicated inflammatory stimuli in activation media for 24h. When required, cells were pretreated for 1h with the indicated drugs. The day of assay, media was changed to Seahorse XF RPMI Medium, pH 7.4 supplemented with 2mM L-glutamine, 25 mM D-glucose and 1 mM pyruvate, and cells were incubated for at least 45 min in a 37ºC incubator without CO_2 incubator to allow outgassing from the plate. Then, cells were ready to be used in XFe24 Seahorse analyzer (Agilent, Sta Clara, CA).

In addition, one day prior to the assay, the sensor cartridge was hydrated with 1000 µL of Seahorse XF calibrant in a 37ºC incubator without CO_2 overnight. The day of assay, the corresponding metabolic modulators were loaded in the cartridge, which was used for Seahorse analyzer calibration for 15 min before use.

M.10.2- Analysis of mitochondrial function by Seahorse Cell Mito Stress Test

The Agilent Seahorse Cell Mito Stress test is based on the sequential injection of three modulators of mitochondrial respiration: oligomycin, carbonyl cyanide-4-(trifluoromethoxy)phenylhydrazone (FCCP) and rotenone/antimycin A (**Figure XV**). The injection of these modulators in the proper order allows the calculation of key parameters in mitochondrial function. To normalize data, cells were quantified by nuclei staining with Hoechst 1 µM. Cell counting was done using Cytation 5 microplate reader (Biotek/Agilent Santa Clara, CA, USA) connected to the Seahorse analyzer. A software owned by Agilent, "Seahorse Analytics", was used to calculate several key parameters (https://seahorseanalytics.agilent.com) such as: basal ECAR (mpH/min/10^4cells), basal respiration (pmol/min/10^4cells), maximal respiration (pmol/min/10^4cells), ATP

production linked to oxidative phosphorylation (pmol/min/10^4cells), proton leak (pmol/min/10^4cells), spare respiratory capacity (pmol/min/10^4cells), and non-mitochondrial respiration (pmol/min/10^4cells), as represented in **Figure XV**.

A variant of this Mito Stress assay was used to characterize the role of glutaminolysis in VIC metabolism both, basally and after cell activation. The variation consisted of the first injection of 3 µM bis-2-(5-phenylacetamido-1,2,4-thiadiazol-2-yl)ethyl sulfide (BPTES), a glutaminolysis inhibitor, or vehicle, as control, followed by the injection of the mentioned modulators in the proper order (**Figure XVI**).This variation allowed the analysis of the metabolism of cells seeded in the same well before and after the injection comparing the effect of BPTES versus vehicle and also, comparing the metabolism after BPTES injection in untreated and activated cells.

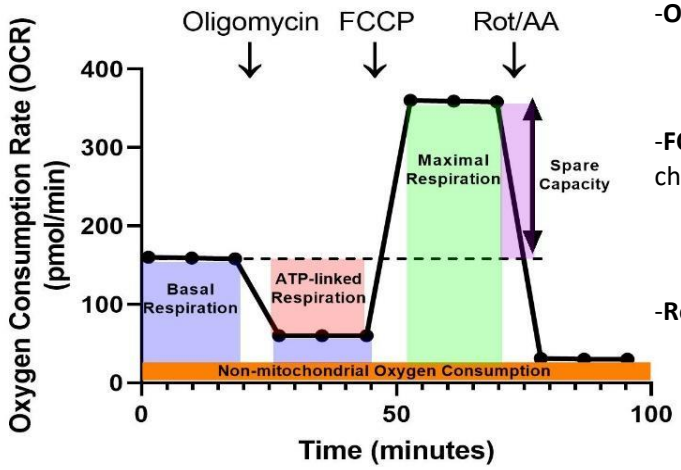

-**Oligomycin** (1.5 µM): ATP synthase inhibitor:
↓ mitochondrial respiration
↓ ATP synthesis

-**FCCP** (2 µM): Uncoupling agent of electron transport chain and oxidative phosphorylation:
↓ mitochondrial membrane potential
↑ complex IV OCR

-**Rotenone/Antimycin** (0.5 µM): Complex I/III inhibitors:
↓ mitochondrial respiration

Figure II. Cell Mito Stress Test profile showing the key parameters of mitochondrial function and the sequence of metabolic modulators injections. This figure illustrates the sequential injection of modulators for the Mito Stress Assay their working concentrations, and their target and the subsequent metabolic effect.

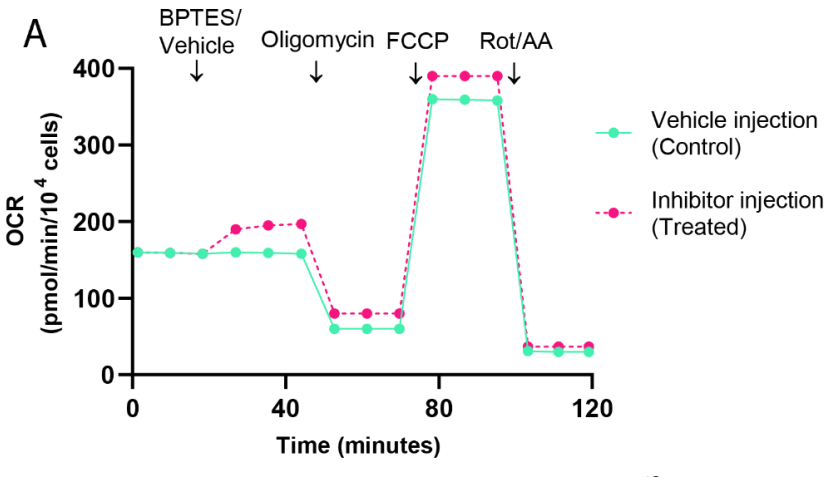

Figure XVI. Schema of Seahorse Mito Stress assay with acute injection. This figure illustrates the injection time course of modulators required for Mito Stress Assay with the acute injection of a glutaminolysis modulator, BPTES.

M.10.3- Measurement of ATP production by Seahorse Real-Time ATP Rate Assay

This assay allows not only the determination of the total adenosine triphosphate (ATP) production, the dominant energy source in cells, but also elucidates the amount of ATP produced by OXPHOS and glycolysis, the two main metabolic pathways responsible for ATP production in mammalian cells.

For the ATP rate assay, a different combination of metabolic modulators was used: oligomycin followed by rotenone/antimycin (**Table VII**). Hoechst 1 µM was added for cell counting using Cytation 5 and the Seahorse analytics software, as indicated above. Key parameters obtained in this assay are glycolytic ATP production rate (GlycoATP, pmol ATP/min/10^4cells), mitochondrial ATP production rate (mitoATP, pmol ATP/min/10^4cells) and total ATP production rate (pmol ATP/min/10^4cells).

Table VII. Metabolic modulators used for Seahorse Real-Time ATP Rate Assay

Port	Inhibitor	Concentration	Target	Effect
A	Oligomycin	1.5 µM	ATP synthase (Complex IV)	Inhibition of total ATP obtained from OXPHOS.
B	Rotenone/ Antimycin	0.5 µM	Complex I/Complex III	Total inhibition of mitochondrial respiration and induction in glycolytic ATP production.

M.10.3.1- Glycolytic ATP production rate calculation

During the conversion of glucose to lactate in glycolysis process, two molecules of ATP, H^+ and lactate are produced as shown in equation 1:

Eq 1: Glucose + 2ADP + 2 Pi → 2 Lactate + 2ATP + $2H_2O$ + $2H^+$

Considering the stoichiometry of the glycolytic pathway, the rate of ATP production by glycolysis (glycoATP production rate) is equivalent to Glycolytic Proton Efflux Rate (GlycoPER) and can be calculated using the same approach validated for Glycolytic rate assay (Romero et al., 2017) as shown in equation 2:

Eq 2: glycoATP production rate (pmol ATP/min) = glycoPER (pmol H^+/min)

M.11.3.2- Mitochondrial ATP production rate calculation

The rate of OCR that is coupled to ATP synthesis linked to OXPHOS can be calculated as the OCR that is inhibited by the ATP synthase inhibitor, oligomycin, as shown in equation 3:

Eq 3: OCR_{ATP} (pmol O_2/min) = OCR (pmol O_2/min) - OCR_{Oligo} (pmol O_2/min)

Conversion of OCR linked to ATP production to the rate of mitochondrial ATP production is done by multiplying by 2 (to convert to Oxygen atoms (O)). Then, it is necessary to multiply the P/O ratio, which is the number of ADP molecules phosphorylated to ATP per atom of O reduced by an electron pair going through the mitochondrial chain (equation 4). Seahorse Analytics software uses an average value for P/O which is 2.75 that was validated by (Romero et al., 2017).

Eq 4: mitoATP Prod Rate (pmol ATP/min) = OCR ATP (pmol O_2/min) * 2 (pmol O/pmol O_2) * P/O(pmol ATP/pmol O)

Finally, the total ATP production rate is the sum of the glycolytic and mitochondrial ATP production rates, as shown in equation 5:

Eq 5: ATP Prod Rate (pmol ATP/min) = glycoATP Prod Rate (pmol ATP/min) + mitoATP ProdRate (pmol ATP/min)

M.10.4- Analysis of Glycolytic function in XFe24 Seahorse Analyzer

There are two different assay protocols for measuring glycolytic parameters using the Seahorse analyzer: (i) the Seahorse Glycolytic Rate assay and (ii) the Seahorse Glycolytic Stress Kit that differ in the set of metabolic modulators and the glycolytic parameters elucidated. The main difference between them is that cells were seeded and activated in glucose-free media for Glycolytic Stress Kit and resuspended before the analysis in Seahorse XF RPMI Medium not supplemented with D-Glucose.

M.10.4.1- Seahorse Glycolytic Rate Assay

The Seahorse Glycolytic Rate Assay provides a precise measurement of glycolysis in live cells. This assay allows to quantify the proton efflux specific to glycolysis by calculating and subtracting mitochondrial-produced acidification. Metabolic modulators used in this assay were: rotenone/antimycin and 2-DG (**Figure XVII**). Cell counting and data analysis were performed as described in M.11.2. This assay allows the quantification of several key parameters such as basal glycolysis (pmol/min/10^4cells), compensatory glycolysis (pmol/min/10^4cells), proton efflux rate (PER) (pmol/min/10^4cells), and glycolytic proton efflux rate (pmol/min/10^4cells) (**Figure XVII**).

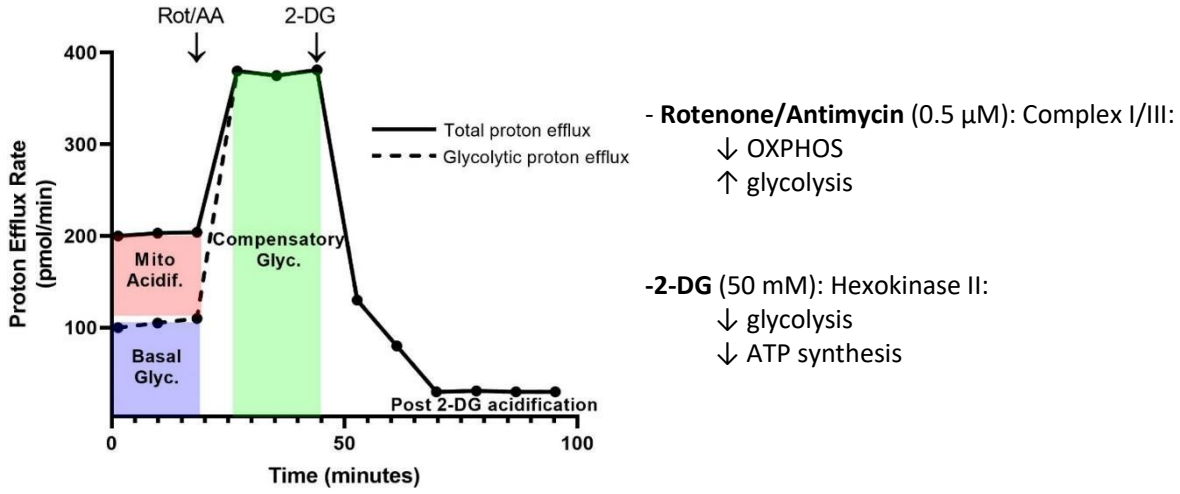

Figure XIIIII. Seahorse Glycolytic Rate Assay profile showing the key parameters of glycolysis and the sequence of metabolic modulators injections. This figure illustrates the sequential injection of modulators required for glycolytic rate assay, their working concentrations, and their target and the subsequent metabolic effect. Glyc=glycolysis. Acidif= acidification.

The Seahorse XF Glycolysis Stress Test is the standard assay for measuring glycolytic function in living cells. It is based in the direct measurement of the extracellular acidification rate (ECAR) reached by a cell after the addition of saturating amounts of glucose and allows to measure key parameters such as basal glycolysis (mpH/min/10^4), glycolytic Capacity (mpH/min/10^4), glycolytic Reserve (mpH/min/10^4), as well as non-glycolytic acidification (mpH/min/10^4). These calculations are based on the acidification caused by the extrusion of protons generated during the conversion of glucose to pyruvate and, later, to lactate. The sequential injection of modulators include glucose, oligomycin and 2-DG (**Figure XVIII**)**.** Cell quantification and analysis were performed as described above (M.11.2).

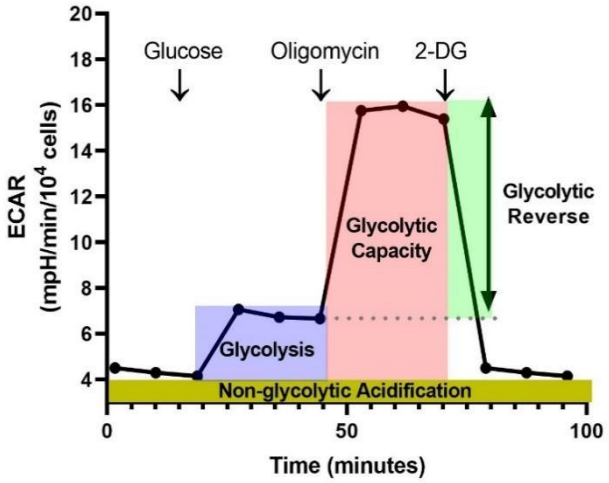

- **Glucose** (10 mM): Glycolysis:
  ↑ glycolysis

-Oligomycin (1.5 µM): ATP synthase:
  ↑ glycolysis
  ↓OXPHOS

-2-DG (50 mM): Hexokinase II:
  ↓ glycolysis

Figure XIVII. Seahorse Glycolysis Stress Test profile showing the key parameters of glycolytic function and the sequence of metabolic modulators injections.

M.11- RNA interference assays for silencing *HIF1A* gene

RNA interference assays were performed for silencing the target gene *HIF1A* and then analyzing VIC response to inflammatory stimuli. VIC were transiently transfected with small interference RNAs (siRNAs) of 20-25 nucleotides directed against the sequence of *HIF1A* mRNA. For this assay, Ambion® Silencer® predesigned and validated siRNA duplexes against *HIF1A* (ID s6539, Thermo Scientific, Carlsbad, MA) and an unspecific Silencer® (Ref. 4390843, Thermo Scientific, Carlsbad, MA) were used as Parra-Izquierdo et al., 2019. First, both siRNAs' duplexes were resuspended in 100 µL of nuclease-free water generating a 50 µM stock solution stored at -20 ºC until use, which further diluted to the working concentration of 10 nM.

The transient transfection of these siRNAs was performed using a lipid-based method with Dharmafect-1 transfection reagent (Dharmacon, Lafayette, CO) as previously reported by our group (Fernández-Pisonero et al., 2012) based on the previous protocols described by Meng et al., (2008). Briefly, VIC were cultured up to 90% confluence in 6-well plates. Then, 4 µL of the 10 nM siRNA duplexes were diluted in 200 µL of Optimem medium (Gibco Invitrogen, Carlsbad, CA) and 6 µL of Dharmafect-1 reagent were also diluted in 200 µL of optimum medium. Both solutions were incubated separately for 5 min at room

temperature. Then, siRNA dilution was added into the Dharmafect dilution and incubated for 20 min at room temperature to allow the formation of RNA-lipid complexes. Finally, 1.6 mL of M199 medium, supplemented with 10% FBSi but no antibiotic, was added to each tube and the mixture was added to the cells and incubated for 24h. Cell medium was then replaced by M199 supplemented with 10% FBSi and 1% antibiotic-antimycotic solution and cells were cultured for 24h. The next day, transfected cells were activated with the indicated stimulus in activation media for additional 24h and gene silencing was confirmed by the analysis of protein or RNA with Western Blot or q-PCR, respectively. In parallel, transiently transfected cells were used for metabolic analysis. 30,000 cells were seeded into Seahorse plates prior to activation with the indicated stimulus for 24 h, and then analyzed in the metabolic analyzer Seahorse XFe24.

M.12- Apoptosis and necrosis assay by flow cytometry

Flow cytometry detection of positive cells for annexin V and propidium iodide was used to evaluate cell apoptosis and necrosis, a method based on the capacity of annexin V to bind to phosphatidylserine residues exposed in the cell surface in the presence of calcium, an early event of canonical apoptosis (Haanen et al., 1995). In addition, propidium iodide is a non-permeable dye that can only enter the cell when the membrane is damaged and binds stoichiometrically to double strand DNA.

For the assay, approximately 100,000 human VIC were grown to confluence and then treated with the indicated stimuli for 7 days in calcification media. Media and stimuli were changed every 2 days. Cells were detached using StemPro Accutase (Thermo Scientific, Carlsbad, CA;), then spun down and the cell pellet was resuspended in Annexin V binding buffer (140 mmol/L NaCl, 2.5 mmol/L CaCl2, 10 mmol/L HEPES pH 7.4). Cell staining was performed following manufacturer's protocol by incubating with FITC ApoScreen® annexin V (Ref. 10040-02, Southern Biotech, Birmingham, AL) for 15 min on ice, followed by two washes and then staining with ApoScreen® propidium iodide (Ref. 10040-01, Southern Biotech, Birmingham, AL). Finally, stained cells were analyzed by a Gallios™ Flow Cytometer (Beckman Coulter Inc, US). Data were analyzed using Kaluza® Flow Analysis Software (Beckman Coulter Inc, US), and expressed as the percentage of apoptotic cells, which was calculated based on the number of annexin-V positive cells (B2+B4 quadrants).

M.13- Caspase 3/7 enzymatic activity assay

For the assay, 20,000 human VIC were seeded in 96-well treated plates. After attaching, cells were activated for 24h in calcification media. Then, caspase-3 and -7 enzymatic activities were determined using the Caspase-Glo® 3/7 assay following manufacturer's protocol (Promega, Madison, WI). Briefly, cells were scraped and mixed with 100 µL of the Caspase-Glo® 3/7 Reagent. The mixture was incubated for 1h at room temperature and then plated in a luminometer white plate for measuring luminescence in a MicroLumatPlusLB96V luminometer (EG&G Berthold, Germany).

M.14- Mitochondrial potential assay by flow cytometry

This assay quantifies changes in mitochondrial membrane potential in live cells by flow cytometry using tetramethylrhodamine methyl ester (TMRM), a cationic cell-permeant dye that accumulates in mitochondria with intact membrane potentials. For the assay, approximately 100,000 human VIC were grown to confluence in a 6-well plate and then treated with the indicated stimuli for 24h in activation media. The next day, cells were washed with PBS and then incubated with 25 nM TMRM) for 30 min at 37^{o}C in darkness. Cells were then detached using StemPro Accutase (Thermo Scientific, Carlsbad, MA), spun down, and washed twice with PBS. Finally, stained cells were analyzed by a Gallios^{TM} Flow Cytometer (Beckman Coulter Inc, US) using a 488 nm laser for excitation and a 570 ±10 nm emission filter. Data analysis was performed using Kaluza® Flow Analysis Software (Beckman Coulter Inc, US).

M.15-Quantitation of intracellular metabolites by Ultra performance liquid chromatography-Mass spectrometry in tandem (UPLC-MS)

Intracellular metabolites produced by glycolysis, TCA, PPP, and nucleotide synthesis were assayed using UPLC-MS in tandem, a method allowing a quantitative analysis of molecules by combining the physical separation abilities of ultra performance liquid chromatography with the mass analysis capabilities of mass spectrometry. While UPLC separates components based on their size, mass spectrometry provides spectral information that helps identify each separated component and quantify the concentration of each component even in low doses. In the study, metabolic fluxes of D-[U^{13}C6] Glucose isotopic tracer were determined. The assay included four steps: (i) Cell culture with D-[U^{13}C6] Glucose(ii) sample preparation, (iii) chromatographic separation and metabolic analysis, and (iv) data analysis.

(i) Cell culture with D-[U^{13}C6] Glucose: Approximately, three 6-well plates of cultured cells grown to confluence were used for each experimental point (3-4·10^{6} cells). First, cells were washed twice with M199 glucose-free media supplemented with 10% FBSi and 1% antibiotic-antimycotic. Then, M199 glucose-free media with 10% FBSi and 1% antibiotic-antimycotic was supplemented with 5.5 mM D-[U^{13}C6] Glucose and activated with indicated stimuli or vehicle for the specified times. In parallel, controls with D-[^{12}C6] Glucose were performed: Then cells were harvested using a trypsin-EDTA solution and centrifuged at 1500 rpm for 5 min. Cells were washed twice with cold-PBS.

(ii) Sample preparation: Metabolite extraction was performed using 1mL of a solution composed by methanol:acetonitrile:H_2O (2:2:1, v/v/v) for lysing cells. The solution was vortexed for 30 seconds and frozen for 1 min in liquid nitrogen (-192^{o}C). Samples were allowed to thaw at room temperature and were sonicated for 15 min at 4^{o}C. Then, a second cycle of freeze and sonication

was performed following the same conditions. Later, samples were incubated for 1h at -20ºC and centrifuged at 16000 x g for 15 min at 4ºC to get deproteinization. Pellets containing proteins were used for protein quantification by the BCA method, while supernatants containing metabolites were collected and evaporated to dryness using a SpeedVac evaporator (Thermo Scientific, Carlsbad, MA). Next, pellets containing metabolites were solubilized in acetonitrile:H_2O (1:1, v/v) and sonicated for 10 min at 4ºC. Then, samples were centrifuged 16000 x g for 15 min to eliminate insoluble particles. Finally, prior to the analysis by UPLC-MS, samples were evaporated to dryness and resuspended in ultrapure water.

(iii) Chromatographic separation and metabolic analysis: It was performed at the molecular analysis and metabolomics facility in the Centro para el Desarrollo de la Biotecnología, CSIC, Boecillo, Spain. The separation was carried out with a Acquity CORTECS UPLC_ C18, 100 x 2.1 mm column with particles of 1.6 µM (Waters, MA) directly interfaced into the electrospray ionization source of a Q-TOF mass spectrometer (SYNAPT HDMS G2, Waters). An elution gradient involving the eluents (A) H_2O:methanol:formic acid (95:5:0.1, v/v/v) with 5 mM ammonium formate, and (B) 100% acetonitrile with 0.1% formic acid and 5 mM ammonium formate, was run from 95% A to 20% A gradient in 4 min, then isocratic until 4.5 min, to rise again to 95% A at 6 min and kept to 95% A for an additional period of 2 min (8 min elution period), at a flow rate of 0.2 mL/min. Of note, chromatographic separation of ac-CoA was performed with a column Luna ® Omega Polar C18, 50 x 2.1 mm, with 1.6 µM particles (Phenomenex, Torrance, CA). The eluent for the separation was composed of (A)H_2O with 15 mM ammonium acetate and (B) methanol:acetonitrile (2:8, v/v) with 8.3 mM of ammonium acetate. Metabolites were detected in the positive ion mode.

(iv) Analysis: MS analysis was performed in the negative ion mode using a MS_E method that allows simultaneous detection of analytes through a low energy function (full scan) and a high energy function (collision energy) with ion partial fragmentation. All the metabolites were detected as M+H when unlabeled carbon or M+2, M+5, M+10 when incorporating ^{13}C from glucose. Data were either expressed as % of incorporation or nmol metabolite/mg protein.

M.16- Measurement of extracellular lactate by bioluminescence

The levels of L-lactate were measured in the supernatants of human VIC by the bioluminescent Lactate-Glo™ Assay (Promega, Madison, Wisconsin), which is based on the coupling of lactate oxidation and NADH production with a bioluminescent NADH detection system, following the manufacturer's protocol. Briefly, for the assay, 30,000 cells were cultured in 96-well plates and incubated with either stimuli or vehicle (in 100 µL of activation media) for 24h. Supernatants were stored at -80ºC until use. Prior to the assay a 1:40

dilution of supernatants in PBS was made. Then, 50 µL of the mixture were incubated with 50 µL of "lactate detection reagent", which contains lactate dehydrogenase (LDH), NAD^+ reductase, reductase substrate and luciferase, prepared as described by the manufacturer, for 1h at room temperature. The luminescent signal, proportional to the amount of lactate in the sample, was measured in a MicroLumatPlusLB96V luminometer. Data were expressed as luminescence arbitrary units referred to basal conditions.

M.17- Determination of reduction/oxidation (redox) state

The term redox potential is used to describe a system's overall reducing or oxidizing capacity, which is intimately related to the metabolic state of the cell. In this study, we were interested in measuring NAD^+/NADH, $NADP^+$/NADPH ratios and GSSG/GSH.

M.17.1- Determination of nicotinamide adenine dinucleotide $(NAD)^+$/NADH ratio

NAD^+ in an enzymatic cofactor involved in many redox reactions acting as a biological carrier of reducing equivalents. Ratios of the oxidized and reduced forms of these coenzymes offer perspective into the metabolic activity of the cell.

The NAD^+/NADH ratio was measured with the NAD^+/NADH Quantitation Kit (Sigma Aldrich), a colorimetric method based on an enzymatic cycling reaction in which NAD is reduced to NADH, which reacts with a probe producing a colored product Instructions provided by the manufacturer were followed. Briefly for the assay, 2 wells out of 6-well plates with 90% confluent cultures of human VIC were used ($1.5\text{-}2\cdot10^5$ cells). Cells were activated with the corresponding stimulus in activation media for 24h and later harvested with trypsin-EDTA and washed twice with cold PBS. Then, cells were extracted with 400 µL of NADH/NAD^+ extraction buffer by 2 cycles of 20/10 min of freeze/thaw on dry ice. Samples were vortexed and centrifuged at 13,000 x g for 10 min to remove insoluble material. Cell lysates were deproteinized before use by filtering through a 10 kDa cut-off spin filter to eliminate enzymes that consume NADH rapidly. Next, 50 µL of the eluted sample were added in duplicate in a 96-well plate to later mix with 100 µL of the master mix reagent and measure total NADH+NAD^+ levels. To detect NADH only, NAD^+ was first decomposed by heating the rest of the extracted samples at 60°C for 30 min. Once samples were cold on ice, 50 µL of this NADH-only fraction were transferred in duplicate to the 96-well plate. Finally, 100 µL of the master reaction mix, prepared as described by the manufacturer, were mixed with the samples, and incubated for 5 min at room temperature to convert NAD^+ to NADH. Then, 10 µL of NADH developer were added in each well and incubated from 1-4 hours at room temperature. Absorbance was measured at 450 nm in a clear bottom plate using Versamax microplate reader (Molecular Devices). Then, NAD^+ and NADH concentrations were calculated using a calibration curve plot with the values of NADH standards, and data were normalized to the total amount of protein, measured by the BCA method described in M.11.2. Data were expressed as NAD^+/NADH ratio.

M.17.2- Determination of nicotinamide adenine dinucleotide phosphate (NADP)$^+$/NADPH ratio

The levels of $NADP^+$ and NADPH were measured using the colorimetric $NADP^+$/NADPH Quantification Kit (Sigma Aldrich). The protocol was performed as recommended by the manufacturer. Briefly for the assay, three 6-well plates with 90% confluence ($3 \cdot 10^6$ VIC) were used per experimental point. Cells were activated with the indicated stimulus in activation media for 24 h and harvested with trypsin-EDTA solution and washed twice with cold PBS. Then, cells were extracted with 800 µL of $NADP^+$/NADPH extraction buffer, placed on ice for 10 min and centrifuged at 10,000 x g for 10 min to remove debris. 50 µL of the total fraction were plated in duplicate in a 96-well plate to later mix with 100 µL of master mix reagent, prepared as described by the manufacturer. To detect NADPH only, $NADP^+$ was previously decomposed by heating the samples at 60ºC for 30 min. Once samples were cold on ice, 50 µL of this NADPH-only fraction were transferred in duplicate to the 96-well plate and mixed with 100 µL of the master reaction mix. Mixture was incubated for 5 min at room temperature to convert NADP to NADPH. Then, 10 µL of NADPH developer were added in each well and incubated from 1-4 hours at room temperature. Absorbance measure and data analysis were performed as described in M.18.1.

M.17.3- Determination of glutathione disulfide (GSSG)/GSH ratio

The levels of GSSG and GSH were evaluated with the colorimetric GSSG/GSH Quantification Kit (Sigma-Aldrich), which is based on the use of DTNB (5,5'-dithiobis-(2-nitrobenzoic acid), a sulfhydryl reagent used to characterize reactive SH groups. When DTNB reacts with SH groups generating a colored product whose absorbance can be measured at 412 nm.

Manufacturer´s instructions were followed. Briefly, 3 plates of 6-well with 90% confluent cultures of human VIC were used for each experimental condition (≈$2 \cdot 10^6$ cells). Cells were activated for 24h in activation media with the indicated stimuli. Then, cells were harvested with trypsin-EDTA and washed twice with cold PBS. For each experimental condition, cells were resuspended with 2 mL of cold PBS, split in two different tubes, and processed differently. One tube was used for determining GSSG, and the other one for the total glutathione (GSSG+GSH). Then, cells were lysed by sonication with 200 µL of cold lysis buffer (50 mM monobasic sodium phosphate pH=7 and 1 mM EDTA disodium salt). 20 µL of the scavenger reagent provided by the commercial kit was added into the GSSG-only tube to degrade the GSH specie, but not to the tube designed to measure total glutathione (GSSG+GSH). Samples were then centrifuged at 10,000 x g for 15 min at 4ºC and supernatants were later deproteinized with 5% orto-phosphoric acid (MPA) prepared in ultrapure water. 65 µL of MPA were added to 25 µL of sample, vortexed and centrifuged 14,000 x g for 5 min. Finally, 6 µL of the supernatant were mixed with 244 µL of the assay buffer. 200 µL of this mixture were transferred to a 96-well plate and mixed with 100 µL of working reagent, prepared as described by the manufacturer and, absorbance at 412 nm was measured at point 0 and after 10 min of incubation.

Calculations of GSH and GSSG concentration were done using a glutathione standard curve as described by the protocol, and normalized to the total amount of protein, measured by the BCA method, as described in M.11.2. Data were expressed as GSSG levels (µM) and GSSG/GSH ratio.

RESULTS

R.1- Characterization of human VIC basal metabolism

First, the metabolic gene profile of human VIC, which are partially activated myofibroblast, was characterized. To achieve this aim, the transcription levels of metabolic genes participating in several catabolic and anabolic pathways were measured by qPCR in untreated VIC (**Figure 1**). As shown in **Figure 1**, glycolytic genes such as pyruvate kinase M2 (*PKM2)* and lactate dehydrogenase A (*LDHA)* were the most abundant in VIC. The transcript levels of other glycolytic genes, such as *PKM1* and monocarboxylate transporter *4 (MCT4)*, genes involved in TCA, and the gene encoding the rate-limiting enzyme controlling PPP, glucose-6-phosphate dehydrogenase (*G6PD)*, were 5-10 times lower. Interestingly, the fatty acid-degrading enzyme, adipose triglyceride lipase (*ATGL*), is also highly expressed in VIC, while enzymes participating in fatty acid (FA) synthesis, glutaminolysis, and OXPHOS are less abundant. Finally, genes participating in NAD synthesis were expressed at lower levels than the aforementioned. Collectively, these data revealed that human VIC exhibited a metabolic gene profile enriched in some glycolytic genes and the FA oxidation gene *ATGL*.

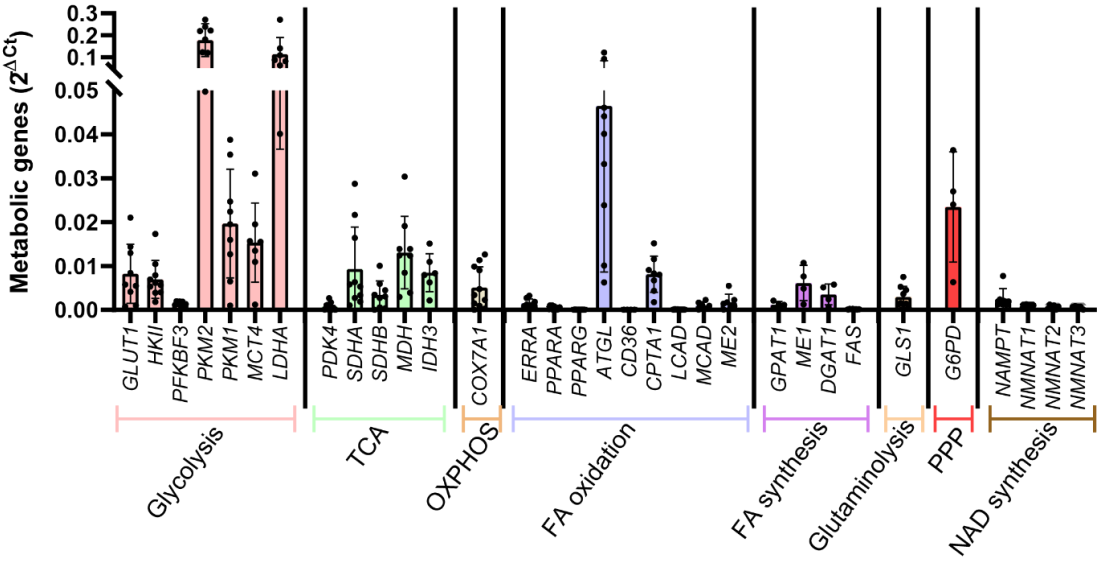

Figure 1. Expression levels of metabolic genes controlling the main anabolic and catabolic pathways in basal VIC. Transcript levels of metabolic enzymes were measured by qPCR in untreated VIC. Data are expressed as $^{2-\Delta Ct}$ (N=4-10). N indicates the number of VIC isolates obtained from independent valve donors.

Next, to measure the contribution and importance of glucose uptake in basal cell metabolism, we performed [U^{13}C]-glucose tracing assays (**Figure 2A**). Liquid chromatography-mass spectrometry results elucidated that the main metabolic fate of glucose was lactate, the end product of aerobic glycolysis. Glucose was readily metabolized into several metabolites. The incorporation of [U-^{13}C]-glucose carbon into intracellular lactate, 35 ± 10% (**Figure 2B**), and acetyl-CoA, 28 ± 3.2% (**Figure 2C**), was detected as early as 6h, further increased at 12h, and maintained until 72h. In contrast, a slower and lower incorporation of [U-^{13}C]-glucose carbon into the TCA metabolites succinic and citric acids, was found (**Figure 2D-E**).

On the other hand, glucose uptake seemed to be important for energy factor and reducing power production, as shown by a quick-6h incorporation of [U-^{13}C]-glucose into the ATP structure, which increased at 12h (**Figure 2F**). Notably, ATP was labeled in 5 carbons (M+5) corresponding to the ribose moiety. Additionally, results highlight the importance of glucose uptake in the synthesis of metabolic cofactors such as NAD and FAD, given the quick incorporation of [U-^{13}C]-glucose carbons into both cofactors, which was increased and maintained until 72h (**Figure 2G-H**). Notably, several labeled forms of NAD were detected, M+10 and M+5 species corresponding to one or two ribose moieties, respectively. Together, data revealed a basal glucose flux into glycolysis, energy production, and PPP for the synthesis of ribose-5-P (R5P).

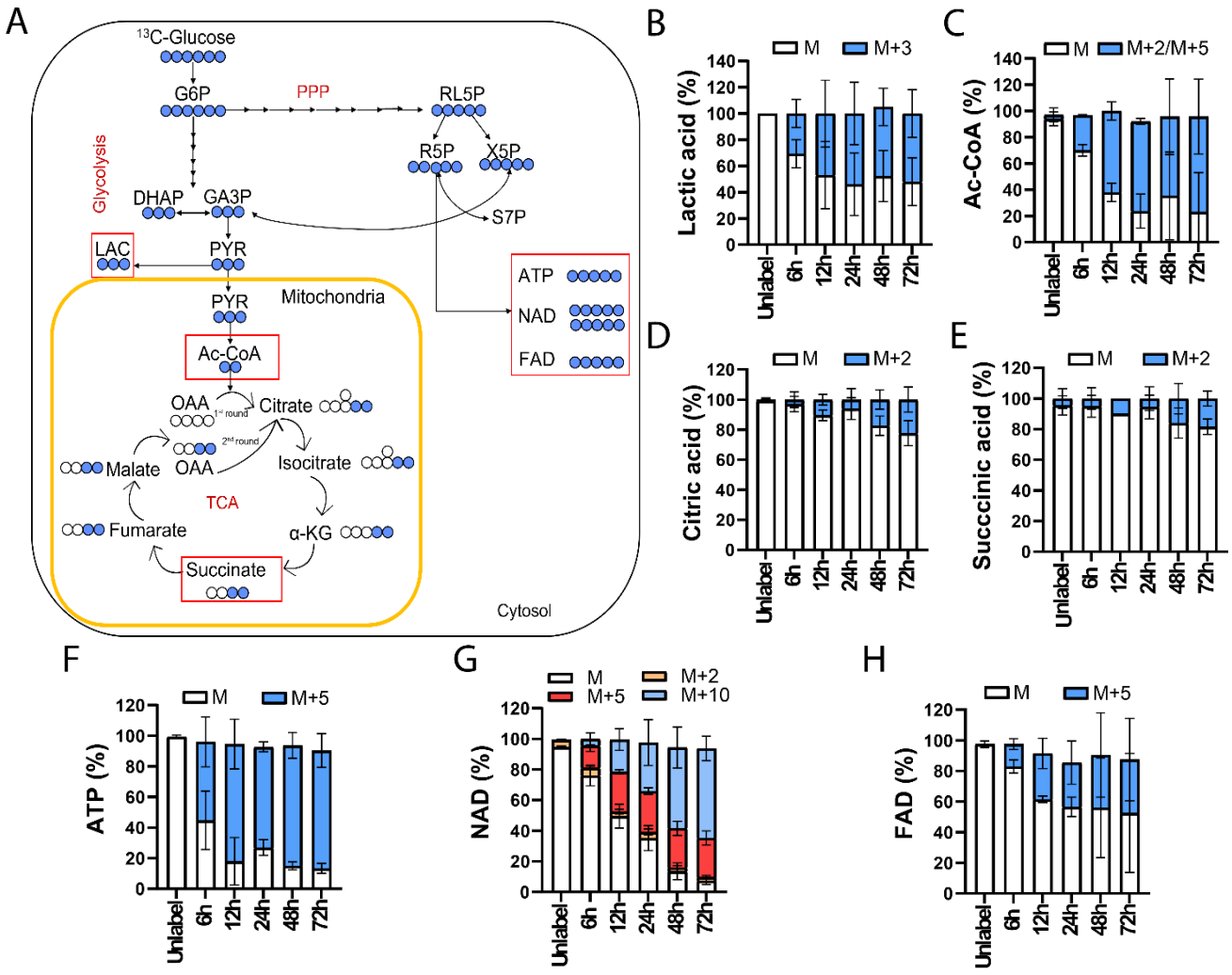

Figure 2. Glucose fluxes into glycolysis, energy production, and PPP in basal VIC. [U-^{13}C]-Glucose tracing analysis of untreated VIC by UPLC/MS. Cells were incubated in M199 supplemented with either 10 mM [U-^{13}C]-glucose for indicated times or [U-^{12}C]-glucose (unlabeled, 24h), the latest used as control of the natural presence of U-^{13}C in metabolites. (A) Schematic showing the primary labeling patterns of [U-^{13}C]-Glucose tracing into glycolysis, PPP, and TCA. (B-G) Graphics show the kinetics of the isotopologue distribution. Data are expressed as the percentage of U-13C incorporated into lactate M+3 (B), acetyl-CoA M+2/M+5 (C), and citric acid (D). succinic acid M+5 (E), ATP M+5 (F), NAD M+2, M+5, M+10 and M+2 (G), and FAD M+5 (G). Data are shown as the mean ± SD (N=3). N indicates the number of VIC isolates obtained from independent valve donors.

Next, real-time metabolic analysis of basal VIC using a Seahorse XFe24 analyzer was performed to assay the contribution of glycolysis and OXPHOS to ATP production. First, Seahorse ATP rate assay quantitation elucidated that ATP production was basally 54 ±10% from OXPHOS and 46±7% from glycolysis in VIC (**Figure 3**), indicating an equal reliance on OXPHOS and glycolysis for ATP generation in basal VIC.

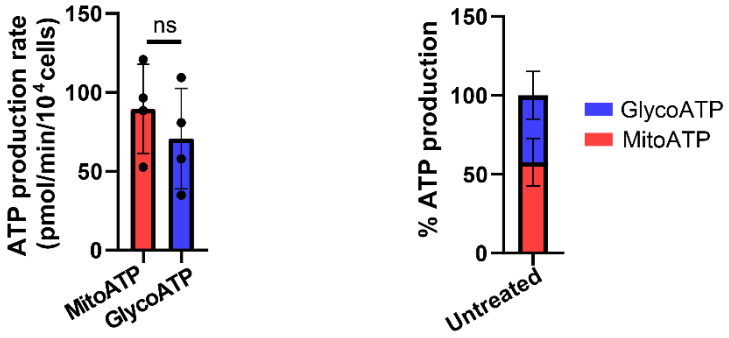

Figure 3. Basal VIC rely equally on OXPHOS and glycolysis for ATP production. Cells were analyzed using the Seahorse ATP rate assay. GlycoATP, indicates glycolytic ATP; MitoATP, mitochondrial ATP; ns, non-significant difference. Graph bars represent mean ± SD (N=4). N indicates the number of VIC isolates obtained from independent valve donors.

Later, to study the contribution of glutaminolysis to basal respiration and acidification, metabolic analysis was performed using Seahorse with acute BPTES injection, an inhibitor of glutaminolysis. Results did not demonstrate any influence of glutaminolysis inhibition on basal extracellular acidification rate (ECAR) values, but the oxygen consumption rate (OCR) was significantly decreased upon BPTES treatment, suggesting the basal contribution of glutaminolysis to OCR, but not to ECAR in VIC (**Figure 4**).

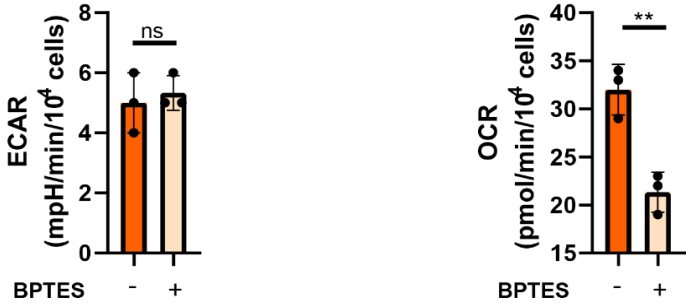

Figure 4. Basal VIC rely on glutaminolysis for mitochondrial respiration. Cells were plated in seahorse plates, and the Mito Stress assay was performed with an acute injection of 1 µM BPTES, a glutaminolysis inhibitor. Measures before and after the acute injection were compared to calculate the participation of glutaminolysis in ECAR and OCR. Data are expressed as the mean ± SD (N=3). N indicates the number of VIC isolates from independent valve donors; ns, non-significant differences; **, p<0.01. Student´s paired t test.

Collectively, the characterization of human VIC metabolism elucidated the abundance of some catabolism-related genes, particularly some glycolytic genes, the glucose uptake with fast carbon incorporation into glycolysis, mainly lactic acid, TCA, and PPP, as well as the reliance on glycolysis and mitochondrial respiration for energy production and on glutaminolysis for feeding the mitochondrial respiratory chain.

R.2- The role of inflammatory cytokines in the metabolic rewiring of human VIC

Several cytokines have been detected in stenotic lesions and related to pathogenic processes, i.e. TNF-α (Kaden et al., 2005 & Lee et al., 2020), TGF-β (Raddatz et al., 2019 & Yousefi et al., 2020), and IFN-α/γ (Parra-Izquierdo et al., 2018). Additionally, increasing evidence links inflammation and metabolic reprogramming not only to cancer but also to immune and cardiovascular disorders (reviewed in Kuhn et al., 2022 & O'Neil et al., 2016), and a metabolic shift from fatty acids to glucose has been reported in cardiomyocytes from patients undergoing CAVD (Heather et al., 2011). Taking this into account, we investigated whether these cytokines induce a metabolic rewiring in human VIC and if this effect was cytokine specific. Metabolic data from the Seahorse analyzer and the Seahorse Mito Stress assay showed that all tested cytokines significantly increased the extracellular acidification rate (ECAR) (**Figure 5A**), while no significant effect on oxygen consumption rate (OCR) (**Figure 5B**), although variability of response among patients. The metabolic profile revealed changes in the main energy source used by VIC exposed to cytokines. The energy map (OCR vs. ECAR plots) showed that all cytokines induced a shift in VIC to a more glycolytic phenotype (**Figure 5C**). Further characterization of VIC metabolism showed no significant alterations in maximal respiration (**Figure 5D**) upon cytokine stimulation but elucidated some cytokine-specific effects. While most cytokines did not alter proton leak, IFN-α specifically decreased it (**Figure 5E**). Also, non-mitochondrial oxygen consumption increased upon TGF-β, IFN-γ, and IFN-α treatment, but not under TNF-α conditions (**Figure 5F**). Moreover, ATP production coupled to OXPHOS was decreased upon IFN-γ and IFN-α treatment, but not by TNF-α, while a minor increase was measured upon TGF- β stimulation (**Figure 5G**).

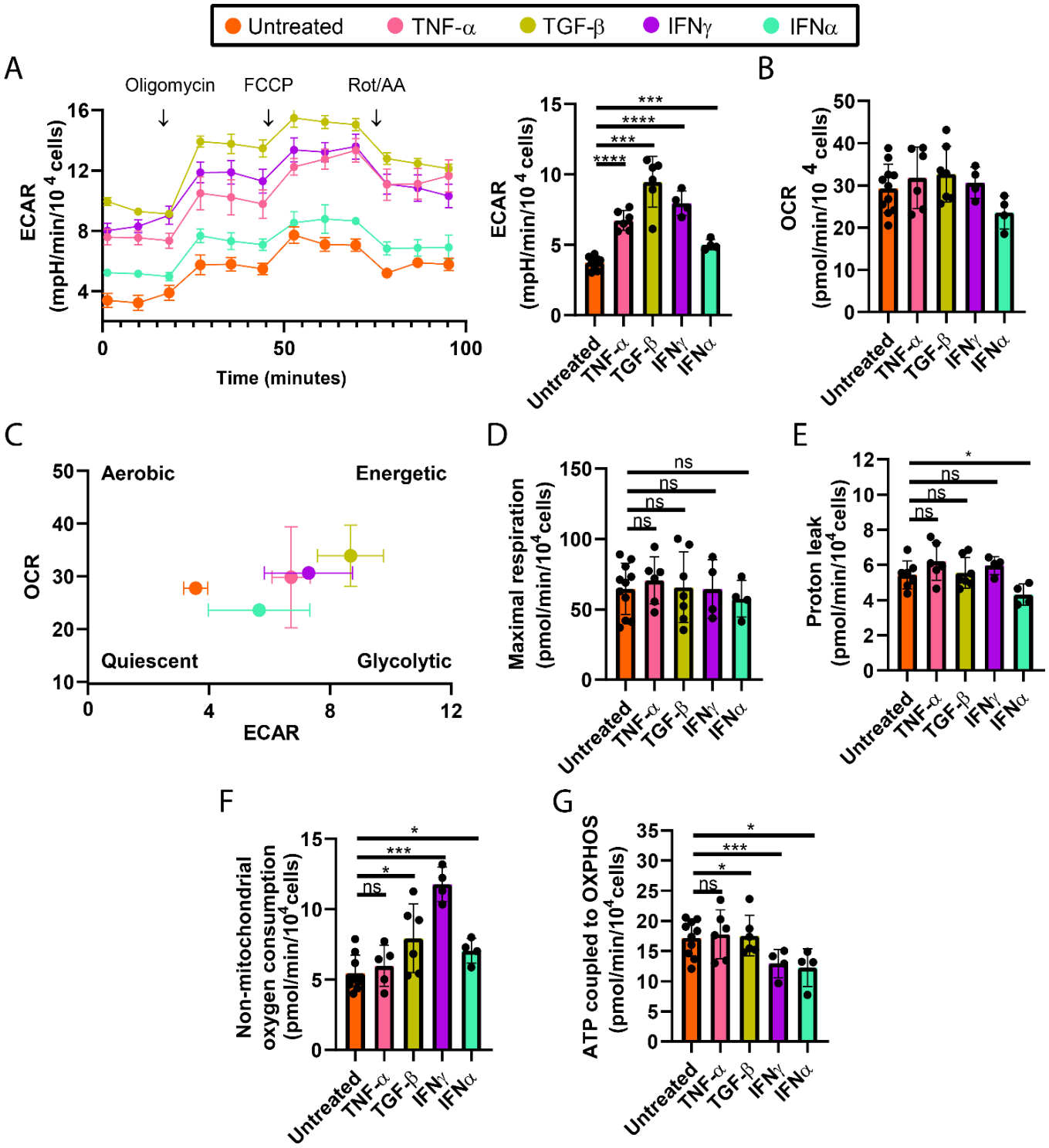

Figure 5. Metabolic reprogramming of VIC is induced by several inflammatory cytokines. Real-time metabolic analysis using Seahorse Cell Mito Stress Assay performed in VIC treated with 5 ng/mL TNF-α, 10 ng/mL TGF-β, 1 µg/mL IFN-γ, 100 ng/mL IFN-α, or vehicle for 24h. (A) Representative ECAR plot (N=5) and its quantitation. (B) Quantitation of OCR (N=5). (D) Energy map (OCR vs. ECAR plots). (D-G) Bar graph corresponding to maximal respiration (D) proton leak (E), non-mitochondrial oxygen consumption (F), and ATP production linked to OXPHOS (G). Data are expressed as mean ± SD (N=6/7). N indicates the number of independent cell isolates; ns, non-statistical significance; *, p<0.05; **, p<0.01. One-way ANOVA followed by Dunnett post-hoc test (vs. untreated).

Together, these data demonstrate that VIC exposed to inflammatory cytokines exhibited a glycolytic shift characterized by increased ECAR and no changes in OCR or maximal respiration. Additionally, data elucidated cytokine-specific effects on some parameters, i.e., proton leak, non-mitochondrial respiration, and ATP production coupled to mitochondrial respiration.

The next aim was to explore whether the co-stimulation of IFN-α/γ with the TLR4 ligand LPS, potentiated the metabolic effects of IFN type I and II, based on previous work of our laboratory linking IFN-TLR4 interplay on VIC calcification and HIF-1α stabilization (Parra-Izquierdo et al., 2018; 2019). Seahorse Cell Mito Stress assay showed no effect of LPS on ECAR or OCR in human VIC (**Figure 6A-B**). Notably, LPS further potentiated IFN-α- and IFN-γ-mediated increase in ECAR, being the effect of LPS + IFN-γ statistically significantly higher (**Figure 6A**) but did not change OCR (**Figure 6B**). Moreover, the energetic map revealed a shift into a more glycolytic phenotype, with maximal changes under co-stimulation with LPS + IFN-γ (**Figure 6C**). Further characterization of respiratory parameters obtained from Seahorse Mito Stress assay, showed non-significant alterations in maximal respiration upon cytokine-only stimulation or by co-stimulation with LPS and IFN-α, but a specific inhibitory effect by TLR4-IFNGR interplay (**Figure 6D**). Inflammatory effects in non-mitochondrial oxygen consumption were specific to IFN-AR, IFNGR and TLR4 activation but there was not a synergy when combining IFNs and LPS (**Figure 6E**). Finally, the downregulation of ATP production linked to OXPHOS seemed to be cytokine-specific and was not additionally altered by co-stimulation with LPS and IFNs (**Figure 6F**).

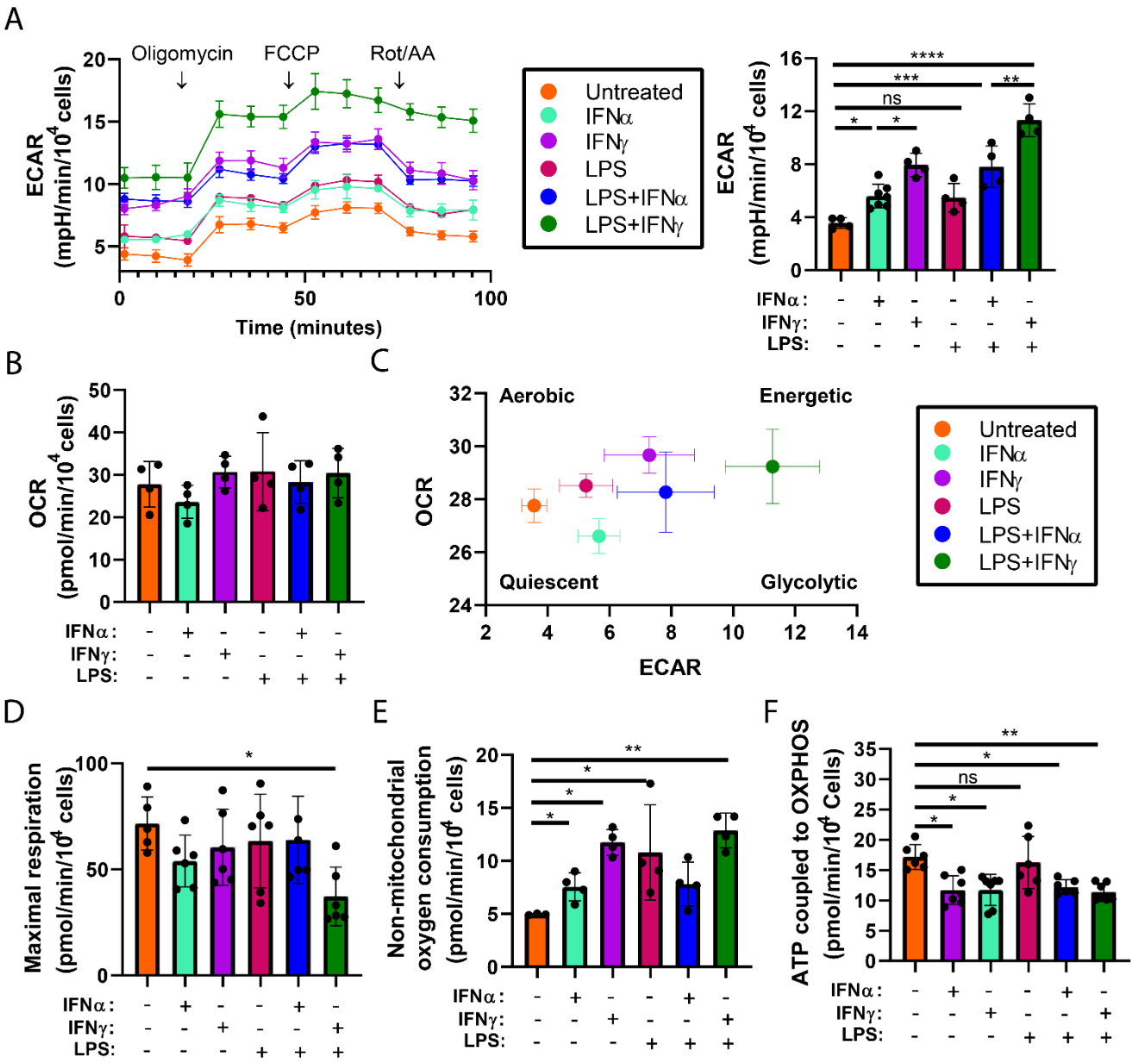

Figure 6. TLR4 activation potentiates the IFNGR/IFNAR-mediated glycolytic shift in VIC. Cells treated with 1 µg/mL IFN-γ, 100 ng/mL IFN-α, and 100 ng/mL LPS for 24h were analyzed with a Seahorse Cell Mito Stress assay. (A) Representative ECAR plot and quantitation (N=4). (B) Quantitation of OCR upon (N=4). (D) Energetic map showing ECAR vs. OCR. (E) Bar graph corresponding to the calculation of maximal respiration, (E) non-mitochondrial oxygen consumption, and (F) ATP production linked to OXPHOS. Data are expressed as the mean ± SD (N=4/6). N indicates, the number of independent cell isolates; ns, non-significant differences; *, $p<0.05$; **, $p<0.01$. One-way ANOVA followed by Dunnett post-hoc test (vs. untreated).

Data in this section demonstrated that human VIC exposed to inflammatory cytokines exhibited a glycolytic shift characterized by increased ECAR and cytokine-specific effects on some parameters. Additionally, the TLR4 ligand LPS induced no metabolic changes, but potentiated the IFN-mediated glycolytic shift in VIC, with the co-stimulation of IFN-γ with LPS exhibiting the maximal changes in glycolysis and maximal mitochondrial respiration.

R.3- Metabolic reprogramming triggered by the interplay of TLR4 and IFNGR signaling routes in human VIC

Due to the cooperation between IFNGR and TLR4 signaling on HIF-1α stabilization reported in human VIC (Parra-Izquierdo et al., 2019) and on metabolic rewiring to a more glycolytic phenotype described in Section R2, we aimed to characterize in depth the metabolic shift in VIC exposed to a highly inflammatory milieu, co-stimulation with LPS and IFN-γ, and the impact on VIC physiopathology.

R.3.1- LPS and IFN-γ team up to enhance glucose metabolism via glycolysis in VIC

Since Seahorse data from **Figure 6** showed that co-stimulation of VIC with LPS and IFN-γ exhibited the highest metabolic shift, increase in ECAR, and no significant changes in OCR, for the rest of the study, we used these inflammatory stimuli to investigate more in depth the metabolic shift in VIC. First, we performed qPCR analysis to quantify the expression levels of HIF-1α-regulated metabolic genes, including several glycolytic genes, such as glucose transporter-1 (*GLUT1* or *SLC2A1*), and glycolytic enzymes i.e., fructose-2,6-bisphosphatase 3 (*PFKFB3*), hexokinase 2 (*HKII*), pyruvate kinase 2 (*PKM2*), and lactate dehydrogenase A *(LDHA*). Results showed an upregulated expression of glucose transporter (*GLUT1*), key glycolytic enzymes as well as lactate transporter (*MCT4*) gene, while no significant changes in *LDHA* expression (**Table 1**).

Table 1. Inflammatory-induced changes in glycolytic gene expression in VIC. RNA from VIC activated or not with LPS + IFN-γ was analyzed by qPCR. Relative transcript levels were calculated based on the $2^{-\Delta\Delta Ct}$ method, where ΔCt is the Ct gene-Ct GAPDH. Fold-change data vs. untreated conditions; mean ± SD (N=8-10). Student's unpaired t-test. Ns, non-significant differences; *, p<0.05; **, p<0.01.

GENE	FOLD CHANGE	STATISTICS
SLC2A1 (GLUT1)	2.89 ± 0.97	**
HKII	2.48 ± 0.60	*
PFKFB3	3.94 ± 1.67	**
PKM2	2.40 ± 0.89	**
LDHA	1.39 ± 0.95	ns
SLC16A4 (MCT4)	4.72 ± 1.28	*

Next, the comparison of the two main isoforms of PKM enzyme, PKM1 and PKM2, was performed. The first one is found to be upregulated in healthy tissues demanding a massive supply of energy, such as the heart, and the second is expressed in proliferating cells, especially in tumors (reviewed in Puckett et al.2021). qPCR analysis revealed that *PKM2* is the most abundant isoform in basal VIC (**Figure 7A**), and in contrast to *PKM2* (**Table 1**), *PKM1* expression was not altered upon cell activation (**Figure 7B**). Furthermore, WB analysis revealed an increase in PKM2 phosphorylation upon cell stimulation (**Figure 7C**) and its detection in both cytoplasmic and nuclear fractions (**Figure 7D**).

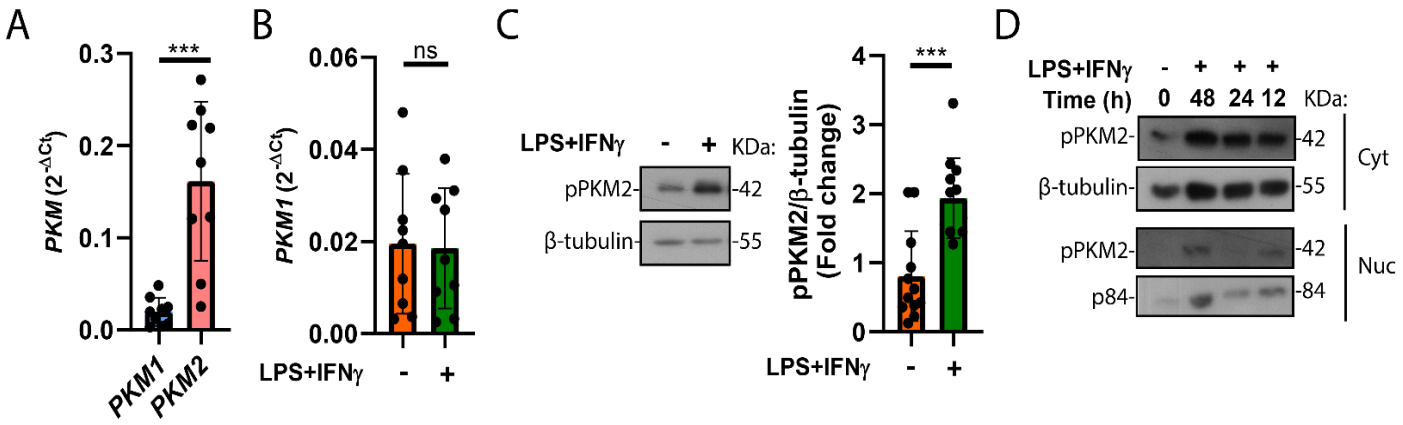

Figure 7. PKM2 is highly expressed in VIC and further increased upon treatment with LPS and IFN-γ. (A) Comparison of basal transcript levels of *PKM* isoforms. (B-D) Cells were activated with 100 ng/mL LPS and 1 µg/mL IFN-γ for 24h: *PKM1* transcript levels (B). Western blot analysis of PKM2 phosphorylation in total cell extracts (C). Cytoplasmic (Cyt) and nuclear (Nuc) protein extracts (D) (representative of N=3). Data are represented as mean ± SD (N=8/9). Ns, non-significant differences; ***, p<0.001. Student's unpaired t-test.

To further assess whether the glycolytic gene expression alterations had a functional effect on glycolysis and given the lack of effects in OCR and the great variability among patients, Seahorse analysis was performed to confirm these results in a higher number of VIC from independent patients (**Figure 8 A-C**).

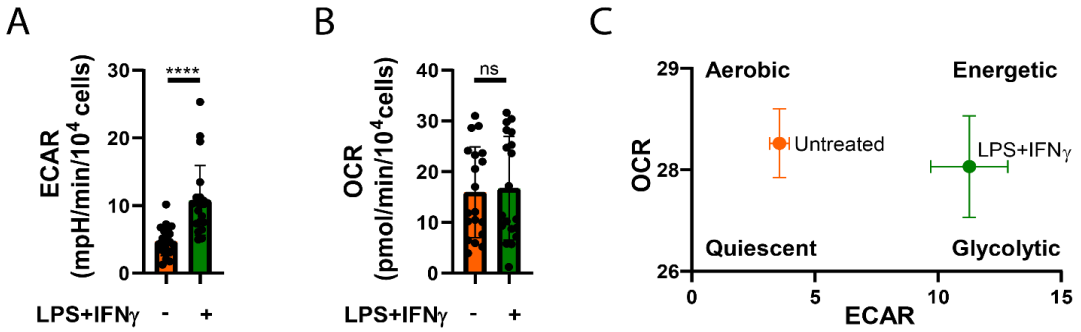

Figure 8. Co-stimulation of VIC with LPS and IFN-γ generates a strong metabolic shift to a glycolytic phenotype. Real-time metabolic analysis using Seahorse Cell Mito Stress Assay was performed in VIC treated with 100 ng/mL LPS and 1 µg/mL IFN-γ for 24h. (A) Representative ECAR plot (N=5). (B) Quantitation of ECAR (N=21). (C) Quantitation of OCR (N=21). (D) Energetics map (ECAR vs. OCR). Ns, non-significant differences; ****, p<0.0001. Student's unpaired t-test.

Next, since the sources of ECAR can include not only lactate secretion and glycolytic proton efflux, but also mitochondrial transport chain proton efflux due to TCA activity, we aimed to elucidate the source of acidification in VIC exposed to inflammatory stimuli. Seahorse Glycolytic rate assay and Glycolysis Stress kit data indicated that the activation of TLR4 and IFNGR signaling increased basal glycolysis (**Figure 9A**), which includes the conversion of glucose to lactate, a metabolite with a crucial role in HIF-1α-driven aerobic glycolysis (reviewed in Vaupel et al., 2019). To determine whether this increase was due to both proton efflux and lactate secretion, further calculations using Seahorse analytics software and the extracellular lactate assay demonstrated that potentiation of both glycolytic proton efflux (**Figure 9B**) and lactate secretion (**Figure 9C**) contributed to the increased extracellular acidification under inflammatory conditions. Notably, %PER from glycolysis was high in basal VIC since ≈75% of protons were from glycolysis (**Figure 9D**),

thus suggesting the relevance of glycolysis in VIC basal bioenergetics. However, under an inflammatory milieu, the contribution of glycolysis further increased to nearly 95%. Moreover, other results suggested the increased relevance of glycolysis in an inflammatory milieu, including an upregulation in compensatory glycolysis upon VIC stimulation (**Figure 9E**), thus indicating the increased ability of VIC to fulfill energetic requirements when OXPHOS was inhibited. Finally, despite the increase in glycolysis and lactate secretion upon stimulation, glucose tracing experiments did not exhibit an increase in labeled intracellular lactate (M+3), in fact, a significant decrease was measured (**Figure 9F**), which is consistent with the increased secretion of lactate (**Figure 9C**).

As the main objective of metabolism is to generate energy, we next analyzed the levels of adenosine triphosphate (ATP), the most important molecule carrying and transferring energy (reviewed in Yin et al., 2021). In healthy differentiated cells, the main ATP source is OXPHOS, as it is the most efficient pathway, although a change in substrate use to aerobic glycolysis has been reported in tumors or highly proliferative cells. Notably, Seahorse ATP rate assay showed an increase in total ATP production upon inflammatory stimulation of VIC, and further revealed a switch in their main ATP source (**Figure 9G**). While basal VIC generated 55% of ATP from OXPHOS (mitoATP) and 45% from glycolysis (glycoATP), activated VIC exhibited decreased mitoATP, up to 23%, in favor of increased glycoATP, up to 77%.

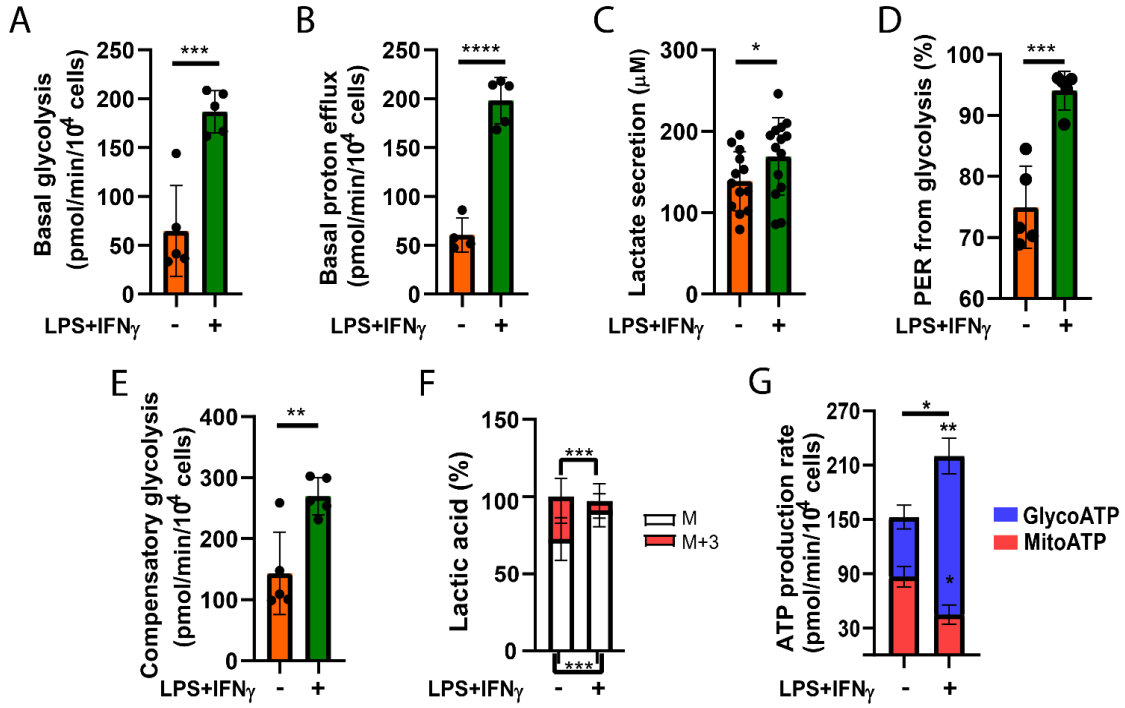

Figure 9. VIC metabolic rewiring is characterized by an increase in glycolytic function. Cells were activated with 100 ng/mL LPS and 1 µg/mL IFN-γ for 24h and then analyzed. Seahorse Glycolytic rate assay showed the contribution of glycolysis (A) and proton efflux (B) in ECAR increase (N=5). (C) Quantitation of extracellular lactate (N=12). (D) Seahorse Glycolytic rate assay calculations of the percentage of protons from glycolytic function and (E) compensatory glycolysis (N=5). (F) Glucose tracing data are expressed as the percentage of incorporation into M+3 lactic acid (N=6). (G) Characterization of ATP source under basal and activated conditions. MitoATP, mitochondrial ATP; glycoATP, glycolytic ATP. Student's unpaired t-test. *p<0.05; **p<0.01, ***p<0.001, ****p<0.0001.

Together, results from this section demonstrated an increase in glycolytic metabolism in VIC upon stimulation. The inflammation-induced increase in the glycolytic phenotype was characterized by an upregulation of glycolytic enzymes that led to increased proton efflux and lactate secretion, as well as both total and glycolytic ATP production.

R.3.2- Inflammatory mediators downregulate the rate-limiting enzyme of the oxidative arm of the pentose phosphate pathway and alter the reduction-oxidation homeostasis

Since co-stimulation with LPS + IFN-γ stabilizes HIF-1α in human VIC (Parra-Izquierdo et al., 2019), and HIF-1α activity has been demonstrated to influence the PPP (Zhao et al., 2010), the next aim was to investigate whether an inflammatory milieu would modulate the PPP. First, the expression of *G6PD*, the rate-limiting enzyme of the oxidative PPP, was evaluated. qPCR revealed a marked decrease in *G6PD* transcript levels (**Figure 10A**). To further confirm if oxidative PPP was affected, we measured $NADP^+$ and NADPH cofactors. Data revealed an increase in $NADP^+$/NADPH ratio due to a marked abrogation of NADPH levels upon immune stimulation (**Figure 10B**). Additionally, due to the role of PPP in reduction-oxidation (redox) homeostasis (Krüger et al., 2011), we sought to measure the expression of NADPH oxidases (NOX), strongly associated with ROS production (reviewed in Bradshaw et al., 2019). qPCR results showed that NOX expression was markedly blunted upon immune stimulation (**Figure 10C**), which agreed with the downregulation of NADPH levels. Moreover, since NADPH is known to be necessary for the conversion of oxidized glutathione (GSSG) to reduced glutathione (GSH), thus preventing oxidative stress, glutathione species were analyzed. [$U^{13}C$]-glucose tracing analysis (**Figure 10D**) disclosed an increased incorporation of glucose carbons into GSSG synthesis upon VIC activation, as indicated by the higher M+2/M ratio (**Figure 10E**). Consistent with these data, the quantitation of GSSG and GSH levels by a commercial kit showed an increase in GSSG/GSH ratios and further revealed higher GSSG levels upon stimulation (**Figure 10F**), which is in accordance with decreased levels of NADPH (**Figure 10B**). Together, these results highlighted the importance of glucose uptake in VIC redox homeostasis and suggested an increased glucose flux into TCA to generate glutamate that is necessary for GSSG synthesis.

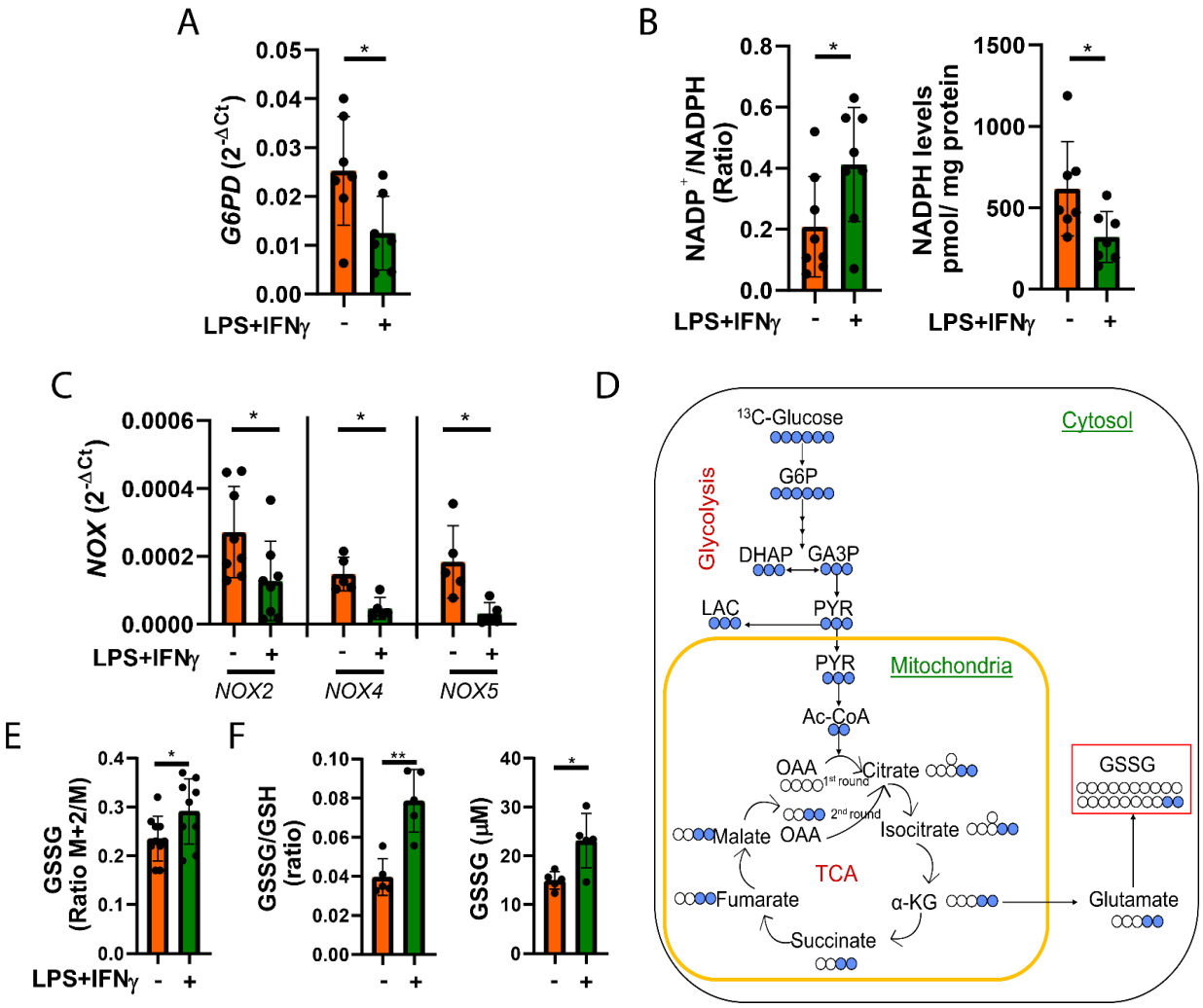

Figure 10. Inflammatory-induced metabolic changes include a reduction in PPP rate-limiting enzyme and alterations in the redox state of VIC. Cells were treated with 100 ng/mL LPS and 1 μg/mL IFN-γ for 24h or vehicle, and then analyzed. (A) Expression levels of *G6PD*. (N=7). (B) $NADP^+$/NADPH ratios and NADPH levels determined with commercial assays (N=6). (C) Expression levels of *NOX2*, *NOX4*, and *NOX5* (N=5). (D) Schematic showing the primary labeling patterns of [U-^{13}C]-glucose tracing in glycolysis, TCA, and GSSG synthesis. (E) [U-^{13}C]-Glucose incorporation into GSSG expressed as the ratio M+2/M (N=10). (F) The GSSG/GSH ratio and GSSG levels measured with commercial assays. *p<0.05; **, p<0.01. Student's unpaired t-test.

Glucose tracing analysis further revealed the induction of [U^{13}C]-glucose flux into the ribose moieties (M+5) of the nucleotide ATP upon VIC stimulation (**Figure 11A-B**). These data disclosed an increased glucose flux into R5P synthesis and suggest that the non-oxPPP may be the source of R5P, since the oxPPP seems impaired (**Figure 11A**). Notably, an enhanced [U^{13}C]-glucose incorporation into 5 (M+5) or 10 carbons (M+10) of NAD was identified, which was also probably due to the upregulation of [U^{13}C]-glucose incorporation into R5P synthesis (**Figure 11C**). Thus, since NAD^+ synthesis was altered upon stimulation, we decided to measure NAD^+/NADH. Measurement of NAD^+/NADH ratios elucidated a downregulation in NAD^+ levels in favor of NADH (**Figure 11D**).

As explained in the introduction, in mammals, NAD^+ is synthesized by the salvage pathway, the Preiss-handler and the *de novo* pathway, and nicotinamide mononucleotide adenylyltransferase (*NMNAT*) is the common ATP-dependent enzyme of both pathways leading to NAD^+ synthesis. We found that this enzyme was significantly downregulated in VIC upon stimulation (**Figure 11E**). In contrast, nicotinamide phosphoribosyltransferase (*NAMPT*), which is the key-limiting enzyme of the salvage pathway, was significantly increased in immune-activated VIC (**Figure 11F**).

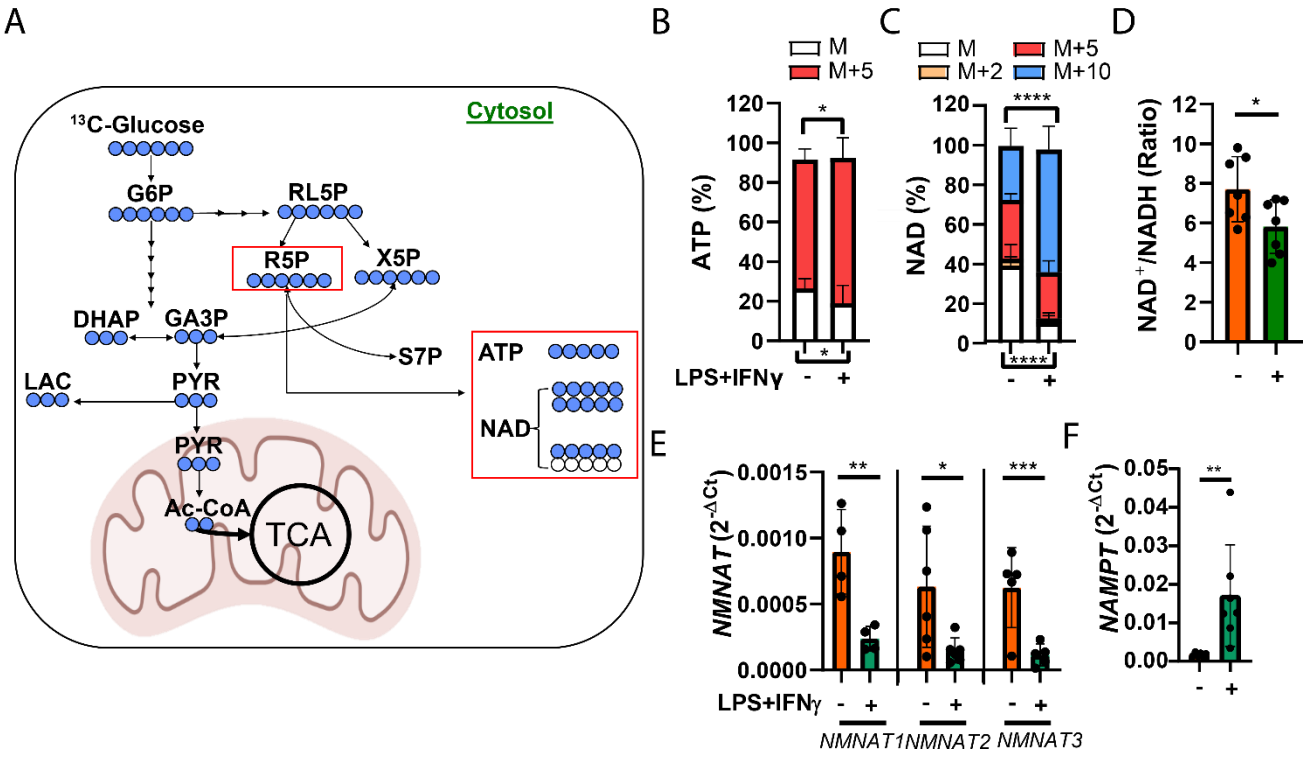

Figure 11. Metabolic rewiring by co-stimulation with LPS and IFN-γ is characterized by an increased glucose flux into the ribose moieties of nucleotides and cofactors. Cells were incubated with M199 media supplemented with 10% FBSi and 10 mM [U-^{13}C]glucose, activated with 100 ng/mL LPS and 1 µg/mL IFN-γ, and the extracted metabolites were analyzed by UPLC-MS. (A) Schema showing the primary labeling patterns of [U-^{13}C]-glucose tracing in glycolysis, PPP, and nucleotide and cofactor synthesis. (B-C) [U-^{13}C] incorporation to ATP M+5 (N=9) (B), NAD synthesis M+2, M+5 and M+10 (N=9) (C). (D) Quantitation of NAD levels, reduced and oxidized species, using commercial assays after 24h activation, expressed as NAD^+/NADH ratio (N=7). (E) Transcript levels of *NMNAT* isoforms (N=5): *NMNAT1, NMNAT2, and NMNAT3*. (F) Expression levels of the rate-limiting enzyme *NAMPT* (N=6). *p<0.05; **, p<0.01; ***, p<0.001; ****, p<0.0001. Student's unpaired t-test.

Once we confirmed that the homeostasis of redox mediators was disrupted in activated VIC, we aimed to assess its effects on VIC redox status. Seahorse Mito Stress assay data revealed that non-mitochondrial oxygen consumption was significantly increased in VIC activated with inflammatory stimuli for 24h (**Figure 12A**). Next, we measured reactive oxygen species (ROS) as they have been related to non-mitochondrial enzyme activity and non-mitochondrial oxygen consumption. DCFH-DA fluorescent probe demonstrated that co-stimulation with LPS and IFN-γ triggered the production of ROS (**Figure 12B**). To further characterize the role of inflammation in ROS production, we analyzed the expression of superoxide (SOD)-2, enzyme

catalyzing the conversion of O^{2-} to H_2O_2. Western blotting data showed increased expression upon inflammatory activation (**Figure 12C**).

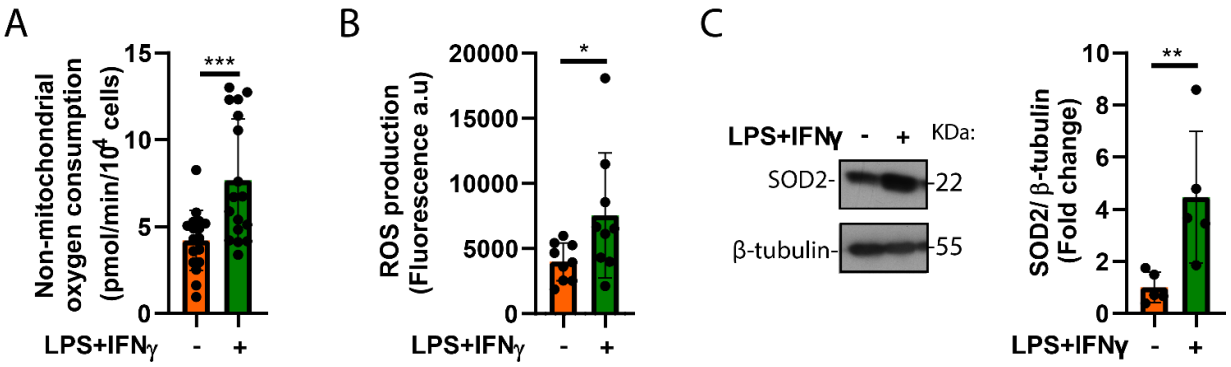

Figure 12. Non-mitochondrial oxygen consumption and ROS production are increased in VIC exposed to inflammatory stimuli. Cells were treated with 100 ng/mL LPS and 1 µg/mL IFN-γ for 24h and then analyzed. (A) Seahorse Mito Stress assay (N=21). (B) Fluorescent probe DCFH-DA for measuring total ROS production. Data were expressed as fluorescence a.u. (N=9). (C) Western blot analysis of SOD2 expression (N=5). Data are expressed as the mean ± SD. *p<0.05; **p<0.01, ***p<0.001. Student's unpaired t-test.

Altogether, results from this section unveiled an inflammatory-induced dysregulation of PPP characterized by the decrease of the rate-limiting enzyme of the oxidative arm, thus altering redox homeostasis. In addition, the non-oxidative arm seemed to be active and upregulated, given the increased glucose carbon incorporation in the ribose moieties of nucleotides and cofactors.

R.3.3- Inflammatory insults favor the entrance of pyruvate into TCA cycle and accumulation of metabolic intermediates

Glycolysis generates pyruvate that can diffuse into the mitochondria and enter the TCA or citric acid cycle (**Figure 13A)**, which generates ATP and TCA related metabolites like fumarate and succinate. Taking this into account, we sought to investigate the status of TCA in VIC exposed to inflammatory conditions. Real-time metabolic analysis using Seahorse Glycolytic rate assay, showed an increase in non-glycolytic acidification (**Figure 13B**), in addition to the glycolytic acidification previously shown (**Figure 8-9**), suggesting an increase in ECAR due to TCA activity. Next, we used fluxomic analysis to trace the uptake of [U-^{13}C]-glucose into the TCA cycle. Data showed a low but consistent increase of [U-^{13}C] incorporation into M+2 and M+5 isotopologues of acetyl-CoA upon LPS + IFN-γ treatment (**Figure 13C**). Additionally, glucose carbon incorporation into M+2 isotopologue of citric acid when expressed as % of incorporation was not affected by cell activation, but the M+2 levels were significantly increased comparing M+2 citrate levels in untreated versus activated VIC (**Figure 13D**). Additionally, an increase of [U-^{13}C]-glucose incorporation into succinic acid synthesis was also detected, in both cases, when calculating % of incorporation, but also M+2 succinic acid upon inflammatory treatment (**Figure 13E**). In contrast, no changes in OAA levels were observed in the presence of inflammatory insults (**Figure 13F**).

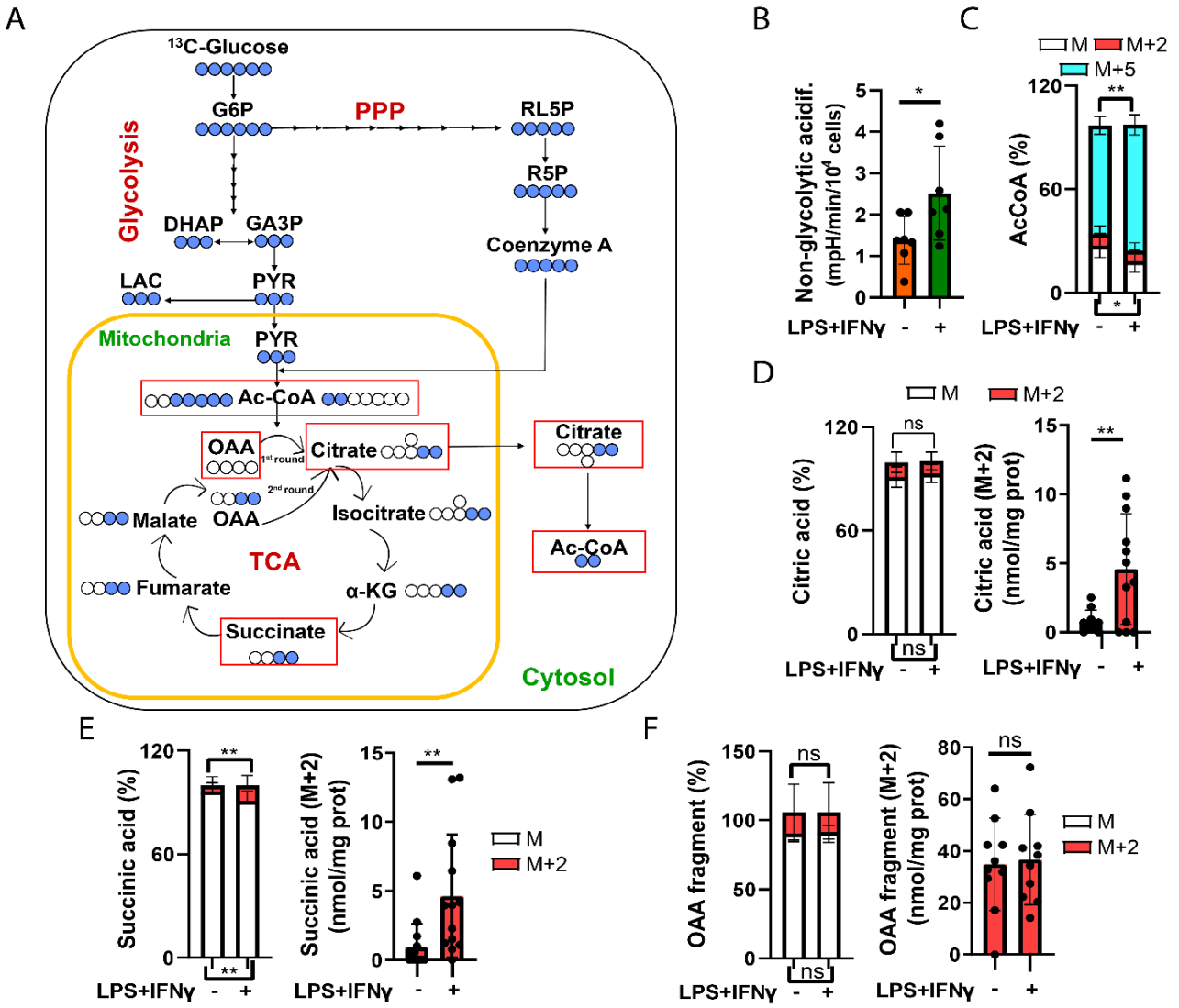

Figure 13. Inflammation-induced metabolic rewiring is characterized by an increased accumulation of some TCA metabolites. (A) Schema showing the glucose catabolism and primary labeling patterns of glucose tracing. (B) VIC were treated with 100 ng/mL LPS and 1 µg/mL IFN-γ for 24h and analyzed using the Seahorse glycolytic stress kit. (C-F) Metabolites extracted from VIC incubated with 10 mM [U-^{13}C]-glucose and activated for 24h were analyzed by LC-MS analysis. The labeled fractions of acetyl-CoA (M+5, M+2) (C), and the label fraction and levels (nmol/mg protein) of: citric acid (M+2); (D) succinic acid (M+2); (E) oxaloacetate (AAA; M+2) (F). Ns, non-significant difference. *p<0.05; **, p<0.01. Data are expressed as mean ± SD (N=9). Student's unpaired t-test.

Acetyl-CoA, a metabolite produced during glucose catabolism to fuel the TCA cycle, which is the essential building block for FA synthesis, is metabolized in the mitochondria to citrate, which can then go out to the cytosol, where it can be converted to acetyl-CoA by the enzyme ATP citrate lyase (ACLY). Thus, to investigate the potential fate of acetyl-CoA in VIC exposed to inflammatory stimuli, we analyzed the activation of ACLY. Western blot analysis of whole cell extracts from VIC revealed a significant increase in the phosphorylated form of ACLY in VIC treated with LPS + IFN-γ (**Figure 14A**), suggesting the activation of ACLY and the subsequent upregulation of cytosolic acetyl-CoA production. The analysis of cytosolic and nuclear

protein extracts further showed an inflammation-induced increase of p-ACLY in the cytoplasm (**Figure 14B**), where it produces acetyl-CoA for fueling FA synthesis and histone acetylation.

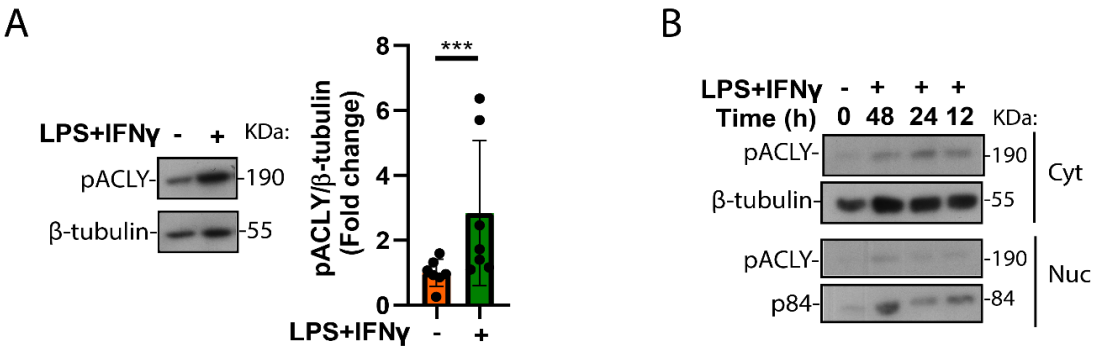

Figure 14. ACLY phosphorylation in the cytosol increases upon inflammatory activation. VIC were treated with 100 ng/mL LPS and 1 µg/mL IFN-γ for 24h and the p-ACLY was analyzed by WB. (A) Analysis of whole cell extracts (N=7). (B) Analysis of cytoplasmic (Cyt) and nuclear (Nuc) protein extracts. Image is representative of N=3. Data are expressed as mean ± SD. ***p<0.001. Student's unpaired t-test

Since recent evidence showed that in addition to the role of TCA in metabolite production, it is also important in NADPH mitochondrial production due to the activity of enzymes in canonical and non-canonical TCA (reviewed in Bradshaw et al., 2018), we aimed to evaluate in VIC the expression of relevant TCA enzymes. qPCR results disclosed the downregulation of genes involved in canonical TCA, i.e., pyruvate dehydrogenase kinase (*PDK4*), a negative regulator of the entrance to TCA, isocitrate dehydrogenase 3 (*IDH3*), and malate dehydrogenase 2 (*MDH2*), as well as the malic enzyme 1 (*ME1*), participating in non-canonical TCA (**Table 2**). In contrast, no transcriptional changes in succinate dehydrogenase subunits A (*SDHA*), B (*SDHB*), or *ME2* were observed upon stimulation (**Table 2**).

Table 2. Inflammatory-induced changes in the expression of genes encoding TCA enzymes in human VIC. RNA from untreated and LPS + IFN-γ-activated VIC was analyzed by qPCR. Relative transcript levels were referred to the Ct of GAPDH and the Ct of untreated conditions. Data are expressed as mean + SD (N=8). Student's unpaired t-test. *p<0.05, **p<0.01, ns; non-significant.

GENE	FOLD CHANGE	STATISTICS
PDK4	0.26 ± 0.06	*
IDH3	0.35 ± 0.05	**
SDHA	1.04 ± 0.27	ns
SDHB	0.99 ± 0.89	ns
MDH2	0.61 ± 0.14	*
ME1	0.32 ± 0.07	*
ME2	0.80 ± 0.19	ns

Altogether, data from this section suggested the upregulation of pyruvate entrance to mitochondria for the TCA cycle and metabolite production that could serve as biomass for cell proliferation and lead to

HIF-1α stabilization in VIC co-stimulated with LPS and IFN-γ. Additionally, the activation of ACLY in the cytosol suggested the inflammatory-induced production of cytoplasmic acetyl-CoA.

R.3.4- Inflammatory stimuli decrease respiratory capacity and impair mitochondrial ATP production

Next, we assessed mitochondrial metabolism, the main source of cellular energy in the form of ATP, since alterations in OXPHOS have been associated with disease (reviewed in Vaupel et al., 2019). First, we evaluated the expression levels of cytochrome C oxidase (*COX7A1*), which encodes complex IV of the respiratory mitochondrial chain, since HIF-1α is reported to upregulate the expression of *COX7A1* (Fukuda et al., 2007). qPCR analysis revealed a decrease in *COX7A1* transcript levels upon VIC activation in response to inflammatory stimuli (**Table 3**). In addition, since mitochondrial function has been related to mitochondrial biogenesis in contexts such as myofibroblast differentiation (Bernard et al., 2015), we assessed the expression of the main marker of mitochondrial biogenesis, *PGC1α* gene (*PPARGC1A1*), and found no alterations upon VIC stimulation (**Table 3**)**.**

Table 3. LPS + IFN-γ-induced downregulation of cytochrome C oxidase gene in human VIC. The relative expression of the indicated genes is expressed as $2^{-\Delta\Delta Ct}$ where ΔCt is the Ct gene-Ct GAPDH, later referred to Ct of untreated. Data are expressed as mean ± SD (N=8). Student's unpaired t-test. *p<0.05, ns; non-significant.

GENE	FOLD CHANGE	STATISTICS
COX7A1	0.42 ± 0.13	*
PPARGC1A1	1.05 ± 0.45	ns

To assess mitochondrial respiration in depth, we performed Seahorse Mito Stress assays (**Figure 15A**). The results revealed the lack of changes in basal OCR upon stimulation (**Figure 15B**), in accordance with the lack of alteration of the mitochondrial biogenesis marker (**Table 3**)**.** In contrast, activated VIC significantly decreased their maximal respiration capacity (**Figure 15B**), which is the maximal oxygen consumption rate achieved by the injection of the uncoupling agent FCCP that mimics a physiological energy demand by stimulating the respiratory chain to operate at full capacity. In addition, a decrease in spare respiratory capacity upon VIC activation was measured (**Figure 15B**), indicating the lack of flexibility of activated VIC to respond to an energetic demand and denoting that they were working less close to their maximal respiration. Notably, mitochondrial ATP production (OXPHOS-ATP) significantly decreased upon VIC stimulation (**Figure 15B**). Considering that basal OCR did not change while the final OXPHOS product, ATP, decreased, the Mito stress assay allowed the calculation of two other parameters, helping to elucidate a potential ineffective respiration. Data disclosed a tendency to increase proton leak, which could lead to an impaired mitochondrial membrane potential (**Figure 15B**) accompanied by a significant abrogation of the coupling efficiency between ETC and OXPHOS after VIC stimulation (**Figure 15C**).

The next goal was to assess the role of ETC in metabolic switch, particularly the reliance of activated and untreated VIC in complexes I/III and ATP synthase for oxygen consumption. OCR measurements after

rotenone/antimycin injection showed a reduced dependency on complex I/II for oxygen consumption after VIC activation (**Figure 15D**), suggesting a potential damage induced by inflammatory agents. Additionally, activated VIC exhibited a decreased dependency on ATP synthase for oxygen consumption (**Figure 15D**). Together, these data supported the notion of inflammatory-induced alteration of mitochondrial respiration.

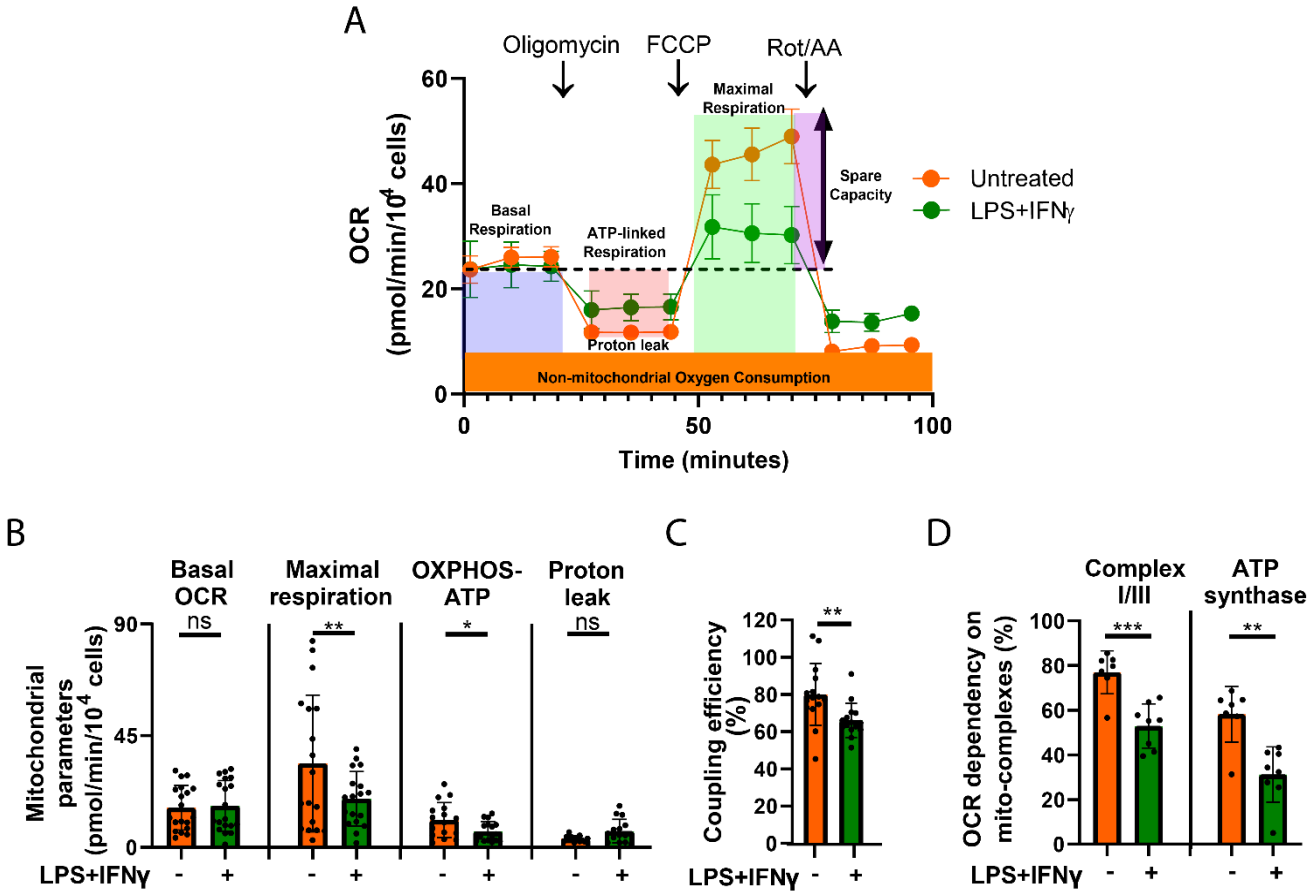

Figure 15. Co-stimulation with LPS and IFN-γ does not affect basal OCR but alters mitochondrial complexes and decreases ATP production in human VIC. (A) VIC were treated with 100 ng/mL LPS and 1 µg/mL IFN-γ for 24h and then analyzed using Seahorse Mito Stress metabolic analysis. (B) Bar graph corresponding to the calculation of basal OCR, maximal respiration, ATP production linked to OXPHOS and proton leak (N=21). (C) Bar graphs corresponding to coupling efficiency (%) (N=10). (D) OCR measures after oligomycin and rot/AA injection were referred to basal OCR for calculating the percentage of reliance in respiratory complexes (N=7/8). Data are expressed as the mean ± SD. Ns, non-significant differences; *, p<0.05; **, p<0.01; ***, p<0.001. Student's unpaired t-test.

Taken together, our data suggested that mitochondrial respiration was partially altered upon activation of VIC, and in consequence, ATP production linked to mitochondrial respiration was reduced.

R.3.5- Glutaminolysis is necessary to fulfill cell energy requirements upon inflammatory activation

Since glutamine is highly present in blood and is a key anaplerotic substrate used by cells to replenish the TCA cycle, and thus participates in ATP synthesis (Altman et al., 2016), we investigated the role of glutaminolysis in VIC. Glutamine is metabolized via glutaminolysis and converted to glutamate by the

mitochondrial enzyme glutaminase (*GLS1*) (**Figure 16A**). qPCR analysis in VIC showed a decrease in transcript levels of the first enzyme metabolizing glutamine, *GLS1*, upon exposure to LPS + IFN-γ (**Figure 16B**).

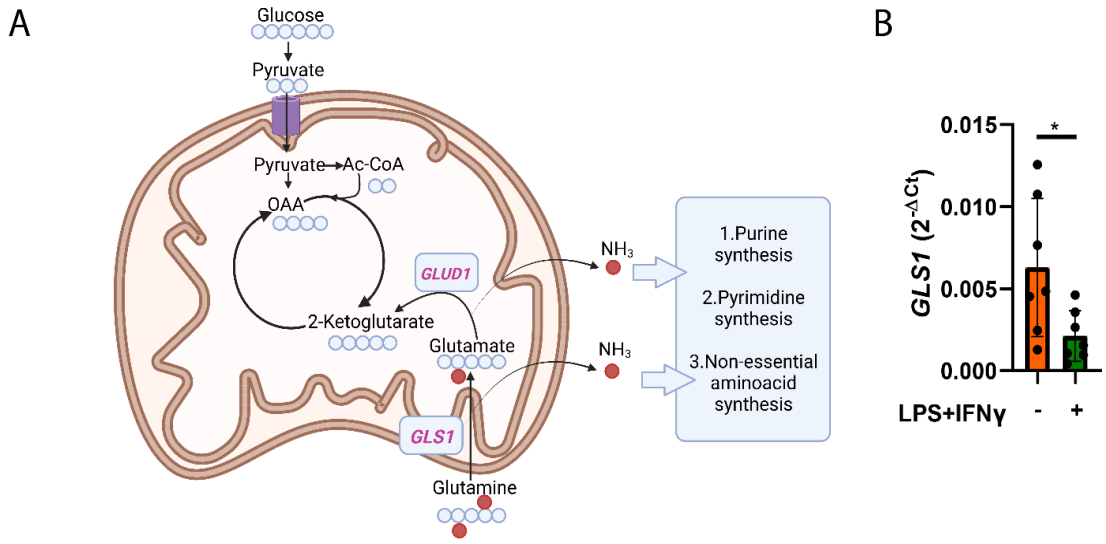

Figure 16. The rate limiting enzyme of glutaminolysis is transcriptionally downregulated in VIC. (A) Schema of glutamine metabolism. (B) VIC were treated with 100 ng/mL LPS and 1 µg/mL IFN-γ for 24h and then transcript levels of *GLS1* were measured by qPCR. Data are expressed as mean ± SD (N=7). *p<0.05. Student's unpaired t-test.

To further characterize the role of glutaminolysis in the inflammation-induced metabolic rewiring in VIC, we used BPTES, a GLS1 inhibitor. Seahorse metabolic analysis data showed a significant decrease of ECAR when glutaminolysis was abrogated in activated VIC, but not in untreated cells (**Figure 17A**). In contrast, OCR was significantly downregulated by BPTES inhibitor in both basal and activated VIC (**Figure 17B**). Interestingly, the contribution of glutaminolysis to the OCR significantly increased upon stimulation (**Figure 17B**). Notably, BPTES reduced the levels of ATP coupled to OXPHOS, thus indicating the participation of glutaminolysis in ATP synthesis in both untreated and inflammatory-activated VIC (**Figure 17C**).

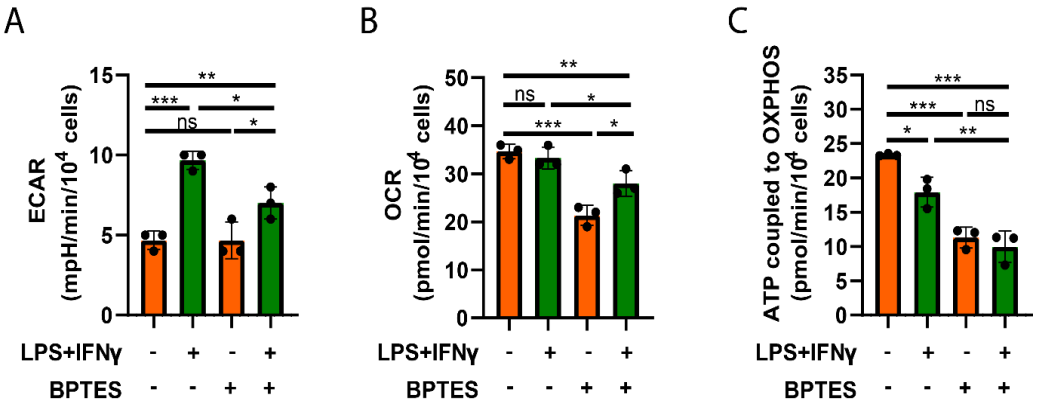

Figure 17. Glutaminolysis participates in extracellular acidification and oxygen consumption upon inflammatory stimuli-induced metabolic rewiring. VIC were plated in seahorse plates and then treated with 100 ng/mL LPS and 1 µg/mL IFN-γ for 24h. (B) ECAR levels of activated and non-activated cells in BPTES and vehicle-injected cells. (C) OCR levels of cells in BPTES injected and control. (D) ATP production linked to OXPHOS in presence or absence of BPTES. Calculations were performed as detailed in M.11.2. Data are expressed as mean ± SD (N=3). Ns, indicates non-statistical significance. *p<0.05, **p<0.01, ***p<0.001. One-way ANOVA followed by Tukey post-hoc analysis.

Altogether, data showed that glutaminolysis played a role in maintaining mitochondrial respiration in activated and basal VIC, increasing its contribution upon immune stimulation. Additionally, glutaminolysis was relevant for extracellular acidification upon inflammatory activation.

R.3.6- Inflammatory environment and metabolic switch affect apoptosis pathways in VIC

Because of the previously established relationship between HIF-1α, metabolic stress, ROS, and apoptosis (Mason et al., 2011), we aimed to study the link between metabolism and apoptosis in VIC. qPCR results indicated a marked induction in FAS ligand (*FAS)*, an extrinsic apoptotic mediator, but no alterations in caspase 8 (*CASP8*) transcription levels upon treatment of VIC with LPS and IFN-γ (**Table 4**). Additionally, upregulation of intrinsic pathway-participating genes, i.e., *BNIP3*, *PMAIP* (NOXA), *BAK*, and *BAX* was detected (**Table 4**). Finally, the common mediators of the extrinsic and intrinsic pathways were analyzed. Although the expression levels of caspase 9 (*CASP9*) were not altered (**Table 4**), the enzymatic activity of caspase 3/7 increased significantly upon VIC activation in a time-dependent manner (**Figure 18A**). To further characterize whether these changes led to apoptosis in VIC, flow cytometry analysis of Annexin V and propidium iodide staining was performed, and the results indicated an inflammation-induced increase in VIC apoptosis (**Figure 18B**).

Table 4. LPS + IFN-γ-induced changes in apoptotic gene expression in human VIC. Relative gene levels were calculated using the $2^{-\Delta\Delta Ct}$ method, where ΔCt is the Ct gene-Ct GAPDH and fold-change data vs. untreated. Data, mean + SD (N=7). Student's unpaired t-test. *p<0.05, **p<0.01, ns; non-significant.

GENE	FOLD CHANGE	STATISTICS
EXTRINSIC PATHWAY		
FAS	10.25 ± 2.5	*
CASP8	0.99 ± 0.40	ns
INTRINSIC PATHWAY		
BNIP3	3.87 ± 1.63	*
PMAIP1 (NOXA)	25.05 ± 3.96	**
BAK	3.47 ± 0.97	*
BAX	2.23 ± 0.65	*
COMMON EFFECTORS		
CASP9	0.87 ± 0.21	ns

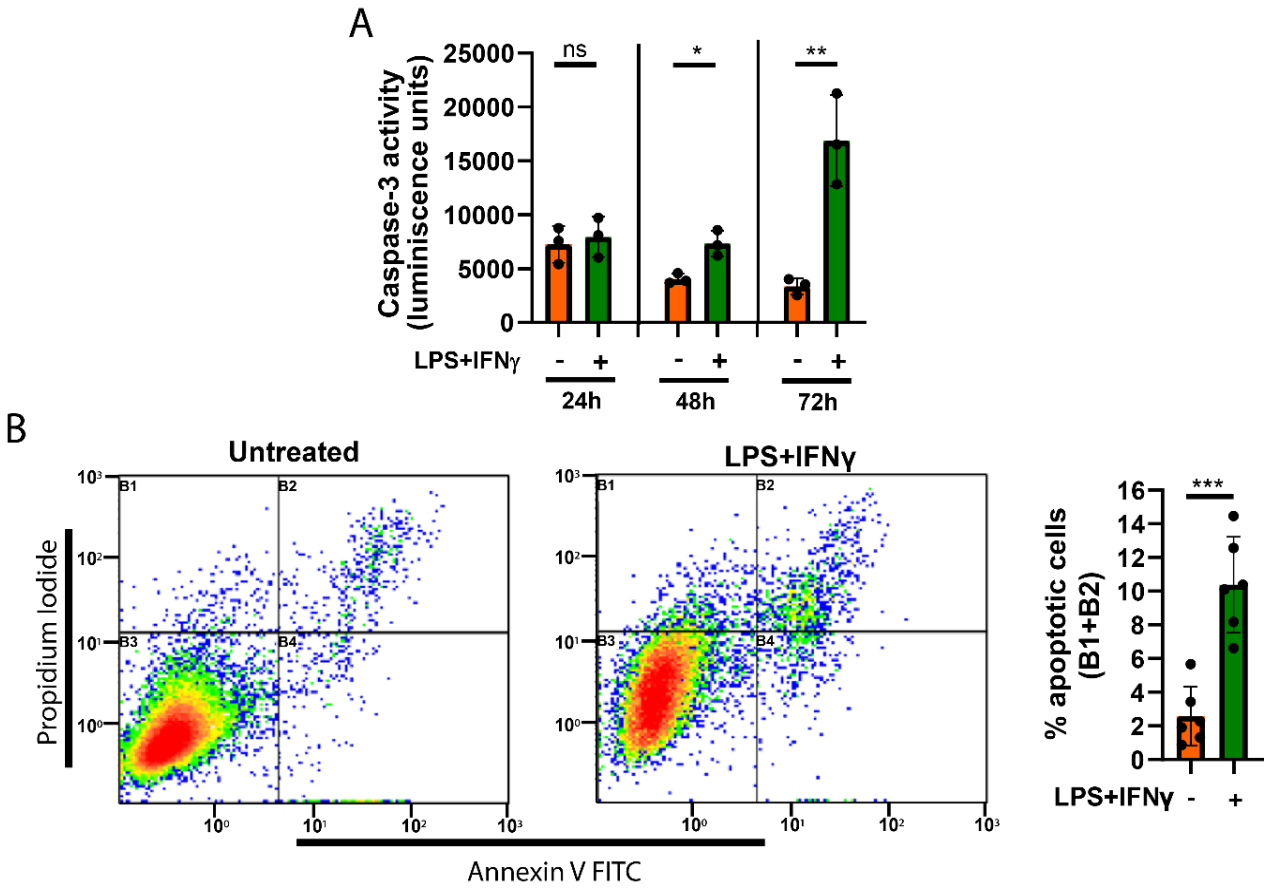

Figure 18. Extrinsic and intrinsic apoptotic pathways are upregulated by LPS + IFN-γ activation in VIC. Cells were treated with 100 ng/mL LPS and 1 µg/mL IFN-γ in calcification media for the indicated times (A) or 1 week (B). (A) Caspase 3/7 activity was determined at different time points (N=3). (B) Apoptosis assay by cytometric analysis of Annexin V-FITC and propidium iodide staining (N=6). Data are expressed as mean ± SD. Ns, non-statistical significance; *, p<0.05; **, p<0.01; ***, p<0.001. Student's unpaired t-test

Together, results demonstrated the LPS + IFN-γ-induced apoptosis in VIC and further suggested the TLR4-IFNGR interplay on the induction of both extrinsic and intrinsic apoptotic pathways.

R.4- Metabolic reprogramming triggered by TLR3 signaling and its cooperation with IFNGR

Poly (I:C), a TLR3 ligand, has been described to stabilize HIF-1α via JAK/STAT, and this effect is further potentiated by IFNGR signaling (Parra-Izquierdo et al., 2021). Based on this evidence, we aimed to study whether Poly (I:C) would cooperate with IFN-γ to promote a metabolic shift and to elucidate potential TLR-specific effects.

R.4.1- Poly (I:C) and IFN-γ team up to enhance glucose metabolism via glycolysis in VIC

To evaluate the metabolic changes exhibited by VIC under TLR3 and IFNGR signaling activation, Seahorse Mito Stress assay was performed. Poly(I:C), a synthetic dsRNA and TLR3 ligand, significantly increased ECAR (**Figure 19A**) in contrast to LPS (**Figure 8**). Conversely, Poly(I:C) potentiated the effects of IFN-γ in ECAR, showed no effect on OCR, and promoted a metabolic shift into a glycolytic phenotype (**Figure 19**) in a comparable manner to the TLR4 ligand LPS (**Figure 8**).

Next, we elucidated the contribution of glycolytic acidification to the total ECAR increase. Seahorse Glycolytic Stress and rate assays revealed an upregulated glycolytic function by Poly(I:C)+IFN-γ treatment since basal glycolysis (**Figure 19D**) and basal glycolytic proton efflux (**Figure 19E**) were significantly increased. Additionally, increased extracellular lactate by Poly(I:C)+IFN-γ demonstrated that, at least in part, extracellular acidification was due to enhanced lactate secretion (**Figure 19F**). Notably, the inflammatory milieu also induced the %PER from glycolysis; ≈ 95% of protons came from glycolysis upon stimulation (**Figure 19G**), as well as compensatory glycolysis (**Figure 19H**), supporting the relevance of glycolysis in VIC activated with Poly(I:C)+IFN-γ.

Next, we analyzed ATP levels. Seahorse ATP rate assay data unveiled an increased total ATP production, but also a switch in the main ATP source (**Figure 19I**); while basal VIC were generating 60% of ATP from OXPHOS (mitoATP) and 40% from glycolysis (glycoATP), activated showed a decrease in mitoATP up to 25% in favor of a significant upregulation of glycoATP up to 75%, similar to the data found in VIC co-stimulated with LPS and IFN-γ (**Figure 9**).

In summary, data disclosed a TLR3-specific effect on extracellular acidification, but similar interplay between TLR3/4 and IFNGR in the induction of a metabolic shift to glycolysis in VIC.

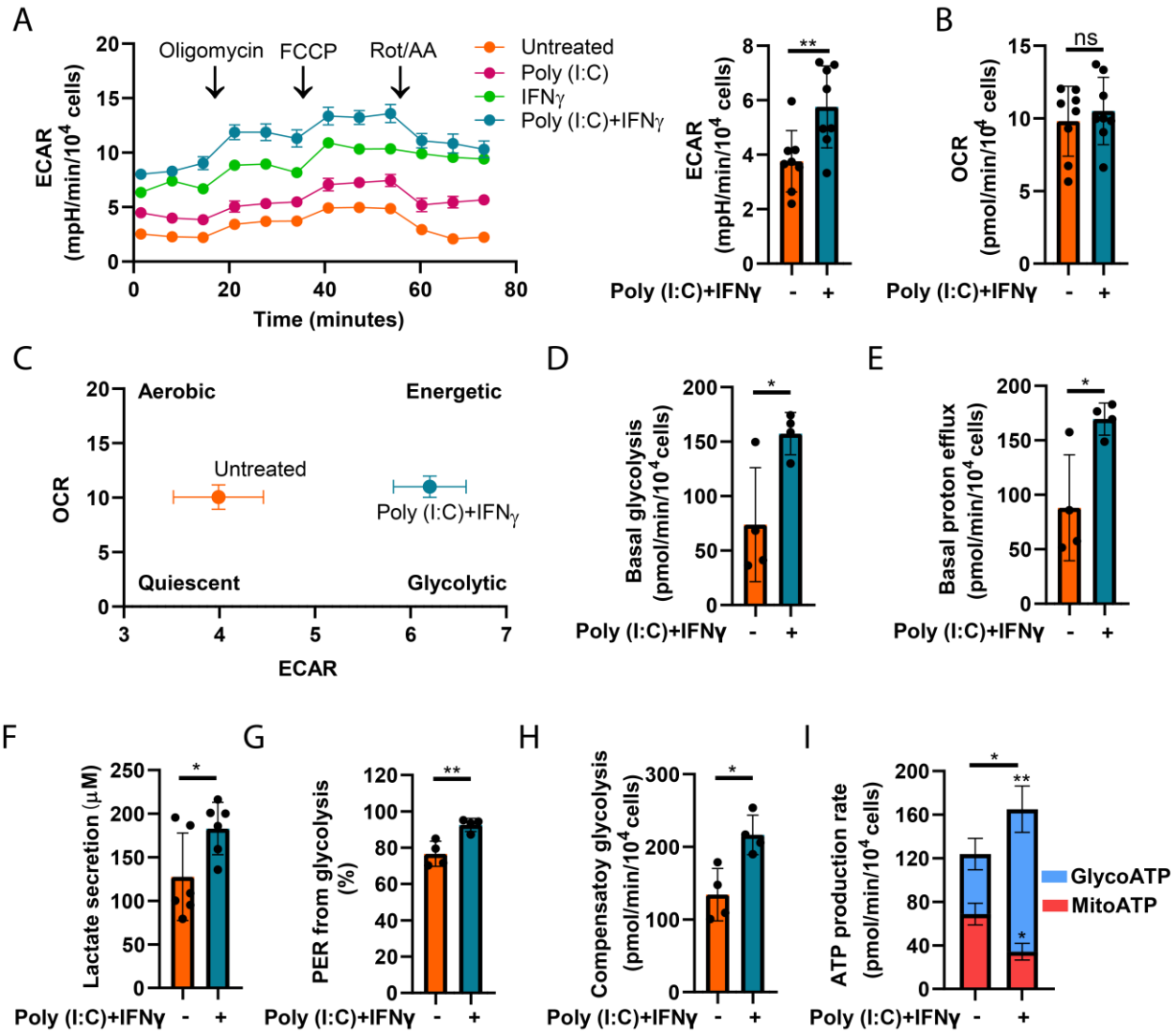

Figure 19. Co-stimulation with Poly (I:C) and IFN-γ inflammatory agents generates a metabolic shift to a glycolytic phenotype in human VIC. Real-time metabolic analysis using Seahorse was performed in VIC treated with 1 μg/mL Poly (I:C) and 1 μg/mL IFN-γ for 24h. (A) Representative ECAR plot (N=8) and its quantitation. (B) Quantitation of OCR (N=8). (C) Energetics map (ECAR vs. OCR). (D-E) Glycolytic rate assay to calculate (E) Basal glycolysis (N=4) and (E) proton efflux (N=4). (F) Quantitation of extracellular lactate (N=6). (G-H) Seahorse Glycolytic Rate assay to calculate (G) Percentage of protons due to glycolytic function and, (H) compensatory glycolysis (N=4). (I) Seahorse ATP rate assay to calculate ATP production (N=5). Data are expressed as the mean ± SD. glycoATP, indicates glycolytic ATP; mitoATP, mitochondrial ATP; ns, non-significant differences; *. p<0.05; **, p<0.01. Student's unpaired t-test.

R.4.2- Poly (I:C) and IFN-γ affect pentose phosphate pathway metabolite synthesis and alter redox homeostasis

Next, we investigated whether Poly(I:C) + IFN-γ would also have an impact on the PPP and redox state in VIC, as observed with LPS + IFN-γ treatment (**Figures 10-12**). Glucose tracing analysis disclosed no changes in the incorporation of [U-^{13}C]-glucose into GSSG (**Figure 20A**), opposite to the results obtained for TLR4 and IFNGR activation in **Figure 10**. However, increased incorporation of [U-^{13}C]-glucose in the ribose moieties of nucleotides such as ATP (**Figure 20B**) and cofactors such as NAD$^+$ (**Figure 20C**) occurred in the same manner as TLR4 and IFNGR activation (**Figure 11**). These results supported the notion of an inflammatory-mediated

increase in the PPP non-oxidative route thus providing a source of ribose-5-P for the enhanced synthesis of nucleotides and cofactors.

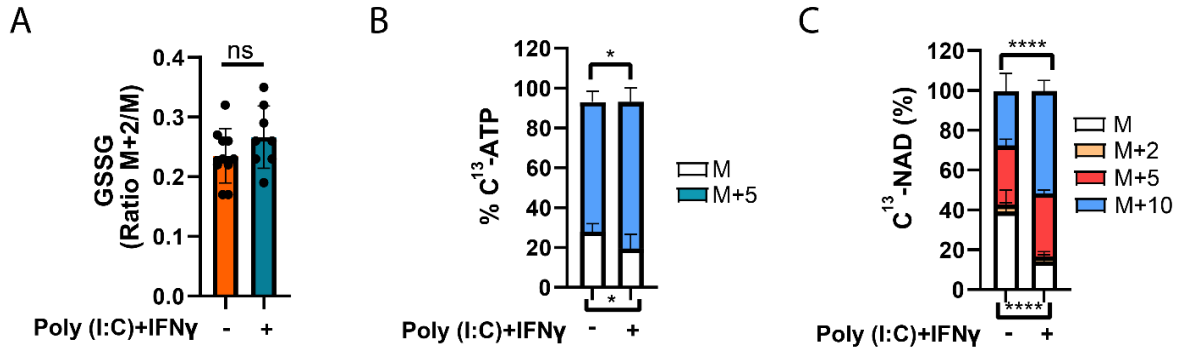

Figure 20. Metabolic rewiring by Poly(I:C)+IFN-γ is characterized by increased glucose flux into the ribose moieties of nucleotides and cofactors. Cells were incubated with M199-10% FBSi and 10 mM [U-^{13}C]-glucose and activated with 1µg/mL Poly (I:C) and 1 µg/mL IFN-γ. Extracted metabolites were then analyzed by UPLC-MS analysis. (A) [U-^{13}C] incorporation into M+2 GSSG expressed as the ratio M+2/M (N=7). (B-C) [U-^{13}C] incorporation into M+5 ATP (N=7); and into M+2, M+5, and M+10 NAD (N=7). Data are expressed as mean ± SD. N indicates the number of VIC isolates from independent valve donors; ns, non-significant differences; *, p<0.05; ****, p<0.0001. Student's unpaired t-test

Subsequently, we studied the potential alterations in redox homeostasis by Poly (I:C) + IFN-γ treatment in VIC, which may be a consequence of PPP impairment. For this purpose, we used a seahorse analyzer and Mito Stress assay to measure non-mitochondrial oxygen consumption, which increased upon activation of VIC (**Figure 21A**). To clarify whether this increase was due to ROS production, we used a fluorescent probe (DCFH-DA) to measure total ROS, and the results showed a significant increase in ROS production upon activation (**Figure 21B**).

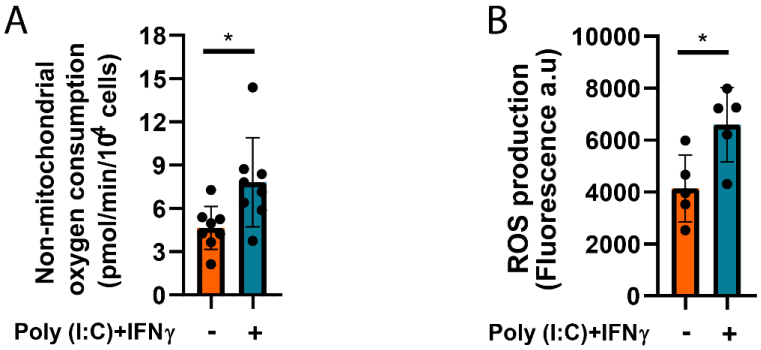

Figure 21. Non-mitochondrial ROS production is increased upon Poly (I:C) + IFN-γ-induced metabolic shift. VIC were treated with 1 µg/mL Poly (I:C) and 1 µg/mL IFN-γ for 24h and then analyzed. (A) Seahorse metabolic analysis of non-mitochondrial oxygen consumption (N=7). (B) ROS production evaluated with the fluorescent DCFH-DA was expressed as fluorescence a.u. (N=5). *p<0.05. Student's unpaired t-test.

R.4.3- Poly (I:C) and IFN-γ team up to increase pyruvate entrance to TCA

Next, we investigated whether Poly(I:C) + IFN-γ would also have an impact on pyruvate entrance to the TCA cycle, as observed with LPS + IFN-γ treatment (**Figures 13).** [U-^{13}C]-Glucose tracing analysis revealed a significant decrease in unlabeled (M) acetyl-CoA while a tendency to increase in [U-^{13}C] glucose flux into

(M+5) acetyl-CoA (**Figure 22A**). Glucose flux into TCA metabolites, such as citrate and succinate, was poorly detected in untreated VIC, although a small but consistent and significant raise in [U-^{13}C]-glucose incorporation was detected (**Figure 22B**, **C).** Moreover, a significant increased incorporation of label glucose into citrate (M+2) was measured. Although the % of incorporation expressed as (M+2/M) was not significant, marked differences were measured when comparing M+2 citrate levels in untreated versus activated VIC (**Figure 22B).** In the case of succinate, differences were significant when expressing data as % of incorporation and when comparing M+2 succinate levels in untreated and activated cells (**Figure 22C**). In contrast, no changes in OAA levels were observed in the presence of inflammatory insults (**Figure 22D**).

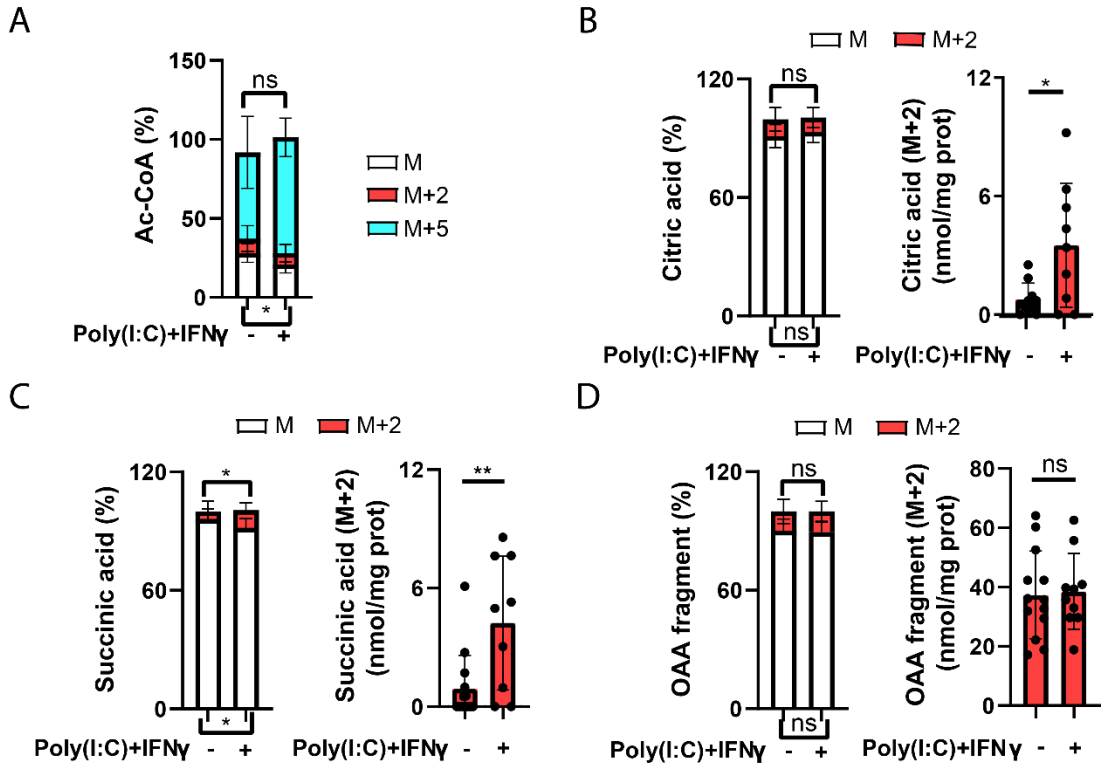

Figure 22. Metabolic rewiring induced by Poly (I:C) + IFN-γ is characterized by glucose flux into TCA.VIC were incubated with M199 -10% FBSi and 10 mM [U-^{13}C]-glucose and activated with 1 µg/mL Poly (I:C) and 1 µg/mL IFN-γ for 24h. Then, metabolite extraction was performed followed by UPLC-MS analysis. (A) % incorporation of [U-^{13}C]-glucose carbon into M+2 and M+5 acetyl-CoA (N=9). (B-D) % incorporation of U-^{13}C and nmol/mg protein (N=9) of (B) M+2 citric acid, (C) M+2 succinic acid, (D) M+2 OAA. Data are expressed as mean ± SD. N indicates the number of VIC isolates from independent valve donor.; ns, non-significant differences. *p<0.05; **p<0. 01.. Student's unpaired t-test.

Together, results showed a tendency to increase the glucose flux into the first metabolite undergoing TCA, acetyl-CoA, while low but consistent incorporation in subsequent TCA metabolites, such as succinic acid and citric acid.

R.4.4- Activated VIC decrease respiratory capacity and impair mitochondrial ATP production

The next step was to assess the status of mitochondrial respiration in VIC exposed to Poly(I:C) + IFN-γ. Real time Seahorse Mito Stress analysis disclosed some differences between TLR3 and TLR4 agonists. Poly (I:C) + IFN-γ had no effect on either basal OCR or maximal respiration capacity but showed a tendency to decrease ATP linked to OXPHOS (**Figure 23A**), in contrast to the reduction of maximal respiration and ATP linked to OXPHOS induced by LPS + IFN-γ treatment (**Figure 15**). Then, we measured proton leak and coupling efficiency to evaluate a potential ineffective respiration. After Poly (I:C) + IFN-γ activation, proton leak showed a tendency to increase, whereas coupling efficiency did not show alterations (**Figure 23A, B**), differing from the results obtained upon co-stimulation with LPS and IFN-γ (**Figure 15**).

Finally, to elucidate the role of mitochondrial respiratory chain after stimulation, we calculated the reliance on complexes I and III for mitochondrial respiration. Cell activation with Poly (I:C) + IFN-γ did not alter the reliance on complex I/III complexes (**Figure 23C**), in contrast to LPS + IFN-γ treatment (**Figure 15**). In contrast, the % dependence of oxygen consumption on ATP synthase diminished upon Poly (I:C)+ IFN-γ activation (**Figure 23C**), as observed in **Figure 15**.

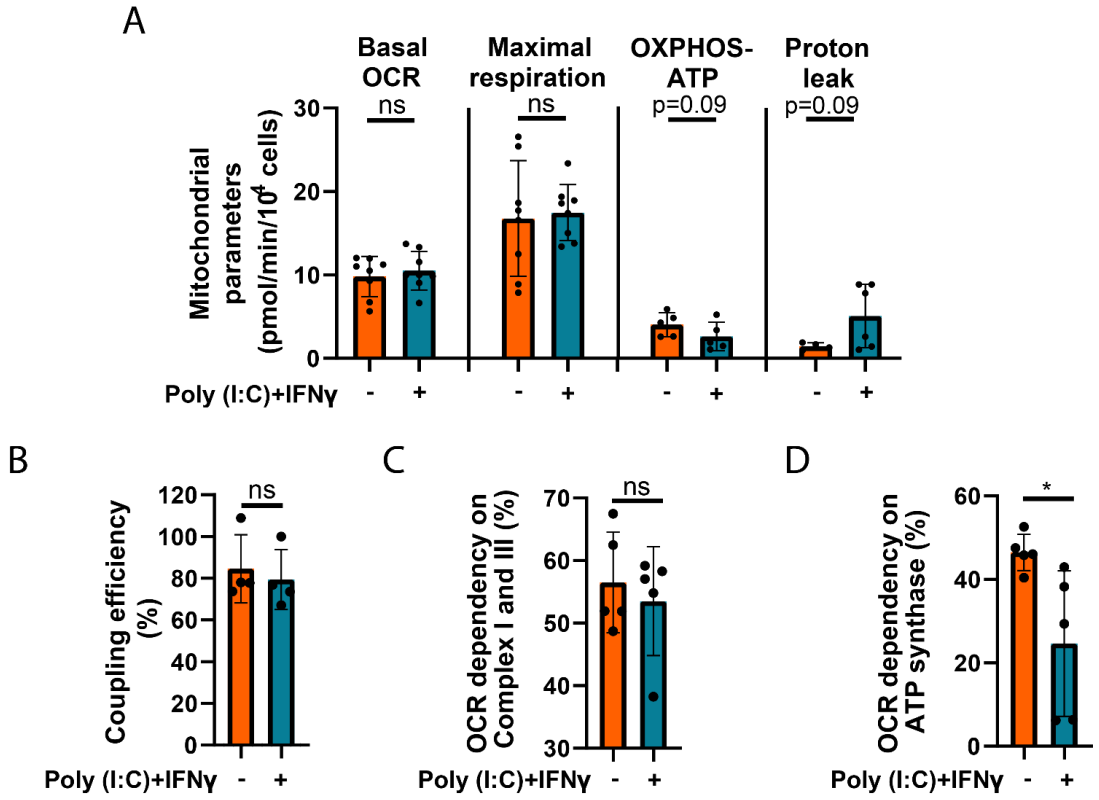

Figure 23. Metabolic reprogramming induced by Poly (I:C) + IFN-γ does not affect mitochondrial respiration parameters. VIC were treated with 1 µg/mL Poly (I:C) and 1 µg/mL IFN-γ for 24h and then analyzed using Seahorse Mito Stress metabolic analysis. (A) Bar graph corresponding to basal OCR, maximal respiration, ATP production linked to OXPHOS and proton leak (N=5/6/7). (B) Bar graphs corresponding to the coupling efficiency (%) (N=4). (C-D) OCR measures after rot/AA and oligomycin injection, respectively, referred to basal OCR for calculating the percentage of reliance in respiratory complexes (N=5). Data are expressed as the mean ± SD. Ns, non-statistical significance; *, p<0.05. Student's unpaired t-test.

Altogether, data revealed a decrease in mitochondrial ATP production, but no changes in oxygen consumption rate or maximal respiration, upon Poly (I:C) + IFN-γ activation that may be due to the proper function of complex I/III but altered ATP synthase. Additionally, these results disclosed some differences between TLR3 and TLR4 in the interplay with IFNGR on mitochondrial respiration in VIC.

R.4.5- TLR3 promotes the activation of apoptotic pathways and decrease the mitochondrial membrane potential in VIC

Considering that (i) the TLR3 agonist Poly (I:C) induced a proglycolytic metabolic shift in VIC (Figure 19), (ii) Poly (I:C) is reported to stabilize HIF-1α and then induce VIC calcification (Parra-Izquierdo et al., 2021), and (iii) HIF-1α has been associated not only with metabolic stress but also with ROS generation and apoptosis (Mason et al., 2011), we aimed to investigate the effects of Poly (I: C) on apoptosis and mitochondrial membrane potential in VIC. qPCR analysis of VIC activated with Poly (I:C) for 24h indicated upregulation of genes related to the extrinsic apoptotic pathway, such as FAS-ligand (*FAS*) receptor and caspase 8 (*CASP8*) (**Table 5**), and genes from the intrinsic pathway, such as *BNIP3, PMAIP* (NOXA), *BBC3* (PUMA), *BAK*, and *BAX* (**Table 5**). Transcription analysis of common effectors revealed no changes in *CASP9* transcripts, but *CASP3* upregulation upon VIC activation (**Table 5**). Thus, the analysis of caspase 3/7 activity showed an increased caspase 3 activity upon stimulation (**Figure 24A**). To further characterize if these changes were leading to membrane damage and mitochondrial potential disruption, we used the fluorescent probe TMRM. FCCP, a potent uncoupler of mitochondrial oxidative phosphorylation, was used as a control. Flow cytometry analysis showed a decrease in fluorescence in Poly (I:C) activated as compared to untreated VIC (**Figure 24B**), thus elucidating a TLR3-induced inhibition of mitochondrial membrane potential that would lead to metabolic changes such as ATP depletion and may later induce VIC apoptosis.

Table 5. Changes in apoptotic gene expression in Poly (I:C)-activated vs. untreated VIC. The comparison of the expression for the indicated genes is expressed as $2^{-\Delta\Delta Ct}$, where ΔCt is the Ct gene-Ct GAPDH. Table includes fold change data vs. untreated, mean + SD (N=5). Student's unpaired t-test. *p<0.05, **p<0.01,***p<0.001, ns; non-significant.

GENE	FOLD CHANGE	STATISTICS
	EXTRINSIC PATHWAY	
FAS	10.05 ± 3.75	***
CASP8	4.00 ± 2.49	*
	INTRINSIC PATHWAY	
BNIP3	3.00 ± 1.59	**
PMAIP1 (NOXA)	12.64 ± 1.21	***
BAK	2.87 ± 0.64	*
BBC3 (PUMA)	2.09 ± 0.74	*
APAF1	2.75 ± 1.10	*
	COMMON EFFECTORS	
CASP9	1.16 ± 0.32	ns
CASP3	2.15 ± 0.64	*

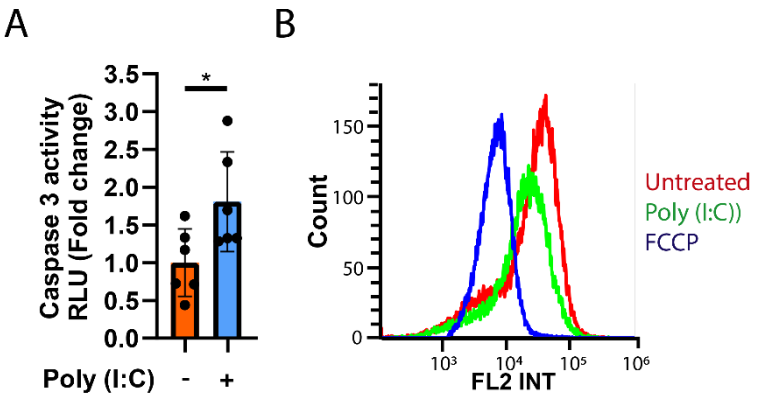

Figure 24. Poly(I:C) upregulates extrinsic and intrinsic apoptotic pathways and reduces the mitochondrial membrane potential of VIC. Cells were treated with 1 µg/mL Poly (I:C) for 24h and then analyzed. (A) Caspase 3 activity in cells activated as indicated for 24h was analyzed with a luminescent assay kit. RLU, relative luminescence units are directly proportional to caspase 3 activity. N=6. (B) Flow cytometry analysis of cells stained with fluorescent dye TMRM, representative of N=3. The uncoupling agent, FCCP, was used as a control. Data are shown as the mean ± SD. *p<0.05. Student's unpaired t-test

Since the main apoptotic changes are mediated by the tumor suppressor p53, which is known to regulate cell metabolism by directly inducing ETC and repressing glycolytic enzymes (Bensaad et al., 2006 & Matoba et al., 2006), the next step was to assess p53 in VIC. WB analysis showed an early increase in p53 expression 8h after Poly (I:C) activation, which decreased after 24h of treatment (**Figure 25A-C**). In addition, WB analysis of nuclear and cytoplasmic protein extracts unveiled Poly (I:C)-induced accumulation of p53 in both cytoplasm and nuclei (**Figure 25D**), where it could function as a transcriptional factor.

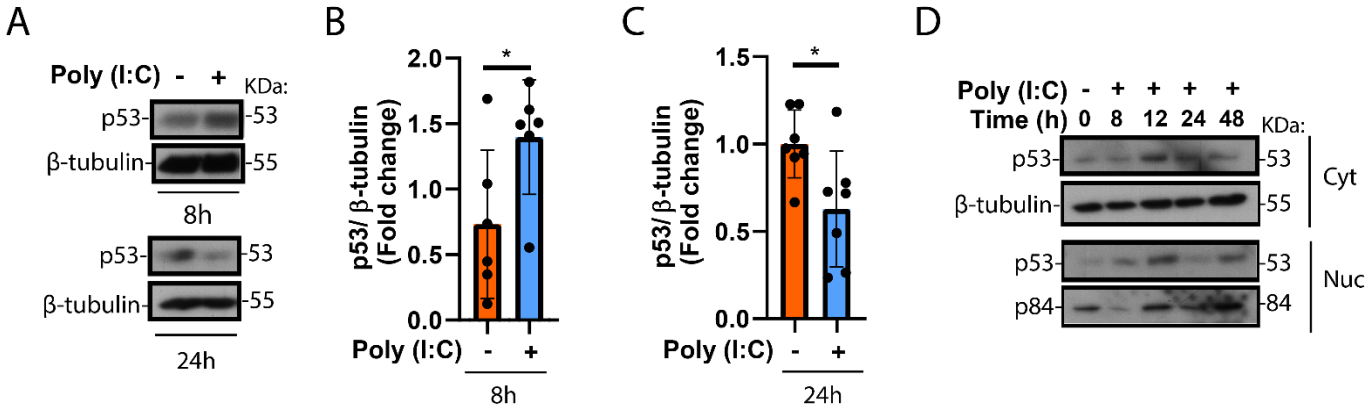

Figure 25. p53 accumulation in both the cytoplasm and nuclei of VIC is increased by Poly (I:C) activation. VIC were treated with 1 µg/mL Poly (I:C) and then analyzed by WB. (A-C) Representative immuno-blot and quantitation of p53 protein in whole cell extracts from cells activated for (B) 8h (N=6) or (C) 24h (N=7). (D) Representatives immunoblot of the time-course of p53 in nuclear (Nuc) and cytoplasmic (Cyt) extracts. Data are shown as mean ± SD. *p<0.05. Student's unpaired t-test.

Together, data disclosed that Poly(I:C) reduced mitochondrial membrane potential and induced intrinsic and extrinsic apoptotic pathways and p53 accumulation in human VIC, suggesting that p53, a key factor in apoptosis regulation, could play an early role in the induction of apoptosis.

R.5-Role of inflammation-induced increase in glycolysis in pathogenic processes underlying CAVD: inflammation, differentiation, and calcification.

Once characterized the TLR4-IFNGR interplay on increased glucose uptake and catabolism, we investigated whether this increase in glycolysis could contribute to CAVD pathological processes such as inflammation, differentiation, and calcification. Firstly, we used the pharmacological blockade of glycolysis via 2-Deoxy-D-glucose (2-DG), a competitive inhibitor of HKII. HKII phosphorylates 2-DG to 2-deoxy-D-glucose-6-phosphate, which cannot be further metabolized (S. Yu et al., 2010). Likewise, due to its structural similarity with mannose, 2-DG exerts a greater competitive effect with mannose than with glucose, since mannose is found in tissues in much lower concentrations (Kurtoglu et al., 2007). To validate the results obtained upon glycolysis inhibition, glucose deprivation was used. Notably, the fact that 2-DG blocks mannose and glucose metabolism affects post-translational protein modifications, such as mannosylation and glycosylation, leading to unfolded protein accumulation and response, and endoplasmic reticulum stress.

R.5.1- 2-DG pre-treatment and glucose deprivation blunt metabolic effects orchestrated by co-stimulation with LPS and IFN-γ

To directly assay the role of glycolysis in the inflammatory-induced metabolic rewiring described in **Figures 8**-**9**, real-time metabolic analysis was performed in presence of 2-DG or in glucose-free conditions. First, Seahorse Mito Stress assay showed that glycolysis blockade significantly blunted the LPS + IFN-γ-triggered increase in ECAR levels and also upregulated OCR levels both in untreated and inflammatory-activated cells (**Figure 26A**-**B**). In addition, the energetic map confirmed the abrogation of the shift to a more glycolytic phenotype acquired upon inflammatory induction by 2-DG (**Figure 26C**). Additionally, Glycolytic rate assay showed that glycolysis blockade significantly decreased some glycolytic parameters that were upregulated upon LPS + IFN-γ treatment: glycolytic acidification, basal glycolysis, and basal proton efflux (**Figure 26D**). Similarly, a Glycolytic Stress assay showed that 2-DG abrogated the LPS + IFN-γ-induction of glycolytic capacity and compensatory glycolysis (**Figure 26E**). Moreover, Seahorse analysis of VIC activated in glucose-free medium further confirmed that glucose deprivation significantly blunted LPS + IFN-γ-induced ECAR (**Figure 26F**), and markedly increased OCR (**Figure 26G**) and reversed the metabolic rewiring induced by inflammatory insults (**Figure 26H**).

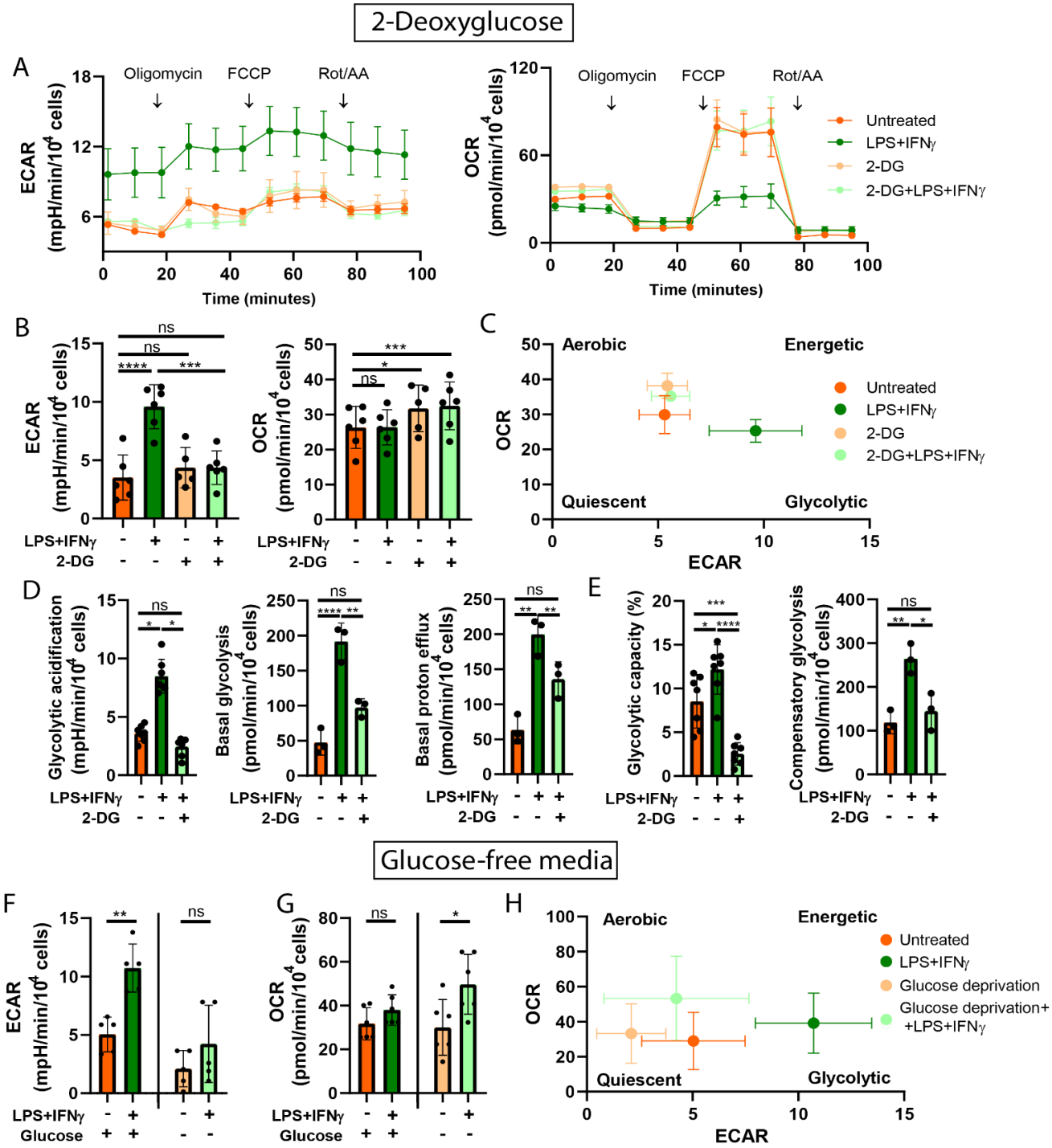

Figure 26. Glycolysis blockade inhibits inflammation-induced glycolytic shift in VIC. (A-E) VIC were pre-incubated with 10 mM 2-DG for 1h and treated with 100 ng/mL LPS and 1 µg/mL IFN-γ for 24h and then analyzed using Seahorse metabolic Mito Stress assay. (A) Representative ECAR and OCR plots. (B) Bar graphs of basal ECAR and OCR (N=6). (C) Energetic map (ECAR vs. OCR plot). (D-E) Bar graphs of the indicated glycolytic parameters (N=3/6/7). (F-H) Cells were activated in glucose-free medium and ECAR and OCR rates were analyzed (N=5/6). (H) Energy map. Data are expressed as the mean ± SD. Ns, non-statistical significance. *p<0.05, **p<0.01, ***p<0.001, ****p<0.0001. One-way ANOVA followed by Tukey's post-hoc test in panels B, D, and E. Student's unpaired t-test in G and H.

Next, we evaluated the impact of glycolysis blockade on other downstream metabolic pathways. Seahorse Mito Stress assay data showed that glycolysis blockade blunted all the mitochondrial respiratory

effects induced by TLR4 and IFNGR stimulation (**Figure 15**). 2-DG reversed the effects of LPS + IFN-γ on maximal respiration, non-mitochondrial oxygen consumption, proton leak, coupling efficiency, and ATP production linked to OXPHOS (**Figure 27A-E**). Additionally, the Seahorse ATP rate assay showed that 2-DG reversed the inflammatory-induced switch in ATP sources in VIC by reducing glycoATP and total ATP levels and increasing mito-ATP (**Figure 27F**).

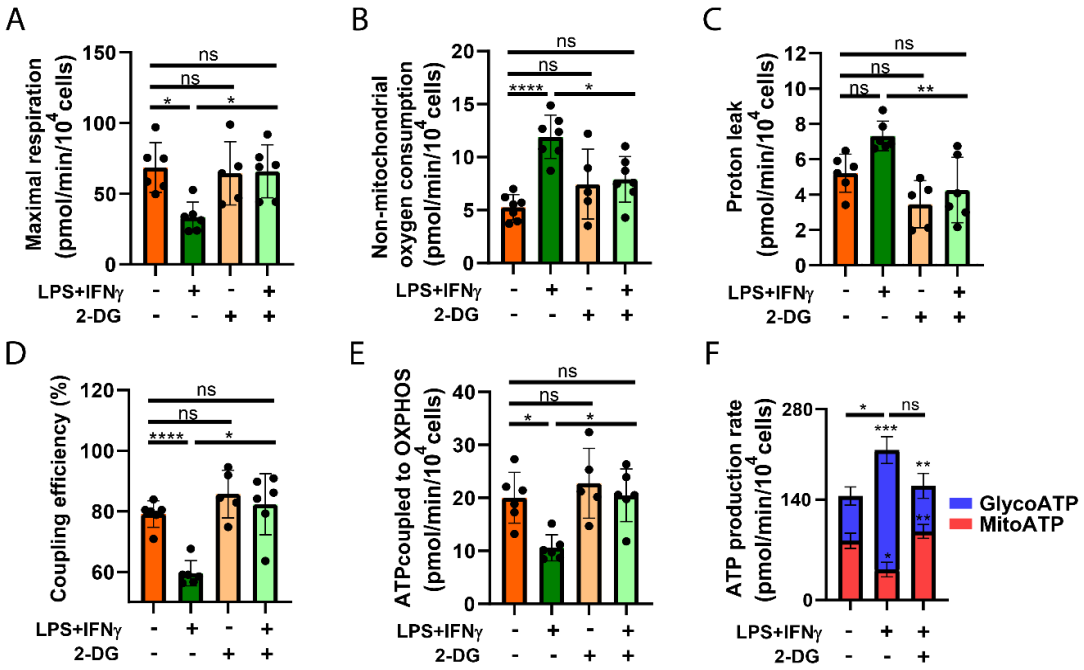

Figure 27. Metabolic changes affecting mitochondrial respiration and ATP production upon LPS + IFN-γ activation are blunted when blocking glycolysis. VIC were pre-incubated with 10 mM 2-DG and then treated with 100 ng/mL LPS and 1 µg/mL IFN-γ for 24h and analyzed mitochondrial parameters by Seahorse Mito Stress Assay. (A) Maximal respiration, (B) non-mitochondrial oxygen consumption, (C) proton leak, (D) coupling efficiency, and (E) ATP production coupled to OXPHOS. (F) ATP production rate assay showing the main sources of ATP. Data are shown as the mean ± SD (N=6/7). N indicates the number of VIC isolates from independent valve donors; ns, non-significant differences. *p<0.05, **p<0.01, ***p<0.001, ****p<0.0001. One-way ANOVA followed by Tukey's post-hoc test.

Given that JAK-STAT1/HIF-1α is reported to mediate LPS + IFN-γ-induced inflammation and calcification in VIC (Parra-Izquierdo et al., 2019), and the role of HIF-1α in metabolic reprogramming (Warburg et al., 1926), we sought to investigate the potential role of glycolysis in the activation of the JAK-STAT1/HIF-1α pathway. Notably, WB results disclosed that glycolysis blockade with 2-DG significantly decreased the STAT1 phosphorylation and HIF-1α stabilization induced upon LPS + IFN-γ treatment, and this effect was reversed by mannose (**Figure 28A-C**). Next, we analyzed the expression of limiting enzymes involved in glucose metabolism regulated by HIF-1α. qPCR data revealed that 2-DG significantly inhibited LPS + IFN-γ-triggered effects on *GLUT1* (**Figure 28D**) and *PDK4* (**Figure 28E**) gene expression. Additionally, the effects of glycolysis inhibition were significantly reversed by mannose treatment (**Figure 28D-E**). To further confirm if the observed 2-DG effects were a consequence of glycolysis blockade, WB analysis in glucose-free

medium showed that blunting glucose uptake in an inflammatory environment significantly decreased HIF-1α stabilization and STAT1 phosphorylation (**Figure 28F-H**).

Altogether, results confirmed that glycolysis blockade inhibits glycolytic flux, thus preventing the glycolytic shift induced by LPS + IFN-γ, and further disclosed that when glycolysis was blunted, VIC tried to restore the mitochondrial respiratory chain to maintain cell bioenergetics and fulfill energy requirements. Notably, glycolysis is required for LPS + IFN-γ-mediated STAT1 activation and HIF-1α stabilization.

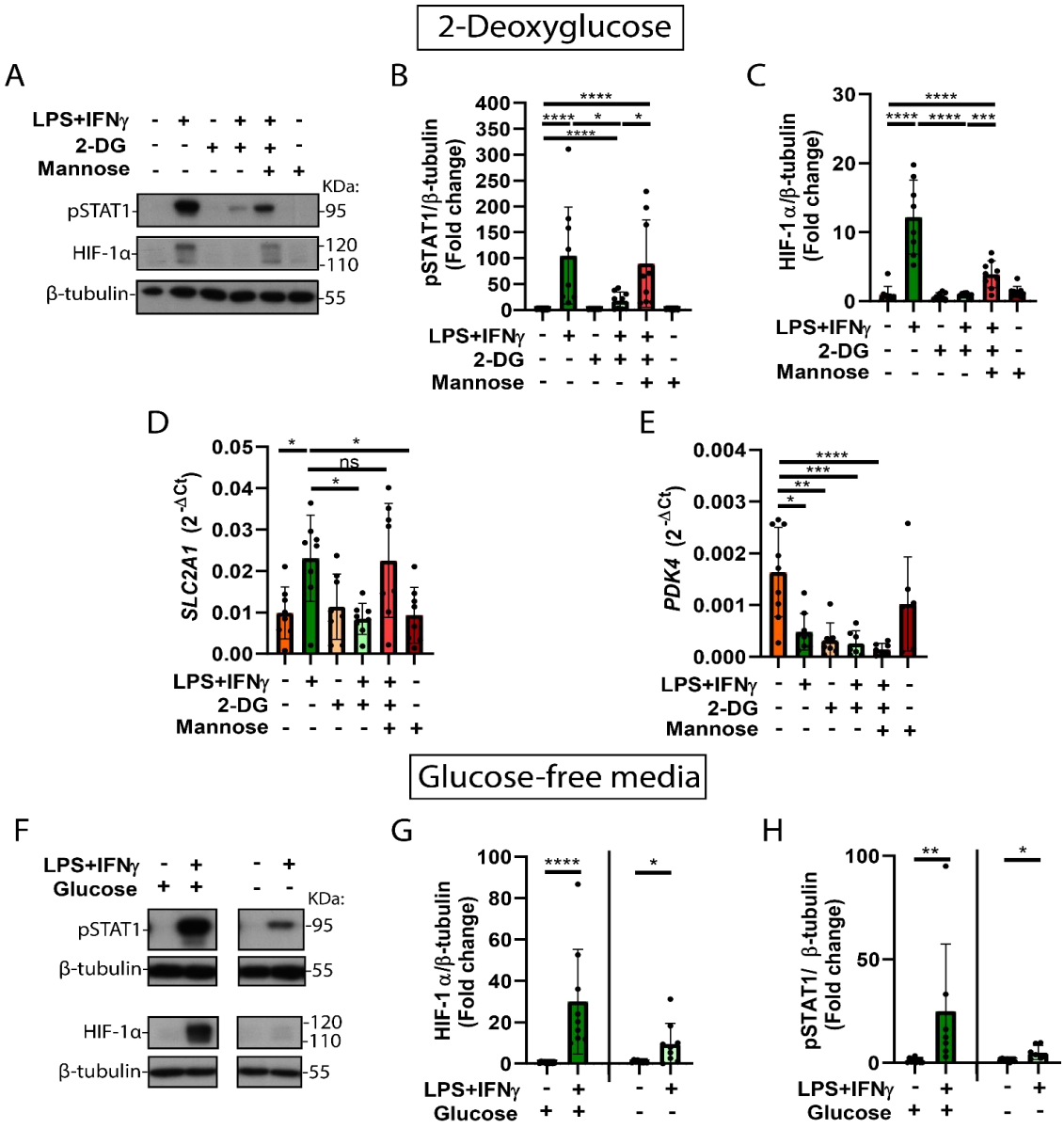

Figure 28. Glycolysis blockade inhibits LPS + IFN-γ-induced STAT1 activation, HIF-1α stabilization, and metabolic gene enzyme alterations, and mannose reverses these effects. (A-E) VIC were pre-incubated with 10 mM 2-DG for 1h and activated with 100 ng/mL LPS, 1 µg/mL IFN-γ and 1mM mannose for 24h. (A-C) Representative blots and quantitation of HIF-1α and pSTAT1. (D) qPCR analysis of *GLUT1 (SLC2A1)* and (E) *PDK4* expression. (F-H) VIC were activated in glucose-free or regular media. Representative blots and quantitation of HIF-1α and pSTAT1. Data are shown as the mean ± SD (N=8/9). Ns, non-significant difference; *, p<0.05; **, p<0.01; ***, p<0.001; ****, p<0.0001. One-way ANOVA with Tukey's post-hoc test in panels B-D. One-way ANOVA followed by Dunnett's post-hoc test (vs. untreated) in E. Student´s unpaired t-test in G and H.

R.5.2- Glycolysis inhibition abrogates inflammation induced upon TLR4 and IFNGR co-stimulation

Given the association of JAK-STAT signaling and inflammation and calcification reported in human VIC (Parra-Izquierdo et al., 2019), we sought to investigate the role of glycolysis on inflammation. WB analysis showed that LPS + IFN-γ induced strong activation of the master regulator of inflammation, NF-κB, and this induction was blunted when glycolysis was blocked, and the effect was reversed by mannose treatment (**Figure 29A-B**). We then explored adhesion molecules regulated by NF-κB, such as ICAM-1 and VCAM-1, whose serum levels were increased in patients with non-rheumatic valve disease (Death et al., 1997). Our data confirmed the LPS + IFN-γ–induction of ICAM-1 (**Figure 29A, C**), as previously reported by our group (Parra-Izquierdo et al., 2019), and further disclosed the upregulation of VCAM-1 protein levels (**Figure 29A,D**). Glycolysis blockade with 2-DG abrogated the LPS + IFN-γ-mediated induction of both adhesion molecules. Notably, 2-DG reduced the molecular weight of both detected proteins (**Figure 29A, C, D**), indicating the inhibition of their post-translational modifications, consistent with the 2-DG disruption of N-glycosylation. Furthermore, 2-DG effects on protein expression and glycosylation were reversed by mannose (**Figure 29A-D**).

Next, a glucose deprivation analysis was performed to confirm the role of glucose uptake in inflammation. WB analysis in glucose-free medium showed that activation of NF-κB by LPS + IFN-γ was blunted in the absence of glucose (**Figure 29E-F**). Additionally, glucose depletion also reduced the inflammatory-induction expression of ICAM-1 and VCAM-1 (**Figure 29E, G, H**).

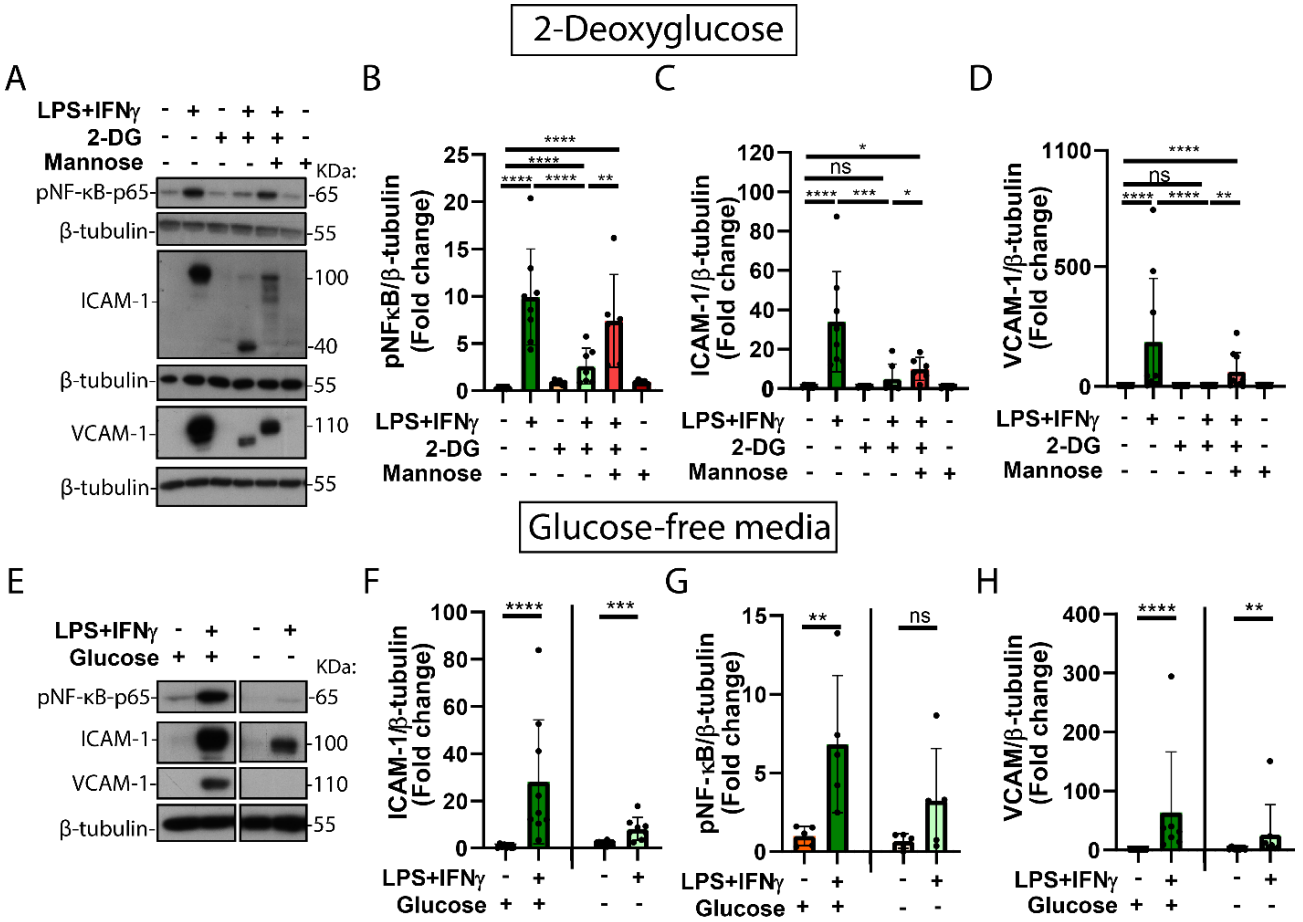

Figure 29. Glycolysis inhibition blunts the inflammation-mediated activation of NF-κB, as well as the expression and post-translational modifications of adhesion molecules. (A-D) VIC were activated and analyzed as in **Figure 28A-C**. Representative blots (glycolysis blockade with 2-DG) and quantitation of pNF-κB, ICAM-1, and VCAM-1 levels. (E) VIC were activated and analyzed as in **Figure 28F-H.** Representative blots (glucose-free medium), and quantitation of pNF-κB, ICAM-1 and VCAM-1, Data, mean ± SD (N=5/7). ns, non-significant differences. *p<0.05, **p<0.01, ***p<0.001, ****p<0.0001. One-way ANOVA with Tukey's post-hoc in panels B, C, D. Student's unpaired t-test performed in F, G, H.

To further examine the role of glycolysis on inflammation, we explored the transcription of inflammatory molecules and cytokines with a reported role in CAVD such as IL-6, IL-8, and COX-2 (*PTGS2*) (Mathieu et al., 2015). qPCR data showed the abrogation of LPS + IFN-γ-induced upregulation of *IL6, IL8,* and *PTGS2* transcripts by pre-incubating VIC with 2-DG, and the effect was reversed by mannose (**Figure 30A-C**). Moreover, ELISA analysis confirmed that co–stimulation of VIC with LPS + IFN-γ significantly induced the secretion of the cytokines IL-6/8 and the lipid mediator and product of the COX-2 pathway prostaglandin E2 (PGE2), which was blunted upon glycolysis inhibition, and further showed a partial reversion by mannose (**Figure 30D-F**). Experiments performed in glucose-free medium confirmed the role of glycolysis by showing a decrease in LPS + IFN-γ-induced *IL6* and *IL8* transcripts and IL-6 secretion in the absence of glucose (**Figure 30G-H**).

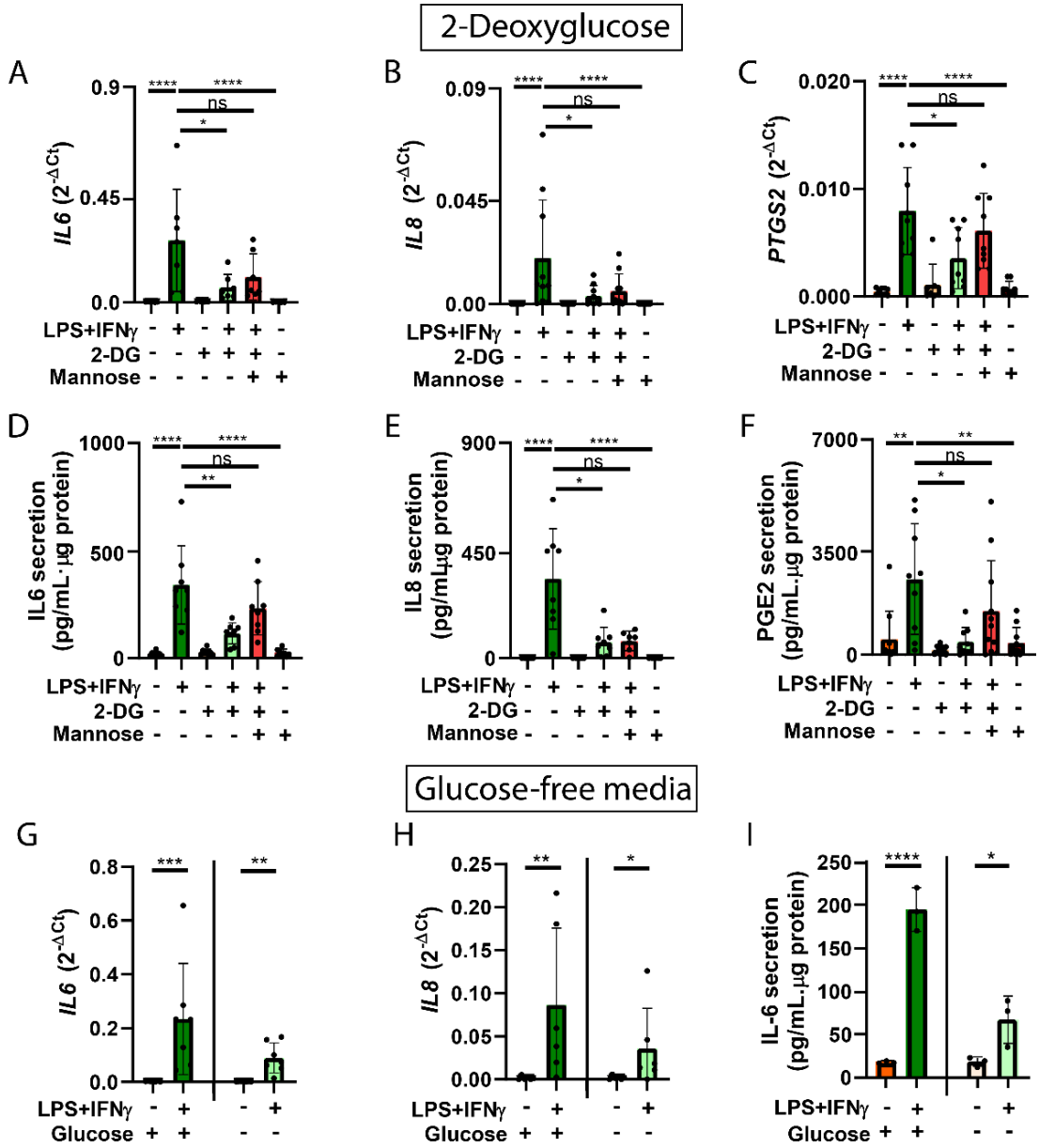

Figure 30. Glycolysis blockade inhibits inflammation-induced expression of COX2 and cytokine secretion. (A-F) VIC were activated and analyzed as in **Figure 28A-C,** (glycolysis blockade with 2-DG). (A-C) qPCR analysis of *IL6, IL8,* and *PTGS2* transcripts. (D) ELISA results showing secretion of IL-6, IL-8, and PGE2. (G-I) VIC were activated and analyzed, as in **Figure 28F-H** (glucose-free medium). (G-H) qPCR analysis of *IL6* and *IL8* in glucose-free medium. (I) IL-6 secretion. Data are expressed as mean ± SD (N=3-8). Ns, non-significant differences; *, p<0.05; **, p<0.01; ***, p<0.001; ****, p<0.0001. One-way ANOVA with Dunnett post-hoc (vs. LPS + IFN-γ) in panels A, B, C, D, E, F. Student's unpaired t-test in G, H, I.

Finally, in contrast to 2-DG (**Figure 30C**), glucose deprivation did not inhibit the upregulation of *PTGS2* transcripts upon activation with LPS + IFN-γ (**Figure 31A**). The inhibition of *PTGS2* by 2-DG treatment could be due to the known role of 2-DG in ER stress induction and the reported role of ER stress in COX-2 expression and glycosylation inhibition (Yu et al., 2010). In fact, inflammatory-induced *PTGS2* levels were significantly decreased upon tunicamycin, a well-known inductor of ER stress (**Figure 31B**).

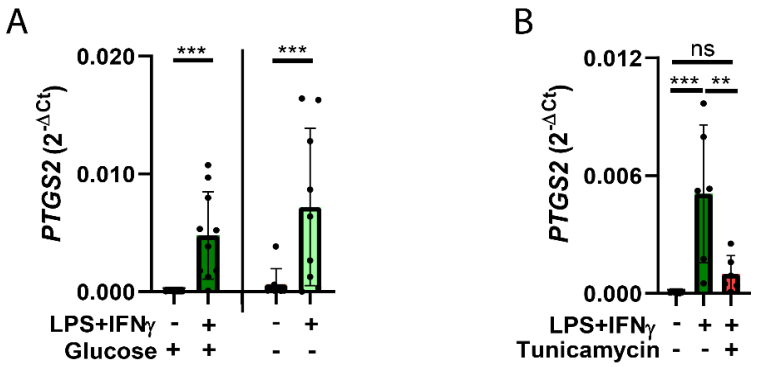

Figure 31. Inflammatory-induced upregulation of *PSTG2* transcripts is not altered by glucose deprivation but inhibited by an ER stress inducer. (A) *PTGS2* expression in VIC activated for 24h with 100 ng/mL LPS and 1 µg/mL IFN-γ with or without 10mM glucose (B) *PTGS2* transcript levels of VIC treated as indicated for 24 h; 100 ng/mL tunicamycin. ns, non-significant differences. **p<0.01, ***p<0.001. Data are expressed as mean ± SD (N=6/7). Student's unpaired t-test.

Together, data disclosed that glycolysis was necessary for the inflammatory-mediated induction of the secretion of cytokines IL-6/8 and the expression of adhesion molecules in human VIC, and further showed that glycolysis is required for the glycosylation of the adhesion molecules ICAM-1 and VCAM-1.

R.5.3-Glycolysis blockade blunts VIC differentiation and matrix remodeling upon LPS + IFN-γ activation

Human calcified valves exhibit overexpression of several osteogenic genes and bone-related pathways compared to healthy valves (Bosse et al., 2009). In fact, our laboratory has previously shown that long-term treatment of cells with IFN-γ induced VIC differentiation to an osteoblast-like phenotype that was further potentiated by TLR4 activation (Parra-Izquierdo et al., 2019). Taking this into account, we addressed whether glycolysis is required for LPS + IFN-γ-triggered differentiation of VIC. Microphotographs showed an osteoblast-like morphology when treating VIC with inflammatory stimuli for 14 days, and notably, glycolysis blockade with 2-DG promoted the dedifferentiation of VIC, as suggested by the acquisition of a fibroblast-like phenotype with large, elongated and spindle-shaped cells (**Figure 32A**). Moreover, qPCR analysis confirmed the loss of the myofibroblast marker alpha-smooth muscle actin (α-SMA; *ACTA2*) in VIC exposed to 2-DG (**Figure 32B**). In addition, the addition of mannose to the media resulted in partial reversion to a myofibroblast-like phenotype (**Figure 32A**).

Next, we addressed the levels of bone morphogenetic protein (BMP)-2, a potent osteogenic signaling morphogen overexpressed in calcified valves (reviewed in Rajamannan et al., 2014) and associated with osteoblast-like differentiation of VIC and the ensuing calcification (Gomez-Stallons et al., 2016). qPCR data disclosed that 2-DG significantly inhibited the upregulation of *BMP2* transcripts upon VIC exposure to LPS + IFN-γ for 24h, and these effects were partially reversed by mannose (**Figure 32C**). Additionally, because exaggerated matrix remodeling is another feature of CAVD (Miller et al., 2011), we explored the role of glycolysis in metalloproteinase expression. qPCR data showed that the upregulation of the matrix

metalloproteinase 1 (*MMP1*) upon stimulation was significantly decreased in the presence of 2-DG, while mannose partially reversed this effect (**Figure 32D**). Furthermore, inflammatory-induced upregulation of *BMP2* and *MMP1* gene expression was reduced in glucose-free medium (**Figure 32E-F**).

Together, data highlighted the role of glycolysis in the inflammatory-induced VIC differentiation into an osteoblast-like phenotype and in the upregulation of osteogenic and matrix remodeling markers in human VIC.

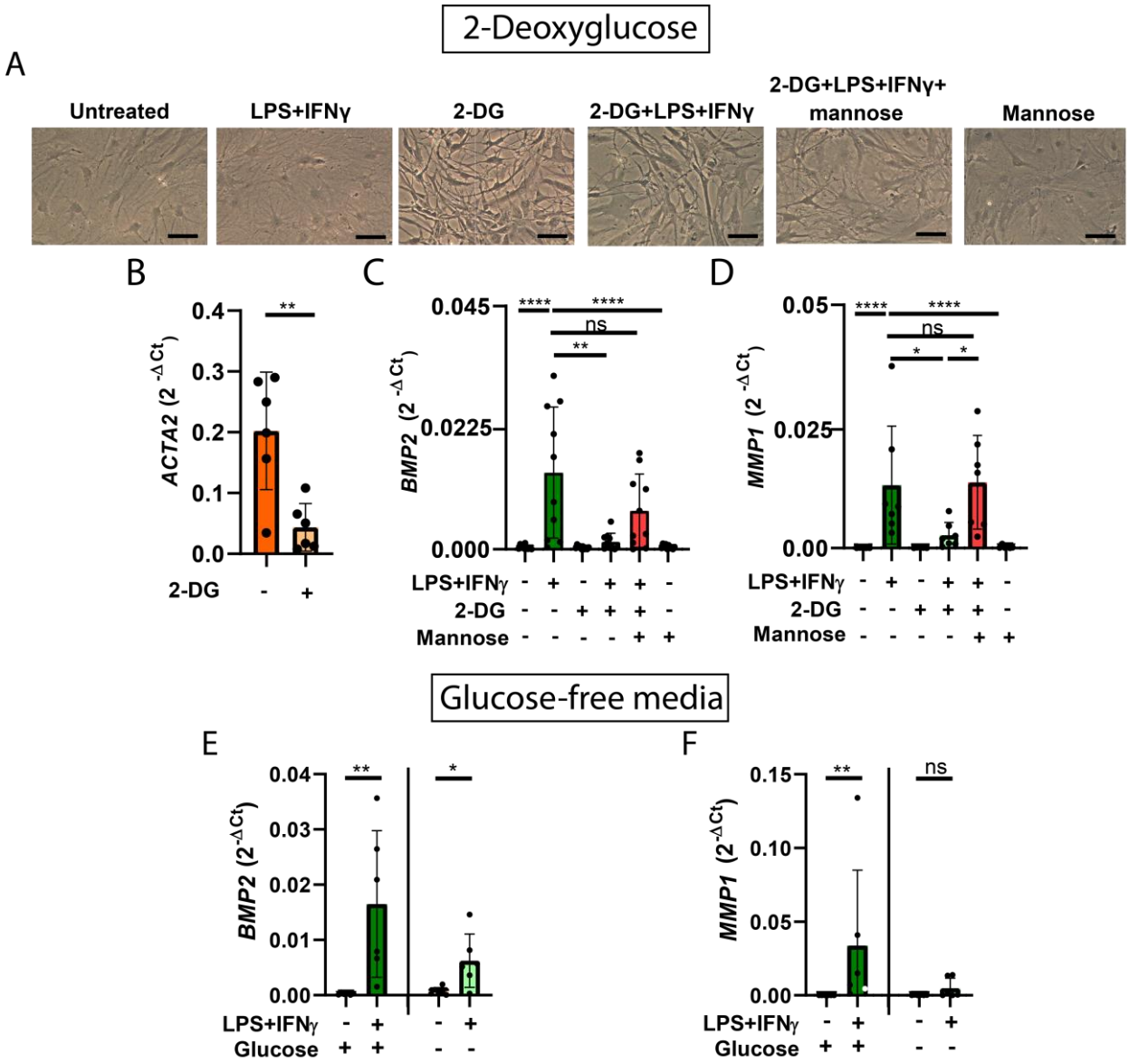

Figure 32. Glycolysis is necessary for the inflammatory-induced osteoblast-like phenotype and upregulation of osteogenic and matrix remodeling markers in VIC. (A) VIC were pre-incubated with 10 mM 2-DG and 1mM mannose and then treated with 100 ng/mL LPS and 1 µg/mL IFN-γ for 14 days in M199+10% FBSi media. Representative of N=3. Black line indicates 50 µm. (B) VIC were treated with 2-DG for 24h and *ACTA2* expression levels were measured by qPCR. (C) *BMP2* and (D) *MMP1* expression levels. (E-F) VIC were pre-incubated with glucose-free medium for 1h and then stimulated as described for later PCR analysis of *BMP2* and *MMP1* expression levels. Data are presented as mean ± SD (N=6/7). Ns, non-significant differences; *, p<0.05; **, p<0.005; ***, p<0.001; ****, p<0.0001. One-way ANOVA with Dunnett's post-hoc test (vs. LPS + IFN-γ) in panel B. One-way ANOVA with Tukey's post-hoc test in panel C. Student's unpaired t-test in E, F.

R.5.4-Glycolysis is necessary for inflammatory-induced calcification and apoptosis in VIC

The next step was to study whether the inflammatory-induced increase of glycolysis had a role in promoting calcification in human VIC. *In vitro* calcification assays revealed both that co-stimulation with IFN-γ and LPS induced mineralization and Ca^{2+} deposition, confirming data from our group (Parra-Izquierdo et al., 2019), which was further blunted by pre-incubation with the glycolysis inhibitor 2-DG (**Figure 33A-B**). Surprisingly, the effect of 2-DG was not reversed by mannose, as expected, but was further potentiated in Ca^{2+} deposits (**Figure 33B**). The role of glycolysis on inflammation-induced calcification was further confirmed by glucose deprivation experiments showing the reduction of LPS + IFN-γ-mediated mineralization and Ca^{2+} deposition in VIC (**Figure 33C-D**).

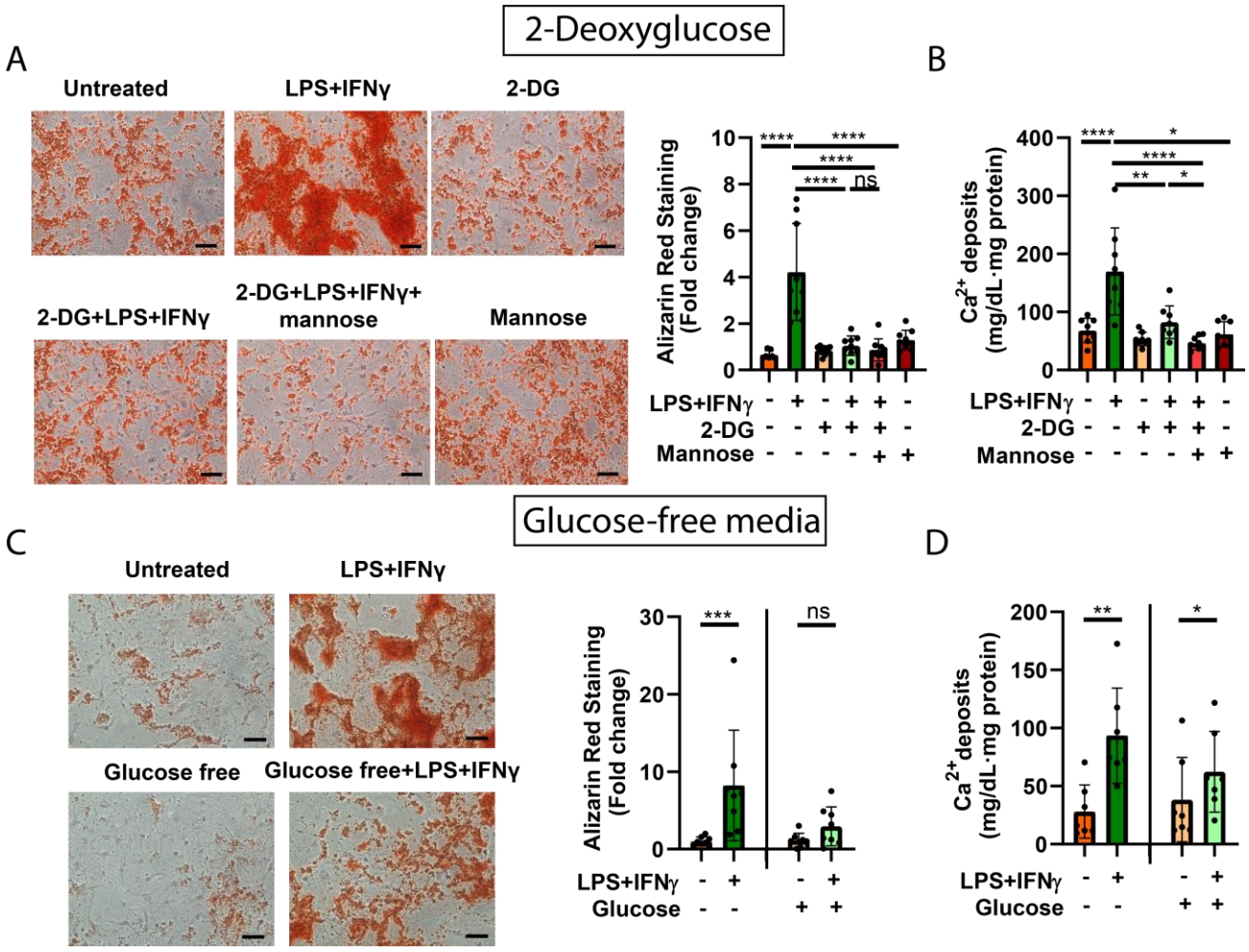

Figure 33. Glycolysis inhibition abrogates inflammatory-induced mineralization and Ca^{2+} deposition in VIC. VIC were pre-incubated with 10 mM 2-DG or glucose-free medium for 1 h and then treated with 100 ng/mL LPS, 1 µg/mL IFN-γ and 1mM mannose for 7 days in calcification media and then analyzed. (A) ARS staining and its quantitation when pre-incubating cells with 2DG. (B) Ca^{2+} deposits. (C) ARS staining and its quantitation in glucose-free medium. (D) Ca^{2+} deposits. Data are expressed as mean ± SD (N=7/8). Black line indicates 50 µm; ns, non-significant differences. *p<0.05, **p<0.01, ***p<0.001, ****p<0.0001. A one-way ANOVA with Tukey's post-hoc test is shown in panels A and B. Student's unpaired t-test is shown in panels C and D.

It is known that both osteogenic and dystrophic calcifications are found in stenotic valves (Torre et al., 2016), and apoptosis has been reported to contribute to LPS + IFN-γ-induced calcification in human VIC (Parra-Izquierdo et al., 2019). For this reason, we aimed to assess apoptosis. Flow cytometry analysis of annexin-stained VIC revealed that glycolysis blockade with 2-DG did not alter the number of apoptotic VIC (**Figure 34A**), while the pre-treatment with mannose further decreased apoptosis (**Figure 34A**). Therefore, results suggested a potential anti-apoptotic role of mannose, which could also explain why the abrogation of VIC calcification by 2-DG was not reversed by mannose (**Figure 33A-B**). The upregulation of a well-known anti-apoptotic gene, B-cell lymphoma 2 (*BCL2*), by mannose also suggested its role as an anti-apoptotic agent in VIC (**Figure 34B**).

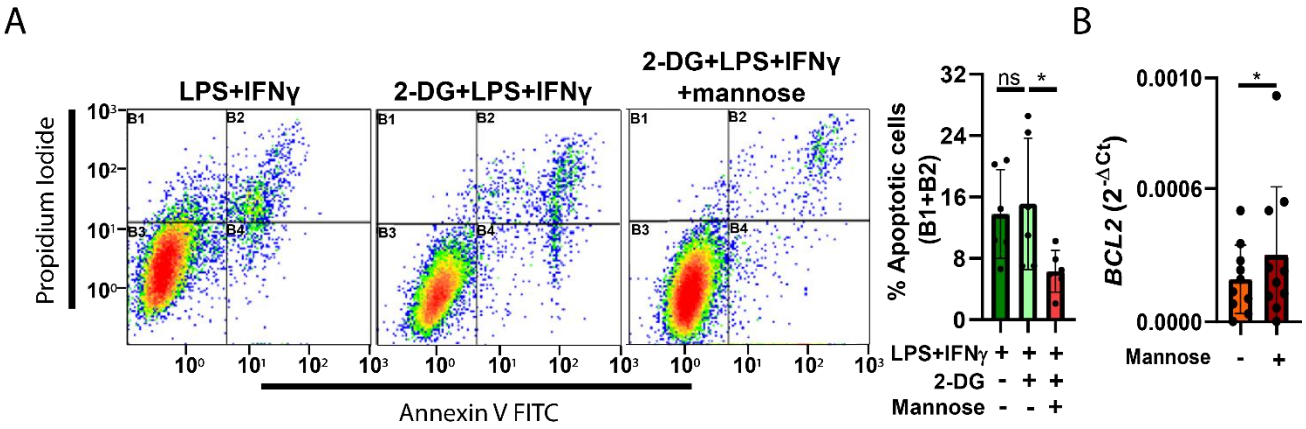

Figure 34. Mannose reduces the apoptosis induced by LPS + IFN-γ and upregulates the anti-apoptotic gene in VIC. (A) VIC were pre-incubated with 10 mM 2-DG and treated with 100 ng/mL LPS, 1 µg/mL IFN-γ and 1mM mannose for 7 days in calcification media and then analyzed by flow cytometry to evaluate Annexin V FITC-stained cells (B2+B4) (N=6). (B) *BLC2* transcription levels in VIC treated with or not with 1mM D-mannose (N=10). Ns means non-significant differences; *, p<0.05. One-way ANOVA with Dunnet post-hoc (vs. 2-DG + LPS + IFN-γ) in panel A. Student's unpaired t-test in B.

Collectively, data highlighted the requirement of glycolysis to support the LPS + IFN-γ-induced calcification and revealed a potential role of mannose as an anti-apoptotic agent.

R.5.5- Increase in PKM2 activity directly contributes to inflammation, differentiation, and calcification processes in VIC

The next aim was to address whether PKM2 activation had a role in the inflammatory-induced glycolytic reprogramming, since *PKM2* expression is upregulated by inflammatory stimuli in VIC (**Figure 7**). This enzyme catalyzes the last step in glycolysis, the conversion of phosphoenolpyruvate to pyruvate generates ATP. Both its conformation and activity can be allosterically modified by metabolic intermediates and pharmacological compounds. Firstly, human VIC were treated with the compound ML-265 (also called TEPP46) which enhances PKM2 tetramerization and converts it into a highly glycolytic enzyme that increases glycolytic flux and decreases pyruvate flux to mitochondria (Anastasiou et al., 2012 & Christofk et al., 2008). Seahorse Mito Stress assay revealed that the activation of PKM2 tetramerization with TEPP46 promoted a significant increase in ECAR, while non-significant changes in OCR, resulting in a metabolic shift to a more

glycolytic phenotype in VIC (**Figure 35A-C**) that resembled the inflammatory-induced shift (**Figures 6,8**). Other metabolic parameters related to OXPHOS showed that PKM2 activation did not alter maximal respiration (**Figure 35D**) but enhanced non-mitochondrial oxygen consumption (**Figure 35E**). Moreover, as expected, VIC treated with TEPP46 showed no changes in proton leak, but decreased ATP production linked to OXPHOS (**Figure 35F-G**). To further characterize if PKM2 participated in glycolytic ATP production, which is the main ATP source in inflammatory-activated cells, Seahorse ATP rate assay was performed. Data showed that PKM2 tetramerization induced glycolytic ATP production and decreased mitochondrial ATP production (**Figure 35H**).

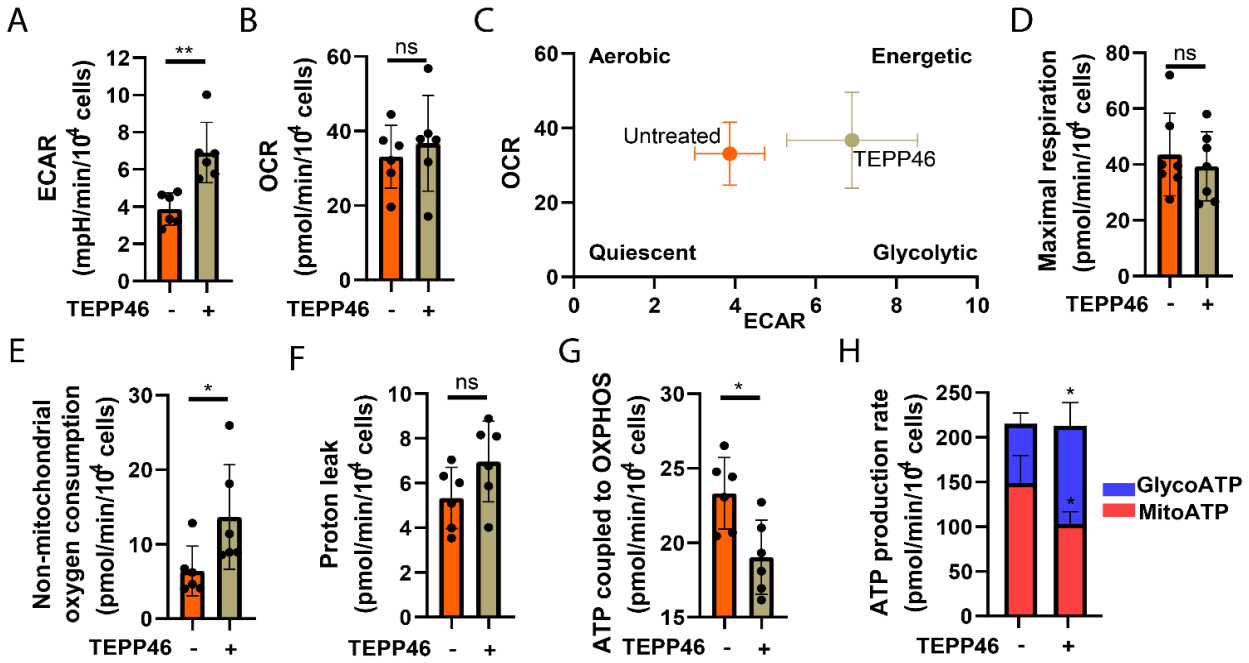

Figure 35. PKM2 tetramerization leads to a glycolytic shift in human VIC. (A-G) Cells were incubated with 50 µM TEPP46 for 24h and then analyzed using Seahorse Mito Stress assay. (A) ECAR quantitation. (B) OCR quantitation (C) Energetic map (ECAR vs. OCR plot). (D) Maximal respiration. (E) Non-mitochondrial oxygen consumption. (F) Proton leak. (G) ATP production linked to OXPHOS. (H) Main sources of ATP were evaluated by ATP rate assay. Data are expressed as the mean ± SD (N=6/7). ns, indicates non-significant differences; *, p<0.05; **, p<0.01. Student's unpaired t-test.

Due to the association between PKM2 and HIF-1α since it has been previously described that dimeric PKM2 is present in the nuclei of tumor cells and is responsible for the Warburg effect by interacting with HIF-1α (reviewed in Puckett et al., 2021), we analyzed HIF-1α stabilization after PKM2 activation. WB analysis showed an increase in HIF-1α stabilization upon PKM2 induction with TEPP46 (**Figure 36A-B**).

Next, we explored the potential role of PKM2 in VIC inflammation. WB blot analysis revealed increased activation of the master inflammation regulator NF-κB, as shown by its phosphorylation (**Figure 36A, C**). Then, the expression of pro-inflammatory cytokines regulated by NF-κB was measured using qPCR. Data elucidated an upregulated expression of *IL6* and *IL8* upon TEPP46 treatment (**Figure 36D-E**), indicating that PKM2 activation was associated with inflammation in human VIC.

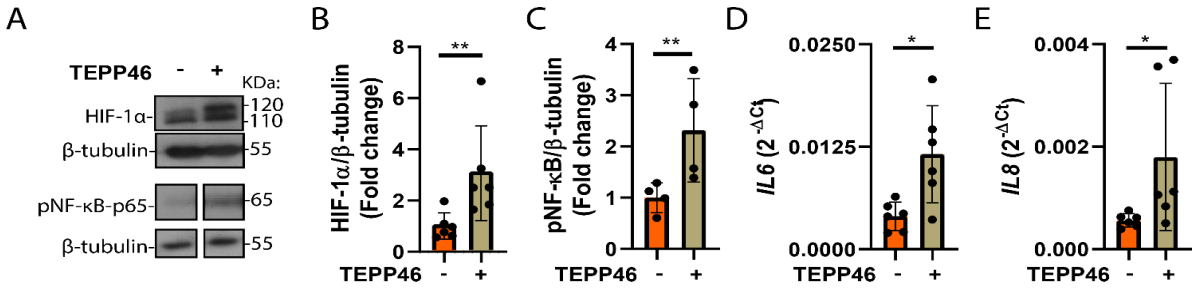

Figure 36. PKM2 activation increases HIF-1α stabilization and inflammation in VIC. VIC were incubated with 50 µM TEPP46 for 24h and then analyzed. (A) Immunoblot showing HIF-1α and NF-κB phosphorylation levels. (B) Quantification of HIF-1α levels. (C) Quantitation of p NF-κB levels. (D) PCR expression levels of *IL6*. (E) qPCR results of *IL8* expression. Data are expressed as the mean ± SD (N=4/6). *p<0.05, **p<0.01. Student's unpaired t-test.

Next, we asked if PKM2 was playing a role in processes such as differentiation and calcification. First, human VIC treated with TEPP46 in growth media for 21 days exhibited some morphological changes resembling an incipient osteoblast-like phenotype (**Figure 37A**). Additionally, qPCR measurement of the osteoblast marker *BMP2,* after 24h of TEPP46 treatment showed a significant induction (**Figure 37B**). Next, *in vitro* calcification assays for 7 days showed that TEPP-46 increased nodule formation and Ca^{2+} deposits (**Figure 37C-D**). Finally, to evaluate the potential mechanisms supporting PKM2-induced calcification, WB analysis revealed enhanced ERK phosphorylation upon TEPP46 treatment (**Figure 37E**), consistent with the reported MAPK signaling activation previously associated with VIC calcification (Gu et al., 2009).

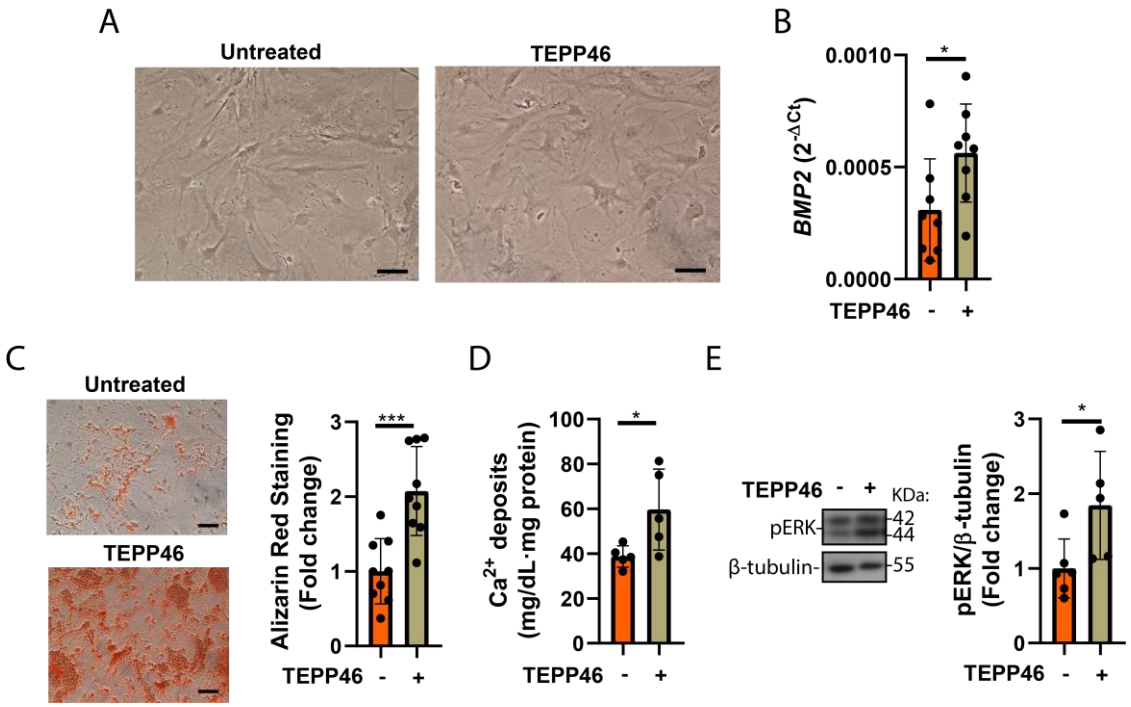

Figure 37. PKM2 activation potentiates VIC differentiation and calcification and promotes ERK activation. (A) VIC were incubated with 50 µM TEPP46 for 21 days and imaged. Images representing N=3. Black line indicates 50 µm. (B) *BMP2* expression levels after 24h of stimulation. (C) VIC were activated for 7 days in calcification media: (C) alizarin red staining images and quantitation (D) and Ca^{2+} deposits. (E) Representative immunoblots and quantitation of ERK phosphorylation upon 24h stimulation. Data are expressed as the mean ± SD (N=5/9). N indicates the number of VIC isolates from independent valve donors; ns, non-significant differences; *, p<0.05; ***, p<0.001. Student's unpaired t-test.

Together, data from this section highlighted the role of PKM2 in VIC metabolic reprogramming and triggering inflammation, cell differentiation, and calcification processes underlying CAVD pathogenesis.

R.5.6- Inflammation-induced lactate secretion has a key role in inflammation, differentiation, and calcification processes in VIC

Considering our previous results showing an increase in lactate secretion (**Figure 9C**) as well as overexpression of the lactate transporter gene *MCT4* (**Table 1**), we sought to assay the role of lactate production in pathogenic processes underlying CAVD by blocking the enzyme LDH with the inhibitor sodium oxamate. Since lactate has been reported to have a direct role in HIF-1α stabilization leading to osteogenesis in osteoblast-lineage cells (Y. Wu et al., 2017), we first analyzed HIF-1α expression. WB data showed that inhibition of lactate production significantly abrogated the stabilization of HIF-1α induced by co-stimulation with LPS and IFN-γ, while no significant effect was observed on STAT1 activation (**Figure 38A-C**).

Later, due to the recent association of lactate to immune induction and inflammation (Beyoğlu et al., 2021 & Haas et al., 2015) and considering the crucial role of inflammation in CAVD pathogenesis, we measured the activation of NF-κB, and the expression of inflammatory molecules regulated by this factor. WB data showed a tendency for LPS + IFN-γ-induced NF-κB phosphorylation to decrease when lactate production was blunted with oxamate (**Figure 38D**), as well as ICAM-1 (**Figure 38E**), and VCAM-1 expression (**Figure 38F**). In addition, sodium oxamate significantly inhibited the expression of *PTGS2*, a gene encoding COX2 (**Figure 38G**) that has been associated with CAVD calcification (Wirrig et al., 2015). Finally, ELISA assay showed that blunting lactate production abrogated the IL-6 secretion induced upon inflammatory stimulation (**Figure 38H**). These data suggest a role for lactate in inflammation triggered by VIC exposure to inflammatory stimuli.

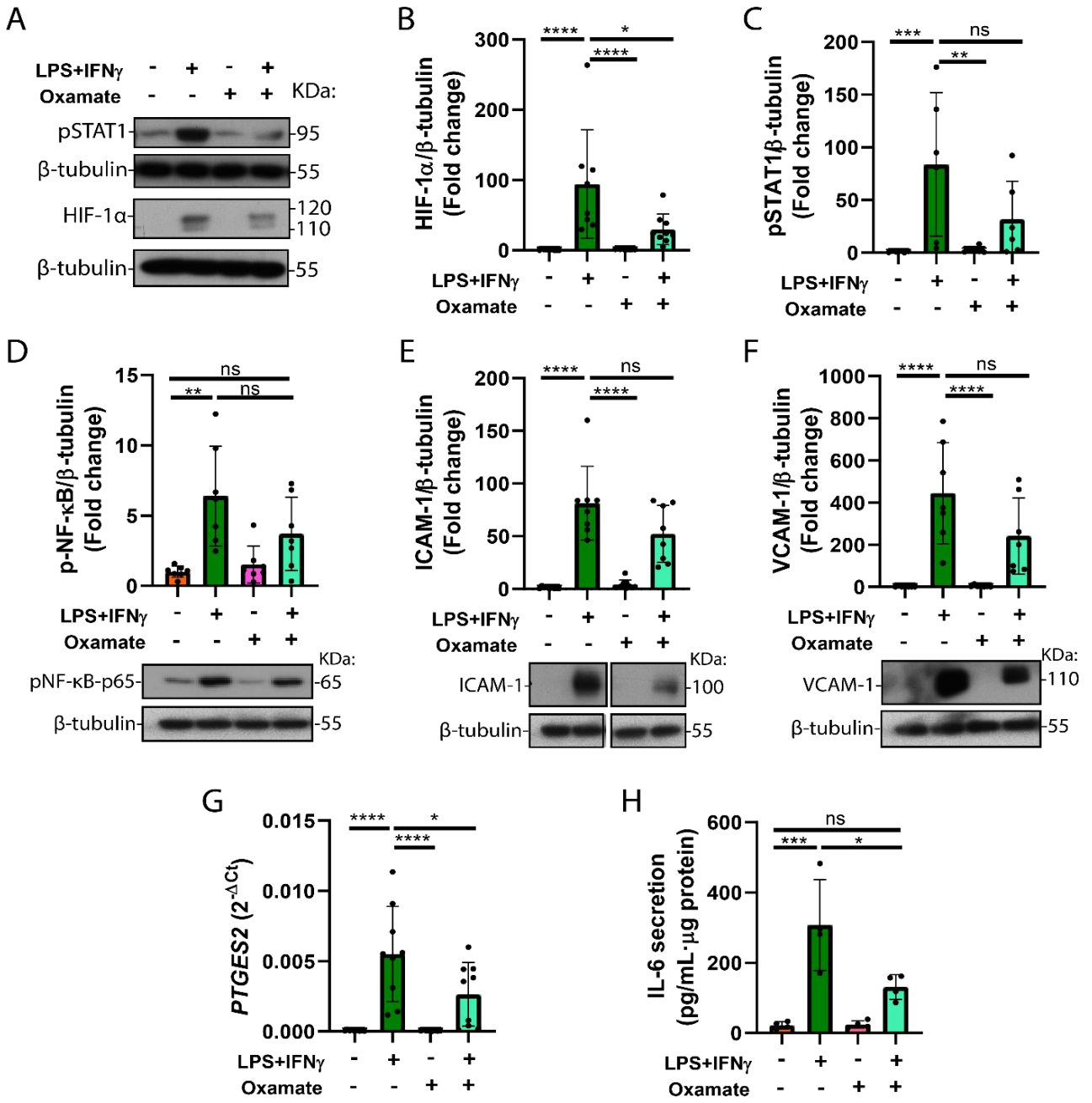

Figure 38. Inhibition of lactate production directly blunts LPS + IFN-γ-induced HIF-1α stabilization and the expression of inflammatory mediators. (A-F) VIC were pre-incubated with 10 mM sodium oxamate and later activated for 24h with 100 ng/mL LPS and 1 µg/mL IFN-γ and analyzed by WB. (A) Representative-blots and quantitation of (B) STAT1 phosphorylation. (C) HIF-1α stabilization. (D) NF-κB phosphorylation. (E) ICAM-1 expression. (F) VCAM-1 expression. (F) qPCR analysis of *PTGES2* (COX2) transcription levels. (G) ELISA for IL-6 secretion Data are expressed as the mean ± SD (N=4/7). Ns, non-significant differences; *, p<0.05; **, p<0.01; ***, p<0.001; ****, p<0.0001. One-way ANOVA with Tukey post-hoc in panels D, H. One-way ANOVA with Dunnett's post-hoc test (vs. LPS + IFN-γ) in B, C, E, F, and G.

Next, we addressed the role of lactate production in VIC differentiation and *in vitro* calcification. The analysis of cell morphology after 21 days of treatment disclosed morphological changes by the inhibition of lactate production with sodium oxamate. Microphotographs unveiled that the inhibition of lactate production partially blunted the osteoblast-like phenotype induced upon LPS + IFN-γ treatment (**Figure 39A**).

Then, *in vitro* calcification assays for 7 days, showed that sodium oxamate blunted the inflammatory-induced mineralization (**Figure 39B**). Notably, sodium oxamate significantly inhibited basal calcification in VIC (**Figure 39B**). Taken together, these data indicate a role for lactate in VIC differentiation and calcification.

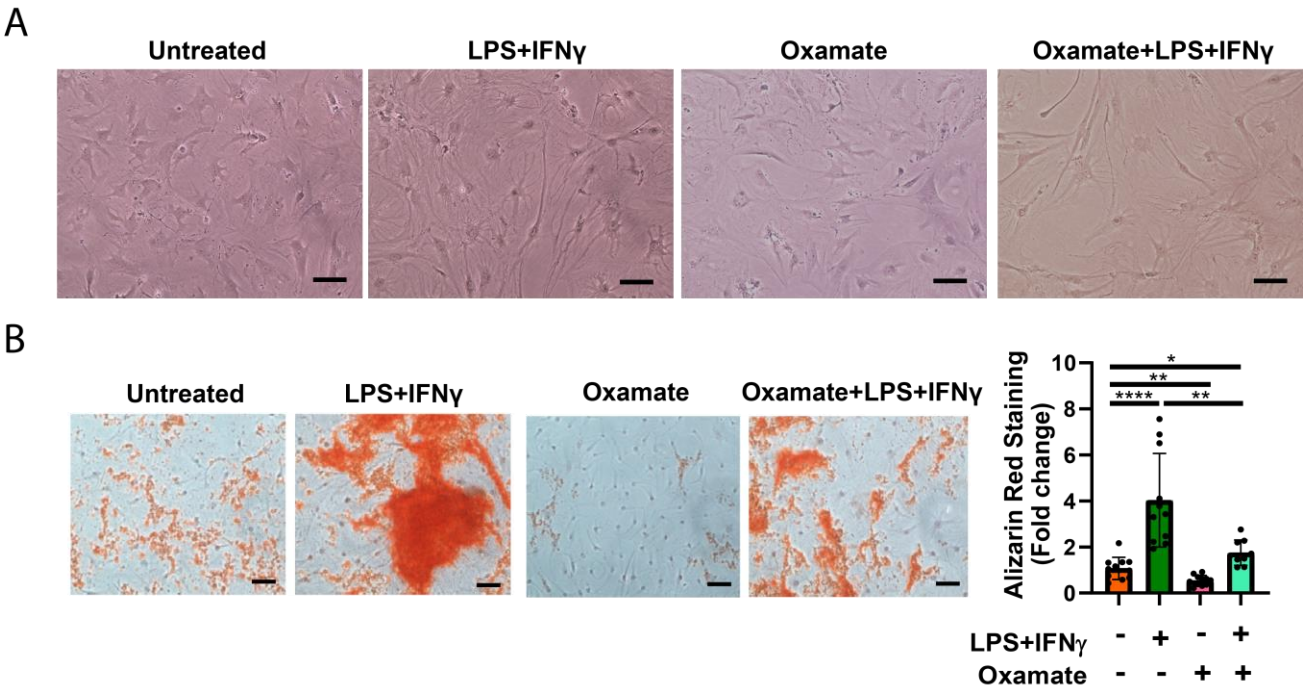

Figure 39. Lactate production blockade significantly inhibits inflammatory-mediated VIC differentiation and calcification. VIC were pre-incubated with 10 mM sodium oxamate and activated with 100 ng/mL LPS and 1 µg/mL IFN-γ. (A) Microphotographs of VIC treated for 21 days in M199 media. Representative of N=4. Black line indicates 50 µm. (B) Representative images and alizarin red staining quantitation of cells treated for 7 days in calcification media and quantitation (N=11). *p<0.05, **p<0.01, ****p<0.0001. One-way ANOVA with Tukey's post-hoc test.

Considering that lactate has been described as a signaling molecule (reviewed in Xiaolu et al., 2022) and the increased lactate secretion detected in the supernatants of activated VIC (**Figure 9C**), we next explored the potential role of secreted lactate in surrounding VIC. For this purpose, we exposed the cells to sodium lactate for 24h and assayed metabolic and pathogenic markers. WB analysis revealed that extracellular sodium lactate induced HIF-1α stabilization in VIC (**Figure 40A**). Moreover, Seahorse Mito Stress assay showed that exposure of VIC to sodium lactate enhanced the ECAR rate (**Figure 40B**), which was consistent with increased HIF-1α stabilization and glycolysis. Interestingly, Seahorse assay unveiled a direct role of extracellular lactate in the upregulation of non-mitochondrial oxygen consumption (**Figure 40C**), suggesting increased ROS production. In addition, sodium lactate significantly inhibited coupling efficiency (**Figure 40D**), suggesting some potential mitochondrial damage leading to a tendency in decreasing mitochondrial ATP production (**Figure 40E**). Furthermore, extracellular lactate altered VIC phenotype since after 21 days of treatment, VIC exhibited an osteoblast-like phenotype when compared with untreated cells (**Figure 40F**).

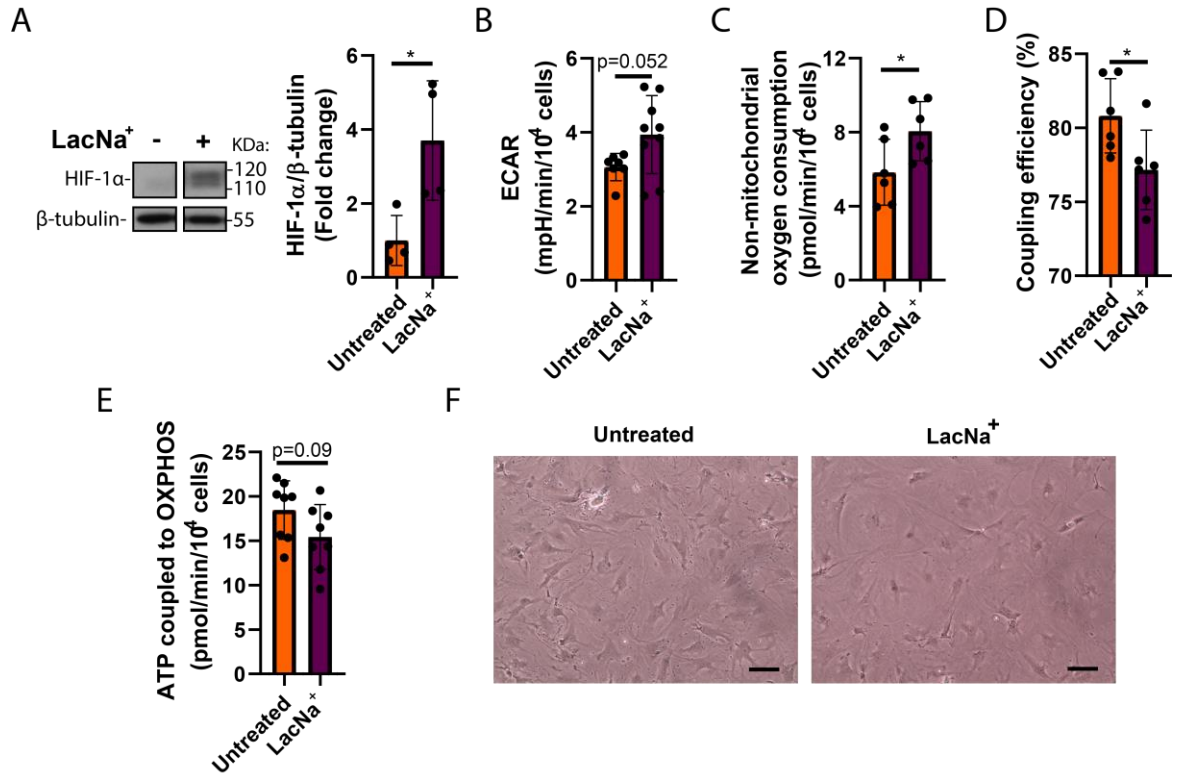

Figure 40. Extracellular lactate induces HIF-1α stabilization, metabolic changes, and VIC differentiation. (A-D) VIC were treated as indicated for 24 h. $LacNa^+$, 15 mM sodium lactate. (A) Western blot analysis of HIF-1α expression. (B) Seahorse Mitrostress assay. ECAR rate. (C) Non-mitochondrial oxygen consumption. (D) Coupling efficiency measure. (E) ATP production linked to OXPHOS. (F) Microphotographs of VIC treated with $LacNa^+$ for 21 days. Representative of N=4. Black line indicates 50 µm. Data, mean ± SD (N=4/8). ns, non-significant differences. *p<0.05, ***p<0.001. Student's unpaired t-test.

Data from this section indicated that lactate production was necessary for inflammatory-induced inflammation, differentiation, and calcification, most likely via HIF-1α stabilization. Notably, this metabolite, secreted by inflammatory activation of VIC, may exert some effects as a signal molecule by inducing metabolic changes in the neighboring VIC.

R.6-Role of pentose phosphate pathway in inflammatory-induced metabolic reprogramming and redox homeostasis

As HIF-1α activity has been demonstrated to influence the pentose phosphate pathway (Majmundar et al., 2010) and considering data suggesting a decrease in the oxidative arm of PPP (oxPPP) based on the downregulation of its rate-limiting enzyme in VIC (**Figure 10**) and its influence in redox homeostasis alteration (**Figure 12**), we addressed the role of the oxPPP in VIC physiopathology by analyzing processes relevant to CAVD pathogenesis as well as in redox alteration.

R.6.1- G6PD inhibition increases glycolytic shift in human VIC

To characterize the role of oxPPP inhibition in disease processes, we used G6PDi, a specific inhibitor of the rate-limiting enzyme, G6PD. Cells were pre-incubated with G6PDi, for at least 45 min and then inflammatory activated for 24h. Seahorse metabolic analysis showed that inhibition of G6PD induced a metabolic rewiring characterized by an increase in ECAR, while no significant changes in OCR (**Figure 41A-B**). Notably, the energy map unveiled that G6PD blockade promoted a similar metabolic rewiring to glycolytic phenotype as the co-stimulation of VIC with LPS and IFN-γ but showed no further potentiation of inflammatory stimuli effects (**Figure 41C**). Next, since metabolism was altered upon oxPPP inhibition, we also measured the transcription levels of key glycolytic genes and found that *PFKFB3* transcript levels were upregulated by G6PDi (**Figure 41D**). Data highlight the role of oxPPP downregulation in glycolytic shift in VIC.

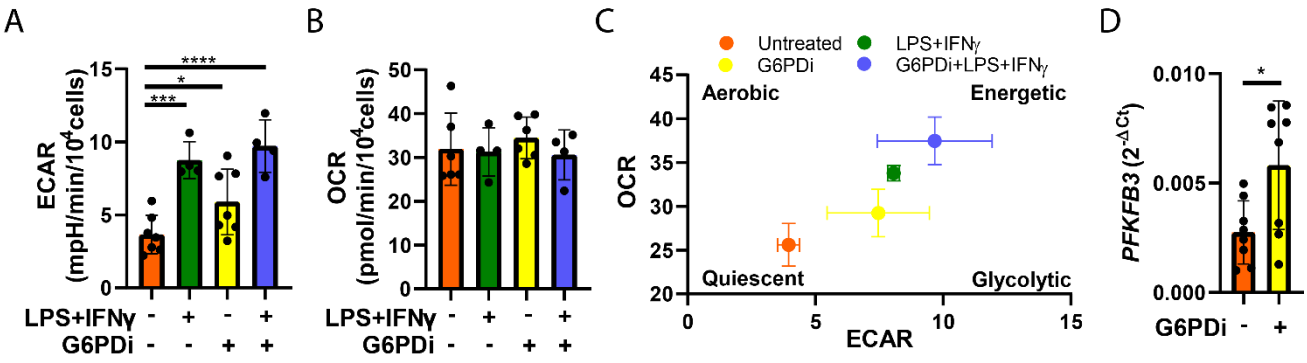

Figure 41. The inhibition of the limiting enzyme of the oxPPP promotes a metabolic rewiring to a glycolytic phenotype. VIC were pre-incubated with 10 µM G6PDi and activated with 100 ng/mL LPS and 1 µg/mL IFN-γ for 24h. (A) ECAR levels (N=4), (B) OCR levels (N=6), and (C) energetic map (ECAR vs. OCR plot). (D) qPCR analysis of *PFKFB3* transcript levels (N=8). *p<0.05, **p<0.01, ****p<0.0001. One-way ANOVA with Dunnett's post-hoc test (vs. untreated) is shown in panel A. Student's unpaired t-test in D.

R.6.2- G6PD inhibition upregulates inflammation, differentiation, and calcification in VIC

To further characterize the role of the oxPPP in other processes underlying CAVD, we assessed the impact of G6PD downregulation on inflammatory responses in human VIC. WB results showed that G6PDi activated the key regulator of inflammation, NF-κB, and further potentiated LPS + IFN-γ-mediated activation of NF-κB (**Figure 42A-B**). Moreover, G6PDi increased the expression of adhesion molecules, such as VCAM-1,

although no further potentiation was observed when combined with inflammatory stimuli (**Figure 42A, C**). In addition, qPCR analysis showed that *IL6* transcript levels were upregulated upon G6PD inhibition (**Figure 42D**). Next, we explored the potential role of the oxPPP inhibition in VIC differentiation and ECM remodeling. Notably, qPCR data disclosed that G6PD inhibition downregulated *ACTA2* expression, while upregulating *BMP2* and *MMP1* transcript levels (**Figure 42E-G**), indicating a role in VIC differentiation and ECM remodeling.

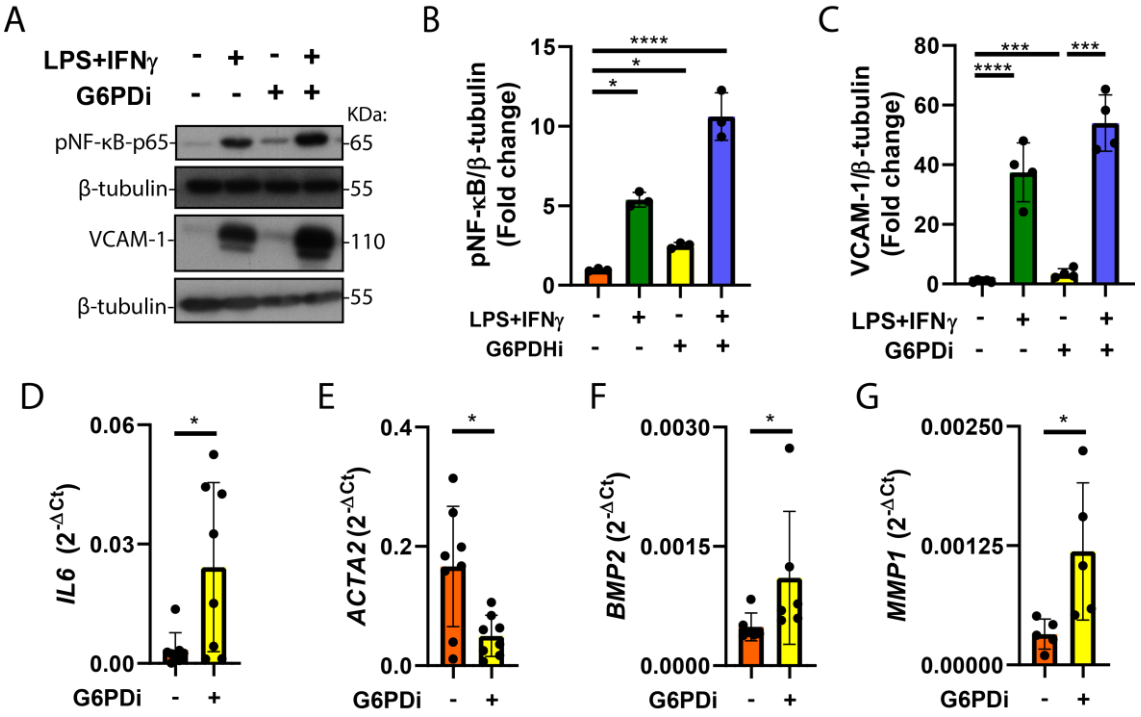

Figure 42. The inhibition of G6DP enzyme induces inflammatory routes and mediators and upregulates markers of differentiation and extracellular matrix remodeling. VIC were pre-incubated with 10 µM G6PDi and then activated with 100 ng/mL LPS and 1 µg/mL IFN-γ for 24h. (A-C) Representative blots and quantitation of NF-κB phosphorylation and VCAM-1 expression (N=3/4). (D-G) qPCR analysis of *IL6, ACTA2*, *BMP2*, and *MMP1* transcript levels (N=5-8). *p<0.05, ***p<0.001, ****p<0.0001. Data are expressed as mean ± SD. One-way ANOVA with Tukey post-hoc analysis in C. One-way ANOVA with Dunnett's post-hoc analysis (vs. untreated) in panel A. Student's unpaired t-test in D-G.

Next, *in vitro* calcification assays unveiled that G6PDi promoted VIC mineralization but was not able to further potentiate the effects of inflammatory stimuli (**Figure 43A**). Later, when addressing the underlying mechanisms, we found that G6PDi significantly increased ERK phosphorylation (**Figure 43B**), thus suggesting the involvement of the ERK pathway in mediating calcification induced by blockade of the oxPPP.

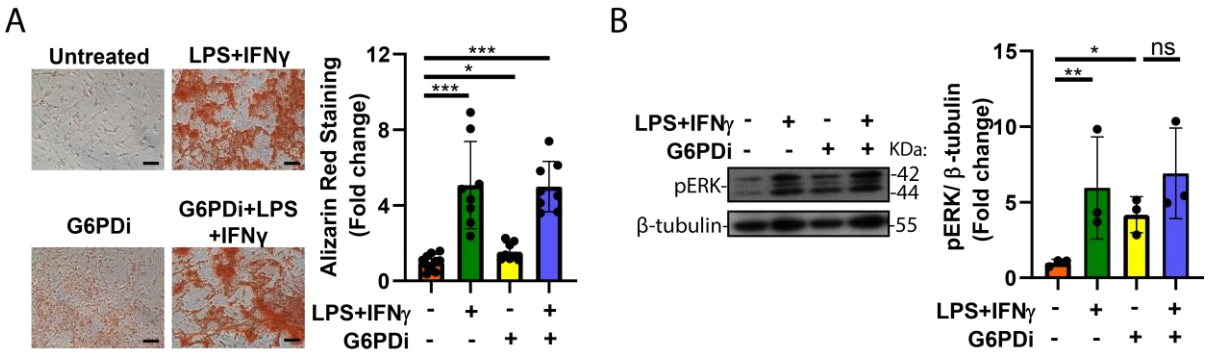

Figure 43. Blockade of the limiting enzyme of the oxPPP increases *in vitro* calcification in VIC and activates the ERK routes. VIC were pre-incubated with 10 µM G6PDi and then activated with 100 ng/mL LPS and 1 µg/mL IFN-γ for 7 days in calcification medium (A), or for 24 h in activation medium and analyzed (B). (A) Representative Alizarin red staining and quantitation (N=8). Black line indicates 50 µm. (B) Representative blot and quantitation of ERK phosphorylation (N=3). Ns, non-significant differences; *, p<0.05; **, p<0.01; ***, p<0.001; ****, p<0.0001. Data are expressed as mean ± SD. One-way ANOVA with Tukey's post-hoc analysis in A. One-way ANOVA with Dunnett's post-hoc analysis (vs. untreated) in B.

R.6.3- G6PD inhibition and a ROS inducer promote non-mitochondrial oxygen consumption in human VIC

To further elucidate the association between oxPPP inhibition and redox homeostasis alteration, as described in other models such as phagocytes and animal models of ischemic stroke (reviewed in Bradshaw et al., 2019), we first analyzed non-mitochondrial oxygen consumption. Seahorse analysis showed that G6PDi triggered non-mitochondrial oxygen consumption, but no further potentiated LPS + IFN-γ effects (**Figure 44A**). Thus, we sought to investigate the potential role of ROS in redox homeostasis and metabolic rewiring. Seahorse metabolic analysis of VIC treated with H_2O_2, a known ROS inducer, showed a direct association between ROS and non-mitochondrial oxygen consumption increase (**Figure 44B**). In addition, H_2O_2 treatment also induced ECAR (**Figure 44C**), suggesting a direct interplay between ROS and metabolic reprogramming.

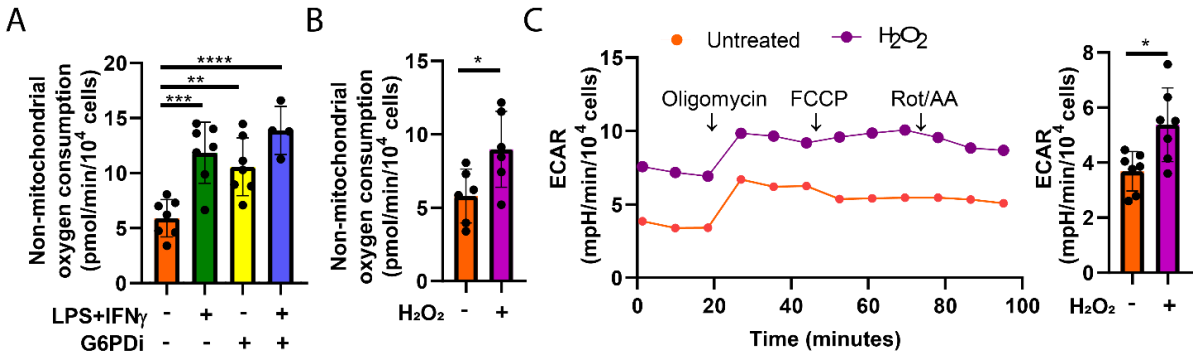

Figure 44. Inhibition of the limiting enzyme of the oxPPP arm and H_2O_2 treatment increase non-mitochondrial oxygen consumption and ECAR. (A) VIC were pre-incubated with 10 µM G6PDi and then activated with 100 ng/mL LPS and 1 µg/mL IFN-γ for 24h and non-mitochondrial oxygen consumption was measured with Seahorse metabolic analyzer. (B-C) Cells were treated with 100 µM H_2O_2 and analyzed by Seahorse Mito Stress assay; (B)Non-mitochondrial oxygen consumption was measured. (C) Representative graph of ECAR and its quantitation. *p<0.05, **p<0.01, ***p<0.001, ****p<0.0001. Data are expressed as mean ± SD (N=6/7). One-way ANOVA with Dunnett post-hoc (vs. untreated) in panel A. Student's unpaired t-test in C, D.

Taken together, results indicated that inhibition of G6PD, the rate-limiting enzyme of PPP, enhanced non-mitochondrial oxygen consumption, which could be associated with an increase in ROS production, and subsequently play a direct role in the induction of glycolytic phenotype induction in VIC.

R.7-Role of oxidative stress in inflammatory-mediated responses in VIC

R.7.1- Reduction of oxidative stress by the antioxidant NAC abrogates inflammation, differentiation, and calcification processes induced in VIC exposed to inflammatory stimuli

Oxidative stress is usually generated by an imbalance between ROS formation and degradation mechanisms. To reduce the cellular damage caused by ROS, N-acetylcysteine (NAC) is converted into metabolites that stimulate the synthesis of glutathione, generating its reduced form (GSH), which functions as a free radical scavenger. Considering this, we sought to further characterize the role of oxidative stress generated by metabolic reprogramming and PPP impairment in inflammation-induced inflammation, differentiation, and calcification. First, WB analysis revealed that the antioxidant NAC partially inhibited the stabilization of HIF-1α, and VCAM-1 expression induced by the co-stimulation of VIC with LPS + IFN-γ (**Figure 45A-B**). Furthermore, the inflammation-induced upregulation of other inflammatory cytokines, such as *IL6* and *IL8*, was significantly blunted when oxidative stress was inhibited (**Figure 45C-D**). To explore the role of oxidative stress in VIC differentiation, *BMP2* marker expression was measured. qPCR data showed downregulation of inflammatory-induced *BMP2* expression by the antioxidant NAC (**Figure 45E**), suggesting that oxidative stress generated upon inflammatory activation triggered osteoblast-like differentiation. Finally, *in vitro* calcification assay elucidated that NAC treatment significantly inhibited the LPS + IFN-γ-induced mineralization (**Figure 45F**).

Together, results suggested a significant role of inflammatory-induced oxidative stress in inflammation, differentiation, and calcification in VIC exposed to an inflammatory milieu.

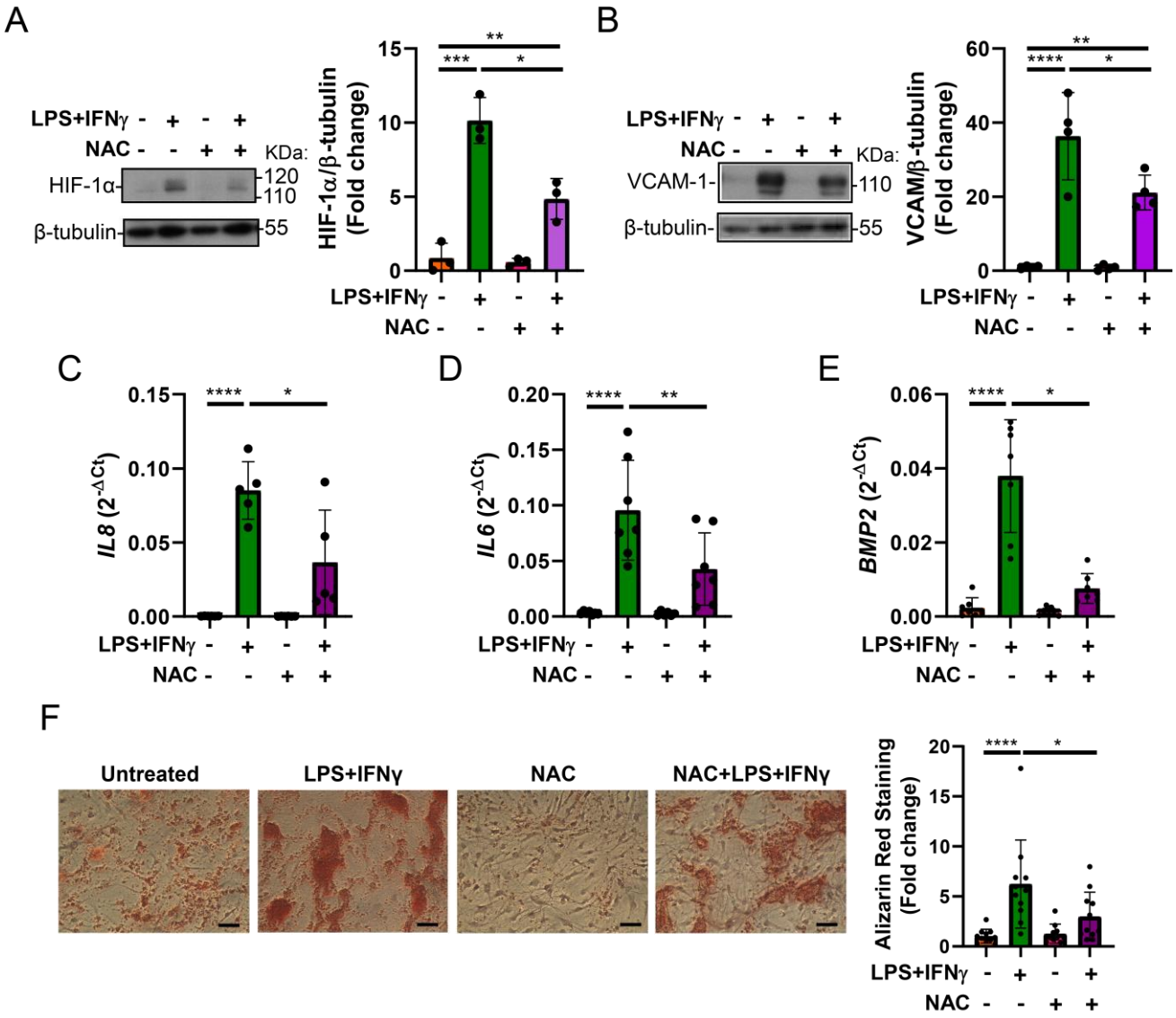

Figure 45. The antioxidant NAC reduces inflammatory-induced effects on HIF-1α stabilization, inflammatory differentiation markers, and VIC mineralization. VIC were pre-incubated with 10 mM NAC and then activated with 100 ng/mL LPS and 1 µg/mL IFN-γ for 24h. (A-B) Representative blot and quantitation of HIF-1α stabilization and VCAM-1 expression (N=3/4). (C-E) qPCR analysis of transcript levels of *IL8*, *IL6*, and *BMP2* (N=5/7). (F) VIC were pre-incubated with 10 mM NAC and then activated for 7 days in calcification media. Alizarin red staining and quantitation (N=10). Black line indicates 50 µm; ns, non-significant differences; *, p<0.05; **, p<0.01; ***, p<0.001; ****, p<0.0001. Data are expressed as mean ± SD. One-way ANOVA with Tukey's post-hoc test in A-B. One-way ANOVA with Dunnett's post-hoc test (vs. LPS + IFN-γ) in C-F.

R.8- Role of the tricarboxylic acid cycle in JAK-STAT/HIF-1α pathway, inflammation, and differentiation in VIC exposed to inflammatory stimuli

As disclosed by fluxomic experiments, [U-^{13}C]-glucose carbons were incorporated into acetyl-CoA synthesis and consequently into some TCA metabolites such as citrate and succinate (**Figure 13**). Acetyl-CoA is produced in the mitochondria and has several fates, as previously described. Taking this information into account, we assessed the role of acetyl-CoA production and pyruvate entry into the mitochondria in CAVD pathological processes. First, we used dichloroacetate (DCA), a pharmacological inhibitor of pyruvate dehydrogenase kinase 4 (PDK4), to mimic the PDK4 decrease observed in LPS + IFN-γ-activated VIC (**Table 2**). As previously mentioned, PDK4 is a negative regulator of PDH that controls the conversion of pyruvate to acetyl-CoA in the mitochondria. WB analysis revealed that direct inhibition of PDK4 by DCA increased HIF-1α stabilization and STAT1 phosphorylation (**Figure 46A-B**), indicating the activation of both transcription factors. Additionally, experiments using UK5099, an inhibitor of mitochondrial pyruvate carrier 1 (MPC1), the transporter of pyruvate to mitochondria, further confirmed the importance of pyruvate entrance for the inflammatory-induced HIF-1α stabilization (**Figure 46C**).

Next, we assayed the effects of pyruvate entry into the mitochondria and acetyl-CoA production on inflammatory routes and mediators. Experiments using DCA showed a significant increase in NF-κB phosphorylation (**Figure 46D, E**), as well as the expression of downstream inflammatory mediators, such as ICAM-1 (**Figure 46D, F**) and *IL6* transcript levels (**Figure 46D,G**), indicating a role of PDK4 inhibition in inflammation.

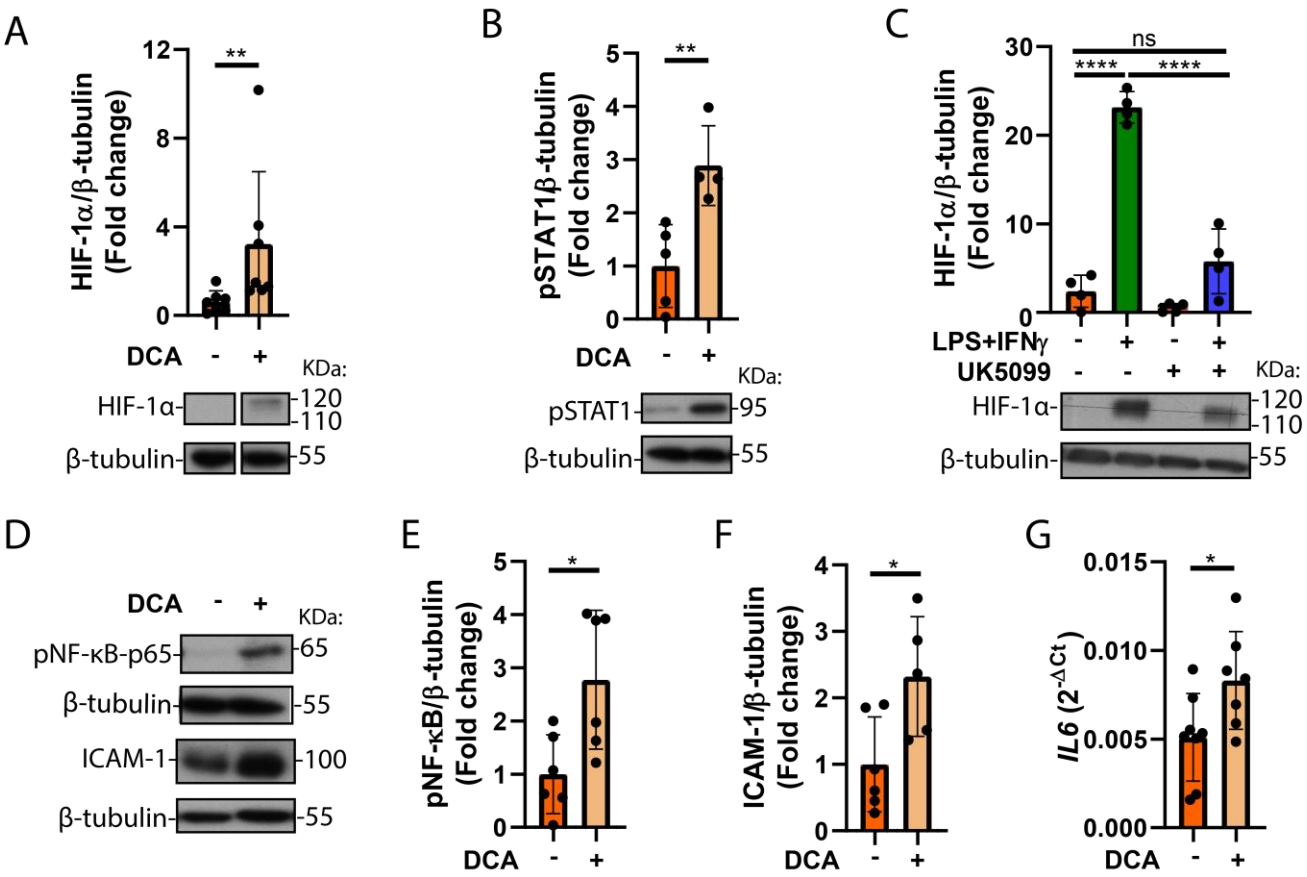

Figure 46. Pyruvate entry into mitochondria and acetyl-CoA production are important in JAK-STAT/HIF-1α and NF-κB pathway activation and downstream production of inflammatory mediators. VIC were incubated with 5mM DCA or pre-incubated for 1h with 50 µM UK5099 and then activated with 100 ng/mL LPS and 1 µg/mL IFN-γ for 24h. (A-B) WB analysis of HIF-1α stabilization and STAT1 phosphorylation upon DCA treatment. (C) WB of HIF-1α stabilization upon UK5099 and inflammatory stimulation. (D-F) Representative immuno-blot of pNF-κB and ICAM-1 upon DCA treatment, and quantification. (G) qPCR results for *IL6* transcription levels. N indicates the number of VIC isolates from independent valve donors; ns, non-significant; *, p<0.05; **, p<0.01; ****, p<0.0001. Data are expressed as mean ± SD (N=4-8). One-way ANOVA with Tukey post-hoc analysis in panel C. Student's unpaired t-test in A, B, E, F, G.

Later, the role of acetyl-CoA production and pyruvate entry into the mitochondria during differentiation and calcification was assessed. qPCR analysis showed that the treatment of VIC with DCA resulted in the downregulation of the myofibroblast marker, *ACTA2* (**Figure 47A**), and upregulation of the osteogenic marker *BMP2* (**Figure 47B**), suggesting that the inhibition of PDK4 and subsequent activation of PDH, which catalyzes the conversion of pyruvate to acetyl-CoA, played a role in VIC differentiation. Then, calcification assays blocking the pyruvate transporter exhibited a reduction in LPS + IFN-γ-induced calcification of VIC (**Figure 47C**). In addition, WB analysis revealed that inhibiting pyruvate transporter with UK5099 inhibited ERK phosphorylation by inflammatory stimuli (**Figure 47D**), while inhibiting PDK4 with DCA increased ERK activation (**Figure 47E**). Data suggest a role of MAPK pathway in induced calcification upon pyruvate entrance to mitochondria and acetyl-CoA production.

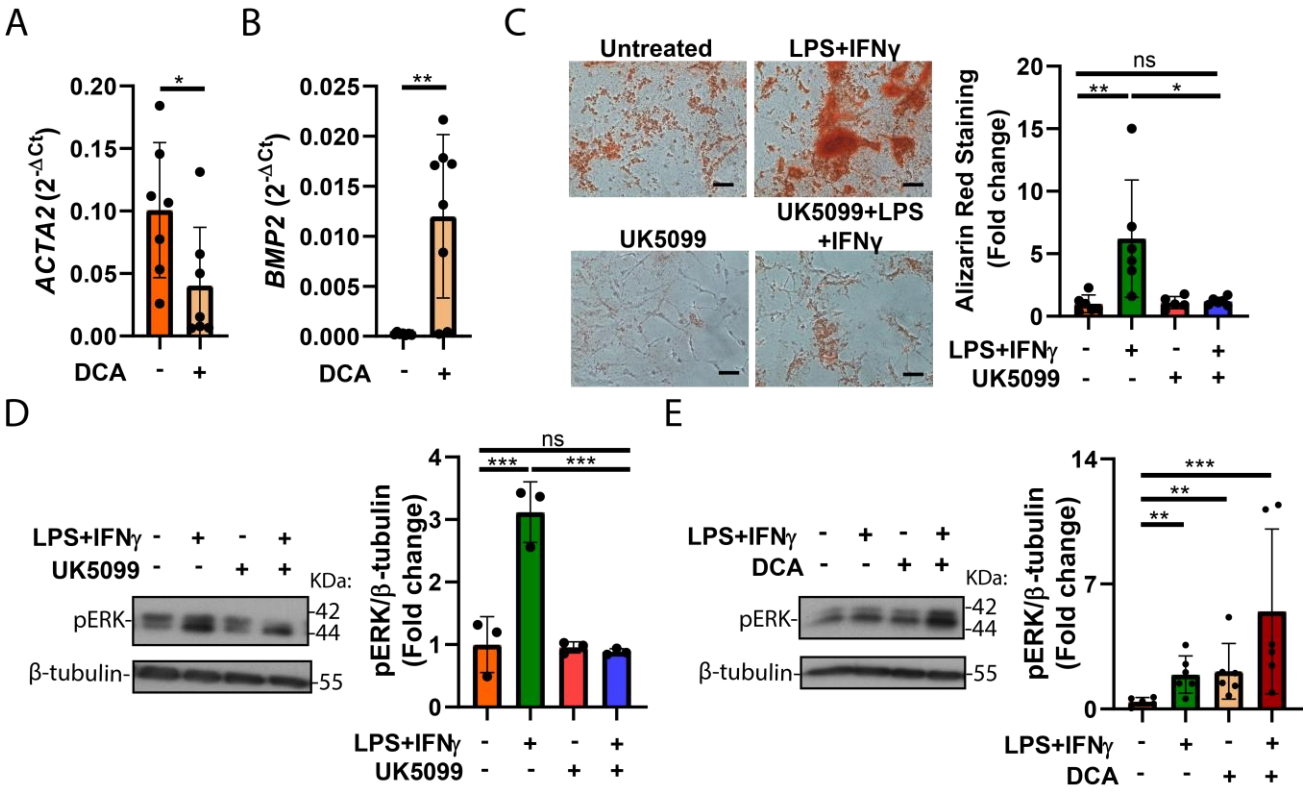

Figure 47. Pyruvate entry into mitochondria and acetyl-CoA production play a role in VIC differentiation and calcification via ERK activation. VIC were incubated with 5mM DCA or pre-incubated for 1h with 50 µM UK5099 and then activated with 100 ng/mL LPS and 1 µg/mL IFN-γ for 24h. (A-B) qPCR analysis of *ACTA2* and *BMP2* transcript levels upon DCA activation. (C) Alizarin red staining and its quantification. (D-E) Western blot analysis of ERK phosphorylation upon indicated treatments. Ns, non-significant differences; *, p<0.05; **, p<0.01; ***, p<0.001. Data are expressed as mean ± SD (N=3-8). One-way ANOVA and Tukey post-hoc test in panels C and D. One-way ANOVA and Dunnett post-hoc (vs. untreated) in E. Student's unpaired t-test in panels A and B.

Finally, to further characterize the role of acetyl-CoA entrance in the TCA cycle and subsequent metabolite production, we used several approaches. First, to assess the role of succinate accumulation in pathological processes, we used dimethyl malonate (DMM), a selective pharmacological inhibitor of SDH subunit A, to mimic the accumulation of succinate observed in VIC exposed to LPS + IFN-γ (**Figure 13**). WB analysis of HIF-1α protein revealed that succinate accumulation did not show a basal effect but further potentiated the inflammation-induced stabilization of HIF-1α (**Figure 48A**). Additionally, to further address the role of succinate, we used diethyl succinate, which can be recognized by the succinate receptor SUCNR1 that typically resides in the endoplasmic reticulum and relocates to the plasma membrane under hypoxic conditions (reviewed in K. Wu et al., 2023). Diethyl succinate treatment induced the stabilization of HIF-1α (**Figure 48B**) as well as changes in VIC morphology (**Figure 48C**), suggesting alterations in VIC phenotype. Finally, due to the importance of TCA metabolite production, but mainly acetyl-CoA, we investigated the role of exogenous citrate, a metabolite that can enter the cell by different transporters, such as plasma membrane-specific variant of SLC25A1 (Mycielska et al., 2018), as well as members of the SLC13 sodium sulfate/carboxylate symporter family (Judge et al., 2020). Taking this evidence into account, we treated VIC

with exogenous citrate for 21 days and observed morphological modifications (**Figure 48C**), suggesting the induction of phenotypic changes.

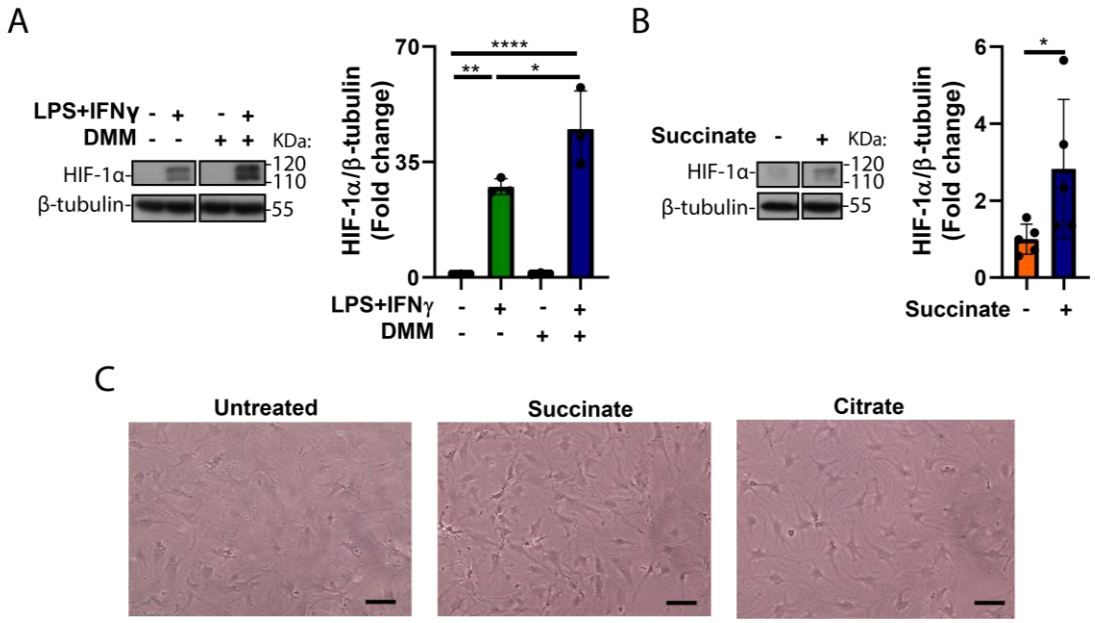

Figure 48. Succinate accumulation potentiates inflammation-induced HIF-1α stabilization and extracellular metabolites alter the VIC phenotype. (A) VIC were pre-incubated with 5mM DMM for 1h and then activated with 1µg/mL LPS and 100 ng/mL IFN-γ for 24 were used for WB analysis of HIF-1α (N=3). (B) VIC were treated with 10 mM diethyl succinate for 24h and were analyzed as in (A) (N=5). (C) VIC were treated with 10 mM diethyl succinate or 5 mM sodium citrate for 14 days in M199 medium. Representative microphotographs of N=3. Black line indicates 50 µm. Succinate indicates 10 mM diethyl succinate; *, p<0.05; **, p<0.01; ****, p<0.0001. Data are expressed as mean ± SD. One-way ANOVA with Tukey post-hoc in panel A. Student's unpaired t-test in B.

Altogether, data suggested that pyruvate entry into mitochondria and TCA metabolites were necessary for HIF-1α stabilization and VIC differentiation. Additionally, pyruvate transport to mitochondria showed a direct role in the activation of inflammatory pathways as well as VIC mineralization.

R.9- Role of OXPHOS modulation in JAK-STAT/HIF-1α pathway and subsequent metabolism rewiring

As described in the Introduction, the respiratory chain is composed of several complexes that allow the transport of electrons through the mitochondrial membrane while creating a proton-motive force that is finally used for ATP synthesis. Therefore, in this section, our aim was to evaluate whether any of the complexes participate in the LPS + IFN-γ-induced metabolic reprogramming of VIC.

R.9.1- Complex I does not play a role in inflammation-induced metabolic shift or subsequent inflammation, differentiation, and calcification in VIC.

To investigate the role of mitochondrial respiration chain complexes in VIC physiopathology, we used pharmacological inhibitors of complex I, rotenone, and metformin. In bioenergetic experiments using Seahorse metabolic analyzer rotenone showed a tendency, even non-significant changes, to increase ECAR in VIC untreated and exposed to inflammatory insults (**Figure 49A**). In contrast, OCR measurement showed a significant inhibition of oxygen consumption by rotenone in basal VIC, while a tendency to decrease OCR in LPS + IFN-γ activated cells (**Figure 49B**). Furthermore, WB analysis of HIF-1α showed no alteration of HIF-1α when inhibiting complex I before LPS + IFN-γ treatment (**Figure 49C**). In contrast, metformin, a well-known antidiabetic drug that is also a complex I inhibitor, significantly blunted the LPS + IFN-γ-induced stabilization of HIF-1α (**Figure 49D**). Later, when assessing the expression of some HIF-1α target genes, we found that metformin reversed the inflammatory-induced effects on *PDK4* gene expression (**Figure 49E**).

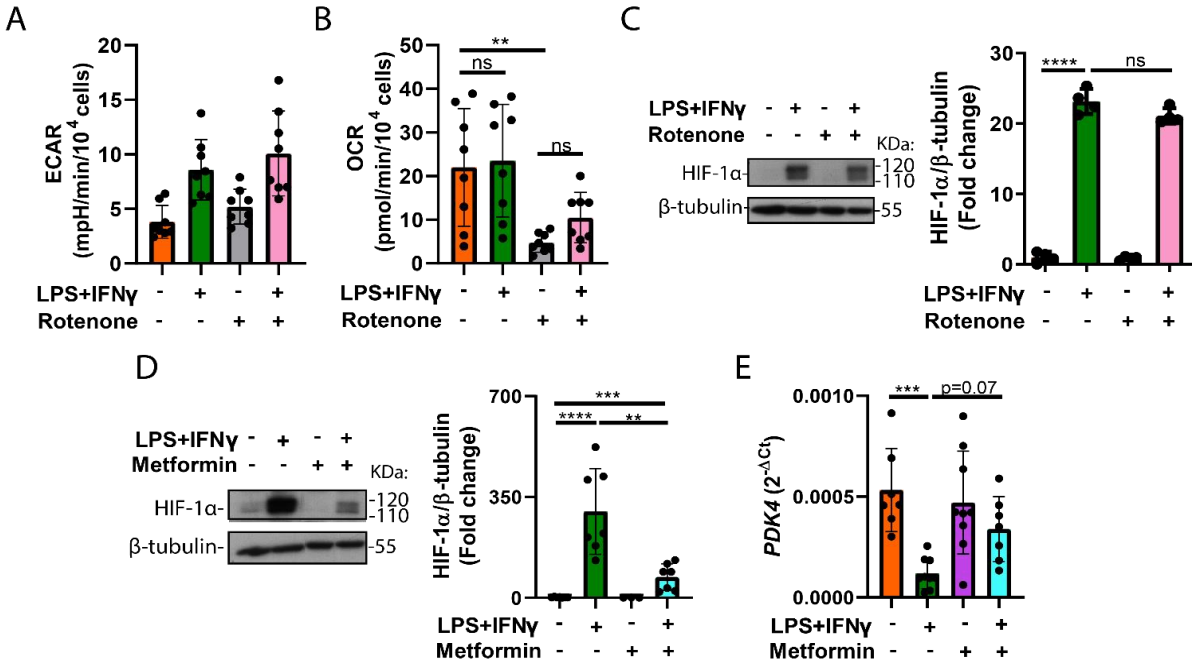

Figure 49. Inhibition of complex I inhibition by rotenone and metformin exhibit opposite effects in HIF-1α stabilization. VIC were pre-incubated with 1 µM rotenone or 5 mM metformin and then activated with 100 ng/mL LPS and 1 µg/mL IFN-γ for 24h. (A-B) Seahorse Mito Stress assay of ECAR and OCR (N=8). (C-D) Representative blot and quantitation of HIF-1α (N=4/7). (E) qPCR analysis of *PDK4* transcript levels (N=7). ns, non-significant differences. **p<0.01, ***p<0.001, ****p<0.0001. One-way ANOVA with Tukey's post-hoc test.

RESULTS

Considering the partial effect that complex I seemed to have in VIC physiopathology, we next addressed the effects in some inflammation and differentiation markers. qPCR results evidenced that although inflammatory effects induced by LPS + IFN-γ in *IL6* and *PTGES2* expression were not significantly altered in the presence of rotenone, a tendency to increase was observed upon rotenone-only treatment (**Figure 50A-B**). As for differentiation markers, rotenone potentiated the upregulation of *MMP1* gene expression by LPS + IFN-γ (**Figure 50C**) but had no effect on *BMP2* transcript levels (**Figure 50D**). In addition, experiments with metformin disclosed a significant effect on inflammatory cytokine expression by inhibiting the inflammatory-induced upregulation of *IL6* and *PTGES2* transcripts, as well as subsequent secretion of PGE_2 (**Figure 50E-G**).

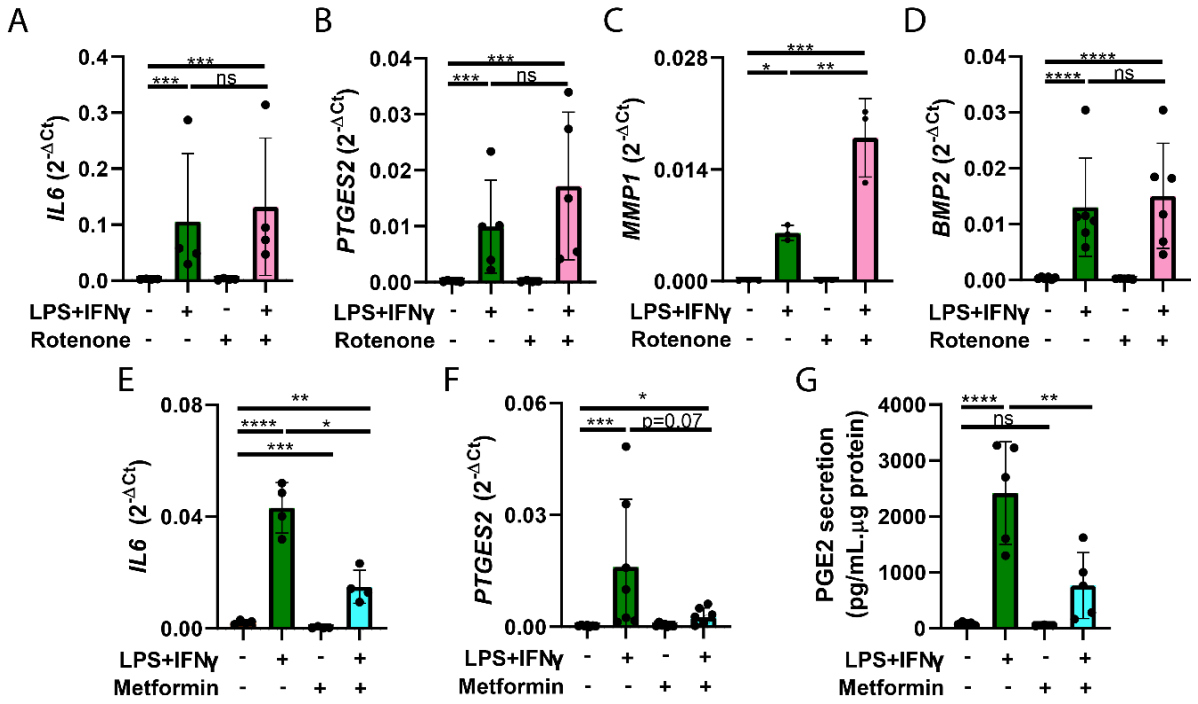

Figure 50. Complex I inhibition by metformin, but not by rotenone, downregulates inflammatory mediators. VIC were pre-incubated with 1 µM rotenone or 5 mM metformin and then activated with 100 ng/mL LPS and 1 µg/mL IFN-γ for 24h. (A-D) qPCR analysis of (A) *IL6*, (B) *PTGES2*, (C) *MMP1*, and (D) *BMP2* after rotenone treatment. (E-F) qPCR analysis of *IL6* and *PTGES2* after metformin treatment. (G) PGE2 secretion. Mean ± SD (N=3-6). ns, non-significant differences. *p<0.05, **p<0.01, ***p<0.001, ****p<0.0001. One-way ANOVA with Tukey's post-hoc test was performed.

Finally, we assayed the role of Complex I in the calcification process. In sights of the different pathways for the effects of rotenone and metformin, both inhibitors were used to perform *in vitro* calcification assays. Rotenone inhibition of complex I did not show significant effects on calcification, either in combination with LPS + IFN-γ or alone (**Figure 51A**). Notably, metformin treatment significantly decreased inflammatory-induced and basal calcification (**Figure 51B**). These differences suggested that metformin was conducting its effects by other pathways, in addition to complex I inhibition. In fact, several other targets have been described for metformin action, i.e., HIF-1α and PKM2. Additionally, recent evidence has shown

that metformin inhibits valvular calcification via AMPK and insulin signaling activation (En et al., 2021). Taking this information into account, we assayed downstream routes, such as PI3K and ERK, by WB. As shown in **Figure 51C-D**, metformin significantly inhibited the inflammatory-induced phosphorylation of ERK while induced AKT phosphorylation, suggesting that both mechanisms could mediate the role of metformin in calcification abrogation, in agreement with previous reports demonstrating a protective role of AKT in VIC calcification (Parra-Izquierdo et al., 2018 & Moorhead III et al., 2020).

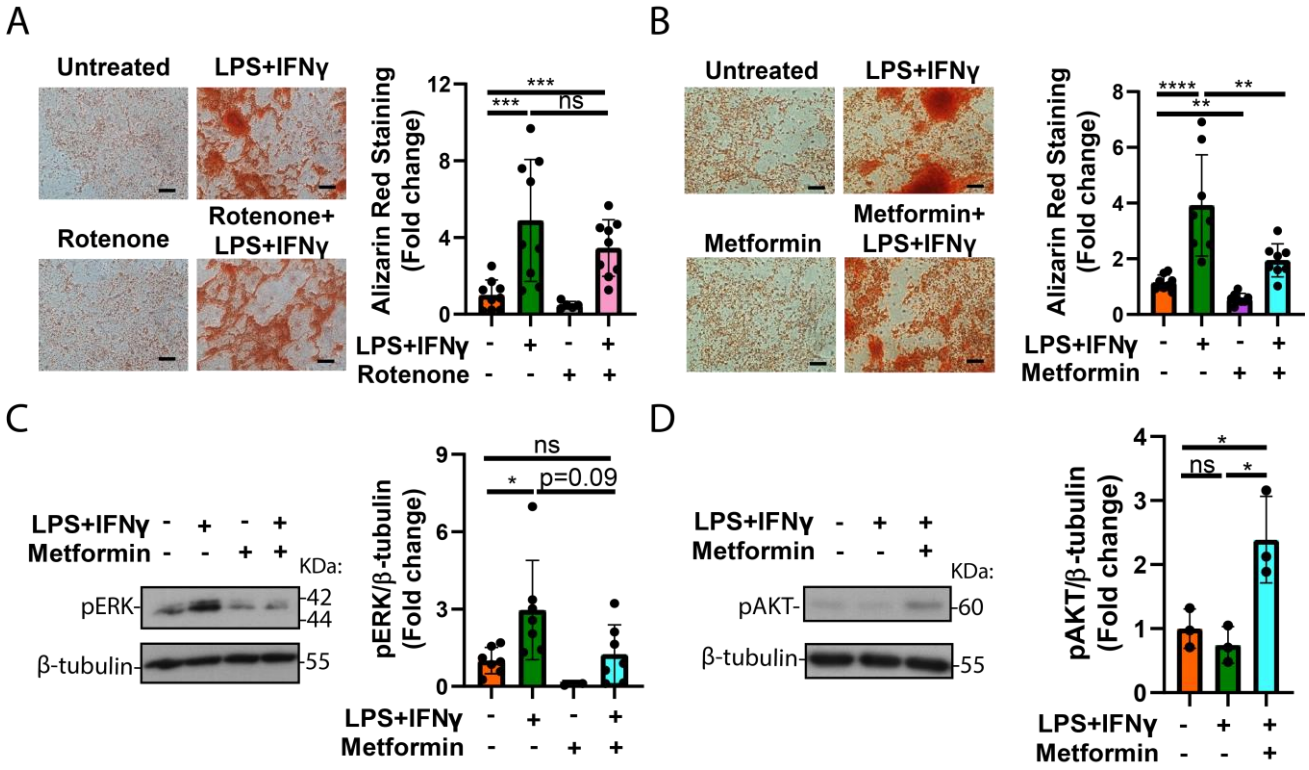

Figure 51. Differential effects of rotenone and metformin on calcification and PI3K and Akt activation. VIC were pre-incubated with 1 µM rotenone or 5 mM metformin and then activated with 100 ng/mL LPS and 1 µg/mL IFN-γ for 1 week in calcification media: (A-B) Alizarin red staining its quantitation. Black line indicates 50 µm. (C-D) Western blot analysis after 24h of activation. (C) ERK phosphorylation and its quantitation. (D) AKT phosphorylation and its quantitation. Data are expressed as the mean ± SD (N=3/6/9). ns, non-significant differences. *p<0.05, **p<0.01, ***p<0.001, ****p<0.0001. One-way analysis with Tukey's post-hoc test.

Together, data suggested that inhibition of complex I by rotenone exhibited no effect on HIF-1α stabilization, metabolic rewiring, cytokine production, or calcification either basally or upon LPS + IFN-γ treatment in VIC. In contrast, metformin inhibited these processes, which could be mediated by the insulin-signaling pathway.

R.9.2- ATP synthase inhibition increases ECAR, inflammatory gene expression, and *in vitro* calcification of human VIC

Next step was investigating ATP synthase or complex V using a pharmacological approach, oligomycin. Bioenergetic experiments showed that oligomycin induced a significant ECAR increase in basal VIC and a tendency to potentiate the effect of activated VIC (**Figure 52A**). In contrast, OCR results showed a significant

inhibition of oxygen consumption after oligomycin treatment in basal VIC, while this inhibition was not significant upon inflammatory stimuli (**Figure 52B**). Subsequently, the impact of oligomycin on the inflammatory gene profile upon LPS + IFN-γ activation was analyzed. qPCR results revealed that ATP synthase inhibition potentiated the effect of immune stimuli on the expression of some inflammatory cytokines and mediators such as *IL6* and *PTGES2*, and the osteogenic marker *BMP2* (**Figure 52C-E**).

To further investigate whether ATP synthase inhibition had a role in the induction of metabolic reprogramming, HIF-1α stabilization was assayed. Western blot analysis showed a tendency to upregulate HIF-1α stabilization upon complex V inhibition, as well as when combining oligomycin and inflammatory stimuli (**Figure 52F**). Based on these data, we investigated the effect on *in vitro* calcification and found that oligomycin increased nodule formation but did not potentiate LPS + IFN-γ-triggered mineralization of VIC (**Figure 52G**).

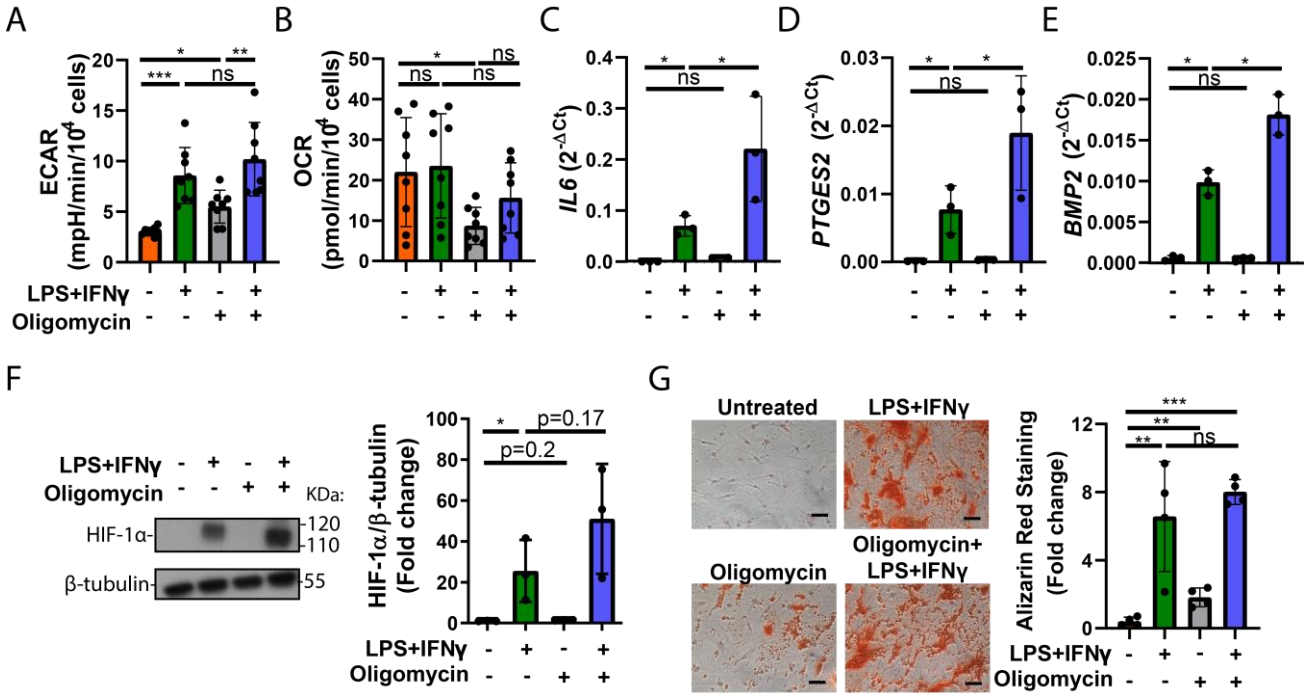

Figure 52. Inhibition of ATP synthase increases ECAR and calcification in untreated VIC and potentiates the upregulation of inflammatory mediators and osteogenic markers in activated VIC. Cells were pre-incubated with 1.5 µM oligomycin and activated with 100 ng/mL LPS and 1 µg/mL IFN-γ (A) ECAR levels after 24h of activation (N=7). (B) OCR levels (N=7). (C-E) qPCR analysis of (C) *IL6*, (D) *PTGES2,* and (E) *BMP2* genes, upon 24h stimulation. (F) WB analysis of HIF-1α stabilization upon 24h incubation with the indicated treatments. (G) ARS after 1 week of treatment and its quantification. Data are expressed as mean ± SD (N=3/4–8). ns, non-significant differences. *p<0.05, **p<0.01, ***p<0.001. One-way ANOVA with Tukey post-hoc in panels A, B, C, D, E, F, G.

Together, data suggested that ATP synthase may play a role in maintaining VIC metabolism by preventing hyperglycolysis and calcification in basal VIC and the upregulation of inflammatory mediators in VIC exposed to an inflammatory milieu.

R.9.3- Increase in mitochondrial respiration abrogates inflammation and calcification processes in VIC exposed to an inflammatory milieu

Based on the alterations in mitochondrial respiration and ATP synthesis promoted by inflammatory stimulation of VIC (**Figure 15**), as well as the recent evidence of a protective role of OXPHOS in the context of immune-induced inflammation in vascular endothelial cells (Xiao et al., 2021), we addressed the effect of increasing mitochondrial respiration in the processes underlying CAVD. To achieve this aim, FCCP, a mitochondrial uncoupler that dissipates the proton gradient between the intermembrane space and the matrix, thus allowing the cell to reach its maximum OCR, was used. Seahorse metabolic analysis using Mito Stress assay demonstrated that FCCP did not alter ECAR basally or upon LPS + IFN-γ activation (**Figure 53A**). In contrast, FCCP significantly increased the OCR (**Figure 53B**). Moreover, WB revealed that FCCP inhibited the inflammation-induced STAT1/HIF-1α pathway (**Figure 53C**) and its downstream metabolic gene *GLUT1* (**Figure 53D**).

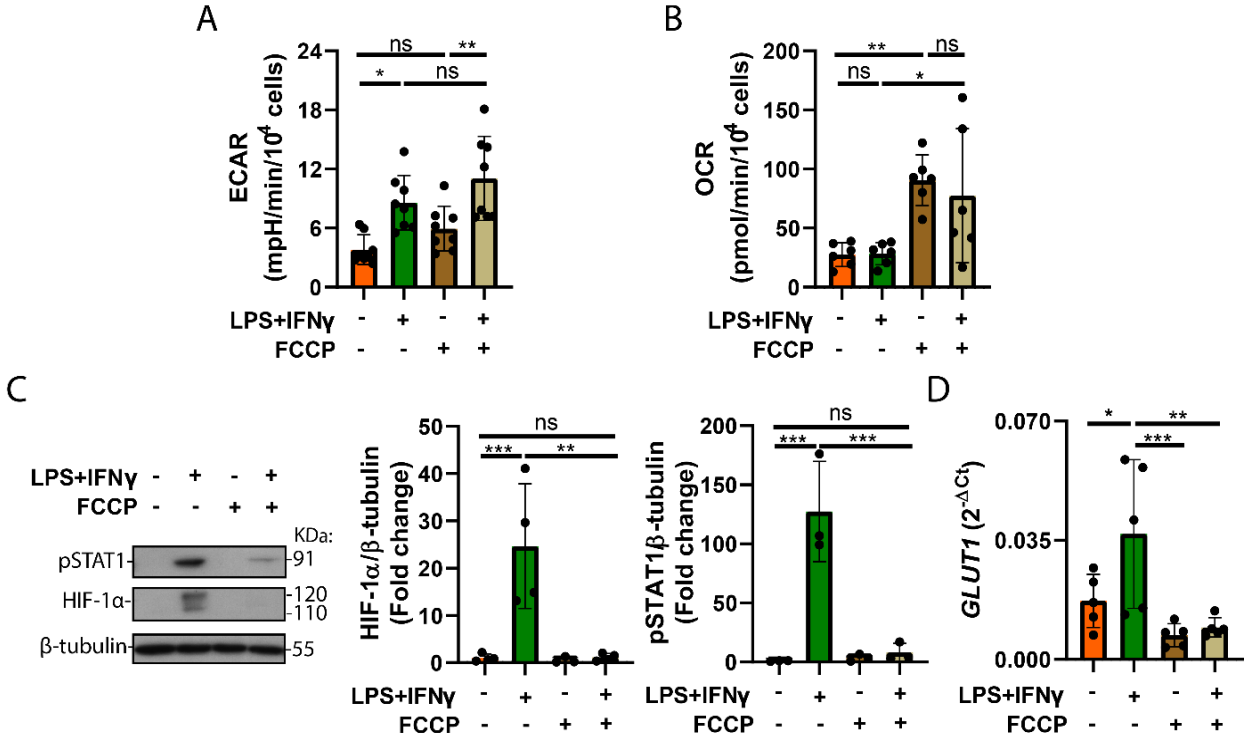

Figure 53. Mitochondrial uncoupling increases OCR and inhibits inflammation-mediated activation of the JAK-STAT/HIF-1α pathway and a HIF-1α-regulated metabolic gene. VIC were pre-incubated with 10 µM FCCP and activated with 100 ng/mL LPS and 1 µg/mL IFN-γ for 24 h. (A-B) Seahorse Mito stress analysis (N=6/8). (A) ECAR measurement and (B) OCR measurement. (C) Western blot analysis of protein lysates (N=4). (D) qPCR analysis of *GLUT1* levels. ns, non-significant differences. *p<0.05, **p<0.01, ***p<0.001. One-way ANOVA with Tukey post-hoc analysis.

Later, the impact of FCCP on apoptotic markers and inflammatory cytokines was assessed. qPCR results elucidated that forcing mitochondria to reach its maximal respiration significantly blunted the inflammatory induction of *BNIP3* expression (**Figure 54A**), a mitochondrial-mediated apoptotic marker (Greijer et al., 2004). In addition, FCCP showed a tendency to decrease the inflammatory-induced

upregulation of *IL8* expression (**Figure 54B**). Moreover, qPCR analysis revealed that LPS + IFN-γ induction of *BMP2* and *MMP1* transcript levels was significantly decreased by FCCP (**Figure 54C-D**), suggesting the inhibition of VIC differentiation and ECM remodeling. Based on this, we performed *in vitro* calcification and found that inflammatory-induced calcification was significantly blunted by FCCP (**Figure 54E**).

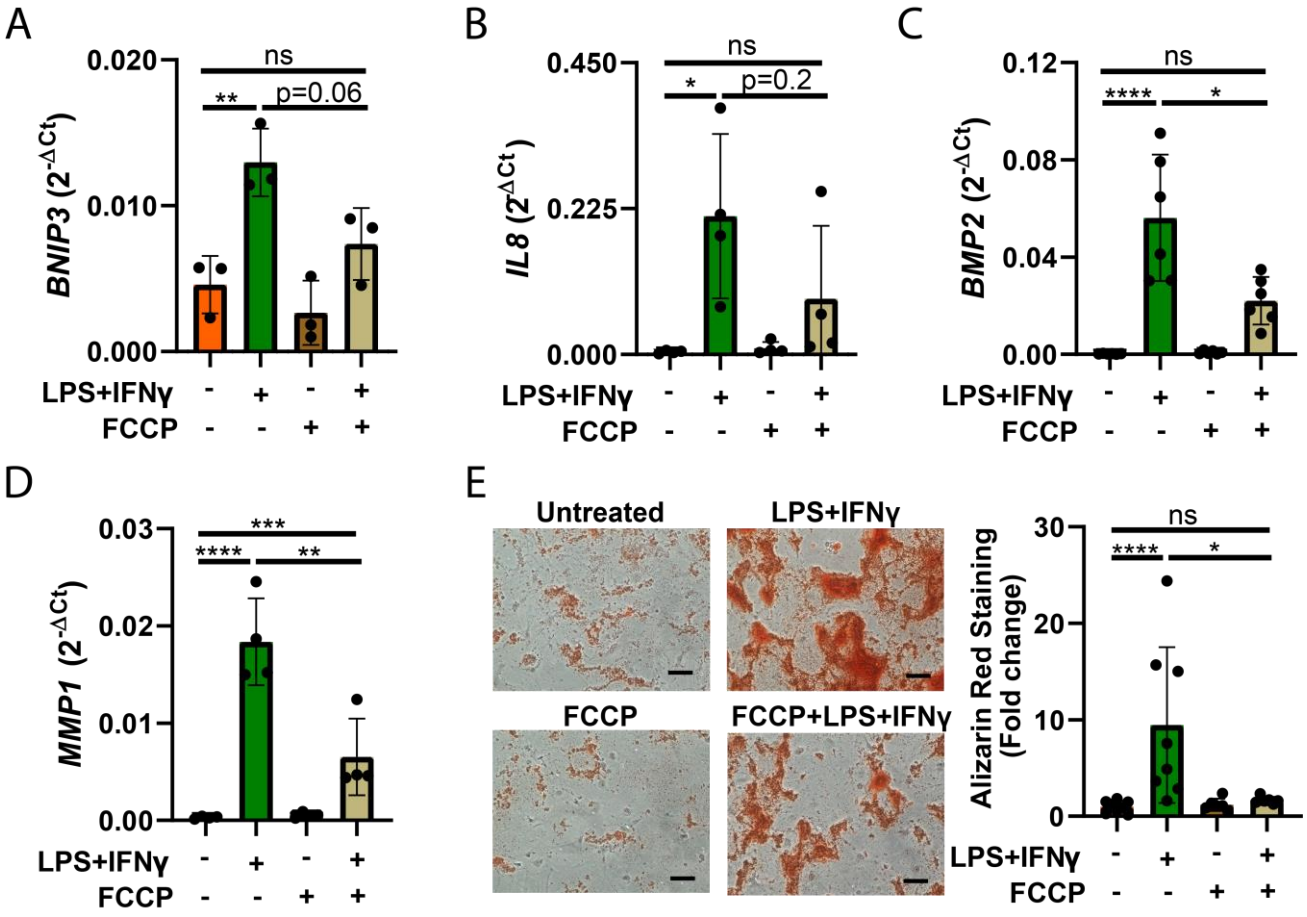

Figure 54. The mitochondrial uncoupler FCCP inhibits the upregulation of osteogenic markers and *in vitro* calcification of VIC exposed to inflammatory stimuli. (A-D) Cells were pre-incubated with 10 µM FCCP, activated with 100 ng/mL LPS and 1 µg/mL IFN-γ, and analyzed. qPCR analysis of apoptotic, inflammatory, and differentiation genes: (A) *BNIP3*, (B) *IL8*, (C) *BMP2*, and (D) *MMP1*. (E) Calcification assay performed for 1 week. Alizarin red staining and its quantitation. Black line indicates 50 µm. Data are represented as mean ± SD (N=3/4/6/8). ns, non-significant differences. *p<0.05, **p<0.01, ***p<0.001, ****p<0.0001. One-way ANOVA with Tukey's post-hoc test

Together, data showed that mitochondrial uncoupling increases OCR and inhibits the JAK-STAT/HIF-1α-mediated upregulation of metabolic genes, differentiation markers, and VIC calcification. These data suggested that mitochondrial respiration may play a protective role in VIC differentiation, inflammation, and calcification.

R.10- JAK-STAT/HIF-1α and NF-κB pathways involvement in metabolic reprogramming

Next, we aimed to elucidate the molecular mechanisms responsible for the metabolic reprogramming induced by LPS + IFN-γ. Our focus was on the JAK-STAT/HIF-1α pathway and other downstream pathways, such as NF-κB, AKT, and MAPK, which are reported to be downstream of IFNGR and TLR4 signaling in VIC (Parra-Izquierdo et al., 2019).

R.10.1- JAK1/2 inhibition partially abrogates the metabolic shift induced upon LPS + IFN-γ treatment

To assay the role JAK-STAT pathway, we used ruxolitinib, a well-known inhibitor of JAK1/2, which is already used in the treatment of other diseases such as cancer and myelofibrosis (Han et al., 2018 & Plosker, 2015). First, we assayed the bioenergetic status of activated VIC in the presence of the inhibitor. As shown by the Seahorse Mito Stress assay**,** the LPS + IFN-γ–induced increase in ECAR was markedly blunted when VIC was pre-incubated with ruxolitinib, while no effects on OCR were observed (**Figure 55A-B**). The energy map revealed that ruxolitinib reversed the inflammation-induced glycolytic phenotype (**Figure 55C**). Next, we investigated respiratory changes and found non-significant differences in the presence of ruxolitinib, although the inflammatory-stimulation of maximal respiration seemed to be partially reversed by JAK-STAT inhibition (**Figure 55D**). In addition, pre-incubation of VIC with ruxolitinib significantly abrogated the inflammation-induced inhibition of ATP production linked to OXPHOS (**Figure 55E**) and coupling efficiency (**Figure 55F**). Furthermore, JAK inhibition showed a tendency to blunt the LPS + IFN-γ induction of non-mitochondrial oxygen consumption (**Figure 55G**). Due to the importance that JAK-STAT signaling seemed to have in the metabolic reprogramming induced by LPS + IFN-γ, we sought to measure the expression of glycolytic enzymes altered by the inflammatory environment (**Table 1,2**). qPCR results shown in **Table 6** disclosed that the inflammatory induced expression of genes related to glycolysis, *GLUT1*, *PDK4*, *HKII*, *MCT4*, and *PFKFB3* was mediated by JAK-STAT signaling.

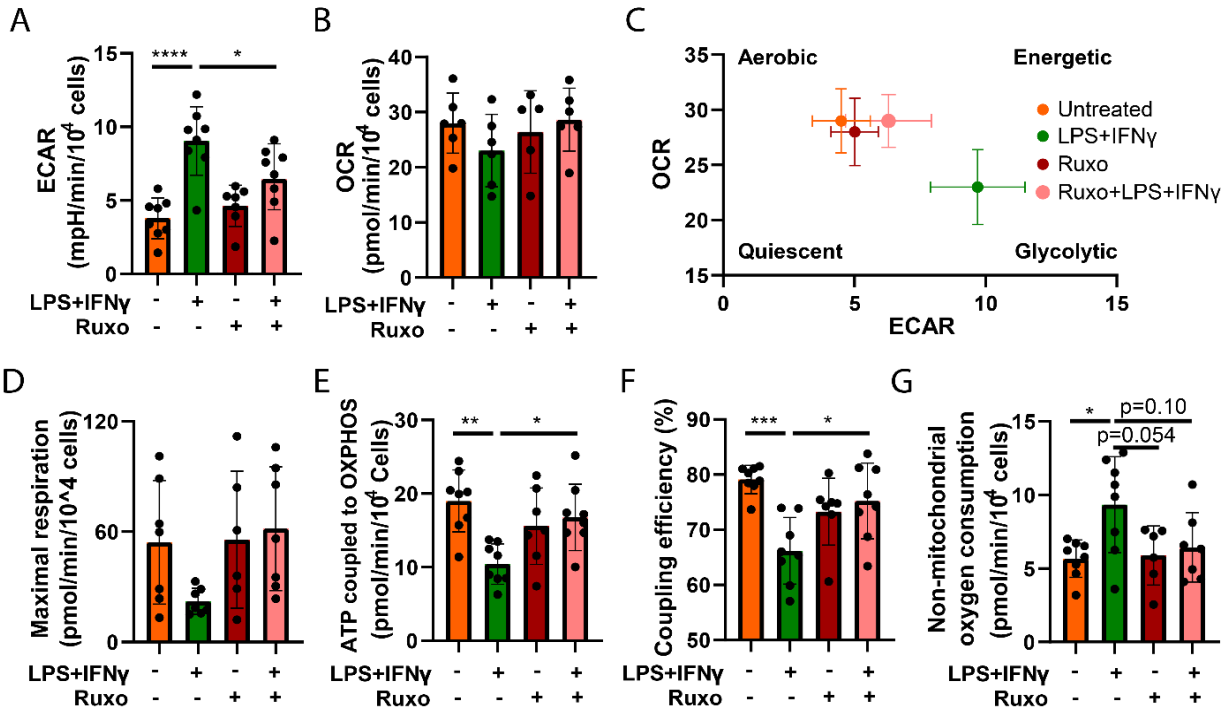

Figure 55. The JAK-STAT pathway mediates the glycolytic shift induced by inflammatory stimuli. VIC were treated with 1 µg/mL IFN-γ and 100 ng/mL LPS for 24h and metabolic analysis was performed. (A) ECAR quantitation (N=8). (B) Quantitation of OCR (N=8). (C) Energetics map (ECAR vs. OCR plot). (D) Maximal respiration (N=5). (E) ATP production linked to OXPHOS (N=5). (F) Coupling efficiency (N=5). (G) Non-mitochondrial oxygen consumption (N=5). Data are represented as the mean ± SD. ns, non-significant differences; ruxo, 6 µM ruxolitinib. *p<0.05, **p<0.01, ****p<0.0001. One-way ANOVA with Tukey's post-hoc analysis.

Table 6. Reversal of LPS + IFN-γ-induced changes in metabolic gene expression by ruxolitinib. Table includes fold change data (mean ± SD (N=6)): the comparison of the expression for the indicated genes is expressed as $2^{-\Delta\Delta Ct}$ where ΔCt is the Ct gene-Ct GAPDH and % of fold change reversion calculated as the % that ruxolitinib reversed the inflammatory induced effect (considered as 100%). Table also shows one-way ANOVA with Tukey post-hoc statistical analysis. *p<0.05, **p<0.01, ***p<0.001, ****p<0.0001, ns; non-significant.

GENE	FOLD CHANGE	% REVERSION BY RUXOLITINIB
SLC2A1 (GLUT1)	2.85±0.58 (***)	24.34±2.52 (****)
PFKFB3	4.52±1.25 (***)	21±1.39 (***)
HKII	1.76±0.46 (*)	60±0.99 (*)
SLC16A4 (MCT4)	4.96±1.56 (**)	37.14±1.98 (*)
PDK4	0.49±0.24 (*)	30±2.98 (***)

Together, data elucidated that the JAK-STAT pathway was partially controlling the inflammatory-induced metabolic rewiring in VIC by regulating metabolic enzyme expression, as well as ECAR and OXPHOS.

R.10.2- Non-hypoxic HIF-1α stabilization mediates the inflammatory induced metabolic rewiring in VIC

Given that LPS + IFN-γ was demonstrated to stabilize HIF-1α downstream of STAT1 in VIC (Parra-Izquierdo et al., 2019), we next addressed the role of HIF-1α in metabolic rewiring using a well-known chemical stabilizer of HIF-1α, $CoCl_2$ (Wu et al., 2011). Bioenergetic assays using Seahorse analyzer showed that $CoCl_2$ increased ECAR (**Figure 56A**), while reducing OCR inhibition (**Figure 56B**), resembling the

proglycolytic shift by LPS + IFN-γ and suggesting the involvement of HIF-1α in extracellular acidification. We then used a selective pharmacological inhibitor of HIF-1α, PX-478 (Koh et al., 2008), which has been reported to inhibit LPS + IFN-γ-mediated stabilization of HIF-1α in VIC (Parra-Izquierdo et al., 2019), and found that PX-478 inhibited ECAR in inflammatory-activated VIC (**Figure 56C**) but had no effect on OCR (**Figure 56D**). The energy map showed a strong shift to glycolysis induced by $CoCl_2$, as well as inhibition of the inflammatory-induced glycolytic phenotype by PX-478 (**Figure 56E**).

To further confirm the involvement of HIF-1α, given that PX-478 may exert some potential off-target effects on transcription at high doses (Venardos et al., 2015), the next step was to perform loss-of-function experiments on *the HIF1A* gene using a siRNA. First, qPCR analysis confirmed the *HIF1A* gene knockdown, as shown by the reduced *HIF1A* transcript levels up to a 35% (**Figure 56F**), and WB analysis confirmed the reduction of inflammatory-induced HIF-1α protein levels up to a 25% (**Figure 56G**). Bioenergetic assays showed that *HIF1A* gene silencing blocked the inflammation-induced increase in the ECAR (**Figure 56H**). Additionally, the abrogation of *HIF1A* expression directly exerted an upregulation effect of OCR levels in both basal and activated VIC when comparing with non-silenced conditions (**Figure 56I**)**.** Moreover, the energetic map showed that *HIF1A* silencing abrogated the inflammatory-induced glycolytic rewiring in VIC (**Figure 56J**), thus demonstrating the involvement of HIF-1α in the metabolic shift.

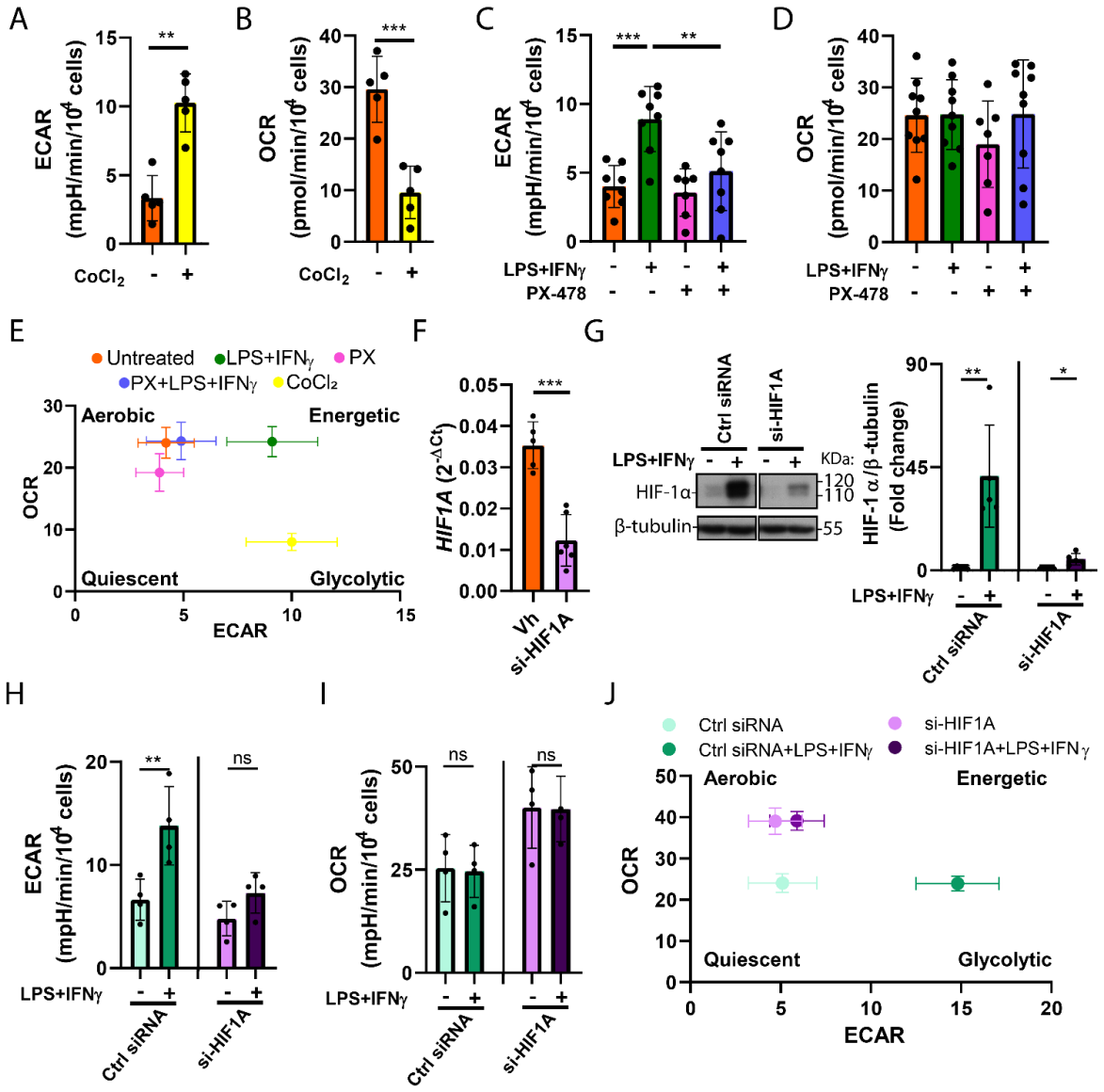

Figure 56. HIF-1α stabilization plays a role in inflammatory-induced glycolytic shift. (A-E) VIC were treated with the indicated compound or stimuli for 24h and then analyzed using Seahorse Mito Stress assay. $CoCl_2$ indicates 100 µM cobalt chloride (HIF-1α inducer), and 40 µM PX-478 (HIF-1α inhibitor), pre-incubated before activation. (A) ECAR levels. (B) OCR levels. (C) ECAR levels. (D) OCR levels. (E) Energetic map (ECAR vs. OCR plot). (F-J) VIC were transfected either siRNA to silence *HIF1A* (si-HIF1A) or a siRNA negative control (Ctrl siRNA) as indicated in methods, and then activated for 24 h. (F) *HIF1A* mRNA levels by qPCR to confirm gene silencing. (G) Western blot analysis of HIF-1α protein upon activation of silenced and unsilenced VIC and its quantitation. (H-J) Seahorse analysis of ECAR and OCR levels and energetic map (ECAR vs. OCR blot). Mean ± SD (N=4/5/8). ns, non-significant differences. *p<0.05, **p<0.01, ***p<0.001. One-way ANOVA with Tukey post-hoc in panels C, D. Student's unpaired t-test in A, B, F, G, H, I.

Later, we further examined some mitochondrial respiration parameters using both approaches: chemical induction of HIF-1α and gene silencing. First, ATP rate assay analysis showed that $CoCl_2$ reduced the production of ATP from mitochondria while increasing the ATP from the glycolytic source in VIC (**Figure 57A**). These data suggest a HIF-1α-induced switch in the main ATP source to glycolysis that resembles the shift observed in VIC under an inflammatory milieu (**Figures 9G and 19I)**, although $CoCl_2$ did not mimic the increase in total ATP. In addition, Mito Stress assay showed a decrease in coupling efficiency (**Figure 57B**)

and maximal respiration capacity after treating VIC with $CoCl_2$ (**Figure 57C**). Moreover, *HIF1A* silencing prevented the decrease in ATP production linked to OXPHOS induced by LPS + IFN-γ treatment (**Figure 57D**), thus confirming the role of HIF-1α in the reduction of mitochondrial ATP under inflammatory conditions.

Finally, considering the effects of HIF-1α on the metabolic rewiring induced upon inflammatory stimuli, we examined the expression of glycolytic genes altered upon inflammatory activation in VIC (**Table 1,2**), which have been previously described as HIF-1α targets (Leung et al., 2017). qPCR analysis using PX-478 and *HIF1A* silencing showed that the inflammatory-induced effects on *SLC2A1/GLUT1, G6PD*, and *PDK4* transcription levels were reversed by the pharmacological inhibition of HIF-1α (**Figure 57E**). Moreover, *HIF1A* knocking-down further confirmed these results (**Figure 57F**), thus indicating the role of HIF-1α in the metabolic shift by regulating their expression.

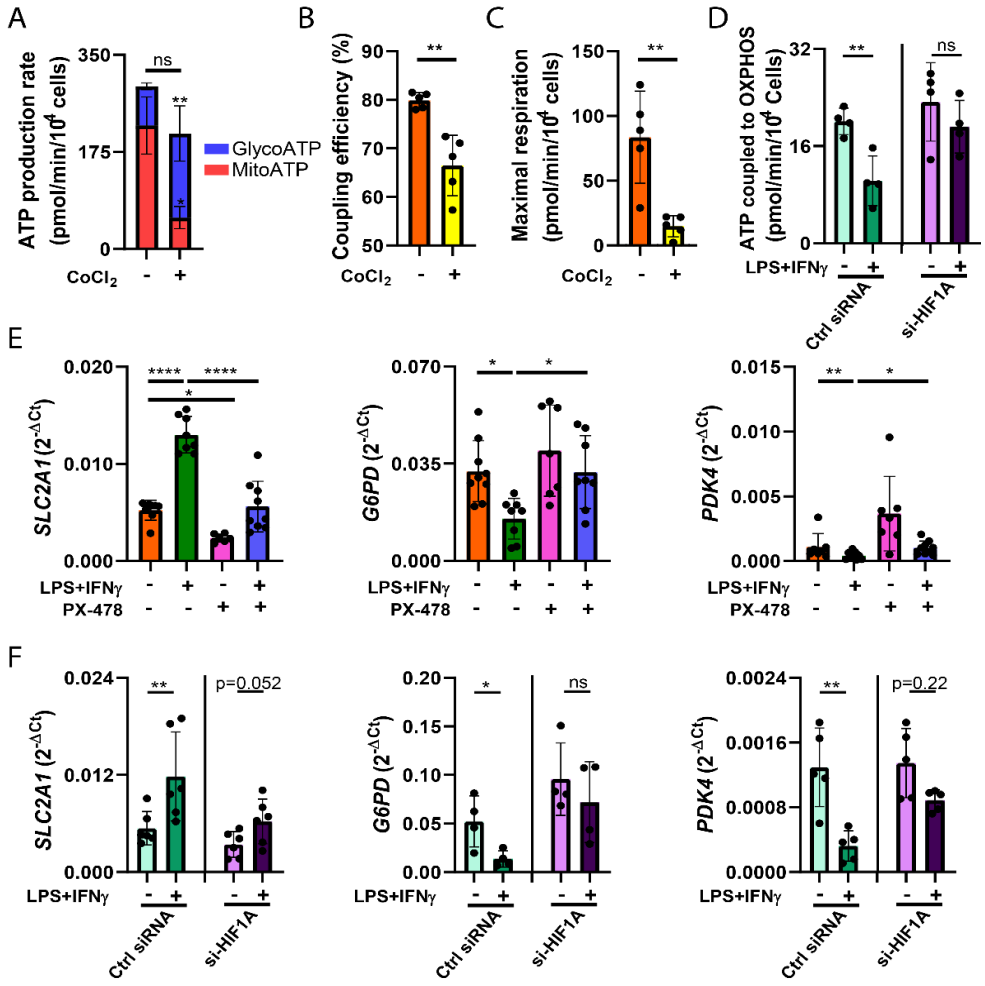

Figure 57. HIF-1α is involved in mitochondrial damage and subsequent reduction of mitochondrial ATP, as well as in the regulation of glycolytic genes induced by inflammatory stimuli. (A-F) VIC were either treated with the HIF-1α inducer $CoCl_2$ (A-C), with the HIF-1α inhibitor PX-478 (E) or transfected and activated as in **Figure 56** (D, F). (A) Seahorse ATP rate assay results showing main sources of ATP production (N=4). (B-D) Seahorse Mito Stress Assay data. (B) Coupling efficiency and (C) maximal respiration (N=5). (D) ATP production linked to OXPHOS. (E) qPCR analysis of *SCL2A1 (GLUT1), G6PD and PDK4* transcripts (N=7-9). (F) siRNA assay for HIF-1α silencing and qPCR analysis as in (E) (N=4-6). $CoCl_2$=100 µM, PX-478=40 µM; IFN-γ, 1 µg/mL IFN-γ, and LPS, 100 ng/mL LPS**.** Data are represented as mean ± SD. ns, non-significant differences. **p<0.01. Student's unpaired t-test.

Together, data from this section indicated that HIF-1α mediated the inflammatory-induced glycolytic rewiring in VIC by regulating the expression of some glycolytic genes, and by promoting mitochondrial damage leading to decreased mitochondrial ATP and the switch in the main source of ATP.

R.10.3- NF-κB pathway participates in metabolic rewiring induced upon LPS + IFN-γ

As aforementioned, NF-κB pathway has been associated with inflammation induction in human VIC exposed to LPS + IFN-γ (Parra-Izquierdo et al., 2019), and recent evidence has demonstrated the role of the NF-κB-PFKFB3 axis in inflammation-induced metabolic rewiring in vascular endothelial cells (Xiao et al., 2021). For this reason, we assessed the role of this pathway in the inflammatory stimuli-induced metabolic reprogramming of VIC. Bioenergetic metabolic analysis by Mito Stress assay showed that NF-κB SN50, a well-known inhibitor of NF-κB translocation to the nucleus, had no effect on the induction of ECAR by co-stimulation with LPS and IFN-γ (**Figure 58A**). Notably, NF-κB SN50 treatment induced non-mitochondrial oxygen consumption in basal VIC and further potentiated the effects of inflammatory stimuli (**Figure 58B**). Finally, qPCR analysis showed a direct role for NF-κB in *PFKFB3* upon inflammatory induction (**Figure 58C**).

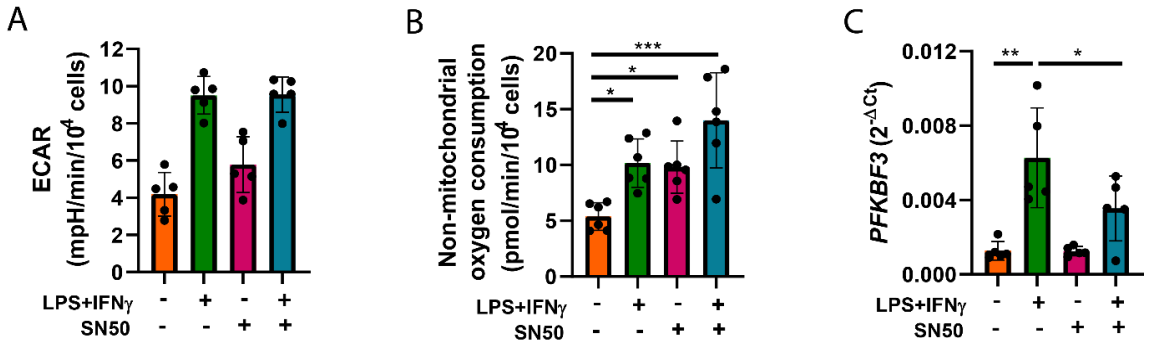

Figure 58. Inhibition of NF-KB shows no inhibitory effects in ECAR and non-mitochondrial oxygen consumption induced by LPS + IFN-γ, but downregulated inflammatory-induced *PFKFB3* expression. VIC were pre-incubated with 50 µg/mL NF-κB SN50 (SN50) for at least 30 min, then treated with 1 µg/mL IFN-γ and 100 ng/mL LPS for 24h, and metabolic analysis was performed. (A) ECAR quantitation (N=5). (B) Non-mitochondrial oxygen consumption (N=6). (C) qPCR analysis of *PFKFB3* mRNA levels (N=5). Data are represented as the mean ± SD. ns, non-significant differences. *p<0.05, **p<0.01, ***p<0.001, One-way ANOVA test with Dunnett post-hoc (vs. untreated) in A, B. One-way ANOVA test with Tukey post-hoc in C.

Together, results from this section elucidated that NF-κB was not directly involved in some of the early metabolic changes induced by an inflammatory milieu, namely extracellular acidification, and non-mitochondrial oxygen consumption, but it had a direct role in regulating the expression of *PFKFB3,* the rate-limiting enzyme of glycolysis, which could later affect metabolic parameters.

R.11- Validation of the inflammation-mediated metabolic rewiring in quiescent VIC and 3D VIC-VEC co-cultures and correlation of metabolic profile changes in valve leaflets and VIC from patients with CAVD

As mentioned in the introduction, interstitial cell population in the human aortic valve comprises a number of different phenotypic states, mostly quiescent fibroblasts (qVIC), with <5% exhibiting an activated phenotype, while *in vitro* cultures exhibit a predominant myofibroblast (aVIC) phenotype (Taylor et al., 2000), resulting in >90% of aVIC (Spadaccio et al., 2016), referred in this thesis as VIC. Therefore, the dominance of the aVIC phenotype in *in vitro* cultures is likely to significantly diminish their accuracy for studying VIC activation or mimicking healthy valve conditions. Our study was performed in human VIC in culture (myofibroblasts) as a model to study osteoblast-like differentiation and subsequent calcification. To study the relevance of inflammation as an inducer of metabolic rewiring that is required for mineralization in CAVD pathogenesis and validate major findings in 2D-human VIC cultures, we evaluated metabolic changes in qVIC dedifferentiated from VIC cultures and in 3D VIC-VEC co-cultures mimicking the valve setting. Further, we compared the metabolic gene profile and bioenergetics of valve leaflets and explanted VIC from patients with or without CAVD.

R.11.1- Quiescent VIC exhibit a metabolic rewiring and phenotypic changes upon exposure to inflammatory stimuli via JAK-STAT/HIF-1α activation

Firstly, we investigated whether qVIC could be metabolically reprogrammed and differentiated upon co-stimulation with LPS and IFN-γ. To get this aim we first used a method described by Latif et al., (2015) based on a fibroblast formulation media (FIB) to dedifferentiate VIC (myofibroblast) to qVIC (fibroblast) phenotype. As shown in **Figure 59A**, qVIC exposed to inflammatory stimuli for 14 days underwent morphological changes that resembled the osteoblast-like phenotype found previously in activated VIC (Parra-Izquierdo et al., 2019). These phenotypic changes were further confirmed by qPCR analysis of markers in cells activated for 24h. We confirmed that *ACTA2* levels were higher in VIC than in qVIC, consistent with their phenotypic differences, and further showed a significant decrease in both cell types after exposure to inflammatory stimuli (**Figure 59B**). Notably, the osteogenic differentiation marker *BMP2* was significantly upregulated after inflammatory stimulation in both qVIC and VIC (**Figure 59C**), thus indicating osteogenic differentiation of qVIC in response to an inflammatory milieu.

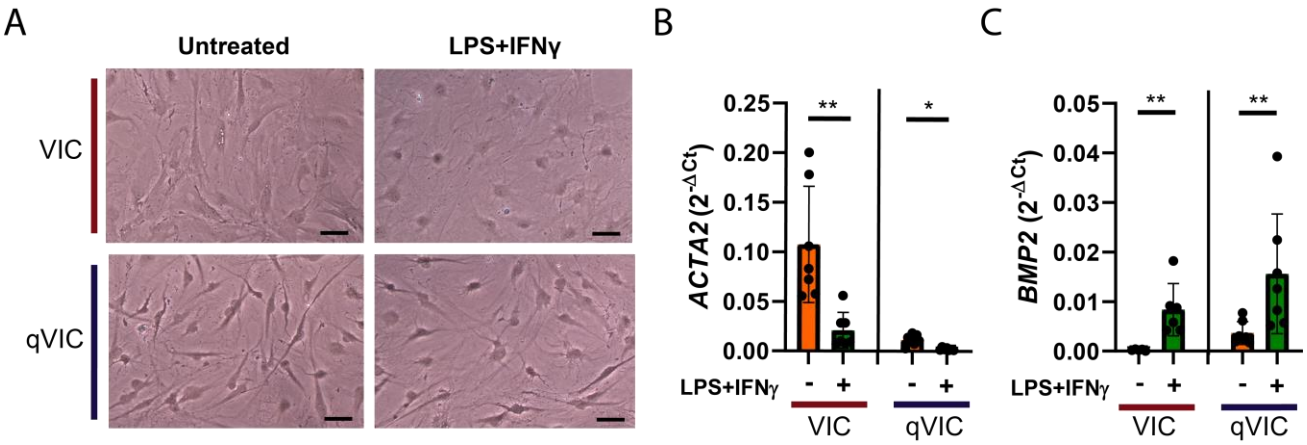

Figure 59. qVIC acquire an osteoblast-like phenotype upon LPS + IFN-γ treatment. VIC were incubated with control media or FIB for 14 days as described in methods and then activated with 100 ng/mL LPS and 1 µg/mL IFN-γ. (A) Representative microphotographs showing morphological changes (N=6). (B) qPCR analysis of *ACTA2*, and (C) *BMP2* levels. Mean ± SD (N=3/6). ns, non-significant differences. *p<0.05, **p<0.01. Student's unpaired t-test.

The next step was to compare the metabolic gene profiles of qVIC and VIC under basal conditions. Notably, qVIC and VIC exhibited distinct metabolic gene profiles, with differences in the transcript levels of metabolic enzymes and transporters such as *GLUT1*, *HKII*, *PKM2*, *MCT4*, *PDK4, and COX7A1* (**Figure 60A**). In line with these results, metabolic analysis using Seahorse unveiled a significantly higher OCR in qVIC than in VIC (**Figure 60B**) while similar ECAR levels in both cell types (**Figure 60C**). The energetic map revealed that qVIC exhibited a more aerobic and energetic metabolism than VIC (**Figure 60D**). Consistently, ATP levels coupled to OXPHOS were markedly higher in qVIC than in VIC (**Figure 60E**). These results were further confirmed using the Seahorse ATP Rate assay, which revealed higher mitochondrial ATP levels in basal qVIC than in VIC, whereas the glycolytic ATP was significantly lower in qVIC, and total production of ATP was similar in both cell types (**Figure 60F**). Together, data disclose a more energetic phenotype in qVIC different from the more glycolytic phenotype exhibited by VIC.

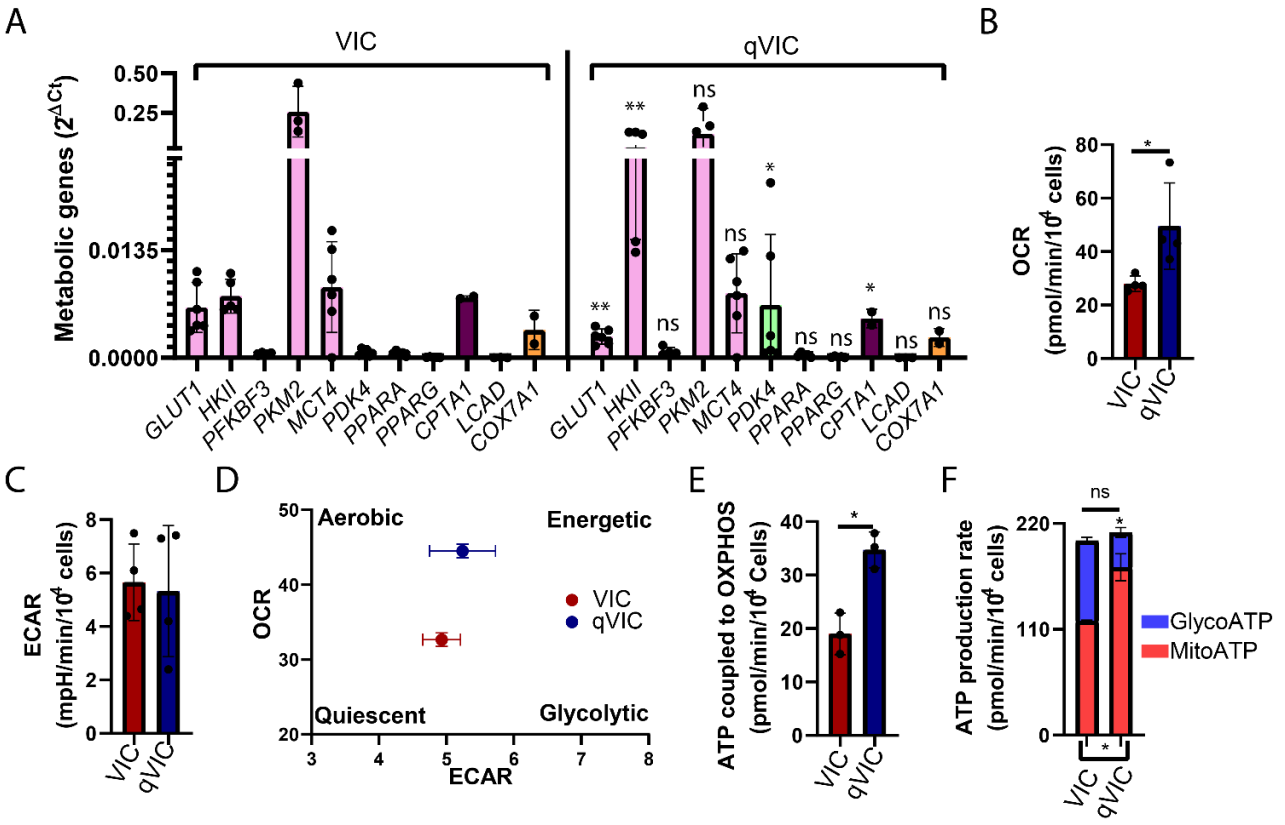

Figure 60. qVIC exhibits a more energetic basal metabolism than VIC with higher ATP coupled to OXPHOS and lower glycolytic ATP. Cells were incubated with control media (VIC) or FIB (qVIC) for 14 days and then analyzed. (A) Metabolic profile showing metabolic gene expression by qPCR analysis: *GLUT1*, *HKII*, *PFKFB3, PKM2, MCT4, PDK4, COX7A1*. (B) Seahorse Mito Stress Assay(B) OCR measure, (C) ECAR measure, (D) Energetic map (ECAR vs. OCR plot). (E) ATP production linked to OXPHOS. (F) Main source of ATP production measured by Seahorse ATP Rate Assay. Data are expressed as mean ± SD (N=3/4/5). Ns, non-significant differences. *p<0.05, **p<0.01. Student's unpaired t-test.

The following step was to compare the metabolic rewiring induced upon LPS + IFN-γ in both VIC and qVIC. Seahorse analysis revealed that in qVIC, the OCR decreased upon activation to reach rates like those of the activated VIC (**Figure 61A**). In addition, an increase in ECAR was observed in both cell types upon stimulation (**Figure 61B**). The energetic map showed an inflammatory-induced shift to a more glycolytic phenotype in qVIC, as observed in VIC (**Figure 61C**). Additionally, Seahorse Mito Stress assay showed that inflammatory-activated qVIC tended to increase non-mitochondrial oxygen consumption (**Figure 61D**). Finally, mitochondrial ATP production significantly decreased upon cell activation in both VIC and qVIC, reaching similar levels (**Figure 61E**). ATP rate assay further confirmed the shift from mitochondrial ATP source to glycolytic ATP in both cases (**Figure 61F**). Subsequently, the expression of metabolic enzymes was measured in both cell types upon inflammatory insults. Data in **Table 7** confirmed that upregulation of *GLUT1*, *PFKFB3*, *PKM2*, and *MCT4*, and downregulation of *PDK4*, *COX7A1*, and *GLS1* were induced by inflammatory agents in both VIC and qVIC. However, in qVIC, HKII levels were basally so high that no changes were measured in qVIC, in contrast to the VIC results.

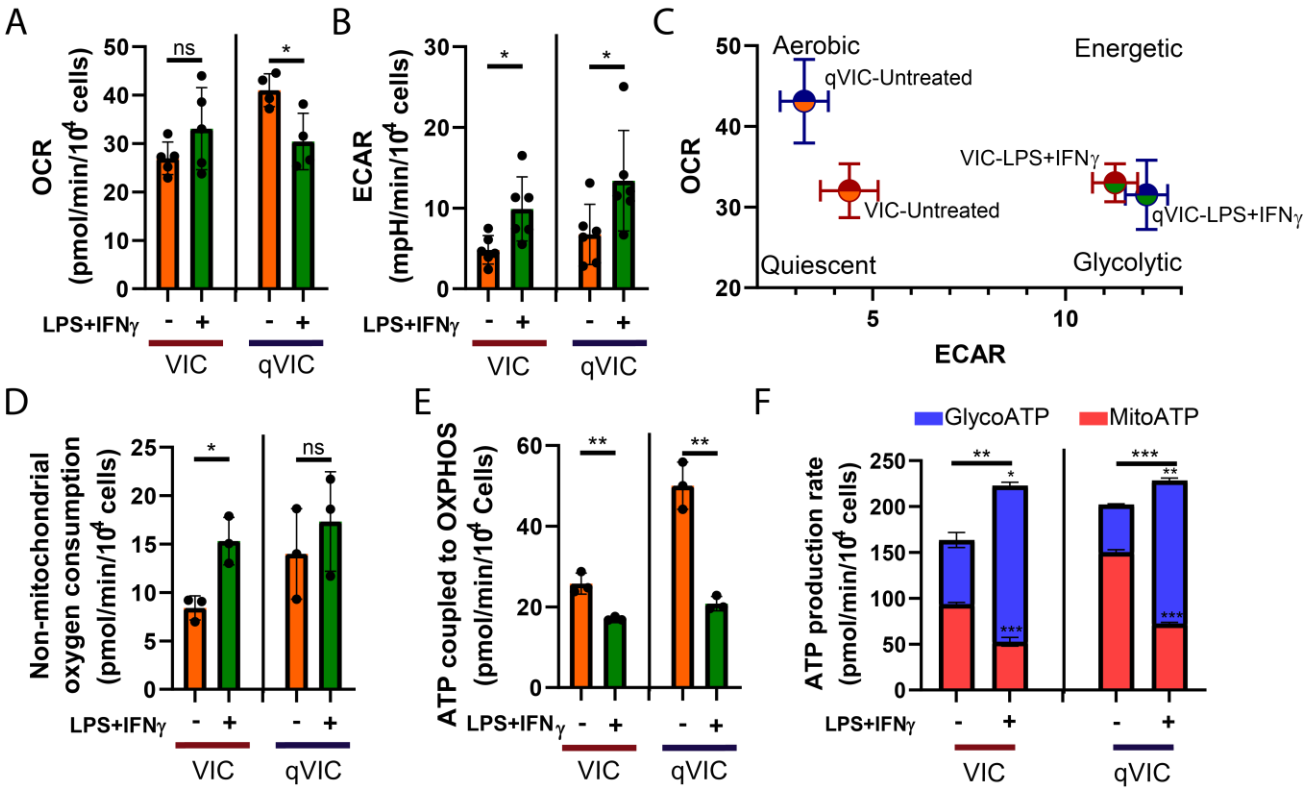

Figure 61. qVIC, as well as VIC, undergo metabolic rewiring to a more glycolytic phenotype upon inflammatory stimulation. VIC were incubated with control media or FIB for 14 days, then activated with 100 ng/mL LPS and 1 µg/mL IFN-γ, and later analyzed in a Seahorse analyzer. (A) OCR quantitation (N=5), (B) ECAR quantitation (N=5), (C) Energetic map (ECAR vs. OCR plot), (E) Oxygen consumption rate by non-mitochondrial processes (N=3). (F) ATP production rate linked to OXPHOS (N=3). (G) ATP Rate Assay showing the main source of ATP production (N=3). Data are expressed as mean ± SD (N=3/5). Ns, non-significant differences; *, p<0.05; **, p<0.01. Student's unpaired t-test.

Table 7. Comparison of inflammatory-induced changes in metabolic gene expression in VIC and qVIC. Cells activated or not with LPS + IFN-γ for 24h were analyzed by PCR. Data (N=5) are expressed as $2^{-\Delta\Delta Ct}$ where ΔCt is the Ct gene-Ct GAPDH, and then compared to untreated. Mean + SD and Student's unpaired t-test. *, p<0.05; **, p<0.01; ns, non-significant.

GENE	FOLD CHANGE (VIC)	FOLD CHANGE (qVIC)
SLC2A1 (GLUT1)	3.11±1.23 (*)	4.98±1.88 (**)
HKII	3.63±0.92 (*)	0.94±0.36 (ns)
PFKFB3	4.61±1.97 (*)	5.74±1.99 (*)
PKM2	2.81±1.06 (*)	2.48±1.36 (p=0.052)
SLC16A4 (MCT4)	3.75±1.10 (*)	10.75±3.40 (**)
PDK4	0.18±0.07 (*)	0.27±0.10 (*)
GSL1	0.13±0.05 (*)	0.33±0.10 (*)
COX7A1 (Cyt C oxidase)	0.42±0.07 (*)	0.21±0.08 (*)

Finally, we sought to characterize whether these inflammation-induced changes in qVIC were mediated by the JAK-STAT/HIF-1α pathway, as described for VIC (**Figure 55,56)**. Western blot analysis demonstrated that both STAT1 phosphorylation and HIF-1α stabilization increased upon inflammatory stimuli in qVIC (**Figure 62A-C**). In addition, another pathway related to calcification in VIC, MAPK, was

analyzed and the phosphorylation of ERK was found to be increased upon activation in qVIC (**Figure 62A, D**). WB was used to characterize the inflammatory profile induced upon inflammatory treatment of qVIC and results showed that the master inflammatory regulator NF-κB was significantly activated (**Figure 62E-F**), and further revealed increased expression of adhesion molecules such as ICAM-1 (**Figure 62E,G**) and VCAM-1 (**Figure 62E,H**).

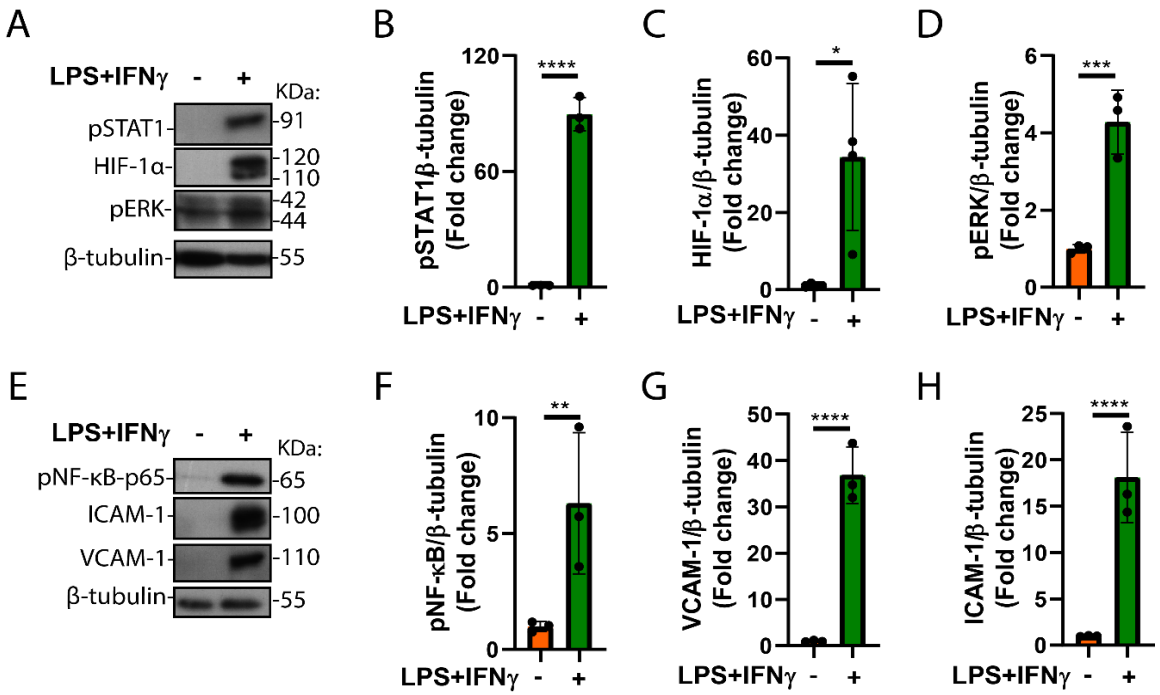

Figure 62. Co-stimulation with LPS and IFN-γ induces the JAK-STAT/HIF-1α and NF-κB pathways in qVIC. VIC were incubated with control media or FIB for 14 days as described in the Methods section, activated with 100 ng/mL LPS and 1 µg/mL IFN-γ, and later analyzed by WB. (A) Representative immuno-blots of the indicated proteins. (B) pSTAT1 quantitation, (C) HIF-1α quantitation and (D) pERK quantitation. (E) Representative immuno-blots of the indicated proteins. (F) pNF-κB quantitation, (G) ICAM-1 quantitation and (H) VCAM-1 quantitation (N=3). Data are expressed as mean ± SD (N=3/4). N indicates the number of VIC isolates from independent valve donors; ns, non-significant differences; *, p<0.05; **, p<0.01; ***, p<0.001; ****, p<0.0001. Student's unpaired t-test.

Collectively, data from this section unveiled different metabolic phenotypes in qVIC and VIC and further disclosed that inflammatory stimuli such as LPS + IFN-γ promoted metabolic reprogramming to a more glycolytic phenotype in both VIC and qVIC, leading to cell differentiation and inflammation.

R.11.2- Validation of metabolic rewiring VIC and VEC 3D co-culture: correlation in HIF-1α upregulation and an altered profile of metabolic genes

Next, we validated data in VIC-VEC 3D co-culture hydrogels to mimic the valve structure. This model was performed with porcine aortic valve interstitial and endothelial cells (PAVIC and PAVEC, respectively), as described in the Methods section. The 3D co-culture was set as described, and hydrogel compaction was observed every day to approach cell differentiation (Gee et al., 2021). Once we determined that the

hydrogel was compacting and cells were differentiating, we directly assayed HIF-1α expression and found increased HIF-1α stabilization in cultures exposed to inflammatory stimuli (**Figure 63**).

Next, we analyzed metabolic genes, some of which are HIF-1α targets. To further confirm the upregulation of metabolic genes, we performed qPCR analysis after seven days of co-culture. Notably, the results revealed the upregulation of several metabolic genes, namely *GLUT1, HKII, PFKFB3, PKM2,* and *MCT4*, while downregulation of *G6PD* and *COX7A1* in LPS + IFN-γ inflammatory conditions in 3D co-culture (**Table 8**), a similar change in metabolic profile compared to that observed in 2D (**Tables 1-3**). Strikingly, osteogenic media promoted a similar change in the metabolic profile of 3D co-cultures (**Table 8**).

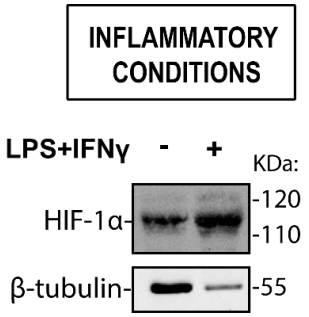

Figure 63. Inflammatory stimuli promote HIF-1α stabilization in 3D VIC-VEC co-culture. Porcine 3D VIC-VEC co-cultures were established as detailed in the methods section and were treated with 100 ng/mL LPS and 5 ng/mL IFN-γ for 1 week. Western blot analysis of HIF-1α stabilization upon inflammatory stimulation (representative of N=2).

Table 8. Comparison of changes in metabolic gene expression in 2D-VIC cultures and 3D-VIC+VEC co-cultures upon activation. Cell cultures, 2D-human VIC, or 3D-porcine VIC+VEC, were treated as indicated and analyzed by qPCR. Gene expression is expressed as relative to housekeeping genes and to untreated conditions. Data are expressed as fold change vs. untreated (mean + SD (N=5)). Student's unpaired t-test. *p<0.05, **p<0.01.

GENE	FOLD CHANGE		
	2D-human VIC (LPS + IFN-γ treated)	**3D- porcine VIC+VEC (LPS + IFN-γ treated)**	**3D- porcine VIC+VEC (OGM treated)**
SLC2A1 (GLUT1)	2.89±0.97 (**)	2.67±0.71 (**)	2.48±1.20
HKII	2.48±0.60 (*)	5.89±1.97 (*)	1.67±0.29 (p=0.09)
PFKFB3	3.94±1.67 (**)	5.98±1.97 (*)	10.79±2.40 (*)
PKM2	2.40±0.89 (**)	3.20±1.02 (*)	1.99±0.33 (**)
SLC16A4 (MCT4)	4.72±1.28 (*)	6.89±1.59 (*)	3.41±0.55 (*)
G6PD	0.51±0.20 (*)	0.67±0.14 (*)	0.67±0.06 (p=0.07)
COX7A1 (Cyt C oxidase)	0.42±0.13 (*)	0.53±0.09 (*)	0.34±0.08 (*)

Together, data from 3D co-cultures of VIC-VEC (swine) revealed an inflammation-induced upregulation of HIF-1α stabilization, as well as inflammatory- and osteogenic-triggered changes in metabolic gene profile that resembled inflammatory-induced alterations in human VIC (2D).

R.11.3- Stenotic human aortic valve tissue and explanted cells mimic the metabolic rewiring induced in VIC exposed to inflammatory stimuli

First, we analyzed potential changes in the metabolic profile of explanted VIC from patients with and without CAVD. Real time metabolic analysis of explanted VIC unveiled an increase in extracellular acidification rate in stenotic VIC as compared to non-stenotic VIC (**Figure 64A**), while similar OCR levels (**Figure 64B**). The energetic map showed a metabolic shift to a more glycolytic phenotype in diseased VIC (**Figure 64C**). In addition, Seahorse Mito Stress assay comparing ATP production rate between control and stenotic VIC further showed a significant decrease in ATP production linked to OXPHOS in stenotic vs. non-stenotic VIC (**Figure 64D**).

Next, the differential metabolic gene profile was analyzed in VIC and valve tissue from patients with and without CAVD. We found upregulation of metabolic enzymes in stenotic VIC as compared to non-stenotic VIC, including some enzymes controlling glycolysis, such as *GLUT1* and *PKM2* (**Figure 64E-F**), while downregulation of the main negative regulator of TCA entrance, *PDK4* (**Figure 64G**). Moreover, qPCR analysis of stenotic and non-stenotic valve tissue elucidated similar alterations in the gene metabolic profile, with upregulation of some limiting enzymes controlling glycolysis, such as *PFKFB3* and *PKM2* (**Figure 64H-I**), while downregulation of *PDK4* in stenotic versus non-stenotic tissue (**Figure 64J**).

Together, data highlight changes in VIC bioenergetics with a metabolic shift to glycolysis in VIC from CAVD patients and changes in metabolic profile to glucose use in both valve leaflets and VIC from CAVD patients, which resembles the metabolic rewiring found in non-stenotic VIC exposed to inflammatory stimuli.

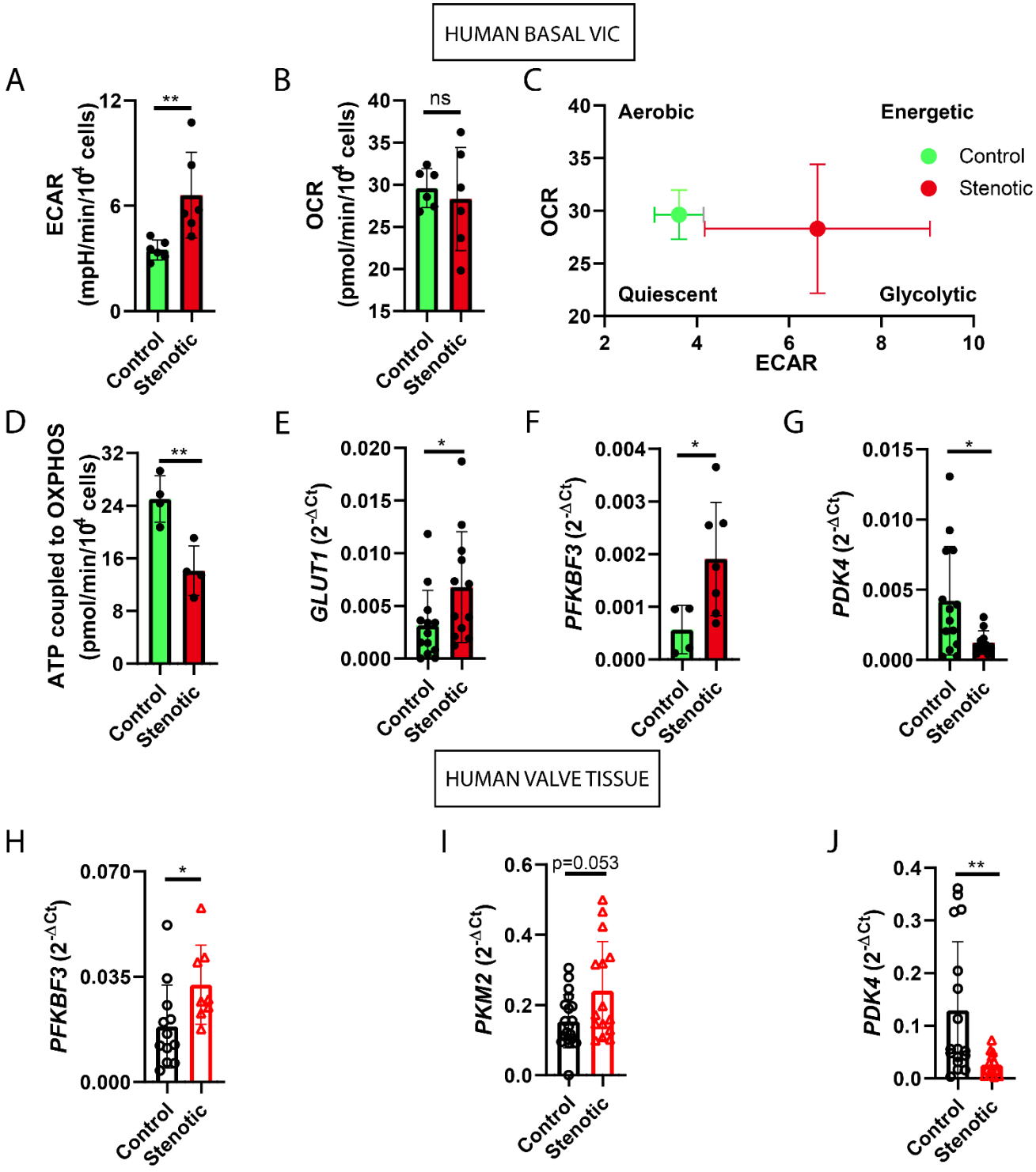

Figure 64. Metabolic rewiring occurs in explanted stenotic VIC and tissue. Analysis of VIC (A-G) and valve tissue from patients with CAVD (stenotic) or without (control) (H-J). (A-D) Seahorse metabolic analysis by Mito Stress assay VIC. (A) Extracellular acidification rate. (B) Oxygen consumption rate. (C) Energetic map (ECAR vs. OCR plot). (D) ATP linked to OXPHOS. (E-G) Analysis by qPCR of (E) *GLUT1*, (F) *PFKFB3*, and (G) *PDK4* in VIC (N≥6 for each group). (H-J) qPCR analysis in control and calcified valves of (H) *PFKFB3*, (I) *PKM2*, (J) *PDK4* (N≥6 for each group). Data are expressed as mean ± SD. In basal VIC experiments N indicates the number of VIC isolates from independent valve donors and in valve experiments N indicates the number of independent valve tissues; ns, indicates non-significant; *, p<0.05; **, p<0.01. Student's unpaired t-test.

DISCUSSION

This study unravels the interrelation between inflammation and metabolism in a cellular model of CAVD, human primary VIC culture, by identifying a novel shift in cell metabolism to glycolysis required for calcification, inflammation, and cell differentiation, and further showing that this shift mimics the metabolic phenotype in calcified valves and stenotic VIC. Moreover, this study demonstrates the role of impairment in other metabolic pathways such as PPP, TCA, and OXPHOS, by generating oxidative stress, in disease. These metabolic changes are mediated through the JAK-STAT/HIF-1α axis and NF-κB pathways. Finally, validation strategies confirm some of the metabolic alterations in diseased human aortic valves in comparison with healthy ones.

D.1- VIC in the basal state exhibit a fast glycolytic catabolism for feeding their higher reliance on glycolysis energy production than qVIC

New finding of this study is the metabolic genotype of human primary VIC and quiescent VIC (qVIC). Human VIC in culture exhibit a metabolic profile with high expression of genes encoding for proteins involved in cellular catabolism, mainly glycolysis, PPP, and fatty acid oxidation, while lower expression of enzymes involved in TCA cycle, OXPHOS, glutaminolysis and other non-canonical pathways. These findings are supported by the fact that glucose tracing demonstrates that lactate and NAD, synthesized using the R5P coming from PPP, are the predominant metabolic fates of glucose in VIC. Additionally, while VIC rely equally in glycolysis and OXPHOS to generate ATP, qVIC show a more energetic phenotype with the most reliance on OXPHOS. Moreover, gene expression analysis disclosed that the basal metabolic phenotype of VIC is different from qVIC, demonstrating differences with a lower expression of *GLUT1* and higher expression of *HKII* and *PDK4* in qVIC.

Therefore, basal VIC metabolism differs from qVIC metabolism. Metabolic differences between myofibroblast and fibroblast have been previously described in several contexts. In fact, a microarray study comparing gene expression between freshly isolated porcine VIC and cultured porcine VIC demonstrated over 4,000 differentially expressed genes in just 6 days of *in vitro* culture, including the upregulation of mitochondrial and lipid metabolism genes in cultured VIC when comparing with freshly isolated qVIC (Wang et al., 2013). Additionally, a recent characterization of fibroblast metabolism has demonstrated the reliance on OXPHOS for energy production (Algieri et al., 2022). Moreover, in several contexts, the metabolic switch from fibroblast to myofibroblast phenotype has been described to be necessary in processes underlying macrophage-induced disease, such as fibrosis (Setten et al., 2022). Specifically, in the context of pulmonary fibroblasts, an increase in OXPHOS and glycolysis has been reported during the TGF-β-mediated transformation into a myofibroblast phenotype necessary for pulmonary fibrosis thus leading to an equal participation of both pathways for maintaining myofibroblast identity (Bernard et al., 2015).

Furthermore, the metabolic reprogramming required for fibroblast differentiation, has been associated with a metabolic gene profile alteration, as happens in this study. For example, in lung fibroblast, TGF-β-mediated myofibroblast differentiation has been described to induce *GLUT1* expression, due to the necessity of increasing glucose uptake for glycolysis (Azuelos et al., 2016). In contrast to our findings, in lung fibroblast, TGF-β has been described to induce differentiation into myofibroblast phenotype, which has higher levels of *HKII* (Bernard et al., 2015). Additionally, in renal fibroblast, TGF-β has been described to induce *PDK* expression, thus leading to PDH inhibition, thus leading to an acetyl-CoA inhibition (Smith et al., 2020), which is opposed to our findings in VIC, arguing for tissue and cell specific effects.

Based on this evidence and our data, VIC seem to have a metabolism adaptable to their environment. One may speculate that in culture, VIC undergo a first metabolic rewiring that supports the change in phenotype from fibroblast to myofibroblast. Additionally, a feasible explanation to the discrepancies observed in the metabolic gene expression of qVIC versus other fibroblast, could be due to tissue and cell specificity or to the stimuli used. Additionally, considering the composition of dedifferentiation FIB media, insulin could be leading to an increased *HKII* expression, since it has been previously described its direct regulation (Vogt et al., 1998).

Strikingly, glucose tracing analysis revealed a fast flux of glucose carbons into the ribose moieties of NAD in basal VIC. This may be relevant for myofibroblast function, i.e., by supporting the synthesis of macromolecules required for the maintenance of the extracellular matrix. Moreover, fluxomics analysis showed that glucose is quickly metabolized into acetyl-CoA, but more slowly and to a lower extent into TCA metabolites such as succinate and citrate. As mentioned above, several studies have described that acetyl-CoA can have different fates, not only its entry in TCA, but also lipid synthesis and histone acetylation (reviewed in Shi et al., 2015). This evidence, together with the lower incorporation of labeled carbon into succinate, suggest that the TCA cycle is active but slowed down or alternatively, TCA metabolites may exhibit a high turnover. Taking this into account, we hypothesize that pyruvate is entering mitochondria and transforming into acetyl-CoA, which next is transformed to citrate. Most of this citrate may be going to the cytosol where it is converted to acetyl-CoA for lipid synthesis and histone acetylation, and the minor part of citrate may be metabolized to isocitrate for continuing in TCA cycle.

Real-time metabolic analysis of VIC also demonstrates that glutaminolysis exhibits a role in maintaining OCR, thus suggesting the incorporation of glutamate derived from glutaminolysis into TCA cycle as α-KG allowing the second part of TCA to fulfill ETC and OXPHOS. Accordingly, glutaminolysis has been described as an alternative pathway to fulfill TCA and OXPHOS in many cellular models (reviewed in Kodama et al., 2020). Therefore, one may hypothesize that in VIC model, glutaminolysis exerts an active role in maintaining mitochondrial respiration via its participation in TCA maintenance. This fact leads to a feasible

explanation of the fact that, even with a low contribution of [^{13}C]-glucose into TCA metabolite synthesis, the cells were able to obtain 50% of their energy from OXPHOS.

Together, our data support the notion that VIC are highly metabolic cells relying on a fast glucose uptake for feeding catabolic routes like glycolysis, OXPHOS and PPP. Notably, qVIC and VIC exhibit distinct metabolic gene profile and bioenergetics. While qVIC exhibit a more aerobic metabolism with higher reliance on mitochondrial ATP, VIC rely on equal ATP production from glycolysis and mitochondria.

D.2- Pro-inflammatory cytokines induce metabolic rewiring to a hyperglycolytic phenotype that is potentiated by PAMP in VIC

This thesis unravels that inflammatory cytokines promote a metabolic shift leading to a more glycolytic phenotype in VIC, mimicking the metabolic alterations occurring in stenotic VIC. This metabolic reprogramming is characterized by an increased glycolysis with no mitochondrial respiration alterations, but an impairment in ATP synthesis linked to OXPHOS, which is cytokine specific.

In agreement with these inflammation-induced effects, metabolic reprogramming induced by inflammatory mediators has been described in several contexts such as immune cells, cancer cells or vascular endothelial cells (Everts et al., 2014; Mancebo et al., 2022; S. Wang et al., 2019; Xiao et al., 2021). Remarkably, TGF-β-induced metabolic reprogramming has been observed in lung fibroblasts, conferring them a myofibroblastic phenotype that promotes fibrosis (reviewed in Hamanaka et al., 2021). However, metabolic rewiring in VIC is peculiar and differs from other systems. While lung fibroblasts exhibit an increased glycolysis but also an enhanced ETC and OXPHOS, human VIC show an increased glycolysis, with no alterations in ETC but impaired OXPHOS-ATP synthesis. One may speculate that this difference may be attributed to the fact that in cultured VIC-myofibroblast, the increase in OCR and OXPHOS has already occurred during the transition from fibroblast to myofibroblast.

In addition to the inflammatory-induced metabolic rewiring, the most striking finding of our study is that VIC explanted from stenotic patients exhibit a metabolic rewiring to hyperglycolysis with no changes in OCR but a decrease in ATP production linked to OXPHOS, which correlates with the metabolic reprogramming observed in cultured VIC in an inflammatory environment. Our data confirm the recent research of Liu et al. (2023), which has described a Warburg effect occurring in stenotic valves and VIC treated under osteogenic conditions. This metabolic reprogramming is characterized by an increased glycolysis, non-altered OCR and mitochondrial ATP, and upregulation of total ATP. In addition to their results, we also found other altered metabolic pathways, as discussed in following sections, i.e., PPP, TCA and OXPHOS.

This study also elucidates cytokine-specific effects on the mitochondrial function of human VIC. While proton leak is not affected by exposure to TNF-α, TGF-β or IFN-γ treatment, it is decreased by treatment with IFN-α without affecting mitochondrial ATP synthesis. Although there are no publications associating IFN-α and proton leak parameter, one may hypothesize that metabolic differences upon IFN-α treatment could be attributed to the specific signaling pathways used by IFN-α, such as the STAT2 factor or the interferon response elements that are specifically activated in response to this cytokine (reviewed in Schindler et al., 2007). An increase in proton leak is linked to a decrease in coupling efficiency, thus having a role in blunting mitochondrial ATP synthesis (reviewed in Nanayakkara et al., 2019). In contrast, in the human VIC context, IFN-α is decreasing proton leak while blunting mitochondrial ATP, which could be explained since although proton leak is the predominant mechanism responsible for the incomplete coupling of substrate oxidation and ATP synthesis, other mechanisms may account for ATP reduction. For example, a slip in the respiratory chain (electron transfer without concomitant proton pumping) can, in principle, cause this phenomenon (reviewed in Divakaruni et al., 2023).

Additionally, our data also elucidate that non-mitochondrial oxygen consumption and ATP synthesis linked to OXPHOS are altered upon treatment with TGF-β, IFN-γ and IFN-α, but not by TNF-α. Cytokine-specific effects on mitochondrial ATP synthesis agree with previous reports demonstrating that cell exposure to IFN-γ exhibited an impairment in ATP synthesis linked to ETC in several cellular models such as cardiomyocytes and antigen-presenting cells (Kiritsy et al., 2021; Silva-Nunes et al., 2021). Conversely, lung fibroblast exposure to TGF-β showed an increase in mitochondrial ATP production (Bernard et al., 2015), which disagrees with the results obtained in our VIC model showing non altered ATP production linked to OXPHOS upon TGF-β stimulation. Additionally, TNF-α has been demonstrated to increase OXPHOS in endothelial cells from vasculature (Xiao et al., 2021). Therefore, the lack of TNF-α effect in mitochondrial ATP synthesis in VIC upon activation is opposite to previous findings. Furthermore, effects induced by IFN-α in mitochondrial ATP induction in dendritic cells metabolic reprogramming upon a viral infection (D. Wu et al., 2016) have been described to be different to the ones measured through this thesis in VIC model.

On the other hand, the effect of inflammatory cytokines on non-mitochondrial oxygen consumption has been described in the context of cardiomyocytes under 48h of IFN-γ and TNF-α co-exposure, which exhibited an upregulated non-mitochondrial oxygen consumption (Silva-Nunes et al., 2021). Additionally, TGF-β has also been described to induce non-mitochondrial oxygen consumption during the differentiation process of lung fibroblast into myofibroblast (Bernard et al., 2015). However, no evidence has associated directly IFN-α with non-mitochondrial oxygen consumption, but with ROS production, mainly in the context of immune cells (Glenon-Alti et al., 2021). Together, data suggest that these cytokine-specific differences in mitochondrial function could be explained by the specific signaling pathways used for each one and by the different responses described through the literature depending on the cell type and/or the time of exposure.

This study further elucidates IFN- and pathogen pattern- specific effects. While ECAR increases by IFN-(α/γ), LPS does not affect ECAR, but potentiates the effects of both IFN types, being the co-stimulation with LPS and IFN-γ signaling the strongest shift into a glycolytic phenotype. The metabolic rewiring induced upon IFN treatment, has been previously reported in other contexts such as immune cell as well as the potentiation of the metabolic effect by LPS has been demonstrated in macrophages (Seim et al., 2019; F. Wang et al., 2018). Conversely, the pathogen pattern LPS did not significantly alter extracellular acidification of VIC. This finding was unexpected, since LPS-induced glycolytic reprogramming has been well documented in immune cells like macrophages and endothelial vascular cells (Seim et al., 2019; F. Wang et al., 2018; Xiao et al., 2021). Discrepancy may be explained by cell-specific differences in the activation of HIF-1α, a transcription factor associated with metabolic reprogramming in various contexts like cancer and immune cells (Tannahill et al., 2013; Semenza et al., 2011), since previous data from Parra-Izquierdo et al., (2019; 2021) showed that IFN and Poly (I:C) independently, but not LPS, promote HIF-1α stabilization in human VIC.

Another finding is that the combination of both, LPS or Poly (I:C) with IFN, significantly inhibits ATP synthesis linked to OXPHOS and LPS potentiates the effects of both IFN. Data are consistent with recent evidence reporting specific effects of IFNAR and IFNGR in the synthesis of ATP linked to OXPHOS in cardiomyocytes and antigen presenting cells (Kiritsy et al., 2021; Silva-Nunes et al., 2021).

This work also elucidates that non-mitochondrial oxygen consumption is induced by both, IFN-γ, IFN-α, Poly (I:C), and LPS. Non-mitochondrial oxygen consumption has been associated with oxidative stress in different contexts such as breast tumor, where it has been related to the induction of apoptosis and neuronal activation (Banh et al., 2016; Liao et al., 2023). This evidence leads us to think that an inflammatory milieu may promote oxidative stress in VIC as a consequence of the induced metabolic alterations.

Collectively, these findings demonstrate that the metabolic phenotype of human VIC is dynamic and under inflammatory environments exhibit a shift to glycolysis that resembles the metabolic phenotype of stenotic VIC. This study further highlights the interplay between IFN receptors and TLR signaling pathways in the metabolic shift to increased glycolysis, and IFN and TLR-specific responses.

D.3- TLR3/4-IFNGR interplay on glycolytic reprogramming supports the processes of inflammation, differentiation, and calcification in VIC and human valves

This thesis unveils the role of inflammatory environment on hyperglycolysis induction, thus promoting glycolytic ATP increase, enzymes, and metabolites. Additionally, pharmacological approaches targeting glycolysis reveal a direct role of glycolysis on VIC inflammation, differentiation, and *in vitro* calcification. This metabolic rewiring is mirrored in stenotic valves and explanted VIC.

D.3.1- Inflammation induces alterations in glycolytic gene profile and its functional effects on glycolysis enhancement in VIC

This study unravels that the co-stimulation of VIC with LPS and IFN-γ alters the metabolic gene expression profile of VIC, with upregulation of main regulators of glycolytic function such as *GLUT1, HKII, PFKFB3* and *PKM2*, and the lactate transporter *MCT4*. These changes correlate with functional alterations characterized by an increased extracellular acidification and lactate, as well as glycolytic ATP production. Importantly, inflammatory-induced increase in glycolytic gene expression has been validated in human qVIC and in porcine 3D co-culture, and in the latter also in osteogenic conditions. Remarkably, some of those changes are observed in calcified valve leaflets from patients. Furthermore, the bioenergetic phenotype of stenotic VIC is mirrored by the metabolic rewiring observed in non-stenotic VIC under pro-inflammatory settings. Together, data confirm this metabolic rewiring as a novel mechanism underlying CAVD and suggest that inflammation triggers a metabolic shift that may be relevant to initial stages of its pathogenesis.

A relevant finding of this thesis is that the expression of *PFKFB3, GLUT1, PKM2* is upregulated in VIC activated with inflammatory stimuli and in stenotic leaflets. The altered expression of metabolic enzymes mediating reprogramming has been previously reported in different contexts. In vascular endothelial cells, PFKFB3 has been described as a key mediator of glycolytic flux and glycolytic ATP production induction upon treatment with TFG-β (Xiao et al., 2021). A recent report in VIC demonstrates that PFKFB3 regulates the calcifying conditions-induced inflammation and differentiation and the palmdelphin-induced inflammation but may not be the key regulator of palmdelphin-induced osteogenic differentiation (S. Wang et al., 2022). Additionally, Heather et al., 2011 elucidated a metabolic shift from fatty acid to glucose in heart biopsies of patients with hypertrophy and aortic valve impairment, which goes through the increase of *GLUT1* and *PKM2* expression. Moreover, B. Fu et al. (2022) in a metabolomics and proteomics-based analysis, have described the higher levels of hypoxia-inducible factor 1 (HIF-1) signaling pathway and GLUT1 protein expression in human stenotic valves versus healthy ones. In line with this report, Liu et al., (2023) have elucidated differences in the metabolic protein profile in stenotic and osteogenic-activated VIC versus control ones with upregulated protein levels of GLUT1, PFK1, HKII and LDHA, in accordance with the results obtained in our study. In agreement with these previous publications, it has been recently described that pressure overload in AS triggers not only structural but also metabolic remodeling increasing the risk of decompensation into heart failure. This metabolic remodeling goes through the downregulation of FA oxidation and the increased reliance on glucose metabolism, thus leading to lipid accumulation and heart failure (reviewed in Monga et al., 2022).

Our data also elucidate the functional role of the inflammatory-induced glycolytic gene expression in VIC metabolic reprogramming. Until these last years there was not much evidence related to the role of VIC metabolism in CAVD. However, recently, Liu et al., (2023) have described a Warburg effect occurring in

stenotic valves and VIC treated under osteogenic conditions. This Warburg effect is mediated by the upregulation of RhoA/ROCK1 pathway, generally activated by shear stress, which inhibits AMPK phosphorylation, thus leading to the metabolic reprogramming characterized by an increased glycolysis, non-altered OCR or mitochondrial ATP, and increased total ATP levels. These changes together have a direct role on *RUNX2* upregulation due to the lack of AMPK-mediated proteasome degradation, thus leading to osteogenesis and calcification. This study is confirming some of our findings, but also is complementary. While Liu et al. described a shear stress-induced pathway, our findings unravel inflammation as a driver of the metabolic reprogramming in VIC. Additionally, our study provides a deeper understanding of the metabolic shift, which is not a mere Warburg effect, but a more complex reprogramming that affects the oxidative PPP route as well as mitochondrial function. In support of a more complex metabolic rewiring, a recent report analyzing the metabolomics and proteomics profiles in cardiac valves from patients with and without CAVD showed significant alterations of 229 metabolites and 549 proteins. After a statistical study of the relationship between altered metabolites and proteins, they found a total of 34 metabolites, 52 proteins, and 23 interconnected signaling. The main metabolic pathways were: (i) adenosine triphosphate-binding cassette transporters, (ii) starch and sucrose metabolism, (iii) hypoxia-inducible factor 1 (HIF-1) signaling, and (iv) purine metabolism. Among the most important hubs, they found the activation of the Ectonucleotide pyrophosphatase/phosphodiesterase 1 (ENPP1) pathway and the decrease of the calcium2+/calmodulin-dependent protein kinase II delta (CAMK2D) pathway, which directly interacted with the low levels of ADP, sorbitol, glucose-6-P, glucose-1-P, OAA, and aspartic acid in diseased valves compared to healthy ones. Additionally, ATP binding cassette subfamily a member 8 (ABCA8), which was decreased, directly interacted with choline levels (B. Fu et al., 2022).

This thesis also unveils that human VIC exposed to inflammatory milieu exhibit no significant effect on OCR despite variability between patients but show a decrease in mitochondrial ATP production. In many cellular models, the glycolytic shift is accompanied by a parallel decrease in OXPHOS. However, the activity of OXPHOS is reported to be dependent on the cellular maturation state, immune context, and stimuli used (Everts et al., 2014; Krawczyk et al., 2021 & O'Neil et al., 2013). For example, in pulmonary fibroblasts an increase in both glycolysis and OXPHOS is required for their differentiation to myofibroblast leading to pulmonary fibrosis (reviewed in Hamanaka et al., 2021; Vaupel et al., 2019). However, different disease models have shown an increase in glycolytic ATP production while a decrease in mitochondrial ATP since although less efficient, cells can generate ATP more quickly via glycolysis and produce metabolic intermediates necessary for the synthesis of other molecules which are necessary for proliferation (reviewed in Liberti et al., 2016).

Additionally, our findings demonstrate that although qVIC and VIC are different cellular types, their exposure to an inflammatory milieu leads them to a similar metabolic rewiring, induction of the glycolytic

phenotype and glycolytic ATP production, and inhibition of mitochondrial ATP production. Conversely to our data, some reports have elucidated a different cytokine-induced metabolic rewiring required for transforming from fibroblast to myofibroblast. For example, in the context of lung fibroblast, the metabolic requirements during TGF-β-induced differentiation of fibroblasts to myofibroblasts involved a parallel increase in OCR and ECAR (reviewed in Hamanaka et al., 2021). However, in the context of some other fibrotic diseases, such as heart, liver and kidney fibrosis, a metabolic rewiring involving an impaired mitochondrial ATP synthesis has been described to leads to apoptosis and disease progress (reviewed in Xinyu Li et al., 2020). Interestingly, in line with our data of ATP sources used by activated VIC and qVIC, which are osteoblast-like cells, it has been described that osteoblasts equally utilize both energy sources, OXPHOS and glycolysis, during the differentiation process, but once differentiated, they become more dependent on glycolysis than OXPHOS (Guntur et al., 2014). Additionally, it has been demonstrated that VSMC and VIC pre-osteoblasts generate most of their ATP through glycolysis during osteogenic process (Liu et al., 2023). These pieces of evidences together with the fact that qVIC undergo the metabolic rewiring and phenotype transformation at the same time-period than VIC could suggest direct transformation from fibroblast into osteoblast-like phenotype, without going through a myofibroblast phenotype, a mechanism recently described in Lu et al., 2019.

Together, our data support the notion that although basal metabolic differences, both VIC and qVIC respond to inflammatory stimuli by acquiring a similar metabolic shift characterized by hyperglycolysis, which could be leading to an osteoblast-like differentiation. Finally, differences in metabolic reprogramming induced in other cell types by other cytokines suggest tissue, cytokine, and cell specific differences.

D.3.2- Inflammation-induced glycolysis mediates VIC differentiation, inflammation, and calcification

One of the main findings of this study is that glycolysis is necessary for inflammatory-induced processes like inflammation, differentiation, and calcification in VIC. Indeed, glycolysis abrogation not only inhibits pathological processes underlying CAVD, but also induces a fibroblast-like phenotype characterized by a more metabolically quiescent phenotype than the one exhibited by qVIC, equal ECAR levels but a decrease in OCR consumption in comparison to VIC.

D.3.2.1- The role of inflammatory-induced glycolysis in VIC phenotype and osteogenic differentiation

This study demonstrates that glycolysis is necessary for inflammatory-induced osteoblast-like differentiation. It further shows that while VIC relies equally on glycolysis and OXPHOS, the exposure to an inflammatory milieu increases the reliance on glycolysis. Since this pro-glycolytic shift correlates with phenotypic changes, one may speculate that the increase in glycolysis provides the energy necessary for the demand required in the differentiation process of VIC. Additionally, the thesis unravels the role of mannose in reverting the inhibitory effects of 2-DG on inflammatory-induced differentiation.

Our findings are consistent with reported evidence describing the requirement of increased glycolysis for cell differentiation in many contexts such as lung fibroblast, immune cells, and cancer (Bernard et al., 2015; Everts et al., 2014; Warburg et al.,1926; S. Wang et al., 2019). Interestingly, it has been recently described that osteoblasts use equally OXPHOS and glycolysis, during the differentiation process, but once differentiated, they become more glycolytic (Guntur et al., 2014). Additionally, last year, S. Wang et al., (2022) manifested that in VIC, palmdelphin directly induced differentiation in a glycolytic-dependent way via NF-κB activation although independent of PFKFB3 while calcifying conditions induced osteogenic differentiation and inflammation in a dependent manner of both, NF-κB and PFKFB3. Therefore, one may conclude that inflammatory-induced glycolytic rewiring is energetically supporting the osteoblast-like differentiation of VIC. Finally, the fact that mannose plays a reverting role in 2-DG blocking immune-effects is because 2-DG is a mannose epimer and exerts a greater competitive effect with it than with glucose, since mannose is found in tissues in much lower concentrations (Kurtoglu et al., 2007).

An interesting finding is that glycolysis is relevant to maintain the VIC phenotype since blocking glycolysis reverts the myofibroblast phenotype to fibroblast-like by acquiring a spindle-shape form and decreasing the expression of *ACTA2*. This finding is consistent with glycolysis blockade of VIC changing the metabolic phenotype to a more energetic and less glycolytic phenotype that resembles the metabolic phenotype of qVIC. Thus, the metabolic phenotype of VIC is dynamic and adaptive, and the increase in glycolysis energetically supports the phenotype and differentiation state. Previous reports have also demonstrated a similar effect in myofibroblasts from other tissues. In myofibroblast from kidney has been described that the inhibition of glycolysis blocks TGF-β-induced activation and therefore reverses the myofibroblastic phenotype and promotes a quiescent fibroblast phenotype (Ding et al., 2017).

Together, these findings support the hypothesis that changes in the reliance on glycolysis are required for the phenotypic changes of interstitial valve cells in homeostasis and disease. These results highlight that adaptations in substrate use occur under inflammatory conditions and may contribute to the metabolic shift in valves from patients with CAVD.

D.3.2.2 -The role of inflammatory-induced glycolysis in VIC inflammatory responses

This thesis reveals that glycolysis is required for the inflammatory response triggered by exposure of VIC to IFNγ and pathogen patterns. The role of glycolysis on inflammation induction has been well documented in several disease models such as macrophage proinflammatory response, atherosclerosis, endothelial to mesenchymal transition and cancer (Tannahill et al., 2013; Xiao et al., 2021). Additionally, the role of inflammatory agents in inflammatory response in VIC as well as the role of inflammation in CAVD initiation and progress have been reported by Boström et al., (2011); New et al., (2011) & Parra-Izquierdo et al., (2018; 2019). Recently, it has also been associated osteogenic-induction and palmdelphin expression in

VIC with an enhanced glycolysis, which directly induces inflammation through TNF-α family and NF-κB activation, thus leading to an upregulation of adhesion molecules expression such as ICAM-1 (S. Wang et al., 2022). Although our data confirm some of their findings, we further identified other metabolic pathways playing a direct role on the metabolic reprogramming-dependent inflammation.

This study also reveals that glycolysis is necessary not only to the inflammation-mediated induction of adhesion molecules, ICAM-1 and VCAM-1, but also to their post-translational modifications in VIC and the effects of 2-DG on these proteins are reverted by mannose. These findings agree with the fact that the tool used for glycolysis blockade, 2-DG, also affects protein modifications in ER due to the lack not only of glycolysis, but also mannose metabolism, both required for post-translational modifications. In line with these results, other reports have described that both proteins VCAM-1 and ICAM-1 are highly glycosylated and mannosylated for proper functioning (He et al., 2014 & Montes-Sánchez et al., 2009). In fact, the lack of post-translational modifications leads to ICAM-1 reduction and diminished inflammatory response in HUVEC and mice. Notably, these effects are reverted by mannose (He et al., 2014). Thus, the effect observed in adhesion molecules expression when blocking glycolysis are consequence not only of glycolysis abrogation and pNF-κB decrease, but also to the lack of post-translational modifications, as a consequence of ER-stress induced by 2-DG and these effects can be reverted by mannose.

Notably, through this thesis, the role of glycolysis in inflammatory-triggered upregulation of *PTGS2* (*COX2)* expression was demonstrated by blockade with 2-DG, but not by glucose deprivation. This apparent discrepancy on the role of glycolysis in *COX2* expression may be due to the reported role of 2-DG in ER-stress. In support of this, our experiments with tunicamycin, an ER stress inducer, mimic the effects of 2-DG on *PTGS2 expression*. Additionally, previous studies reported that ER-stress induced by 2-DG reduced *COX2* expression and N-glycosylation and induces a loss of COX2 activity in rabbit articular chondrocytes (Yu et al., 2010), although this is controversial since the opposite conclusion has been reported in human chondrocytes (Rasheed., 2012). Therefore, data and evidence show the need to study in depth the mechanism underlying this 2-DG-induced ER-stress and its subsequent effect on *COX2* expression and translational modifications in human VIC.

Collectively, evidence and data together highlight the role of glycolysis upregulation upon inflammatory stimulation on triggering inflammatory response that could further contribute to pathological processes like calcification in human VIC.

D.3.2.3- The role of glycolysis in inflammation-triggered calcification of VIC

This study unravels the role of increased glycolysis and glycolytic ATP in supporting and fueling the inflammatory-induced *in vitro* calcification in VIC as well as the potential effect of mannose as an anti-apoptotic agent. Several previous publications in the atherosclerosis context have associated glycolysis

upregulation with calcification. A recent study has related glycolysis upregulation and OXPHOS impairment with VSMC calcification due to an increased mitochondrial calcium overload and apoptosis (Zhu et al., 2023). Other studies have associated mitochondrial dysfunction and VSMC calcification with an increase in oxidative stress, apoptosis, aerobic glycolysis, mitochondrial fission, and a decrease in OXPHOS, mitochondrial biosynthesis, and mitochondrial fusion and mitophagy (reviewed in Izquierdo-García et al., 2022).

In the context of CAVD, two recent studies have described a direct association between glycolysis and calcification. First, S. Wang et al., (2022) described that palmdelphin overexpression induced a glycolysis enhancement, under control and calcifying conditions, which is required for later calcification occurring via caspase 3-dependent apoptosis. Later, Liu et al., (2023) have described a Warburg effect occurring in stenotic valves and osteogenic-activated VIC characterized by an increased glycolysis, which has a direct role on RUNX2 upregulation and calcification. Therefore, our data confirm some of their findings on the role of glycolysis in VIC calcification, but we further demonstrate the importance of inflammation as a driver of a metabolic shift leading calcification that is characterized not only by a glycolytic shift, but by additional metabolic changes also contributing to calcification. Their studies are focused on characterizing the role of shear-stress-induced pathway Rho/ROCK1 and other initiation factors such as genetics, hypertension, diabetes, and elevated phosphate, in metabolic reprogramming on CAVD context.

When addressing the role of glycolysis, mannose was used to reverse glycolysis blockade by 2DG. We found that mannose does not revert the effect of glycolysis-blockade on VIC calcification, while it does on VIC differentiation and inflammation, which could be explained by a role of mannose on apoptosis. This idea was supported by the fact that mannose reduced the apoptosis induced by inflammatory agents and 2-DG in VIC, as well as the increased expression of the anti-apoptotic gene, *BCL2*, induced in VIC by mannose. However, the role of mannose on apoptosis is controversial. A recent study has proposed mannose as a new strategy for tumor treatment due to its role in apoptosis induction, thus leading to the sensitizing of tumors to antitumoral drugs (Gonzalez et al., 2018). Conversely, other studies performed in the context of rat chondrocytes demonstrated the role of mannose treatment in promoting proliferation, enhancing autophagy, and reducing apoptosis upon IL-1β-treated chondrocytes, thus suppressing osteoarthritis (Lin et al., 2021). Therefore, we speculate the potential role of mannose as an anti-apoptotic effector that could prevent dystrophic calcification of VIC. However, further experiments characterizing the role and mechanisms of action of mannose in VIC would be necessary.

Collectively, our findings support the notion that enhanced glycolysis is required to support the process of calcification in VIC exposed to an inflammatory milieu.

D.3.2.4- Interplay between glycolysis blockade and other catabolic pathways induction

Beyond the role of glycolysis in pathological processes in CAVD, this thesis also unravels the interplay between glycolysis and other metabolic pathways. Glycolysis blockade in VIC triggers ETC and OXPHOS as well as glutaminolysis in both basal stimulated conditions, probably as a compensatory mechanism for energy production and homeostasis maintenance. A compensatory mechanism has recently been described in different contexts. On the one hand, long-term intermittent treatment of mice with 2DG showed an increase of the proteome of the respiratory chain in the heart without affecting vascularization, hypertrophy, or fibrosis (Dodson et al., 2022). On the other hand, in cancer cells the blockade of glycolysis upregulates mitochondrial function, thus shifting their metabolism towards OXPHOS, mainly through glutaminolysis, which allows the entry of metabolites into the second half of the TCA cycle, thereby promoting the proper function of ETC and OXPHOS (Shiratori et al., 2019). In fact, the increase in OXPHOS could be acting not only as a compensatory but also as a protective mechanism, based on a recent study disclosing a protective role of OXPHOS against inflammation and EndMT in vascular endothelial cells (Xiao et al., 2021). Conversely, in the context of CAVD, Zhong et al. (2023) reported that stenotic patients have increased Piezo 1, an ion channel, expression levels in AV tissue, and elevated glutaminolysis in plasma. Deeper *in vitro* experiments revealed that the induction of Piezo 1 by an agonist induced an overload of intracellular Ca^{2+}, thus leading to the increased expression of YAP protein (calcium-dependent Yes-associated), which is responsible for the induction of GLS1 and glutaminolysis. This increase in glutamine metabolism later affects the TCA cycle by increasing the production of acetyl-CoA, which finally influences the acetylation of histone 3 of *the RUNX2* promoter, inducing the expression of *RUNX2* and subsequent osteogenesis.

Therefore, our data manifests that glycolysis is necessary for maintaining the VIC phenotype but hyperglycolysis leads to CAVD pathology. However, glycolysis blockade forces VIC to fulfill their energetic requirements using other pathways such as OXPHOS, as shown by the increase in mitochondrial ATP upon 2-DG treatment. Taking evidence in the literature showing the downregulation of β-oxidation in CAVD, and our results showing the participation of glutaminolysis in VIC metabolism basally and upon activation, one may hypothesize that glutaminolysis is the pathway implicated in OXPHOS maintenance when glycolysis is blocked. However, more experiments would be required for confirming our hypothesis.

D.3.3- The role of Pyruvate kinases in metabolic reprogramming of VIC and subsequent calcification, differentiation, and inflammation processes

This study identifies *PKM2* as the most abundant metabolic gene in VIC, and further highlights its role in the inflammatory-induced metabolic shift of VIC leading to calcification, differentiation, and inflammation. PKM2 is the only isoform transcriptionally upregulated upon stimulation, and is found as dimers, as shown by its phosphorylation in Y105, and tetramers, assayed using TEPP46, in activated VIC. Dimeric PKM2 is

reported to be the isoform related to metabolic reprogramming in different contexts such as tumor cells (reviewed in Yang et al., 2013). Additionally, PKM2 has been also recognized for its role in regulating gene expression as a co-activator of transcription factors in other disease models of heart, kidney, liver, lung, adipose tissue, and pancreas (reviewed in Puckett et al., 2021). Notably, PKM2 isoform has been associated with pulmonary hypertension progression in a rat model (reviewed in Puckett et al., 2021). Beyond these reports, PKM2 has been described to participate in the phosphorylation of histone 3 by its direct interaction with it, which is required for the later dissociation of histone deacetylase from gene promoters and subsequent histone 3 acetylation, thus leading to gene expression (Yang et al., 2012).

This thesis also shows that PKM2 is phosphorylated at Y105 in activated VIC. These data suggest the existence of PKM2 in its dimeric form, which is located in the nucleus upon immune stimulation of VIC. According to the literature, PKM2 is associated with different activities depending on its conformation and localization (reviewed in Boukouris et al., 2016). Dimeric PKM2 has lower glycolytic activity and can function as a transcriptional coactivator of HIF-1α by dimerizing with it (reviewed in Yang et al., 2013). This complex can later activate the transcription of genes involved in cell proliferation and differentiation in epithelial to mesenchymal transition (Hamabe et al., 2014), metabolism (reviewed in Vaupel et al., 2019), inflammation (Palsson-Mcdermott et al., 2015) and apoptosis (reviewed in Puckett et al., 2021). Of note, PKM2 dimer has been also reported to have a dual role in apoptosis. Some reports demonstrate its role in protecting against apoptosis when it is translocated to mitochondria in response to H_2O_2 to phosphorylate and stabilize Bcl2 (Saleme et al., 2019). Conversely, other authors have described PKM2 to form a complex with MDM2 and p53 in the nucleus and function as a master regulator of pro-apoptotic genes (H.Wu et al., 2016).

Our study also discloses that tetrameric PKM2 plays a role in metabolic rewiring, inflammation, differentiation, and calcification in VIC. Some previous reports have described the higher glycolytic activity of PKM2 tetramers leading to increased lactate production and a decreased pyruvate flux and propose that this is likely due to the formation of a supramolecular complex with lactate dehydrogenase (Anastasiou et al., 2012 & Christofk et al., 2008). Interestingly, tetrameric PKM2 has been reported to induce the mitochondrial fusion leading to the decrease of mitochondrial ATP levels and the reduction of expression level of ETC complex I, III and V (reviewed in Puckett et al., 2021). Surprisingly, tetrameric PKM2 has also been associated with apoptosis depending on the intracellular redox state; in highly oxidized environments, PKM2 tetramer is oxidized in its cysteine 423 and it suppresses p53 activity while in a reduced environment exhibits the opposite effect (Saleme et al., 2019).

Together, our data indicate the coexistence of both dimeric and tetrameric forms of PKM2 in activated VIC. One may speculate that each of these isoforms can be acting differently. The detection of PKM2 in the nuclei of activated VIC suggests that the dimeric PKM2 form could be acting as a co-factor of HIF-1α leading to the transcription of glycolytic genes, as described in murine macrophages (Palsson-McDermott et al.,

2015) or directly participating in histone phosphorylation and acetylation (Yang et al., 2012), a process previously related to VIC calcification (Fu et al., 2019; Song et al., 2017). On the other hand, data upon PKM2 tetramerization, discloses that tetrameric PKM2 increases glycolysis and stabilizes HIF-1α, and subsequently induces VIC calcification, inflammation, and differentiation. Additionally, both isoforms could promote apoptosis leading to dystrophic calcification, but more experiments would be required to demonstrate the link. Supporting our findings of isoforms coexistence, it has been previously described that once the tetramer or dimer has performed its activity, it can be converted into the other form (Christofk et al., 2008). Accordingly, one may speculate that PKM2 plays a dual role in the disease depending on the active isoform. However, further experiments would be required in our system to develop a solid hypothesis regarding the activity and isoforms of PKM2. Additionally, the fact that PKM2 activity can also be regulated by post-translational modifications such as phosphorylation, acetylation, or oxidation (Yang et al., 2013) makes it more difficult to formulate a definitive hypothesis.

D.3.4- The role of lactate in inflammation-induced differentiation, calcification, and inflammation in VIC

This thesis unveils the role of lactate production and secretion, as a by-product of glycolysis, in inflammatory-induced inflammation, differentiation, and calcification of VIC. We found increased aerobic glycolysis and lactate secretion after exposure of VIC to an inflammatory milieu. There is compelling evidence of lactate production under fully aerobic conditions. Lactate production has been linked to metabolic rewiring and disease in several contexts, where it has been reported not only as a source of energy, i.e., in cancer cells (reviewed in Beyoğlu et al., 2021), but also as a direct HIF-1α stabilizer that further leads to osteogenesis of osteoblast-lineage cells (Y. Wu et al., 2017). Additionally, lactate accumulation has been associated with the generation of chronic inflammation in several diseases such as cancer and arthritis rheumatoid (reviewed in Certo et al., 2021). Finally, a recent report links lactate to vascular calcification via fibroblast differentiation to osteoblast-like phenotype and via dystrophic calcification induced by ROS and mitochondrial damage (Zhu et al., 2020).

Therefore, blockade of lactate production by LDH inhibition allows us to speculate that inflammatory-triggered lactate production is directly involved in HIF-1α stabilization leading to inflammation, differentiation, and *in vitro* calcification. Additionally, our findings support a role of increased lactate secretion in VIC metabolic reprogramming acting as a HIF-1α stabilizer. These findings agree with the notion that lactate production is essential for HIF-1α stabilization in macrophages (Colegio et al., 2014). The fluxomics analysis of basal VIC, showed a rapid incorporation of the carbons of [^{13}C]-labeled glucose into lactic acid, but it did not statistically change upon VIC activation for 24h. This apparent inconsistency could be explained by the fact that lactate is readily secreted to extracellular media, and fluxomics analyzes intracellular metabolites.

One finding of this study is that lactate can function as a signaling molecule in VIC. Extracellular lactate can be captured by VIC and induces VIC differentiation, mitochondrial uncoupling, non-mitochondrial oxygen consumption and HIF-1α stabilization. There is compelling evidence of the role of lactate as a signal molecule. Lactate is reported to function as an intercellular and inter-tissue redox signaling molecule not only in neighboring cells but also in distant cells through circulation (reviewed in Xiaolu et al., 2022). As a signaling molecule, lactate has been demonstrated to regulate fibroblast and macrophage IL-6 secretion through a specific lactate transporter. Extracellular lactate has been described to be captured via monocarboxylate transporter (MCT) or G protein-coupled receptors, specifically GPR81 and it carries out several functions.

On the one hand, lactate has been associated with ROS production and metabolic reprogramming. In dermal fibroblasts cultured in a medium where lactate was the only energy source, they exhibited reduced PDH activity, thus inhibiting TCA cycle and impairing OXPHOS leading to a glycolytic shift mediated through ROS-mediated HIF-1α stabilization (Kozlov et al., 2020). Additionally, lactate oxidation by lactate oxidase leads to the generation of ROS, which can result in oxidative damage to cells (reviewed in Corkey et al., 2020). Additionally, lactate has been associated with the modification of lysine residues of histones (reviewed in Certo et al., 2021). They showed that lactate-derived lactylation of histone lysine residues serves as an epigenetic modification that directly stimulates gene transcription from chromatin.

Therefore, although the mechanism of lactate entering to VIC is not identified in this study, extracellular lactate can be captured by VIC leading to impairment in ATP mitochondrial production and HIF-1α stabilization, and mostly inducing metabolic rewiring and ROS production. Additionally, we could hypothesize that lactate could be acting as an histone-activity modulator in VIC, leading to an increase in gene transcription. However, deeper investigations would be required for identifying the mechanisms of lactate action and the exact role of lactate in metabolic rewiring in VIC exposed to an inflammatory milieu.

D.4- TLR3/4- IFNGR interplay on downregulating the rate-limiting enzyme of the oxPPP and its role in inflammation, differentiation and calcification in VIC and human valves

Our data indicate a complex role of the PPP in VIC physiopathology. One of the most striking findings of our study is the downregulation of the limiting enzyme of the oxidative phase of PPP induced by inflammatory stimuli and its further association to VIC calcification. On the other hand, the non-oxidative phase remains active and further potentiated upon inflammatory stimuli. This conclusion is based on the increase of labeled R5P synthesis found incorporated into cofactors and energetic factors.

D.4.1- Inflammatory stimuli downregulate G6PD and promote VIC inflammation, differentiation, and calcification

This study discloses the inflammatory-mediated downregulation of *G6PD*, the rate-limiting enzyme of oxPPP via HIF-1α, thus leading to NADPH levels decrease and oxidative stress. These findings are supported by the pharmacological blockade of G6PD, which demonstrates the protective role of oxPPP against inflammation-induced differentiation, inflammation, calcification, and redox alterations in VIC. The inhibition of *G6DP* expression has been validated in the 3D VIC-VEC co-culture model.

Silencing and pharmacological evidence revealed that HIF-1α participates in the inflammatory-induced downregulation of *G6PD* and redox homeostasis alteration. Several previous reports demonstrate that HIF-1α activity influences PPP. Specifically, Zhao et al., 2010 described in drug resistant leukemia cells that HIF-1α could directly increase the non-oxidative phase of the PPP, while decreasing oxPPP by directly inhibiting the G6DP enzyme. Moreover, R5P is considered the main product of non-oxPPP (reviewed in Tong et al., 2009) while the production of NADPH by the oxPPP has been described as the main mechanism maintaining redox homeostasis, thus NADPH is used as a marker of the state of oxPPP (reviewed in Krüger et al., 2011). NADPH is further required for the conversion of oxidized glutathione (GSSG) to reduced glutathione (GSH), necessary for eliminating ROS (Aon et al., 2012; Bradshaw, 2019). In the context of ROS generation, NADPH oxidases (NOX), whose levels are NADPH-dependent, have been described as the main enzymes producing ROS upon inflammasome activation (reviewed in Bradshaw, 2019). However, controversial reports about NOX expression in stenotic valves have been published (reviewed in Greenberg et al., 2022). For example, the analysis of *NOX2* and *NOX4* mRNA levels in calcified regions of stenotic valves were significantly decreased when compared to normal valve tissue. However, in contrast to these findings, another study revealed a marked increase in NOX2 expression around calcifying regions in human sclerotic and stenotic valves (reviewed in Greenberg et al., 2022). In addition, the fact that *NOX* are downregulated in the VIC model exposed to inflammatory stimuli suggest that they are not the responsible for ROS production in VIC. These findings could be explained by the activity of dioxygenases, which in a reaction involving three co-substrates: divalent iron, 2-oxoglutarate, and molecular oxygen, provide the oxygen atom for the hydroxyl group, while decarboxylates 2-oxoglutarate to succinate and generates ROS as a by-product in the form of superoxide anion (Sengupta et al., 2020). In addition to this potential explanation, other sources of ROS in CAVD has been reported, i.e., inducible nitric oxide synthase or semicarbazide-sensitive amine oxidase, which is able to generate H2O2 from endogenous amines (reviewed in Greenberg et al., 2022).

We found that the inhibition of G6PD mimics the inflammation-induced metabolic shift and redox alteration in VIC. This fact agrees with previous reports in the context of breast cancer cells demonstrating that when the main enzymes controlling PPP are silenced, G6PD and transketolase, glycolytic flux is upregulated, lipid synthesis is reduced, and glutamine uptake is increased. Additionally, this silencing also

directly induces oxidative stress while reducing proliferation and cell survival (Benito et al., 2017). Additionally, data from this thesis parallel the changes found in the hypertrophied hearts, which demonstrates that changes in alternative glucose pathways such as PPP directly affects the reliance on glycolysis for energy production (reviewed in Kolwicz et al., 2011). Moreover, redox alterations, based on non-mitochondrial respiration changes, have been associated with ROS production, which have been later associated with calcification processes due to the induction of apoptosis (reviewed in Qiao, 2022).

Based on the blockade of G6PD emulating the inflammatory-induced shift and VIC responses, an important finding of this thesis is that calcification, inflammation, and differentiation are coupled to impairment of the oxPPP. The main explanation for this data could be due to the glycolytic reprogramming induced upon G6PDi treatment, since all the mentioned processes have been demonstrated to be glycolysis dependent in section D3. On the one hand, the role of G6PD inhibition in calcification has been previously described in the context of vascular cells (Dhagia et al., 2021). This work states that G6PD knockdown significantly decreases histone deacetylase, leading to gene expression, SMC differentiation, and calcification. Finally, the role of G6DP in inflammation has been published in several studies, ones in the line of our results, and others in the opposite line. Some reports supporting our findings show the protective role of PPP against the oxidative and inflammatory state as well as the EndMT of endothelial vascular cells (Xiao et al., 2021). Additionally, in a model of HeLa cells, it has been demonstrated that the overexpression of *G6PD* and upregulation of NADPH levels were associated with higher levels of GSH, lower levels of ROS, and reduced activation of the NF-κB factor, thereby preventing inflammation (Schafer et al., 2001). In contrast to our findings, in the context of immune cells, the upregulation of oxPPP has been associated with inflammatory activation (Britt et al., 2022 & Prange et al., 2018).

Together, one may conclude that inflammatory-induced metabolic changes in PPP regulation are stimulus and cell specific. In VIC, the inflammation-induced oxPPP impairment may lead to ROS production as a consequence of $NADP^+$/NADPH and GSSG/GSH disequilibrium, and also contribute to a glycolytic shift necessary to support VIC inflammation, differentiation, and calcification. Thus, we can speculate the potential protective role of the PPP against pathological processes in CAVD, likely due to its role in maintaining cellular homeostasis and its protective role against ROS production. In fact, the relationship between ROS and metabolic reprogramming is supported by our data obtained upon VIC treatment with H_2O_2, which directly induces a metabolic reprogramming towards a glycolytic phenotype and ROS production in VIC.

D.4.2- Non-oxidative phase of PPP is active in VIC exposed to an inflammatory environment

Although we have not directly explored the non-oxidative PPP in VIC, the inflammation-induced increase in the flux of [U-^{13}C]-glucose carbons into the ribose moieties of coenzyme A of acetyl-CoA, NAD^+, and ATP show a major contribution of the PPP to the production of enzyme cofactors and nucleotides.

Interestingly, in some other contexts, there has been a parallel potentiation of non-oxPPP despite the inhibition of the oxPPP as a direct consequence of HIF-1α stabilization (reviewed in Majmundar et al., 2010). This mechanism was possible because the non-oxPPP could be maintained thanks to the direct incorporation of metabolites generated in glycolysis, such as glyceraldehyde-3-phosphate or fructose-6-phosphate (reviewed in Ge et al., 2020). Additionally, although no role of PPP has been demonstrated in myofibroblast differentiation during fibrosis process, high levels of R5P has been found in lung tissue from patients with pulmonary fibrosis while metabolic tracing experiments have shown that flux through the oxidative arm of the PPP is low in lung fibroblasts and not induced by TGF-β (reviewed in Hamanaka et al., 2021). Finally, in the context of endothelial cells from vasculature, Xiao et al. (2021) described that upon LPS treatment the incorporation of [^{14}C]-glucose into R5P was increased.

On the other hand, several pathways have been described to participate in the synthesis of NAD^+. The most common altered upon disease is the salvage pathway, which synthesize NAD from nicotinamide (NAM), nicotinic acid (NA), nicotinamide riboside (NR), and nicotinamide mononucleotide (NMN) via the rate-limiting enzyme NAMPT (reviewed in Xie et al., 2020). Additionally, salvage pathway has been described as the most important in mammalian cells. In fact, the deletion of *NAMPT* gene in mice has been reported to be lethal (reviewed in Audrito et al., 2020). Furthermore, recently, the direct regulation of NAMPT transcription by the transcription factors STAT1, HIF-1α and NF-κB has been described in several contexts such as tumor-associated macrophages (reviewed in Audrito et al., 2020). Interestingly, in the context of immune cells and fibroblast, *NAMPT* expression has been described to be induced by LPS as well as by pro-inflammatory cytokines induced as a response to LPS stimulation via HIF-1α stabilization (reviewed in Audrito et al., 2020).

Together, data highlight the role of TLR4 and IFNGR interplay on downregulating the rate-limiting enzyme of oxPPP, in a HIF-1α-dependent manner, and its association to VIC calcification. Additionally, our findings support the inflammatory-induced non-oxPPP activation for R5P synthesis and its later incorporation into nucleotide synthesis, which seems to be maintained via transketolase and transaldolase reactions despite the oxPPP inhibition. One may speculate that the salvage pathway is involved, as suggested by the upregulation of the rate-limiting enzyme NAMPT upon VIC activation, in NAD synthesis, and that STAT1 may be involved in the transcription of NAMPT. However, more experiments analyzing specific enzymes or intermediates of non-oxidative PPP would be required for confirming these hypotheses.

D.5- TLR4-IFNGR interplay promotes oxidative stress with a role in inflammatory-induced differentiation, calcification, and inflammation in VIC

An important finding of this study is that the inflammation-induced redox imbalance caused by the increase of ROS and the alterations of NAD^+/NADH, $NADP^+$/NADPH and GSSG/GSH ratios generates oxidative stress, subsequently promoting HIF-1α stabilization, inflammation, differentiation, and calcification of VIC.

D.5.1- Inflammation-induced ROS production and redox disequilibrium

This study has demonstrated an inflammatory-induced ROS production, despite the upregulation of SOD2 antioxidant, and further showed a direct association of ROS, using H_2O_2, with glycolytic rewiring in VIC.

Our findings are consistent with previous reports supporting the importance of ROS in valve sclerosis, by the induction of DNA damage (Branchetti et al., 2013). Additionally, Branchetti et al. (2013) described the downregulation of antioxidant enzymes such as SOD2 in stenotic valves when comparing with control ones. Their study also elucidated that H_2O_2 treatment of VIC, directly induces DNA damage and further histone H2AX phosphorylation and its subsequent accumulation in the nuclei, thus leading to the transcription of differentiation factors such as *RUNX2*. This study was consistent with a previous one describing a direct role of H_2O_2 on CAVD (Miller et al., 2008). In fact, H_2O_2 was found close to calcified regions, in valve cusps at the initial stages of CAVD due the dysregulation of antioxidant mechanisms (Miller et al., 2008). In another study of diseased valves, it has been demonstrated that inflammation triggers an uncoupling between nitric oxide synthase and the nitric oxide scavenger thus leading to a reduction in catalase activity and higher levels of H_2O_2, which directly induced osteogenic genes (Byon et al., 2008). Additionally, in the context of cancer cells, H_2O_2 has been reported to exert a role in glycolytic reprogramming, due to the damage of OXPHOS (Molavian et al., 2016). However, the fact that the antioxidant enzyme SOD2 is upregulated upon VIC stimulation is not consistent with previous reports. Thus, one may speculate that upon inflammatory stimulation, cells are attempting to counteract oxidative stress caused by O_2^- by generating H_2O_2 via SOD2. H_2O_2 may not be eliminated probably due to catalase dysfunction. However, more experiments studying catalase activity would be required for confirming this theory.

This study elucidates an imbalance in redox state by alterations in the NAD^+/NADH and the increase in $NADP^+$/NADPH and GSSG/GSH ratios in VIC in response to inflammatory activation as a mechanism underlying ROS production. Previous reports have described that the alteration of NAD^+/NADH ratios are due to the action of glycolytic and TCA enzymes, which are known to require NAD^+ as a cofactor for electron transfer, thus generating NADH (reviewed in Bradshaw et al., 2019). The maintenance of NAD^+/NADH ratio plays a role in inhibiting mitochondrial ROS production since NADH acts as a redox hinge directing electrons to OXPHOS and to antioxidant systems through transhydrogenase via NADPH (reviewed in Bajic et al., 2019). In fact, in models of old mice the decline in NAD^+ levels in skeletal muscle correlates with compromised

mitochondrial function, decreased expression of mitochondrial respiratory units, and promotes an imbalance in mitochondrial ATP production (Gomes et al., 2013). Interestingly, we found similar changes in activated VIC. Additionally, lactate, whose secretion is upregulated in VIC, can also contribute to the changes in NAD^+/NADH ratios, like reported in T lymphocytes where lactate was found to limit lymphocyte proliferation by altering the NAD^+/NADH redox state (Iii et al., 2020). Additionally, in dendritic cells, a recent work has determined that lactate promotes the decrease of NAD^+ in favor of NADH production (reviewed in Navarro et al., 2021). In the context of macrophages, LPS has been demonstrated to decrease NAD^+ levels as a consequence of the induction of ROS, which induce DNA damage, thus leading to the activation of NAD^+-dependent enzymes. Moreover, the decrease in NAD^+ is generally accompanied by an increase in NAMPT, the rate limiting enzyme of the synthesis of NAD^+ through the salvage pathway (reviewed in Navarro et al., 2021).

Beyond the role of the NAD^+/NADH in metabolism and ROS production, ratios are also important in the function of other enzymes such as CD37 and sirtuins (SIRT), which are NAD^+-dependent for its activity. CD37 deficit has been associated with calcification progress in CAVD (reviewed in Audrito et al., 2020). Additionally, sirtuins are deacetylases distributed in the nucleus (SIRT1, SIRT6, and SIRT7), cytoplasm (SIRT2), and mitochondria (SIRT3-5). Sirtuins can modulate the cell adaptation to the energy state through controlling the acetylation or deacetylation of genetic material (Chalkiadaki et al., 2015). Thus, low levels of NAD^+ inhibit sirtuin activity and, therefore, histone deacetylation, later promoting the initiation and progression of calcification, inflammation and osteogenic differentiation in VIC, as previous studies have shown (Fu et al., 2019 & Song et al., 2017). In fact, in another study of old mouse skeletal muscle, the decrease in NAD^+ levels concurred with a decrease in SIRT1 activity, and these events were associated with an increase in HIF-1α and defective mitochondrial ATP synthesis (Gomes et al., 2013).

Based on these evidence and our data, one may speculate that NAD^+/NADH ratio alterations could be due to a possible damage in mitochondrial respiration complexes that are not able to oxidize all the generated NADH to NAD^+ and/or to mitochondrial shuttles alteration. Additionally, some glycolytic enzymes may not be able to oxidize all NADH when excessive amounts of NADH are generated by catabolic routes. Furthermore, one may speculate that alterations in NAD^+/NADH ratios could be affecting ROS production. Finally, an alternative hypothesis is that the alteration of NAD^+/NADH ratios may have a role in initiation and progression of calcification due to its role in sirtuins activity. However, more experiments would be required to confirm our hypothesis.

Our data unveils increased $NADP^+$/NADPH ratio in VIC upon immune stimulation due to a decrease in NADPH linked to an increased GSSG/GSH ratio and GSSG levels. As discussed before (D.4), this decrease in NADPH production linked to the increase of GSSG is mainly due to the inhibition of the oxPPP. However, other sources of NADPH have been described, such as malic enzyme 1, an enzyme of the non-canonical TCA.

Additionally, the interconnection of NADH and NADPH by directing electrons from NADH to NADPH is important for mitochondria to control ROS emission through the GSSG/GSH redox system (Aon et al., 2012). Interestingly, the balance of GSSG/GSH represents the main redox buffer in cells, and under healthy conditions, GSH is the predominant form (reviewed in Schafer et al., 2001). Many studies have linked an imbalance in this ratio to the development of cardiovascular diseases, not only due to the generation of oxidative stress, but also of protein glutathionylation (reviewed in Narasimhan et al., 2015). In fact, patients with atherosclerosis show increased levels of serum glutathionylated proteins that can later induce apoptosis (Nonaka et al., 2007).

Together, data unveil that ROS may be both the cause and the consequence of inflammatory-triggered metabolic reprogramming in VIC. While ROS are partially generated through the redox disequilibrium generated upon metabolic rewiring induction, they also seem to exert a role in glycolytic reprogramming, through the accumulation of H_2O_2.

D.5.2- Inflammation-induced oxidative stress and its effect on VIC inflammation, differentiation, and calcification

Increasing evidence highlights the role of ROS in cardiovascular diseases, particularly in the initiation and propagation of the CAVD (reviewed in Greenberg et al., 2022). Our findings associate Inflammation-mediated increase in ROS production and oxidative stress with VIC differentiation and calcification, based on pharmacological approaches.

D.5.2.1- The role of ROS an oxidative stress in VIC calcification

Data obtained through our work showing a direct effect of oxidative stress on VIC calcification are supported by previous reports elucidating that high levels of ROS and oxidative stress play a significant role in the initiation and development of vascular and valvular calcification (reviewed in Qiao, 2022; Xue et al., 2017). Moreover, in porcine VIC, inflammatory cytokines such as TGF-β1 are found to induce the production of ROS, which directly contributes to calcium nodule formation via the MAPK cascade and MEK1/2/ERK1/2 pathways (Das et al., 2013). The mechanism of ROS action in calcification is not well understood, but recent studies highlight their role on: (i) Activation of apoptosis, which can occur via endoplasmic reticulum stress-dependent or other pathways (reviewed in Redza-Dutordoir et al., 2016). (ii) Activation of the NLRP3 inflammasome, which can subsequently induce apoptosis (Xu et al., 2020). (iii) Activation of oxidative stress-mediated autophagy, which ultimately leads to vascular calcification (reviewed in Lee et al., 2020).

Together, data and evidence do not allow us to elucidate the exact mechanism by which ROS are inducing calcification in VIC, but one may hypothesize that it is related to the glycolytic rewiring induced by ROS, previously shown to be necessary for apoptosis and calcification.

D.5.2.2- The role of ROS and oxidative stress in VIC differentiation

Our findings unveil a potential association between oxidative stress and VIC differentiation, as shown by pharmacological approaches targeting oxidative stress generation. These data agree with the previous description of a direct relation between ROS, DNA-damage response and cellular transdifferentiation, which is reversible by antioxidant enzymes (Branchetti et al., 2013). Additionally, VSMC differentiation into osteoblast-like cells has been described to be due to ROS-induction of osteoinductive signals that may be regulated by Gas6/Axl pathway or AMP-activated protein kinase (AMPK) (reviewed in Lee et al., 2020). Additionally, ROS has been linked to epigenetic phenomena, including altered microRNA levels, DNA methylation, and histone modifications that are also linked to osteogenic gene expression (reviewed in Lee et al., 2020). In addition to the already explained role of histone modification in CAVD (Fu et al., 2019 and Song et al., 2017), DNA methylation has been also associated with VIC calcification (Zhou et al., 2019). Moreover, other cellular phenomena that affect ROS-mediated osteoinductive intracellular signaling, include autophagy, ER stress, and mitochondrial dysfunction (reviewed in Lee et al., 2020). Finally, conversely to our data, other mechanisms related to osteoblastic VIC differentiation has been the reduction in antioxidant enzyme levels markers in human VIC (Xue et al., 2017).

Taken together, data highlight the association between oxidative stress and VIC differentiation. Regarding the mechanism, one may hypothesize that oxidative stress could be activating VIC differentiation through different signaling pathways: ER-stress, MAPK, histone modifications, autophagy, and mitochondrial dysfunction, but more experiments would be required to identify the exact mechanisms. Additionally, the fact that we found an increase in SOD2 concurrent with VIC differentiation could be explained as in section D.5.1.

D.5.2.3- The role of inflammatory-induced oxidative stress in HIF-1α stabilization in VIC

Our data unravels the direct role of the inflammation-triggered oxidative stress on HIF-1α stabilization, which could be later important for further inducing glycolytic reprogramming. These findings agree with previous reports demonstrating a direct relationship between ROS and HIF-1α stabilization, which leads to glycolytic reprogramming in human umbilical vein endothelial and microvascular endothelial cells (Paik et al., 2017). In this work, they demonstrate that human endothelial cells under hypoxic conditions, directly stabilize HIF-1α through the ROS-activated protein-C-kinase pathway. A recent report has also demonstrated a direct role of lactate-induced ROS in HIF-1α stabilization and its subsequent role in osteoblast-like differentiation through a glycolytic reprogramming mediated by PDC in fibroblasts (Kozlov et al., 2020).

Together, all data from section D.5.2 based on antioxidant NAC pharmacological approaches, demonstrate the role of ROS and oxidative stress in the response of VIC to inflammatory activation,

particularly in the induction and maintenance of HIF-1α stabilization, which subsequently leads to the activation of the glycolytic reprogramming necessary for the inflammation-induced VIC calcification, inflammation, and differentiation. One may speculate that both the increase in glycolysis and lactate production, as well as the inhibition of the oxPPP and the uncoupling of ETC and OXPHOS, contribute to the direct alteration of redox homeostasis and the production of ROS.

D.6- TLR3/4-IFNGR interplay in TCA dysregulation and its role in inflammatory-induced differentiation, calcification, and inflammation in VIC

Main findings of this research related to the status of TCA cycle upon VIC inflammatory stimulation elucidate the downregulation of *PDK4*, a negative regulator of TCA and the increase of cytosolic ACLY, the enzyme generating acetyl-CoA in the cytosol. Notably, *PDK4* downregulation has been validated in valve tissue from stenotic patients. Based on pharmacological approaches, the study elucidates a role of mitochondrial pyruvate on inflammation-induced VIC calcification, as well as the relevance of *PDK4* downregulation on VIC differentiation, inflammation, and calcification pathways. Additionally, data also unravel the importance of TCA metabolites on VIC differentiation.

D.6.1-The role of inflammatory environment in TCA unbalance

A remarkable finding of this study is that there is an increase in the readily glucose flux into acetyl-CoA and, low but consistent, into citrate, and succinate but not OAA upon inflammatory-stimulation of VIC. Consistent with this increase, the expression of the negative regulator of TCA entrance, *PDK4*, is downregulated upon stimulation, thus suggesting an increased activity of PDH and conversion of pyruvate into acetyl-CoA. Additionally, the co-stimulation of VIC with LPS and IFN-γ induces the activation of ACLY, which catalyzes the production of cytosolic acetyl-CoA.

The role of TCA metabolite production and accumulation in disease have been reported in context such as cancer (reviewed in Beyoğlu et al., 2021), or immune cells (reviewed in Martínez-Reyes et al., 2020) for biosynthetic purposes, as signaling molecules with functions controlling chromatin modifications, DNA methylation, the hypoxic response, and immunity. In fact, in immune cells, several different possible TCA alterations have been described upon inflammatory (reviewed in Pearce et al., 2013): (i) in activated neutrophils or M1 macrophages stimulated with TLR agonists, a Warburg reprogramming through glycolysis induction is the strongest response, with most of the pyruvate going to lactate. In this environment, TCA is decreased leading to an inhibited OXPHOS, but maintenance of mitochondrial potential to maintain cell survival. (ii) In activated T cells both OXPHOS and glycolysis are triggered. Although most pyruvate is excreted as lactate, some is entering TCA. Additionally, glutaminolysis is also participating in maintaining TCA and OXPHOS.

DISCUSSION

In line with our findings, recent evidence supports the notion of an “alternative” TCA participating in cell differentiation (Arnold et al., 2022). Through this study, they performed experiments in totally differentiated cells as well as in more dedifferentiated cells. In fact, when comparing not fully differentiated cells, such as myoblasts, with differentiated myotubes, they found that myoblasts rely the more on the non-canonical pathway. Among this non-canonical TCA, citrate derived from the mitochondria is quickly exported to the cytoplasm, where it is metabolized by ACLY to cytoplasmic acetyl-CoA and OAA, which can re-enter mitochondria to complete the cycle. Through this reaction, citrate (M+2) is metabolized into labeled acetyl-CoA (M+2) while unlabeled OAA. They also consider that low levels of M+2 TCA intermediates downstream of citrate can reflect the degree to which cells engage the transport of citrate to the cytosol (Arnold et al., 2022). Therefore, considering this study, one may speculate that inflammatory stimulation of VIC leads to an altered TCA. The low increase in M+2 citrate found in fluxomics analysis could be due to its rapid conversion into cytosolic acetyl-CoA by ACLY. Thus, the exit of acetyl-CoA to cytoplasm could explain, at least in part, why low [U-^{13}C]-glucose flux is detected in subsequent TCA metabolites. Additionally based on the study of Arnold et al., 2022 we speculate that although part of citrate is rapidly transported to cytosol, a small amount of citrate enters the TCA and produces a low rise of M+2 succinate. Moreover, the fact that glucose tracing reveals an increased incorporation of [U-^{13}C]-glucose into GSSG in activated VIC, indirectly demonstrates that TCA is active for feeding cells requirements, since α-ketoglutarate is the precursor of GSSG. Finally, the lack of increase in M+2 OAA upon VIC stimulation could be explained by the fact that the OAA liberated upon ACLY activity is non-labeled and [U-^{13}C] succinate is accumulating without being metabolized into OAA.

Additionally, our study points to the generation of cytosolic acetyl-CoA as a potential event participating in disease. Acetyl-CoA has been reported as a critical substrate for *de novo* synthesis of fatty acids and sterols and could be used for lipid synthesis, a reaction that requires NADPH. Moreover, acetyl-CoA can donate an acetyl group for histone acetylation, which is known to contribute to chromatin relaxation that facilitates gene transcription. In fact, acetyl-CoA levels control the activity of histone acetyltransferases and histone deacetylase. In this line, recent evidence highlights the link between the reduction of histone deacetylase 6 and VIC calcification (Fu et al., 2019). Thus, we speculate that once acetyl-CoA is in the cytoplasm, it may be used by VIC for histone acetylation or for FA and lipid synthesis that could later be accumulated and favor valve calcification (reviewed in Nsaibia et al., 2022).

In conclusion, further analysis of the citrate-malate shuttle, which transports citrate to the cytosol and back to mitochondria the malate generated upon citrate conversion into OAA and, later, into malate, as well as study of histone acetylation, and lipid synthesis anabolic pathways would be required to confirm our hypothesis.

D.6.2- The role of inflammatory-stimuli-induced TCA alterations on VIC inflammation, differentiation, and calcification

Based on pharmacological approaches blocking mitochondrial pyruvate carrier (MPC1), the study unravels the importance of pyruvate entrance to mitochondria on inflammation-induced VIC calcification. Moreover, the pharmacological inhibition of PDK4 demonstrates its role on VIC differentiation, inflammation, and calcification pathways. Additionally, this thesis elucidates the importance of TCA metabolite accumulation on HIF-1α stabilization, and VIC differentiation.

To discuss our findings is important to note that there is an important connection between pyruvate entrance to mitochondria, PDK4 downregulation, PDH activation and pyruvate transformation into acetyl-CoA, thus PDK4 is considered the main regulator of metabolic reprogramming. Additionally, it is important to note that in VSMC, PDK4 isoform has been the only one found to be regulated and to control PDC phosphorylation (reviewed in Ma et al., 2020). However, there are several controversial publications related to this topic. On the one hand, in the same line as our results, mitochondrial pyruvate has been associated with β-glycerophosphate-induced VSMC differentiation (Alesutan et al., 2020). Additionally, Xiao et al., 2021 described a direct role of TNF-α and LPS in inhibiting *PDK4* expression in endothelial cells, thus leading to a direct increase in OXPHOS and the subsequent protection against inflammation and EndMT transition. This is not exactly the mechanism occurring in VIC, since PDK4 inhibition in VIC does not lead to an increase in OXPHOS nor inhibition of inflammation. However, oppositely to our results and Xiao et al., 2021, in VSMC, the induction of PDK4 leading to PDH and acetyl-CoA inhibition, has been described to play a direct role in VSMC osteogenesis and calcification via glycolysis induction and OXPHOS inhibition (reviewed in Ma et al., 2020). In line with this evidence, in TGF-β-mediated myofibroblast differentiation and fibrosis induction, the most important isoform participating in metabolic rewiring is PDK1, which is upregulated upon treatment and its inhibition leads to fibrosis blockade (reviewed in Hamanaka et al., 2021). These findings disagree with the findings of this thesis, since in VIC the pharmacological inhibition of PDK4 leading to PDH activation and acetyl-CoA production, leads to pathological processes such as VIC differentiation and inflammation.

Therefore, according to the fact that pyruvate entrance and TCA inhibition leads to abolishing pathological calcification in VIC, our data from pharmacologically induction of TCA via inhibiting PDK4 shows an increase of VIC differentiation and inflammation. The possible explanation for the differences between VSMC and VIC behavior could be due to the fact that VSMC is going through a metabolic reprogramming that differs in terms of mitochondrial metabolism from the rewiring undergone by VIC. Additionally, another important factor to consider is that PDK4 is not only regulated transcriptionally, but also by protein modifications such as phosphorylation (reviewed in Ma et al., 2020).

As previously mentioned, our findings highlight the role of succinate accumulation on inflammation-mediated stabilization of HIF-1α, and VIC differentiation. These data are based on fluxomics experiments

revealing an increased incorporation of [U-^{13}C]-glucose into succinate, but not in OAA. Additionally, these findings are supported by pharmacological approaches mimicking succinate accumulation, and extracellular succinate and citrate treatment of VIC.

Our findings are consistent with several reports. In the context of macrophage polarization, it has been described a metabolic rewiring going through an increase in glycolysis reliance for energy production accompanied by a decrease in ATP synthesis through OXPHOS maintaining the flow of TCA metabolites with succinate being a key metabolite. In this context through the action of complex II of ETC (SDH), succinate is metabolized to fumarate, generating $FADH_2$ that donates electrons to the ETC, subsequently leading to reverse electron transport from complex II towards complex I. This process promotes an increase in ROS production and, consequently, a decrease in ATP production through OXPHOS (Mills et al., 2016). Although this model fits with the metabolic rewiring found in VIC upon inflammatory stimulation: increased glycolysis, active TCA, and defective OXPHOS, the evidence supporting the idea of succinate accumulation, the potential possible alteration of complex II discussed in D.7.1, lead us to think that this may not be the mechanisms in activated VIC. Additionally, succinate accumulation upon VIC activation, even non-transcriptional alteration of SDHA or B, could be due to the fact that other isoforms are participating, or the regulation occurs at the protein level. In this line, the maintenance of an altered TCA cycle downstream acetyl-CoA has been described to later lead to an abnormal electron flux through ETC generating more ROS and a maintenance of mitochondrial oxygen consumption while decreasing OXPHOS ATP as reviewed in cancer cells (Shiratori et al., 2019).

Supporting the idea of the role of TCA metabolites in HIF-1α stabilization, VIC differentiation, and disease progression, several reports have associated the accumulation of TCA metabolites with neurometabolic disorders and tumors (reviewed in Kang et al., 2021). In fact, in some disease models the regulation of TCA cycle has been described to be inhibited by pathological NADH levels (reviewed in Martínez-Reyes et al., 2020), and this situation could be occurring in VIC. Additionally, in macrophages, succinate acts as an inflammatory signal reported to induce IL-1β through HIF-1α stabilization (Tannahill et al., 2013). Furthermore, succinate as well as fumarate, have been described to inhibit histone demethylation, as well as promote histone succinylation thus promoting the transcription or repression of different genes leading to the altered expression of genes participating in cell differentiation (reviewed in Kang et al., 2021). In addition to the role of intracellular succinate accumulation, it can be secreted and function as extracellular signal, which has been associated with epithelial damage, macrophage activation, and fibroblast transdifferentiation via SUCNR-1-mediated signaling pathways (reviewed in K. Wu et al., 2023).

To sum up, VIC exposed to an inflammatory environment exhibits an altered TCA cycle, which later exerts a role in processes underlying CAVD pathogenesis, probably via HIF-1αinduced metabolic reprogramming.

D.7- TLR3/4- IFNGR interplay in mitochondrial metabolism impairment and its role in VIC inflammation, differentiation, and calcification

Mitochondrial metabolism is an important source of ATP in VIC in the basal state, but it is decreased by inflammatory stimuli. Our findings elucidate the alteration of the ETC as well as OXPHOS upon inflammatory-stimulation, in a JAK-STAT/HIF-1α dependent manner and point to a potential role of mitochondrial respiration in protecting VIC against calcification. Additionally, these findings correlate with data in qVIC, and VIC explanted from stenotic valves as compared to controls.

It is important to note that in addition to generating ATP, mitochondria is involved in several process that have also been associated with CAVD disease, such as calcium caption, ROS generation, and apoptotic cell death induction (reviewed in Redza-Dutordoir et al., 2016).Therefore, an altered mitochondrial function could be the responsible for VIC pathological processes. Additionally, our findings agree with different metabolic reprogramming reported. First, the Warburg effect was originally described as a consequence of mitochondrial damage (Warburg et al., 1926). However, recent evidence has demonstrated that not only defective OXPHOS can occur during aerobic glycolysis (reviewed in Vaupel et al., 2019), but also an increase in OXPHOS has been described in many contexts during metabolic reprogramming.

D.7.1-Inflammatory-induced alterations in mitochondrial respiratory complexes and its role in VIC mitochondrial oxygen consumption

This thesis highlights the TLR-IFNGR interplay in the reduction of mitochondrial maximal respiration in VIC and differential responses depending on the pathogen pattern, Poly (I:C)+IFN-γ or LPS+IFN-γ, while no alteration in basal respiration. Several pieces of evidence support the fact that maximal respiration can be affected without changes in basal respiration, and different regulatory mechanisms of basal and maximal respiration have been elucidated (Dranka et al., 2010 & Pfleger et al., 2015). Notably, oxidative stress has been associated with maximal respiration alterations while no basal respiration changes: low levels of ROS have minimal impact on basal respiration, but they have a significant impact on maximal respiratory capacity, as a result of protein modifications like S-thiolation in the ETC (Dranka et al., 2010). Finally, other factors involved in the regulation of basal mitochondrial respiration include mitochondrial homeostasis, represented by the mitochondrial biogenesis marker, PGC-1α (Vazquez et al., 2013), which is not altered in VIC upon inflammatory stimulation.

Inflammatory stimuli reduce the maximal respiratory capacity and, in parallel, ATP production from OXPHOS in VIC. The maximal respiratory capacity is the mitochondrial capacity to fulfill energy demands that exceed the basal level in response to cellular stress, to avoid a crisis in ATP synthesis. This parameter

determines the health status of the mitochondria, and low levels of maximal respiration have been associated with pathological conditions, particularly cardiovascular diseases (reviewed in Hill et al., 2012). It has been described that decreased maximal respiration may correspond to mitochondrial dysfunction, not detectable under basal conditions, but evident when the respiratory ratio approaches its upper limit (reviewed in Li et al., 2020). Maximal respiratory capacity can be influenced by several factors: (i) the availability of nutrients that fuel the TCA cycle or fatty acid oxidation, (ii) the activity of respiratory chain components, and (iii) the proper assembly of ETC components (Carbognin et al., 2016). Additionally, a decrease in maximal respiration has been associated with all ETC complexes.

This thesis elucidates a potential role of complex I in maximal respiration abrogation. Data demonstrates that the % dependence of oxygen consumption on complex I/III is reduced by co-stimulation with LPS + IFN-γ. This finding is supported by our data showing a decrease in the NAD^+/NADH upon stimulation since it is well known that complex I is the first catalyzing the oxidation of NADH. Additionally, it is important to note that tetrameric PKM2, the isoform discussed in D.3.3, has been described to directly inhibit the function of complex I and III (reviewed in Pucket et al., 2021). Our speculations agree with previous reports demonstrating that overexpression of Complex I is responsible for supporting elevated levels of maximal respiration in mouse embryonic stem cells (Carbognin et al., 2016). Additionally, B. Fu et al. (2022) have recently described in a proteomics and metabolomics-based assay the higher accumulation of rotenone metabolite in aortic valve tissue from CAVD patients in comparison with control ones, thus suggesting a potential inhibition of complex I during disease. Therefore, one may hypothesize the possible functional or structural alteration of complex I upon stimulation. However, we must consider that rotenone alone does not affect inflammatory-induced differentiation, calcification, or inflammation in VIC, thus suggesting that complex I alone may not account for the induction pathological processes of CAVD in VIC.

Considering data of succinate accumulation and its role in cell differentiation discussed in section D.6.2, this thesis unveils a potential altered function of complex II (SDH) upon inflammatory activation of VIC. Complex II has been described in cardiomyocytes as the main source of the reserve respiratory capacity that is regulated by metabolic sensors (Pfleger et al., 2015). In fact, the direct inhibition of the SDHA (complex II) abrogates maximal respiratory capacity without affecting basal respiration (Pfleger et al., 2015). Based on this evidence and our findings we speculate that the reason why complex I basal inhibition with rotenone-only does not have harmful effects on VIC could be explained since complex II is still functionally active. Additionally, considering the results of succinate accumulation, we speculate that the impaired function of complex II upon inflammatory activation of VIC could account for the decrease in maximal respiratory capacity.

According to our findings, reduction in the % dependence of oxygen consumption on complex I/III points to complex III as a potential responsible for inflammatory stimuli-induced reduction of maximal

respiration. In fact, previous publication also associated a defective complex III with maximal respiration abrogation in leukemia cells (Sriskanthadevan et al., 2016). However, we did not study complex III and its effect independently, thus further experiments using a specific inhibitor of this complex would be necessary.

This thesis unveils that complex IV, responsible for transferring electrons to O_2 and maintaining basal OCR, is not altered upon stimulation although a decrease in expression of cytochrome C oxidase (*COX7A1*, complex IV). Supporting this finding, previous studies have demonstrated that not only transcription alterations of complex IV but also enzymatic, can also lead to a decrease in maximal respiration in cardiomyocytes under stress conditions (J. Chen et al., 2001). One may speculate that in our VIC model, complex IV is not damaged since it is the terminal complex of the mitochondrial respiratory chain, responsible for about 90% of oxygen consumption in mammals (reviewed in Brown., 2001). However, more experiments would be required for confirming our hypothesis.

Therefore, data and evidence together allow us to conclude that maximal respiratory capacity depends on multiple mitochondrial parameters, and it is not possible to identify a single regulatory mechanism, which can be different depending on the cell type. However, taking data obtained in VIC into account, one may speculate that complex I and II are damaged upon immune stimulation leading to a decrease in maximal respiratory capacity without affecting basal oxygen consumption, relying on the most in complex IV. In fact, the transcription factor PGC-1α controlling mitochondrial biogenesis is not altered in activated VIC, supporting the idea of a basal OCR maintenance. However, to clearly elucidate the participation of each complex, I would perform more experiments of oxygen consumption reliance on each complex in an independent way.

D.7.2- The protective role of mitochondrial respiration in VIC calcification

A remarkable finding of this work is the role of mitochondrial respiratory capacity in protecting VIC against the inflammatory-induced responses leading to VIC differentiation, inflammation, and *in vitro* calcification.

According to our highlight, several reports have associated mitochondrial respiration with disease specifically with cardiovascular calcification (reviewed in Qiao et al., 2022). Three models have been proposed for the association of mitochondria with calcification: (i) decrease of mitochondrial function by mineral overload in mitochondria such as calcium and phosphate, which leads to apoptosis and calcification, (ii) increase of ROS production, previously associated also with VIC apoptosis and calcification in porcine VIC (reviewed in Qiao et al., 2022), and (iii) decrease in NAD^+/NADH ratios leading to defective histone deacetylation and complex II dysfunction (Finley et al., 2011). The latter is relevant to VIC, since the lack of histone deacetylation has been related to VIC calcification (Fu et al., 2019 & Song et al., 2017). Additionally, SIRT3, dependent of NAD^+, has been described to directly control the deacetylation of SDHA at lysine 13,

resulting in increased enzymatic activity (Finley et al., 2011), thus low levels of NAD^+ would result in a decrease of SIRT3 activity and SDHA function.

Beyond the role of mitochondrial dysfunction in disease, it has also been reported the protective role of mitochondrial respiration. The exposure of neurons to FCCP, a mitochondrial uncoupler forcing mitochondrial respiration, reduces the membrane potential and inhibits mitochondrial calcium uptake, thereby preventing cell death induced by excessive calcium accumulation (Nicholls et al., 2000). Additionally, increased membrane potential has been associated with ROS levels and apoptosis. In the context of immune cells, the inhibition of mitochondrial membrane potential with and uncoupler agent significantly inhibits ROS production, thus inhibiting apoptosis (reviewed in Mills et al., 2026). Finally, a recent study by Xiao et al., (2021) has postulated the protective role of mitochondrial respiration and OXPHOS on immune-induced inflammation and the subsequent EndMT of endothelial vascular cells.

Collectively, our data suggest that the impairment of mitochondrial respiration upon VIC immune stimulation is leading to processes such as inflammation, differentiation, and calcification. One may speculate that several mechanisms participate in mitochondrial-induced calcification, such as ROS accumulation, mineral mitochondrial overload, and NAD^+/NADH ratios alteration. Thus, one may think that upregulating mitochondrial respiration through pharmacological approaches may prevent the inflammation-triggered pathological processes in VIC. In this context, it is important to highlight the importance of optimal FCCP dose that leads to uncontrolled respiration without inducing early cell death, since an excess of FCCP could exert the opposite effect inducing ROS-dependent cell death (reviewed in Kunz, 2003). Our hypothesis is further supported by comparing metabolic data of qVIC and VIC: mitochondrial respiration contributes to maintaining the metabolic phenotype of qVIC while changes in the environment will alter mitochondrial respiration and cell differentiation.

D.7.3-Inflammation-induced impairment of proton leak, coupling efficiency and mitochondrial ATP and its role in VIC calcification, inflammation, and differentiation

A relevant finding of this thesis is the decrease in the coupling efficiency between ETC and OXPHOS resulting in reduced production of mitochondrial ATP in VIC exposed to LPS + IFN-γ. In fact, the reduction in mitochondrial ATP synthesis directly induces calcification and potentiates the inflammatory stimuli-induced differentiation and inflammation in VIC.

Through the years, coupling efficiency has been described as the ability of coupling the proton-motive forces generated through ETC and OXPHOS for ATP synthesis. Decoupling has been described to occur when protons leak back from the intermembrane space to the mitochondrial matrix, thus reducing the mitochondrial membrane potential and causing uncoupling between ETC and OXPHOS-ATP synthesis (reviewed in Nanayakkara et al., 2019). Several factors have been described as responsible for decoupling. The excess of substrate oxidation and imbalance in NAD^+/NADH ratios can exceed the capacity of complex IV

to transfer electrons to molecular oxygen, thus leading to premature electron leakage, the production of mitochondrial ROS, and the impairment in mitochondrial ATP synthesis (reviewed in Vercellino et al., 2022). Notably, in some contexts, the inhibition of ATP synthase has been associated with a phenomenon called mitohormesis, which is an induced mechanism to compensate for the defect in ATP synthesis by OXPHOS, via AMPK and NF-κB by inducing glycolytic metabolism (reviewed in García-Aguilar et al., 2018). This phenomenon had been previously reported in Bernard et al. (2015) in lung fibroblasts, who demonstrated that blocking ATP synthase, directly induced glycolysis.

Therefore, our hypothesis is a role of inflammatory environment in decoupling ETC and OXPHOS in VIC due to the accumulation of NADH and the collapse of mitochondrial complexes leading to proton leak and the loss of proton-motive gradient resulting in the inhibition of mitochondrial ATP synthesis. Based on reported evidence of the compensatory mechanism called mitohormesis, we propose a protective role of mitochondrial ATP synthesis against the glycolysis-mediated immune-induced HIF-1α, calcification, inflammation, and differentiation of VIC. This potential protective role is further supported by the fact that qVIC exhibit a higher mitochondrial ATP synthesis than VIC.

D.7.4- Different interplay between TLR4 and TL3 and IFNGR in maximal mitochondrial respiration and coupling efficiency in VIC

We found similar effects of TL3/4-IFNGR interplay on the metabolic shift in VIC but striking differential response of VIC in maximal respiration and coupling efficiency upon IFNGR and TLR3 or TLR4 activation. While LPS + IFN-γ decrease maximal respiration and coupling efficiency, Poly (I:C) + IFN-γ do not affect any of those mitochondrial parameters, which is consistent with the fact that Poly (I:C)+IFN-γ stimulation does not affect the % dependence of oxygen consumption on complex I/III while LPS + IFN-γ does.

Conversely, previous reports have demonstrated the role of TLR3 signaling in inducing mitochondrial dysfunction through the decrease in maximal respiration in human hepatocytes (Djafarzadeh et al., 2011), although cells were not co-stimulated with IFN. Oppositely, previous evidence supports the idea of different effects of TLR4 and TLR3 due to their signaling pathways. In fact, metabolic effects have been found to be different upon TLR4 or TLR3 monocyte stimulation (Lachmandas et al., 2017). In this work they show that Poly (I:C) increases the oxidative capacity of monocytes while LPS decreases OXPHOS. They suggest that since TLR4 signals through both TRIF and MyD88 signaling pathways while TLR3 exclusively through TRIF, it is unlikely that LPS is contributing to OXPHOS decrease via TRIF but through MyD88. Therefore, distinct roles of TLR ligands may depend on the time exposure, concentration, the way of treatment delivery, and cell type (Kurte et al., 2020). Considering our data, previous reports do not agree at all with our statements, since in VIC model, Poly (I:C) + IFN-γ stimulation is not having any effect, increase nor decrease, different from the context of monocytes. This could be explained by the participation of IFNGR/JAK-STAT signaling in combination with TLR3-TRIF.

To note, *HIF1A* silencing shows that the decrease in maximal respiration upon LPS + IFN-γ directly depends on HIF-1α stabilization in VIC. However, HIF-1α has been described to reach similar levels of non-hypoxic immune stabilization via JAK-STAT upon Poly (I:C) + IFN-γ and LPS + IFN-γ treatments of VIC, leading to calcification, differentiation, and inflammation (Parra-Izquierdo et al., 2019; 2021). Taking this into account, a feasible hypothesis could be that the co-stimulation of TLR3 and IFNGR, either via TRIF-dependent pathway or other routes, could lead to the activation of some factors regulating maximal respiration. A deeper study of mitochondrial function status would be necessary to elucidate the exact differential mechanism between TLR3 and TLR4 stimulation in maximal respiration and coupling efficiency.

D.8-The potential interplay between metabolic rewiring, mitochondrial damage, and apoptosis upon inflammatory stimulation of VIC

A new finding of this study is that inflammatory stimulation induces apoptosis through intrinsic and extrinsic pathways in a HIF-1α dependent way, as suggested by the HIF-1α-dependent expression of the apoptotic gene *BNIP3*. Both pathways lead to mitochondrial caspase-3 mediated apoptosis in VIC.

A link between metabolism, mitochondria, and apoptosis has been reported in cancer cells. Besides the production of ATP, mitochondria participate in buffering cellular calcium, generation of ROS, and apoptotic cell death initiation (reviewed in A. Li et al., 2022). Interestingly, factors related to intrinsic apoptotic pathway, such as BNIP3, BAX, or BAK, have been previously implicated in inducing cell death under conditions of anoxia due to defects in mitochondrial respiration (reviewed in Yin et al., 2021). In fact, HIF-1α has been demonstrated to inhibit anti-apoptotic proteins such as Bcl2 while increasing Bax, Fas/CD95, Bnip3 and activating caspases-3/8 and-9 in human uterosacral ligament fibroblast (Greijer et al., 2004). In contrast, several studies have demonstrated a protective role of HIF-1α-BNIP3 pathway against lactate-induced valvular calcification (Zhu et al., 2020), renal ischemia (Zong-jie Fu et al., 2020), myocardial ischemia-reperfusion injury and renal fibrosis (J. Li et al., 2023) by inducing mitophagy and ROS inhibition.

This thesis also discloses that p53 expression in VIC upon TLR3 ligand exposition is time-dependent: it is increased in short periods and decreased upon longer expositions. Along the literature, p53 is recognized as a key regulator of apoptosis. Interestingly, several and controversial connections have been established between p53 and cellular metabolism, indicating that p53 can directly respond to the metabolic state of the cell to induce cell death (Bensaad et al., 2006). For example, the synthesis of cytochrome C oxidase 2, which is required for the assembly of the respiratory chain complex IV, is dependent on p53. Cells with impaired p53 signaling show decreased mitochondrial oxygen consumption and compensatory increase in glycolysis rates (Matoba et al., 2006). Beyond that, p53 downregulates the expression of certain glycolytic enzymes to redirect metabolites towards the PPP and protect against ROS (Bensaad et al., 2006). Accordingly, enhanced glycolysis can inhibit p53 protecting cells from apoptosis (reviewed in Mason et al., 2011). Supporting these

publications, tetrameric glycolytic PKM2 has been described to be able to regulate p53 depending on redox status of the cell (Saleme et al., 2019).

Therefore, our findings in VIC suggest that apoptotic mechanisms involving mitochondria occur upon TLR3/4 and IFNGR activation in VIC and they may be associated with impaired mitochondrial respiration and OXPHOS, thus leading to apoptosis and dystrophic VIC calcification. In addition, one may speculate a dual role of p53 upon VIC activation. As shown, p53 is upregulated in short periods, while downregulated in longer ones. Thus, we propose that in short periods p53 leads to an early mitochondrial damage, which triggers apoptotic events and induces an upregulated glycolysis to compensate for the lack of proper mitochondrial function. Later, the induction of glycolysis could lead to p53 inhibition, as described in Mason et al., 2011. However, more experiments would be required for confirming our hypothesis.

D.9- JAK-STAT/HIF-1α and NF-κB pathways mediate the inflammation-induced glycolytic rewiring in VIC

This thesis unravels the mechanisms mediating the inflammatory-induced metabolic rewiring in VIC, JAK-STAT/HIF-1α and NF-κB pathways. While JAK-STAT/HIF-1α directly exerts a role in the inflammatory-mediated effects on ECAR, glycoATP, and glycolytic and apoptotic genes upregulation as well as on maximal mitochondrial respiration, mitoATP and *G6PD* and *PDK4* downregulation, NF-κB is directly regulating *PFKFB3* transcription. Our findings agree with the fact that glycolytic genes have been previously reported as HIF-1α direct targets in different contexts such as tumors (Leung et al., 2017). Additionally, as mentioned in section D.4.1 and D.8, the inhibition of G6PD and the induction of BNIP3 have been reported to be controlled directly by HIF-1α (Zhao et al.,2010 & Zhu et al., 2020). However, some discrepancies exist in the context of PDK4, in VSMC, HIF-1α correlates positively with PDK4 expression, leading to a protective mechanism against the calcification induced by glycation end-products (Yang et al., 2019). In addition, JAK-STAT pathway has been also recently associated with hypoxia-induced lipid metabolic reprogramming in cancer (Yang et al., 2022) as well as previously reported to mediate inflammatory-induced inflammation, calcification, and differentiation of VIC in a HIF-1α-dependent manner (Parra-Izquierdo et al., 2019).

Finally, the potential role of NF-κB-PFKBF3 pathway on metabolic rewiring elucidated in VIC model agrees with recent studies demonstrating a direct role of NF-κB-PFKFB3 pathway in metabolic reprogramming of vascular endothelial cells leading to EndMT and atherosclerosis progression (Xiao et al., 2021). However, last year, S. Wang et al., (2022) described the role of PFKFB3-mediated glycolysis in VIC differentiation, calcification, and inflammation upon calcifying stimuli but they stated that *PFKFB3* increase expression mediated by palmdelphin overexpression was not dependent on NF-κB activation in VIC. The differences of our results with S. Wang et al. (2022) study could be explained by other targets of palmdelphin that could be exerting the opposite role than NF-κB inhibitor on *PFKFB3* expression. Finally, some studies in

lung fibroblast have identified the MAPK pathway as a mediator of the energetic reprogramming induced by TGF-β during fibrosis process. In addition, the recent study of Liu et al., 2023 demonstrates that Rho/ROCK1 pathway is also mediating the metabolic rewiring in VIC via AMPK/RUNX2 pathway.

Considering all the evidence, one may speculate that the metabolic rewiring in VIC could be mediated by a combination of signaling pathways working synergistically. Therefore, JAK1 and JAK2 inhibitor, ruxolitinib, which is and FDA-approved drug, may be a potential therapeutic strategy for CAVD treatment.

Overall, our data, summarized in **Figure 65,** uncovers a fresh insight into the mechanisms underlying inflammation-induced development of CAVD. Inflammation, the main trigger of the initial stages of the disease, has been identified as a driver of a complex metabolic remodeling of human VIC that is necessary to provide energy, metabolites, and cofactors required for the major cellular remodeling occurring during the differentiation and calcification processes. A recent report disclosed a metabolic reprogramming in VIC mediated by the shear stress-induced pathway RhoA/ROCK1 (Liu et al., 2023), while this thesis unravels another pathway mediating inflammation-induced metabolic reprogramming: NF-κB and JAK-STAT/HIF-1α pathways, thus suggesting potential targetable pathways in CAVD treatment. Together, evidences from Liu and colleagues and from this thesis support that VIC metabolic remodeling necessary for VIC calcification can be initiated by either mechanical strain or inflammation and suggest its potential relevance in early stages of CAVD. Additionally, our data provides a more comprehensive analysis of metabolic reprogramming and unveils a more complex metabolic remodeling than a Warburg effect. Furthermore, this thesis presents a complex interconnected metabolic rewiring of several catabolic pathways going through an increased glycolysis that produces higher levels of ATP in a quicker way, thus leading to an impaired TCA cycle, which ultimately promotes impaired OXPHOS. Notably, a novel finding of this study is that an important pathway for biomass synthesis and oxidative stress protection, PPP, is dysregulated with a decreased oxPPP. Together, these metabolic alterations lead to the production of ROS and the generation of oxidative stress, which is closely related to the pathological processes underlying CAVD: inflammation, differentiation, and calcification, a previous described (reviewed in Greenberg et al., 2022). Additionally, as summarized in **Figure 66**, data further disclose that quiescent VIC exhibit a more energetic metabolic phenotype with higher reliance on OXPHOS for energy than VIC, and undergo a similar metabolic rewiring than VIC in an inflammatory milieu characterized by the upregulation of glycolytic enzymes and subsequent increase in ATP from glycolysis and decrease in ATP from OXPHOS.

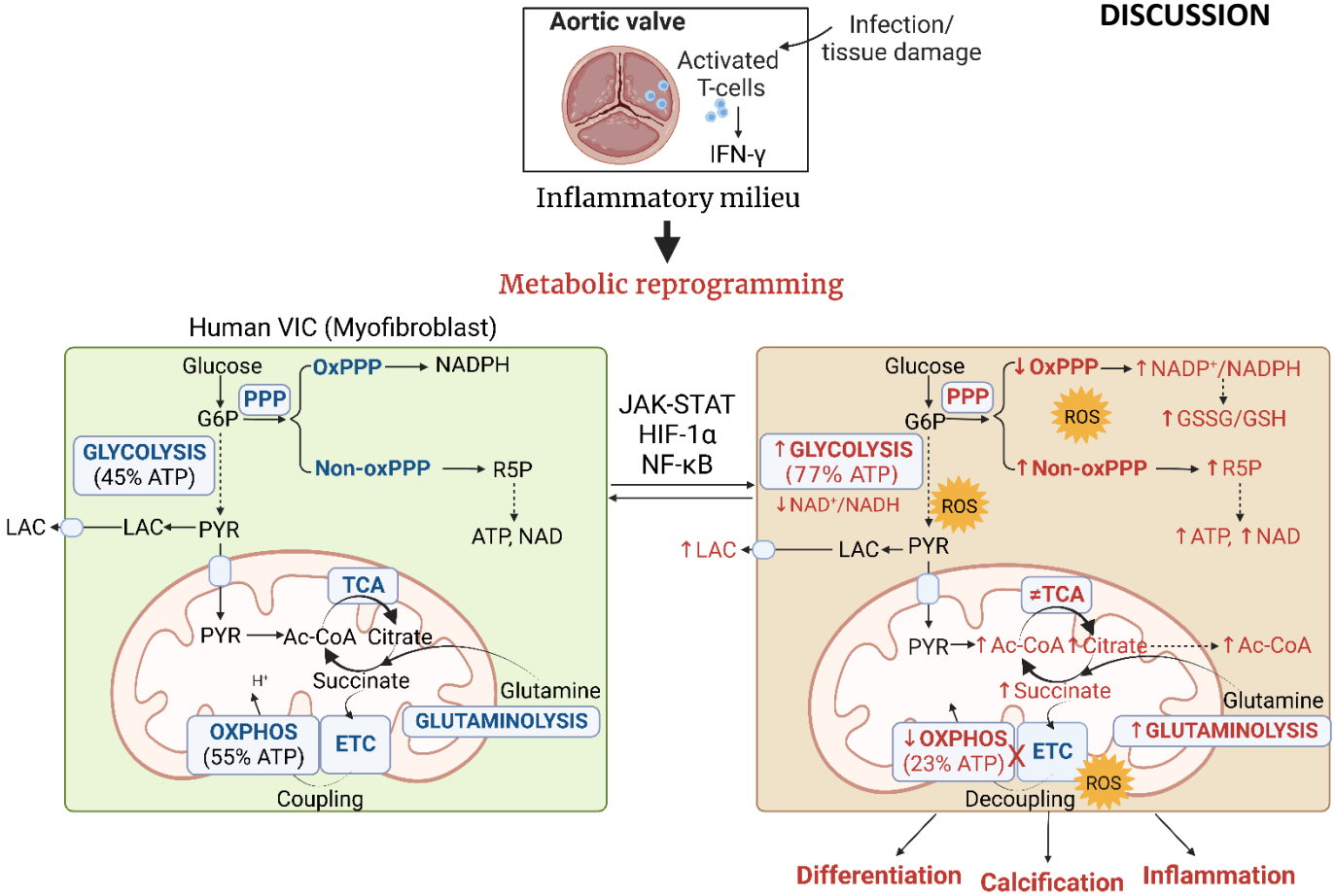

Figure 65. Schematic representation of inflammatory-induced metabolic reprogramming and ROS production in VIC and its role in VIC differentiation, inflammation, and calcification. Ac-CoA indicates acetyl-CoA; ATP, adenosine triphosphate; ETC, electron transport chain; GP6, glucose-6-phosphate dehydrogenase; GSSG/GSH, Glutathione disulfide oxidized/ glutathione reduced; LAC, lactate; NAD, nicotinamide adenine dinucleotide; NADPH, nicotinamide adenine dinucleotide phosphate; non-oxPPP, non-oxidative phase of PPP; OXPHOS, oxidative phosphorylation; oxPPP, oxidative phase of PPP; PPP, pentose phosphate pathway; PYR, pyruvate; ROS, reactive oxygen species; R5P, ribose-5-phosphate; TCA, tricarboxylic acid cycle. Created with BioRender.com.

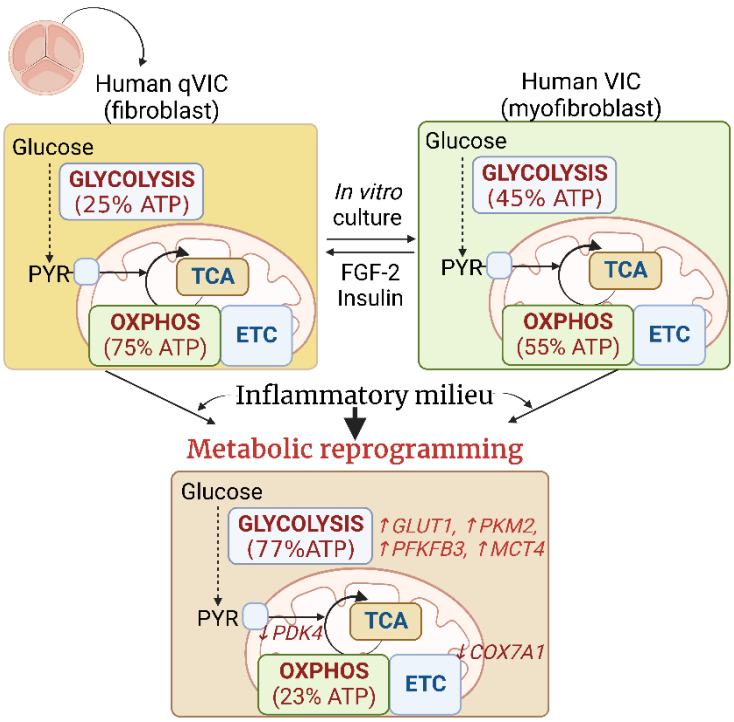

Figure 66. Schematic representation of differences in bioenergetics between qVIC and VIC, and the similar metabolic rewiring undergone upon exposure to an inflammatory environment. *COX7A1*, cytochrome oxidase C; ETC, electron transport chain; *GLUT1*, glucose transporter 1; *MCT4*, monocarboxylate transporter 4; OXPHOS, oxidative phosphorylation; *PKM2*, pyruvate kinase M2; *PFKFB3*, 6-phosphofructo-2-kinase/fructose-2,6-bisphosphatase; PYR, pyruvate; TCA, tricarboxylic acid cycle. Created with BioRender.com.

D.10- Limitations of the study

Throughout this study, we have faced numerous difficulties that have slowed down or complicated the research. Firstly, a low availability of control valves, due to shortage in heart transplantation, and of stenotic valves, due to the smaller number of patients undergoing surgery replacement in favor of TAVI. In addition, the experimental work conducted from 2019 until 2023, has been delayed due to COVID-19 restrictions preventing access to the laboratory and the hospital stopped providing valve samples for a year and a half.

Furthermore, our CAVD disease model is based on a 2D cell culture system that has been used in the last decades. Culture plate's plastic surfaces have the limitation of being stiffer than the extracellular matrix, leading to the activation of quiescent fibroblasts, which populate the healthy valve into a partially activated VIC phenotype. Nevertheless, despite that human VIC are in a pre-pathological state of activation and exhibit a myofibroblastic phenotype, they are a valuable model to study inflammation-mediated osteogenic differentiation and calcification since a potential therapeutic intervention at the early stages of CAVD is likely only plausible when VIC are already activated, as diagnostic tools and biomarkers for CAVD are currently insufficient to detect its initiation during the initial transition from qVIC to VIC. Moreover, to overcome this limitation, we have validated the main findings in cellular models preserve a fibroblastic phenotype. The use of a dedifferentiation medium formula that reverses the VIC phenotype to qVIC (Latif et al., 2015 & Porras et

al., 2017), validated the inflammation-triggered metabolic shift (**Figure 66**). Further, some findings were validated 3D co-culture model hydrogels that not only maintains the qVIC phenotype, but also mimics the valve structure and VIC-VEC interactions (Butcher et al., 2006). However, not every finding has been validated in the 3D co-culture model due to time limitations, as it was a technique performed during a short stay in Cornell University, and due to the technical difficulties of integrating this 3D culture model into a Seahorse analyzer.

We have also been constrained by the significant individual variability observed among patients, as metabolism is highly influenced by other medical conditions such as diabetes, obesity, hypertension, and cholesterol levels. We have attempted to find a relationship between different medical variables, but the limited availability of valves from different patients with the same co-morbidities has not allowed us to perform statistical analysis.

On the technical level, we have been limited by the number of cells available for conducting experiments. VIC are primary cell cultures, which grow very slowly and take a long time to proliferate and multiply, making it challenging to obtain a large number of cells from the same patient at the same passage for experiments. Additionally, there were some experiments that required a significant quantity of cells, such as UPLC-MS or some commercial kits. In addition, we have also faced the difficulty of finding effective antibodies that can efficiently recognize proteins involved in metabolism. Therefore, we have been unable to measure metabolic proteins in addition to measuring the transcriptional levels of some metabolic genes.

The use of 3D co-culture model had some limitations. Validation of data from VIC was shown in 3D VIC-VEC co-cultures and not in 3D VIC cultures due to some technical issues. (i) The concentrations of inflammatory stimuli in hydrogel cultures had to be significantly reduced to avoid cell death /apoptosis. (ii) The survival rate of 3D VIC cultures after 7 days exposure to inflammatory agents significantly decreased, thus resulting in insufficient amounts of RNA or protein for conclusive data. It should be noted that despite this limitation, validation of metabolic changes in a 3D model grouping VICs and VECs is physiologically relevant since this model system arraigns these cellular populations in a more physiologically relevant format, with VEC lining the pseudo-tissue surface and VIC within the intimal space and recapitulates VIC-VEC communication (Gee et al, 2021).

Furthermore, the results obtained in valvular tissue through qPCR would require further investigation with more precise techniques such as western blotting, immunohistochemistry, or transcriptomics and proteomics. Since our discoveries are confined to *in vitro* experiments and the examination of valve tissue, it would be valuable to assess the impact of immune mediators and inflammatory cytokines in suitable animal models of the disease.

D.11- Future perspectives

As mentioned above, several aspects remain open to future studies. This thesis identifies a novel shift in VIC metabolism required for calcification, particularly hyperglycolysis, as well as alterations in PPP routes, and further shows that this shift can be blocked via JAK-STAT/HIF-1α inhibition; however, further studies are needed to deepen on the functional relevance of these results and identify potential therapeutic targets. Future investigations should address glucose catabolic routes in depth, particularly the less-studied pentose phosphate routes, as well as explore potential sex differences in the metabolic shift. Other interesting lines of investigation would be the identification of the specific sources of ROS in VIC under inflammatory exposure, the investigation of potential alterations in mitochondrial metabolism and function, and the analysis of other metabolic pathways, such as β-oxidation and lipid synthesis. It would of great benefit to the field to further study the metabolic signature of initiating events such as inflammation and mechanical strain; and exploring the potential interplay between mechanical strain and inflammatory agents will mimic a more physiologically relevant setting that may provide novel metabolic routes or metabolites with an important role in early stages of the disease. Finally, the identification of the JAK-STAT/HIF-1α-dependent metabolic changes will provide new cues for therapeutic intervention using Jakinibs.

In future studies, it would be of interest to evaluate real-time metabolism in human valve leaflets -subdivided into portions representing disease progression-, as well as in 3D cultures of human VIC, VEC, and VIC-VEC co-cultures. Furthermore, the use of cutting-edge techniques such as proteomics and metabolomics, using intraleaflet subclassification to help removing individual variability and clinical severity, will allow the identification of metabolic signatures that specifically define a progressing valvular pathology.

CONCLUSIONS

The conclusions of this thesis are:

1. Human aortic valve interstitial cells (VIC) in culture are metabolically active myofibroblasts exhibiting equal reliance on glycolysis and oxidative phosphorylation for energy production, which differs from the more energetic metabolism relying on oxidative phosphorylation (OXPHOS) exhibited by quiescent VIC.
2. The inflammatory milieu generated by inflammatory cytokines related to valve disease, induces a metabolic shift to a more glycolytic phenotype in VIC, which is potentiated by pathogen patterns recognized by Toll-like receptors (TLR)-3 and 4, and exhibits some cytokine- and TLR-specific differences.
3. Co-stimulation of human VIC with interferon (IFN)-γ and pathogen patterns LPS or Poly (I:C) induces metabolic rewiring to a hyperglycolytic phenotype, characterized by increased expression of glycolytic enzymes, accumulation of aerobic glycolysis metabolites, and synthesis of glycolytic ATP, thus providing energy and biomass necessary to support inflammatory-induced differentiation, calcification, and inflammation in VIC.
4. The interplay between the IFN-γ receptor and TLR4 signaling in VIC leads to impairment of the oxidative phase of the pentose phosphate pathway (PPP), with the inhibition of the rate-limiting enzyme leading to the induction of hyperglycolytic reprogramming, thus generating oxidative stress and fueling processes such as inflammation, differentiation, and *in vitro* calcification in VIC.
5. The exposure of VIC to IFN-γ and TLR4 ligand leads to increased acetyl-CoA synthesis, followed by a slow accumulation of tricarboxylic acid cycle (TCA) metabolites. The entry of pyruvate into the mitochondria and subsequent TCA metabolites play a role in HIF-1α stabilization, differentiation, and *in vitro* calcification in VIC.
6. Co-stimulation with IFN-γ and TLR4 ligand promotes alterations in the mitochondrial electron transport chain (ETC) with an impaired maximal respiratory capacity and non-altered basal respiration, in parallel with the uncoupling of ETC and OXPHOS, thus resulting in blunted mitochondrial ATP synthesis, which subsequently leads to mitochondria-mediated apoptosis and calcification in VIC.
7. Inflammation-induced metabolic alterations include increasing reliance on glucose for energy, metabolite, and cofactor production and the generation of oxidative stress in VIC inducing reactive oxygen species (ROS) production and redox homeostasis alteration in VIC. Notably, oxidative stress plays a role in HIF-1α stabilization and subsequent inflammation, differentiation, and *in vitro* calcification in VIC.

CONCLUSIONS

8. Metabolic rewiring induced by the inflammatory milieu is controlled by the JAK-STAT/HIF-1α and NF-κB pathways, and this shift can be blocked by ruxolitinib, a Jakinib currently used in clinics.
9. Inflammation-driven metabolic reprogramming in 2D-VIC cultures is reproduced in quiescent VIC as well as in the 3D VIC-VEC co-culture model. Moreover, calcified valve leaflets and VIC from stenotic patients exhibit glycolytic gene profile and metabolism, thus arguing for the relevance of metabolic changes in the initial stages of valve disease.

General conclusion

Collectively, data unveil inflammation as a driver of metabolic rewiring in human VIC and further show this shift mimics the glycolytic profile in calcified cells and valves. JAK-STAT/HIF-1α-triggered hyperglycolysis and impairment of the oxidative PPP provide rapid fuel, metabolites, cofactors, and oxidative stress necessary to support a major cell remodeling during differentiation and calcification processes, which are relevant to the initial stages of valve disease pathogenesis. Also, this thesis provides new cues for therapeutic intervention by targeting JAK-STAT/HIF-1α and NF-κB-mediated glycolysis and suggests the potential second use of drugs like Jakinibs and metformin that are currently used in other diseases.

Las conclusiones de esta tesis son las siguientes:

1. Las células intersticiales de la válvula aórtica humana (VIC) en cultivo son miofibroblastos metabólicamente activos que dependen por igual de la glucólisis y la fosforilación oxidativa para la producción de energía, esto difiere del metabolismo más enérgico basado en la fosforilación oxidativa (OXPHOS) que muestran las VIC quiescentes.
2. El entorno inflamatorio generado por citoquinas inflamatorias relacionadas con enfermedades de la válvula induce un cambio metabólico hacia un fenotipo más glucolítico en VIC, el cual se potencia mediante patrones de patógenos reconocidos por los receptores tipo Toll (TLR)-3 y 4, y muestra algunas diferencias dependiendo de las citoquinas y los TLRs.
3. La coestimulación de las VIC humanas con interferón (IFN)-γ y patrones de patógenos como LPS o Poly (I:C) induce una reprogramación metabólica hacia un fenotipo glucolítico, caracterizado por un aumento en la expresión de enzimas glucolíticas, acumulación de metabolitos de la glucólisis aeróbica y síntesis de ATP glucolítico, proporcionando así la energía y biomasa necesaria para la inducción inflamatoria de calcificación, inflamación, y diferenciación de VIC.
4. La interacción entre el receptor de IFN-γ y la señalización de TLR4 en VIC conduce a la alteración de la fase oxidativa de la vía de la pentosa fosfato (PPP), que cursa con la inhibición de la enzima limitante. Esta inhibición induce la reprogramación glucolítica, generando así estrés oxidativo y alimentando procesos como la inflamación, la diferenciación y la calcificación *in vitro* en las VIC.
5. La exposición de las VIC a IFN-γ y ligandos de TLR4 conduce a un aumento en la síntesis de acetil-CoA, seguido de una lenta acumulación de metabolitos del ciclo de ácido tricarboxílico (TCA). La entrada de piruvato en las mitocondrias y los siguientes metabolitos del TCA desempeñan un papel en la estabilización de HIF-1α, la diferenciación y la calcificación in *vitro* en las VIC.
6. La coestimulación con IFN-γ y ligandos de TLR4 promueve alteraciones en la cadena de transporte de electrones mitocondrial (ETC) con una capacidad respiratoria máxima disminuida y una respiración basal inalterada, junto con un desacoplamiento de ETC y OXPHOS, lo que resulta en una síntesis de ATP mitocondrial disminuida, lo que posteriormente conduce a la apoptosis mediada por mitocondria y la calcificación en VIC.
7. Las alteraciones metabólicas inducidas por la inflamación incluyen una mayor dependencia de la glucosa para la producción de energía, metabolitos y cofactores, y la generación de estrés oxidativo en VIC, induciendo la producción de especies reactivas de oxígeno (ROS) y alteración de la homeostasis redox. Además, el estrés oxidativo desempeña un papel en la estabilización de HIF-1α y la posterior inflamación, diferenciación y calcificación *in vitro* en VIC.

CONCLUSIONS

8. La reprogramación metabólica inducida por el entorno inflamatorio es principalmente controlada por las vías JAK-STAT/HIF-1α y NF-κB, y este cambio puede ser bloqueado por ruxolitinib, un Jakinib actualmente utilizado en la práctica clínica.
9. La reprogramación metabólica mediada por agentes inflamatorios en cultivos de VIC en 2D se reproduce tanto en VIC quiescentes como en un modelo de cocultivo 3D de VIC-VEC. Además, las válvulas calcificadas y las VIC de pacientes estenóticos también muestran un metabolismo glucolítico y un perfil de genes glucolíticos exacerbados. Esto apoya el papel relevante de los cambios metabólicos en las primeras etapas de la patogénesis de CAVD.

Conclusión general:

En conjunto, los datos revelan que la inflamación es un inductor de la reprogramación metabólica en VIC humanas y demuestran que este cambio imita el perfil glucolítico que ocurre en las células y válvulas calcificadas. El aumento glucolítico mediado por JAK-STAT/HIF-1α y la alteración de la PPP oxidativa proporcionan rápidamente energía, metabolitos, cofactores y estrés oxidativo necesarios para respaldar la remodelación celular de VIC que ocurre durante los procesos de diferenciación y calcificación, lo cual es relevante para las primeras etapas de la patogénesis de CAVD. Además, esta tesis proporciona nuevas pistas para la intervención terapéutica de la enfermedad. Propone dianas terapéuticas como la vía JAK-STAT/HIF-1α y NF-κB, y sugiere el potencial uso de medicamentos como los Jakinibs y la metformina que se utilizan actualmente en otras enfermedades.

BIBLIOGRAPHY

BIBLIOGRAPHY

1. Aikawa, E., Nahrendorf, M., Sosnovik, D., Lok, V. M., Jaffer, F. A., Aikawa, M., & Weissleder, R. (2007). Multimodality molecular imaging identifies proteolytic and osteogenic activities in early aortic valve disease. *Circulation*, *115*(3), 377–386.
2. Aikawa, E., & Otto, C. M. (2012). Look more closely at the valve: Imaging calcific aortic valve disease. *Circulation*, *125*(1), 9–11.
3. Akahori, H., Tsujino, T., Naito, Y., H, S., M, S., M, F., & Masuyama, T. (2014). Nuclear factor-κB-hypoxia-inducible factor-2 pathway in aortic valve stenosis. *J. exp. med.*, *23*(5), 558–566.
4. Akira, S., Uematsu, S., & Takeuchi, O. (2006). Pathogen recognition and innate immunity. *Cell*, *124*(4), 783–801.
5. Algieri, C., Bernardini, C., Trombetti, F., Schena, E., Zannoni, A., Forni, M., & Nesci, S. (2022). Cellular Metabolism and Bioenergetic Function in Human Fibroblasts and Preadipocytes of Type 2 Familial Partial Lipodystrophy. *Int. J. Mol. Sci.*, *23*(8659), 1–10.
6. Alesutan, I., Moritz, F., Haider, T., Shouxuan, S., & Gollmann-tepeköylü, C. (2020). Impact of β -glycerophosphate on the bioenergetic profile of vascular smooth muscle cells. *J. Mol. Med.*, *98*, 985–997.
7. Alushi, B., Curini, L., Christopher, M. R., Grubitzch, H., Landmesser, U., Amedei, A., & Lauten, A. (2020). Calcific Aortic Valve Disease-Natural History and Future Therapeutic Strategies. *Front. Pharmacol.*, *11*, 1–12.
8. Anastasiou, D., Yu, Y., Israelsen, W. J., Jiang, J., Matthew, B., Hong, B. S., & Cantley, L. C. (2012). Pyruvate kinase M2 activators promote tetramer formation and suppress tumorigenesis. *Nat. Chem. Biol.*, *8*(10), 839–847.
9. Anderson, R. H., Ho, S. Y. E. N., & Becker, A. E. (2000). Anatomy of the Human Atrioventricular Junctions Revisited. *The Anatomical Record*, *260*, 81–91.
10. Aon, Miguel Antonio, Stanley, B. A., Sivakumaran, V., Kembro, J. M., Rourke, B. O., Paolocci, N., & Cortassa, S. (2012). Glutathione/thioredoxin systems modulate mitochondrial H2O2 emission : An experimental-computational study. *J. gen. physiol.*, *139*(6), 479–491.
11. Arcy, J. L., Coffey, S., Loudon, M. A., Kennedy, A., Pearson-stuttard, J., Birks, J., & Prendergast, B. D. (2016). Large-scale community echocardiographic screening reveals a major burden of undiagnosed valvular heart disease in older people : the OxVALVE Population Cohort Study †. *Eur. Heart J.*, *37*, 3515–3522.
12. Ariza, A. C., Deen, P. M. T., & Robben, J. H. (2012). The succinate receptor as a novel therapeutic target for oxidative and metabolic stress-related conditions. *Front. Endocrinol.*, *3*(February), 1–8.
13. Arjunon, S., Rathan, S., Jo, H., & Yoganathan, A. P. (2017). Aortic Valve: Mechanical Environment and Mechanobiology Sivakkumar. *Ann. Biomed. Eng..*, *41*(7), 1331–1346.
14. Arnold, P. K., Jackson, B. T., Paras, K. I., Brunner, J. S., Hart, M. L., Newsom, O. J., & Finley, L. W. S. (2022). A non-canonical tricarboxylic acid cycle underlies cellular identity. *Nature*, *603*(17), 477–483.
15. Audrito, V., Messana, V. G., & Deaglio, S. (2020). NAMPT and NAPRT : Two Metabolic Enzymes With Key Roles in Inflammation. *Front. Oncol.*, *10*(March), 1–17.
16. Azuelos, I., Selvarajah, B., Forty, E., Plate, M., Brunori, G., Edwards, L., & Chambers, R. (2016). mTOR regulates glucose metabolism during TGFβ-Induced fibroblast to myofibroblast differentiation. *Int. J. Med*, *23*(11), 3–4.
17. Babu, A. N., Meng, X., Zou, N., Yang, X., Wang, M., Song, Y., & Fullerton, D. A. (2008). Lipopolysaccharide Stimulation of Human Aortic Valve Interstitial Cells Activates Inflammation and Osteogenesis. *Ann. Thorac. Surg.*, *86*(1), 71–76.
18. Bajic, V. P., Neste, C. Van, Obradovic, M., Zafirovic, S., Radak, D., Bajic, V. B., & Isenovic, E. R. (2019). Glutathione "Redox Homeostasis" and Its Relation to Cardiovascular Disease. *Oxidative Med. Cell. Longev.*, *2019*, 1–13.
19. Baldini, C., Moriconi, F. R., Galimberti, S., Libby, P., & Caterina, R. De. (2021). The JAK – STAT pathway : an emerging target for cardiovascular disease in rheumatoid arthritis and myeloproliferative neoplasms. *Eur. Heart J.*, *42*, 4389–4400.
20. Banh, R. S., Iorio, C., Marcotte, R., Xu, Y., Cojocari, D., Zhang, S., & Habu, T. (2016). PTP1B regulates non-mitochondrial oxygen consumption via RNF213 to promote tumour survival during hypoxia. *Nat. Cell. Biol.*, *18*(7), 803–813.
21. Bartoli-leonard, F., Zimmer, J., & Aikawa, E. (2021). Innate and adaptive immunity : the understudied driving force of heart valve disease. *Cardiovasc. Res.*, *117*, 2506–2524.
22. Benito, A., Polat, I. H., Noé, V., Ciudad, C. J., & Cascante, M. (2017). Glucose-6-phosphate dehydrogenase and transketolase modulate breast cancer cell metabolic reprogramming and correlate with poor patient outcome. *Oncotarget*, *8*(63), 106693–106706.
23. Bensaad, K., Tsuruta, A., Selak, M. A., Vidal, M. N. C., Nakano, K., Bartrons, R., & Vousden, K. H. (2006). TIGAR , a p53-Inducible Regulator of Glycolysis and Apoptosis. *Cell*, *126*, 107–120.
24. Bernard, K., Logsdon, N. J., Ravi, S., Xie, N., Persons, B. P., Rangarajan, S., & Thannickal, V. J. (2015). Metabolic Reprogramming Is Required for Myofibroblast Contractility and Differentiation. *J. Biol. Chem*, *290*(42), 25427–25438.
25. Bertazzo, S., Gentleman, E., Cloyd, K. L., Chester, A. H., Yacoub, M. H., & Stevens, M. M. (2013). Nano-analytical electron microscopy reveals fundamental insights into human cardiovascular tissue calcification. *Nature Materials*, *12*(6), 576–583.
26. Beyoğlu, D., & Idle, J. R. (2021). Metabolic Rewiring and the Characterization of Oncometabolites. *Cancers*, *13*(12), 1–18.
27. Bian, W., Wang, Z., Sun, C., & Zhang, D. (2021). Pathogenesis and Molecular Immune Mechanism of Calcified Aortic Valve Disease. *Front. Cardiovasc. Med.*, *8*(765419), 1–7.
28. Bogdanova, M., Kostina, A., Enayati, K., Zabirnyk, A., Malashicheva, A., Stensløkken, K., & Rutkovskiy, A. (2018). Inflammation and Mechanical Stress Stimulate Osteogenic Differentiation of Human Aortic Valve Interstitial. *Front.*

Physiol., *9*(1635), 1–14.
29. Boshuizen, M. C. S., & Winther, M. P. J. De. (2015). Interferons as Essential Modulators of Atherosclerosis. *Arterioscler. Thromb. Vasc. Biol.*, *35*, 1579–1588.
30. Bosse, Y., Miqdad, A., Fournier, D., Pibarot, P., & Mathieu, P. (2009). Refining Molecular Pathways Leading to Calcific Aortic Valve Stenosis by Studying Gene Expression Profile of Normal and Calcified Stenotic Human Aortic Valves. *Circulation Cardiovascular Genetics*, *10*, 489–498.
31. Boström, K. I., Rajammanan, N. M., & Towler, D. A. (2011). The Regulation of Valvular and Vascular Sclerosis By Osteogenic Morphogens. *Circ. Res.*, *109*(5), 564–577.
32. Boukouris, A. E., Zervopoulos, S. D., & Michelakis, E. D. (2016). Metabolic Enzymes Moonlighting in the Nucleus : Metabolic Regulation of Gene Transcription. *Trends Biochem.Sci.*, *12*, 1–19.
33. Bours, M. J. L., Swennen, E. L. R., Virgilio, F. Di, Cronstein, B. N., & Dagnelie, P. C. (2006). Adenosine 5 ′ -triphosphate and adenosine as endogenous signaling molecules in immunity and inflammation. *Pharmacol. Ther.*, *112*, 358–404.
34. Boskovsky, M.T., & Gleason, T.G. (2021). Current therapeutic options in aortic stenosis. *Circ. Res., (128), 1398-1417.*
35. Boxel-dezaire, A. H. H. Van, Rani, M. R. S., & Stark, G. R. (2006). Complex Modulation of Cell Type-Specific Signaling in Response to Type I Interferons. *Immunity*, (25), 361–372.
36. Bradshaw, P. C. (2019). Cytoplasmic and mitochondrial NADPH-coupled Redox systems in the regulation of aging. *Nutrients*, *11*(3), 504–538.
37. Branchetti, E., Sainger, R., Poggio, P., Grau, J. B., Patterson-, J., Bavaria, J. E., & Levy, R. J. (2013). Antioxidant Enzymes Reduce DNA Damage and Early Activation of Valvular Interstitial Cells in Aortic Valve Sclerosis. *Arterioescler. Thromb. Vasc. Biol.*, *33*(2), 1–20.
38. Britt, E. C., Lika, J., Giese, M. A., Schoen, T. J., Seim, G. L., Huang, Z., & Fan, J. (2022). Switching to the cyclic pentose phosphate pathway powers the oxidative burst in activated neutrophils. *Nature Metabolism*, *4*, 389–403.
39. Brown, G. C. (2001). Regulation of mitochondrial respiration by nitric oxide inhibition of cytochrome c oxidase. *Biochimica et Biophysica Acta*, *1504*, 46–57.
40. Butcher, JT., & Nerem, RM. (2004). Porcine aortic valve interstitial cells in three-dimensional culture: comparison of phenotype with aortic smooth muscle cells. *J. Heart Valve Dis.*. May;13(3):478-85.
41. Butcher, J. T., & Nerem, R. M. (2006). Valvular Endothelial Cells Regulate the Phenotype of Interstitial Cells in Co-culture : Effects of Steady Shear Stress. *Tissue Eng.*, *12*(4).
42. Butcher, J. T., Tressel, S., Johnson, T., Turner, D., Sorescu, G., Jo, H., & Nerem, R. M. (2006). Transcriptional Profiles of Valvular and Vascular Endothelial Cells Reveal Phenotypic Differences Influence of Shear Stress. *Arteriosler Thromb Vasc Biol*, *30*, 70–77.
43. Byon, C. H., Javed, A., Dai, Q., Kappes, J. C., Clemens, T. L., Darley-usmar, V. M., & Chen, Y. (2008). Oxidative Stress Induces Vascular Calcification through Modulation of the Osteogenic Transcription Factor Runx2 by AKT Signaling *. *J. Biol. Chem.*, *283*(22), 15319–15327.
44. Carbognin, E., Betto, R. M., Soriano, M. E., Smith, A. G., & Martello, G. (2016). Stat3 promotes mitochondrial transcription and oxidative respiration during maintenance and induction of naive pluripotency. *EMBO J.*, *35*(6), 618–634.
45. Certo, M., Tsai, C., Pucino, V., Ho, P., & Mauro, C. (2021). Lactate modulation of immune responses in inflammatory versus tumour microenvironments. *Nat. Rev. Immunol.*, *21*(March), 151–169.
46. Chalkiadaki, A., & Guarente, L. (2015). The multifaceted functions of sirtuins in cancer. *Nature Publishing Group*, *2*, 1–17.
47. Chen, J., Henderson, G. I., & Freeman, G. L. (2001). Role of 4-Hydroxynonenal in Modification of Cytochrome c Oxidase in Ischemia / Reperfused Rat Heart. *J. Mol. Cell. Cardiol.*, *33*, 1919–1927.
48. Chen, J., Ying, C., Yip., Sone, ED., Simmons, CA. (2009). Identification and Characterization of Aortic Valve Mesenchymal Progenitor Cells with Robust Osteogenic Calcification Potential. Am. J. Path., 174(3), 1109-1119.
49. Chen, P., Cai, L., Huffman, K., Minna, J. D., Xiao, G., Deberardinis, R. J., & Sekine, I. (2019). Metabolic Diversity in Human Non-Small Cell Lung Cancer Cells Resource Metabolic Diversity in Human Non-Small Cell Lung Cancer Cells. *Mol. Cell.*, *76*(5), 838–851.
50. Chini, C. C. S., Zeidler, J. D., Kashyap, S., Warner, G., & Chini, E. N. (2021). Perspective Evolving concepts in NAD + metabolism. *Cell metab..*, *33*(6), 1076–1087.
51. Christofk, H. R., Heiden, M. G. Vander, Harris, M. H., Ramanathan, A., Gerszten, R. E., Wei, R., & Cantley, L. C. (2008). The M2 splice isoform of pyruvate kinase is important for cancer metabolism and tumour growth. *Nature*, *452*(March), 230–233.
52. Coffey, S., Chen, M., Sarano, M. E.-, Zühlke, L., & Prendergast, B. D. (2021). Global epidemiology of valvular heart disease. *Nat. Rev.*, *18*, 853–864.
53. Colegio, O. R., Chu, N.-Q., Szabo, A. L., Chu, T., Rhebergen, A. M., Jairam, C., & Medzhitov, R. (2014). Functional polarization of tumour-associated macrophages by tumour-derived lactic acid. *Nature*, *513*(7519), 559–563.
54. Corkey, B. E., & Deeney, J. T. (2020). The Redox Communication Network as a Regulator of Metabolism. *Front. Physiol.*, *11*, 1–10.
55. Côté, N., El Husseini, D., Pépin, A., Guauque-Olarte, S., Ducharme, V., Bouchard-Cannon, P., & Mathieu, P. (2012). ATP acts as a survival signal and prevents the mineralization of aortic valve. *J. Mol. Cell. Cardiol.*, *52*(5), 1191–1202.
56. Coté, N., Mahmut, A., Bosse, Y., Couture, C., Pagé, S., Trahan, S., & Mathieu, P. (2013). Inflammation Is Associated with

the Remodeling of Calcific Aortic Valve Disease. *Inflammation*, *36*(3), 573–581.
57. Dahal, S., Huang, P., Murray, B. T., & Mahler, G. J. (2017). Endothelial to mesenchymal transformation is induced by altered extracellular matrix in aortic valve endothelial cells. *J. Biomed. Mater. Res. - Part A*, *105*(10), 2729–2741.
58. Das, D., Holmes, A., Murphy, G. A., Mishra, K., Anke, C., Horowitz, J. D., & Kennedy, J. A. (2013). TGF-β1-Induced MAPK Activation Promotes Collagen Synthesis , Nodule Formation , Redox Stress and Cellular Senescence in Porcine Aortic Valve Interstitial Cells. *J. Heart Valve Dis.*, *22*(5), 621–630.
59. Death, S. C., Risk, R., Analysis, U., Risk, R., & Analysis, M. (1997). Elevated levels of circulating soluble adhesion molecules in patients with nonrheumatic aortic stenosis. *Excerpta Medica*, *12*(7), 980–982.
60. Deb, N., & Lacerda, C. M. . (2022). The Individual and Combined Effects of Shear , Tension , and Flexure on Aortic Heart Valve Endothelial Cells in Culture. *Cardiovasc. Eng. Technol.*, *13*(3), 443–451.
61. Decano, J. L., Iwamoto, Y., Goto, S., Lee, J. Y., Matamalas, J. T., Halu, A., & Aikawa, E. (2022). A disease-driver population within interstitial cells of human calcific aortic valves identified via single-cell and proteomic profiling. *Cell reports*, *39*(2), 110685.
62. Deck, J. D. (1986). Endothelial cell orientation on aortic valve leaflets. *Cardiovasc. Res.*, *20*, 760–767.
63. Dhagia, V., Kitagawa, A., Jacob, C., Zheng, C., D'Alessandro, A., Edwards, JG., Rocic, P., Gupte, R., & Gupte, SA. (2021). Treatment Strategies for Glucose-6-Phosphate Dehydrogenase Deficiency: Past and Future Perspectives. *Am. J. Physiol. Heart Circ. Physiol.*, Mar 1;320(3):H999-H1016.
64. Ding, H., Jiang, L., Xu, J., Bai, F., Zhou, Y., Yuan, Q., & Yang, J. (2017). Inhibiting aerobic glycolysis suppresses renal interstitial fibroblast activation and renal fibrosis. *Am. J. Renal Physiol.*, *313*(22), 561–575.
65. Divakaruni, A. S., & Brand, M. D. (2023). The Regulation and Physiology of Mitochondrial Proton Leak. *Physiology*, *26*, 192–205.
66. Djafarzadeh, S., Vuda, M., Takala, J., Ochs, M., & Jakob, S. M. (2011). Toll-like receptor-3-induced mitochondrial dysfunction in cultured human hepatocytes. *Mitochondrion*, *11*(1), 83–88.
67. Dodson, M., Benavides, G. A., Darley-usmar, V., & Zhang, J. (2022). Differential Effects of 2-Deoxyglucose and Glucose Deprivation on 4-Hydroxynonenal Dependent Mitochondrial Dysfunction in Primary Neurons. *Front. Aging Neurosci.*, *3*, 1–10.
68. Dranka, B. P., Hill, B. G., & Darley-usmar, V. M. (2010). Mitochondrial reserve capacity in endothelial cells: the impact of nitric oxide and reactive oxygen species. *Free Radic. Biol. Med.*, *48*(7), 905–914.
69. Driscoll, K., Cruz, A. D., & Butcher, J. T. (2021). Inflammatory and Biomechanical Drivers of Endothelial-Interstitial Interactions in Calcific Aortic Valve Disease. *Circ. Res.*, *128*, 1344–1370.
70. El-Hamamsy, I., Chester, A.H., & Yacoub, M.H.,. (2010). Cellular regulation of the structure and function of aortic valves. *J. Adv. Res.*, *1*(1), 5-12.
71. En, Q., Zeping, H., Yuetang, W., Xu, W., & Wei, W. (2021). Metformin alleviates the calcification of aortic valve interstitial cells through activating the PI3K / AKT pathway in an AMPK dependent way. *Mol. Med.*, *27*(156), 1–16.
72. Everts, B., Amiel, E., Huang, S. C. C., Smith, A. M., Chang, C. H., Lam, W. Y., & Pearce, E. J. (2014). TLR-driven early glycolytic reprogramming via the kinases TBK1-IKKε supports the anabolic demands of dendritic cell activation. *Nature Immunology*, *15*(4), 323–332.
73. Flammer, A. J., Gössl, M., Li, J., Matsuo, Y., Reriani, M., Loeffler, D., & Khosla, S. (2012). Patients with an HbA1c in the Prediabetic and Diabetic Range Have Higher Numbers of Circulating Cells with Osteogenic and Endothelial Progenitor Cell Markers. *J. Clin. End. Met.*, *97*(12), 4761–4768.
74. Fernández-pisonero, I., Dueñas, A. I., Barreiro, O., Montero, O., Sánchez-madrid, F., Barreiro, O., García-Rodríguez, C. (2012). Lipopolysaccharide and Sphingosine-1-Phosphate Cooperate To Induce Inflammatory Molecules and Leukocyte Adhesion in Endothelial Cells. *J. Immunol.*, *189*, 5402–5410.
75. Finley, L. W. S., Haas, W., Desquiret-Dumas, V., Wallace, D. C., Procaccio, V., Gygi, S. P., & Haigis, M. C. (2011). Succinate Dehydrogenase Is a Direct Target of Sirtuin 3 Deacetylase Activity. *PLOS ONE*, *6*(8), e23295.
76. Fried, L. P., N.O., B., P., E., C.D., F., J.M., G., R.A., K., & Weiler, P. G. (1991). The cardiovascular Health Study: Design and rationale. *Annals of Epidemiology*, *1*(3), 263–276.
77. Fu, B., Wang, J., Wang, L., Wang, Q., Guo, Z., Xu, M., & Jiang, N. (2022). Integrated proteomic and metabolomic profile analyses of cardiac valves revealed molecular mechanisms and targets in calcific aortic valve disease. *Front. Cardiovasc. Med.*, 1–15.
78. Fu, Zong-jie, Wang, Z., Xu, L., Chen, X., & Li, X. (2020). HIF-1α-BNIP3-mediated mitophagy in tubular cells protects against renal ischemia / reperfusion injury. *Redox Biology*, *36*, 101671.
79. Fu, Zurong, Li, F., Jia, L., Su, S., Wang, Y., Cai, Z., & Xiang, M. (2019). Histone deacetylase 6 reduction promotes aortic valve calcification via an endoplasmic reticulum stress-mediated osteogenic pathway. *The Journal of Thoracic and Cardiovascular Surgery*, *158*(2), 408-417.e2.
80. Fukuda, R., Zhang, H., Kim, J., Shimoda, L., & Dang, C. V. (2007). HIF-1 Regulates Cytochrome Oxidase Subunits to Optimize Efficiency of Respiration in Hypoxic Cells. *Cell*, (129), 111–122
81. Garaikoetxea, M., Mart, E., Navarro, A., Matilla, L., Fern, A., Arrieta, V., Jover, E & López-Andrés, N. (2022). Targeting Fatty Acid-Binding Protein 4 Improves Pathologic Features of Aortic Stenosis. *Int. J. Mol. Sci.*, *23*(8439), 1–15.
82. García-aguilar, A., & Cuezva, J. M. (2018). A Review of the Inhibition of the Mitochondrial ATP Synthase by IF1 in vivo:

Reprogramming Energy Metabolism and Inducing Mitohormesis. *Front. Physiol.*, *9*, 1–10.
83. García-rodríguez, C., Parra-izquierdo, I., & Castaños-mollor, I. (2018). Toll-Like Receptors , Inflammation , and Calcific Aortic Valve Disease. *Front. Physiol.*, *9*(March), 1–8.
84. Ge, T., Yang, J., Zhou, S., Wang, Y., Li, Y., & Tong, X. (2020). The Role of the Pentose Phosphate Pathway in Diabetes and Cancer. *Front. Endocrinol.*, *11*(June), 1–11.
85. Gee, T. W., Richards, J. M., Mahmut, A., & Butcher, J. T. (2021). Valve endothelial-interstitial interactions drive emergent complex calcific lesion formation in vitro. *Biomaterials*, *269*(20), 1–14.
86. Gerald Litwack. (2018). Chapter 4. Proteins. Non-essential aminoacid synthesis. In *Human Biochemistry* (pp. 63–93).
87. Gomes, A. P., Price, N. L., Ling, A. J. Y., Moslehi, J. J., Magdalene, K., Rajman, L., & Sinclair, D. A. (2013). Declining NAD+ induces a Pseudohypoxic state disrupting nuclear-mitochondrial communication during aging. *Cell*, *155*(7), 1624–1638.
88. Gomez-stallons, M. V., Wirrig-schwendeman, E. E., Hassel, K. R., Simon, J., & Yutzey, K. E. (2016). BMP signaling is required for aortic valve calcification. *Arterioscler*, *36*(7), 1398–1405.
89. Gonzalez, P. S., Prey, J. O., Cardaci, S., Barthet, V. J. A., Sakamaki, J., Beaumatin, F., & Ryan, K. M. (2018). Mannose impairs tumor growth and enhances chemoterapy. *Nature*, *563*, 719–722.
90. Gotoh, T., Kuroda, T., Yamasawa, M., Nishinaga, M., Mitsuhashi, T., Seino, Y., … Shimada, K. (1995). Correlation between lipoprotein(a) and aortic valve sclerosis assessed by echocardiography (the JMS Cardiac Echo and Cohort Study). *Am. J. Cardiol.*, *76*(12), 928–932.
91. Gough, D. J., Messina, N. L., Hii, L., Gould, J. A., Sabapathy, K., Ashley, P. S., & Ricky, W. (2010). Functional Crosstalk between Type I and II Interferon through the Regulated Expression of STAT1. *PLOS Biology*, *8*(4), 1–12.
92. Gould, R. A., & Butcher, J. T. (2010). Isolation of Valvular Endothelial Cells. *Journal of Visualized Experiments*, *46*, 6–10.
93. Greenberg, H. Z. E., Zhao, G., Shah, A. M., & Zhang, M. (2022). Role of oxidative stress in calcific aortic valve disease and its therapeutic implications. *European Society of Cardiology*, *118*, 1433–1451.
94. Gregory, C. A., Gunn, W. G., Peister, A., & Prockop, D. J. (2004). An Alizarin red-based assay of mineralization by adherent cells in culture : comparison with cetylpyridinium chloride extraction. *Analtical Biochemistry*, *329*, 77–84.
95. Greijer, A. E., & Wall, E. Van Der. (2004). The role of hypoxia inducible factor 1 (HIF-1) in hypoxia induced apoptosis. *Journal of Clinical Pathology*, *1*, 1009–1014.
96. Gu, X., & Masters, K. S. (2009). Role of the MAPK / ERK pathway in valvular interstitial cell calcification. *J Physiol Heart Physiol*, *10*(296), 1748–1757.
97. Guntur, A. R., Le, P. T., Farber, C. R., & Rosen, C. J. (2014). Bioenergetics during calvarial osteoblast differentiation reflect strain differences in bone mass. *Endocrinology*, *155*(5), 1589–1595.
98. Haanen, C., Steffens-nakken, H., & Reutelingsperger, C. (1995). A novel assay for apoptosis Flow cytometric detection of phosphatidylserine expression on early apoptotic cells using fluorescein labelled Annexin V. *Journal of Immunological Methods*, *184*(95), 39–51.
99. Haas, R., Smith, J., Rocher-ros, V., Nadkarni, S., & Montero-, T. (2015). Lactate Regulates Metabolic and Pro-inflammatory Circuits in Control of T Cell Migration and Effector Functions. *PLOS Biology*, *16*, 1–24.
100. Hamabe, A., Konno, M., Tanuma, N., Shima, H., & Tsunekuni, K. (2014). Role of pyruvate kinase M2 in transcriptional regulation leading to epithelial – mesenchymal transition. *Pnas*, *111*(43), 1–6.
101. Hamanaka, R. B., & Mutlu, G. M. (2021). Metabolic requirements of pulmonary fibrosis: role of fibroblast metabolism. *FEBS Journal*, *288*(22), 6331–6352.
102. Han, E. S., Wen, W., Dellinger, T. H., Wu, J., Lu, S. A., & Yim, J. H. (2018). Ruxolitinib synergistically enhances the anti-tumor activity of paclitaxel in human ovarian cancer. *Oncotarget*, *9*(36), 24304–24319.
103. He, P., Srikrishna, G., & Freeze, H. H. (2014). N-glycosylation deficiency reduces ICAM-1 induction and impairs in fl ammatory response. *Glycobiology*, *24*(4), 392–398.
104. Heather, L. C., Howell, N. J., Emmanuel, Y., Cole, M. A., Frenneaux, M. P., Pagano, D., & Clarke, K. (2011). Changes in cardiac substrate transporters and metabolic proteins mirror the metabolic shift in patients with aortic stenosis. *PLOS ONE*, *6*(10), 1–6.
105. Hilaire, C. S., Jansen, F., Goettsch, C., & Jansen, F. (2022). Editorial : Comorbidities and Aortic Valve Stenosis: Molecular Mechanism , Risk Factors and Novel Therapeutic Options. *Front. Cardiovasc. Med.*, *8*(January), 2021–2023.
106. Hill, B. G., Benavides, G. A., Jr, J. R. L., Ballinger, S., Italia, L. D., Zhang, J., & Darley-usmar, V. M. (2012). Integration of cellular bioenergetics with mitochondrial quality control and autophagy. *Biol. Chem.*, *393*(12), 1485–1512.
107. Hjortnaes, J., Butcher, J., Figueiredo, J. L., Riccio, M., Kohler, R. H., Kozloff, K. M., & Aikawa, E. (2010). Arterial and aortic valve calcification inversely correlates with osteoporotic bone remodelling: A role for inflammation. *Eur. Heart J.*, *31*(16), 1975–1984.
108. Zheng, K.H., Sotirios, T., Pawade, T., Kroon, J., Jenkins, W., Mhairi, D., White, A., Timmers, N., Hjortnaes, J., Rogers, M. A., Aikawa, E., & Arsenault, B. J. (2019). Lipoprotein(a) and Oxidized Phospholipids Promote Valve Calcification in Patients With Aortic Stenosis. *J. Am. Coll. Cardiol.*, *73*(17), 2150–2162.
109. Huang, Z., Xie, N., Illes, P., Virgilio, F. Di, Ulrich, H., Semyanov, A., & Tang, Y. (2021). From purines to purinergic signalling : molecular functions and human diseases. *Nature*, *6*(162), 1–19.
110. Iii, W. J. Q., Jiao, J., Teslaa, T., Wallace, D. C., Baur, J. A., Beier, U. H., & Beier, U. H. (2020). Lactate Limits T Cell Proliferation via the NAD (H) Redox State. *Cell reports*, *33*, 1–10.

BIBLIOGRAPHY

111. Isoda, K., Matsuki, T., Kondo, H., Iwakura, Y., & Ohsuzu, F. (2010). Deficiency of Interleukin-1 Receptor Antagonist Induces Aortic Valve Disease in BALB / c Mice. *Arterioescler. Thromb. Vasc. Biol.*, *28*, 708–715.
112. Ivashkiv, L. B. (2018). IFNγ: signalling, epigenetics and roles in immunity, metabolism, disease and cancer immunotherapy. *Nat. Rev.*, *18*(9), 545–558.
113. Ivashkiv, L. B., & Donlin, L. T. (2014). Regulation of type I interferon responses. *Nat. Rev. Immunol.*, *14*(1), 36–49.
114. Izquierdo-garcia, J. L., Liu, Y. Z., Li, Z. X., Zhang, L. L., & Wang, D. (2022). Phenotypic plasticity of vascular smooth muscle cells in vascular calcification : Role of mitochondria. *Front. Cardiovasc. Med.*, *9*, 1–16.
115. Judge, A., & Dodd, M. S. (2020). Metabolism. *Essays in Biochemistry*, *64*, 607–647.
116. Junco-vicente, A., Rodriguez, I., Solache-berrocal, G., Cigarran, H., & Martin, M. (2020). Válvula aórtica bicúspide :Revisión actualizada de sus aspectos clínicos y fisiopatológicos. *Archivos de Cardiologia de Mexico*, *90*(4), 520–528.
117. Kaden, J. J., Dempfle, C., Grobholz, R., Fischer, C. S., Vocke, D. C., Asl, V., & Borggrefe, M. (2005). Inflammatory regulation of extracellular matrix remodeling in calcific aortic valve stenosis B. *Cardiovasc. Pathol.*, *14*, 80–87.
118. Kaltoft, M., Langsted, A., & Nordestgaard, G. B. (2020). Obesity as a Causal Risk Factor for Aortic Valve Stenosis. *J. Am. Coll. Cardiol.*, *75*(2), 163–176.
119. Kang, W., Suzuki, M., Saito, T., & Miyado, K. (2021). Emerging Role of TCA Cycle-Related Enzymes in Human Diseases. *Int. J. Mol. Sci.*, *22*(13057), 1–14.
120. Katz, R., Wong, N. D., Kronmal, R., Takasu, J., Shavelle, D. M., Probstfield, J. L., & Brien, K. D. O. (2006). Features of the Metabolic Syndrome and Diabetes Mellitus as Predictors of Aortic Valve Calcification in the Multi-Ethnic Study of Atherosclerosis. *Circulation*., ;113, 2113-2119.
121. Kawasaki, T., & Kawai, T. (2014). Toll-like receptor signaling pathways. *Front. Immunol.*, *5*, 1–8.
122. Khurshed, M., Molenaar, R. J., Lenting, K., Leenders, W. P., & Noorden, C. J. F. Van. (2017). In silico gene expression analysis reveals glycolysis and acetate anaplerosis in IDH1 wild-type glioma and lactate and glutamate anaplerosis in IDH1 -mutated glioma. *Oncotarget*, *8*(30), 49165–49177.
123. Kiritsy, M. C., Mccann, K., Mott, D., Holland, S. M., Behar, S. M., Sassetti, C. M., & Olive, A. J. (2021). Mitochondrial respiration contributes to the interferon gamma response in antigen- - presenting cells. *Immunology and Inflammation*, *10*, 1–34.
124. Kodama, M., & Nakayama, K. I. (2020). A second Warburg-like effect in cancer metabolism: The metabolic shift of glutamine-derived nitrogen: A shift in glutamine-derived nitrogen metabolism from glutaminolysis to de novo nucleotide biosynthesis contributes to malignant evolution of cancer. *BioEssays*, *42*(12), 1–11.
125. Koh, M. Y., Spivak-Kroizman, T., Venturini, S., Welsh, S., Williams, R. R., Kirkpatrick, D. L., & Powis, G. (2008). Molecular mechanisms for the activity of PX-478, an antitumor inhibitor of the hypoxia-inducible factor-1α. *Mol. Cancer Ther.*, *7*(1), 90–100.
126. Kolwicz, S. C., & Tian, R. (2011). Glucose metabolism and cardiac hypertrophy. *Cardiovasc. Res.*, *90*, 194–201.
127. Kong, W. K. F., Bax, J. J., Michelena, H. I., & Delgado, V. (2020). Sex differences in bicuspid aortic valve disease. *Progress in Cardiovascular Diseases*, *63*(4), 452–456.
128. Kotenko, S. V., & Durbin, J. E. (2017). Contribution of type III interferons to antiviral immunity: Location, location, location. *Journal of Biol. Chem.*, *292*(18), 7295–7303.
129. Kozlov, A. M., Lone, A., Betts, D. H., & Cumming, R. C. (2020). Lactate preconditioning promotes a HIF-1 α -mediated metabolic shift from OXPHOS to glycolysis in normal human diploid fibroblasts. *Scientific reports*, *20*(8388), 1–16.
130. Krawczyk, C. M., Holowka, T., Sun, J., Blagih, J., Amiel, E., Deberardinis, R. J., & Pearce, E. J. (2021). Toll-like receptor-induced changes in glycolytic metabolism regulate dendritic cell activation. *Blood J.*, *115*, 4742–4749.
131. Krüger, A., Grüning, N. M., Wamelink, M. M. C., Kerick, M., Kirpy, A., Parkhomchuk, D., & Ralser, M. (2011). The pentose phosphate pathway is a metabolic redox sensor and regulates transcription during the antioxidant response. *Antioxid. Redox Signal.*, *15*(2), 311–324.
132. Kuhn, A., & Van Bilsen, M. (2022). Oncometabolism : A Paradigm for the Metabolic Remodeling of the Failing Heart. *Int. J. Mol. Sci.*, *23*(13902), 1–25.
133. Kunz, W. S. (2003). Different metabolic properties of mitochondrial oxidative phosphorylation in different cell types – important implications for mitochondrial cytopathies. *Experimental Physiology*, *88*(1), 149–154.
134. Kurte, M., Vega-letter, A. M., Luz-crawford, P., Djouad, F., & Noël, D. (2020). Time-dependent LPS exposure commands MSC immunoplasticity through TLR4 activation leading to opposite therapeutic outcome in EAE. *Stem Cell Res. Ther.*, *11*(416), 1–14.
135. Kurtoglu, M., Maher, J. C., & Lampidis, T. J. (2007). Differential toxic mechanisms of 2-Deoxy-D-Glucose verus 1-Fluorodeoxy-D-Glucose in hypoxic and normoxi tumor cells, *9*(9).
136. Lachmandas, E., Boutens, L., Ratter, J. M., Hijmans, A., Hooiveld, G. J., Joosten, L. A. B., & Stienstra, R. (2017). Microbial stimulation of different Toll-like receptor signalling pathways induces diverse metabolic programmes in human monocytes. *Nature Microbiology*, *2*(16246), 1–10.
137. Laemmli, U. (1970). Cleavage of Structural Proteins during the Assembly of the Head of Bacteriophage T4. *Nature*, *227*(15).
138. Langston, P. K., Nambu, A., Jung, J., Shibata, M., Aksoylar, H. I., Lei, J., & Horng, T. (2019). Glycerol phosphate shuttle enzyme GPD2 regulates macrophage inflammatory responses. *Nat. Immunol.*, *20*, 1186–1195.

139. Latif, N., Quillon, A., Sarathchandra, P., & Mccormack, A. (2015). Modulation of Human Valve Interstitial Cell Phenotype and Function Using a Fibroblast Growth Factor 2 Formulation. *PLOS ONE*, 1–19.
140. Lebedeva, E., Bagaev, A., Pichugin, A., Chulkina, M., Lysenko, A., Tutykhina, I., & Ataullakhanov, R. (2018). The differences in immunoadjuvant mechanisms of TLR3 and TLR4 agonists on the level of antigen-presenting cells during immunization with recombinant adenovirus vector. *BMC Immunol.*, *19*(26), 1–14.
141. Lee, S. J., Lee, I., & Jeon, J. (2020). Vascular Calcification — New Insights into Its Mechanism. *Int. J. Mol. Sci.*, *21*(2685), 1–32.
142. Lehti, T. E., Knuutila, H. Ö. M., Karppinen, H. K. H., & Strandberg, R. T. T. (2021). Symptom burden in community - dwelling older people : temporal trends in the Helsinki Aging Study. *Aging Clin. Exp. Res.*, *33*(11), 3065–3071.
143. Leung, E., Cairns, R. A., Chaudary, N., Vellanki, R. N., Kalliomaki, T., Moriyama, E. H., & Milosevic, M. (2017). Metabolic targeting of HIF-dependent glycolysis reduces lactate , increases oxygen consumption and enhances response to high-dose single-fraction radiotherapy in hypoxic solid tumors. *BMC Cancer, 17(418),* 1–12.
144. Li, A., Gao, M., Liu, B., Qin, Y., Liu, H., Wu, H., & Gong, G. (2022). Mitochondrial autophagy: molecular mechanisms and implications for cardiovascular disease. *CDD Press*, 1–15.
145. Li, H., Wu, X., Xu, A., & Hoo, R. L. (2021). A-FABP in Metabolic Diseases and the Therapeutic Implications : An Update. *Int. J. Mol. Sci.*, *22*(9386), 1–22.
146. Li, J., Lin, Q., Shao, X., Li, S., Zhu, X., Wu, J., & Zhang, M. (2023). HIF1α-BNIP3-mediated mitophagy protects against renal fibrosis by decreasing ROS and inhibiting activation of the NLRP3 inflammasome. *Nature*, *14*(200), 1–12.
147. Li, Xinyu, Zhang, W., Cao, Q., Wang, Z., Zhao, M., Xu, L., & Zhuang, Q. (2020). Mitochondrial dysfunction in fibrotic diseases. *Cell Death Discov.*, *6*(80), 1–14.
148. Li, Y., Lui, K. O., & Zhou, B. (2018). Reassessing endothelial-to-mesenchymal transition in cardiovascular diseases. *Nat. Rev. Cardiol.*, *15*, 445–456.
149. Liao, Y.-C., Lim, Y. S., Chu, P.-W., & Chen, S. (2023). Inflammatory Milieu Induces Mitochondrial Alterations and Neuronal Activations in Hypothalamic POMC Neurons in a Time-Dependent Manner. *Mol. Neurobiol.*, *60*, 1164–1178.
150. Liberti, M. V, Locasale, J. W., Biology, C., & Biology, C. (2016). The Warburg Effect : How Does it Benefit Cancer Cells ? *Trends Biochem.Sci.*, *41*(3), 211–218.
151. Lin, Z., Miao, J., Zhang, T., He, M., Zhou, X., Zhang, H., & Bai, L. (2021). D -Mannose suppresses osteoarthritis development in vivo and delays IL-1 β -induced degeneration in vitro by enhancing autophagy activated via the AMPK pathway. *Biomedicine & Pharmacotherapy*, *135*, 1–11.
152. Linefsky, J. P., OBrien, K. D., Katz, R., De Boer, I. H., Barasch, E., Jenny, N. S., & Kestenbaum, B. (2011). Association of serum phosphate levels with aortic valve sclerosis and annular calcification. *J. Am. Coll. Cardiol.*, *58*(3), 938-947.
153. Liu, H., Yin, H., Wang, Z., Yuan, Q., Xu, F., Chen, Y., & Li, C. (2023). Rho A/ROCK1 signaling-mediated metabolic reprogramming of valvular interstitial cells toward Warburg effect accelerates aortic valve calci fi cation via AMPK/RUNX2 axis. *Cell Death and Dis. 14*(108), 1–17.
154. López, J., Fernández-pisonero, I., Dueñas, A. I., Maeso, P., San, J. A., Sánchez, M., & García-rodríguez, C. (2012). Viral and bacterial patterns induce TLR-mediated sustained in fl ammation and calci fi cation in aortic valve interstitial cells. Int. J. Cardiol., *158*, 18–25.
155. Lu, Z., Chiu, J., Lee, L. R., Schindeler, A., Jackson, M., Ramaswamy, Y., & Zreiqat, H. (2019). Reprogramming of human fibroblasts into osteoblasts by insulin-like growth factor-binding protein 7. *Tissue eng. and Regenerative Medicine*, *9*, 403–415.
156. Ma, W., Sun, X.-J., & Liu, N.-F. (2020). PDK4 promotes vascular calcification by interfering with autophagic activity and metabolic reprogramming. *Cell Death and Dis.*, *11*(991), 1–23.
157. Mahler, G. J., Farrar, E. J., & Buther, J. T. (2008). Inflammatory cytokines promote mesenchymal transformation in embryonic and adult valve endothelial cells. *Aterioscler. Thromb. Vasc. Biol.*, *23*(1), 1–7.
158. Majmundar, A. J., Wong, W. J., & Simon, M. C. (2010). Hypoxia-Inducible Factors and the Response to Hypoxic Stress. *Mol. Cell.*, *40*(2), 294–309.
159. Mancebo, C., Fernandez, J. J., Herrero-Sanchez, C., Alvarez, Y., Alonso, S., Sandoval, T. A., & Sanchez-Crespo, M. (2022). Fungal Patterns Induce Cytokine Expression through Fluxes of Metabolic Intermediates That Support Glycolysis and Oxidative Phosphorylation. *J. Immunol.*, *208*(12), 2779–2794.
160. Manduteanu, I., Popov, D., Radu, A., & Simionescu, M. (1988). Calf Cardiac Valvular Endothelial Cells in Culture: Production of Glycosaminoglycans , Prostacyclin and Fibronectin Cell isolation At confluency , the cells were detached by a Cell growth To assess the growth of VEC , duplicate cul- Cell culture Cell-con. *J. Mol. Cell. Cardiol.*, *118*, 103–118.
161. Martínez-reyes, I., & Chandel, N. S. (2020). Mitochondrial TCA cycle metabolites control physiology and disease. *Nature Communications*, *11*(102), 1–11.
162. Mason, E. F., & Rathmell, J. C. (2011). Cell metabolism: An essential link between growth and apoptosis. *BBA - Mol. Cell. Research*, *1813*(4), 645–654.
163. Masoud, G. N., & Li, W. (2015). HIF-1α pathway: Role, regulation and intervention for cancer therapy. *Acta Pharm. Sin. B B*, *5*(5), 378–389.
164. Mathieu, P., Bouchareb, R., & Boulanger, M. (2015). Innate and Adaptive Immunity in Calcific Aortic Valve Disease. *J. Immunol. Res.*, *20*, 1–11.

BIBLIOGRAPHY

165. Matoba, S., Kang, J.-G., Patino, W. D., Wragg, A., Boehm, M., Gavilova, O., & Hwang, P. M. (2006). p53 Regulates Mitochondrial Respiration. *Science*, *312*, 1650–1653.
166. Meng, X., Ao, L., Song, Y., Babu, A., Yang, X., Wang, M., & Fullerton, D. A. (2008). Expression of functional Toll-like receptors 2 and 4 in human aortic valve interstitial cells: Potential roles in aortic valve inflammation and stenosis. *American Journal of Physiology - Cell Physiology*, *294*(1), 29–35.
167. Michl, B. Y. J., Ohlbaum, D. J., & Silverstein, S. C. (1976). 2-Deoxyglucose selectively inhibits Fc and complement receptor-mediated phagocytosis in mouse peritoneal macrophages. *J. exp. med.*, *144*, 1484–1493.
168. Miller, J. D., Chu, Y., Brooks, R. M., Richenbacher, W. E., Peña-silva, R., & Heistad, D. D. (2008). Dysregulation of Antioxidant Mechanisms Contributes to Increased Oxidative Stress in Calcific Aortic Valvular Stenosis in Humans. *J. Am. Coll. Cardiol.*, *52*(10), 1–8.
169. Miller, J. D., Weiss, R. M., & Heistad, D. D. (2011). Calcific aortic valve stenosis: methods, models and mechanisms. *Circ. Res.*, *108*(11), 319–356.
170. Mills, E. L., Kelly, B., Logan, A., Costa, A. S. H., Varma, M., Bryant, C. E., & O'Neill, L. A. (2016). Succinate Dehydrogenase Supports Metabolic Repurposing of Mitochondria to Drive Inflammatory Macrophages. *Cell*, *167*(2), 457-470.e13.
171. Mohty, D., Pibarot, P., Despre, J., Co, C., Arsenault, B., Cosnay, P., … Mathieu, P. (2007). Association Between Plasma LDL Particle Size , Valvular Accumulation of Oxidized LDL , and Inflammation in Patients With Aortic Stenosis. *Arterioescler. Thromb. Vasc. Biol.*, 187–193.
172. Molavian, H. R., Kohandel, M., & Sivaloganathan, S. (2016). High Concentrations of H2O2 Make Aerobic Glycolysis Energetically More Favorable for Cellular Respiration. *Front. Physiol.*, *7*(August), 1–6.
173. Moncla, L. M., Briend, M., Bossé, Y., & Mathieu, P. (2023). Calcific aortic valve disease: mechanisms, prevention and treatment. *Nat. Rev.*, *20*, 546–559.
174. Monga, S., Valkovic, L., Tyler, D., Lygate, C. A., Rider, O., Myerson, S. G., & Mahmod, M. (2022). Insights Into the Metabolic Aspects of Aortic Stenosis With the Use of Magnetic Resonance Imaging. *JACC-Cardiovasc. Imag.*, *15*(12), 2022.
175. Montes-sánchez, D., Ventura, J. L., Mitre, I., Frías, S., Michán, L., Espejel-nuñez, A., & Zentella, A. (2009). Glycosylated VCAM-1 isoforms revealed in 2D western blots of HUVECs treated with tumoral soluble factors of breast cancer cells. *BMC Chemical Biology*, *13*, 1–13.
176. Moorhead III, W. J., Chu, C. C., Cuevas, R. A., Iv, J. C., Wong, R., Regan, C., & Hilaire, C. S. (2020). Dysregulation of FOXO1 Drives Calcification in Arterial Calcification due to Deficiency of CD73 and Is Present in Peripheral Artery Disease. *Arterioescler. Thromb. Vasc. Biol.*, *40*(July), 1680–1694.
177. Myasoedova, V. A., Ravani, A. L., Frigerio, B., Valerio, V., Moschetta, D., Songia, P., & Poggio, P. (2018). Novel pharmacological targets for calci fi c aortic valve disease : Prevention and treatments. *Pharmacol. Res., 136*(August), 74–82.
178. Mycielska, M. E., Dettmer, K., Petra, R., Prehn, C., Milenkovic, V. M., Jagla, W., & Geissler, E. K. (2018). Extracellular Citrate Affects Critical Elements of Cancer Cell Metabolism and Supports Cancer Development In Vivo. *Met. Chem. Biol., 18*, 2513–2523.
179. Nagy, E., Anderson, D. C., Caidahl, K., Eriksson, M. J., Eriksson, P., Franco-Cereceda, A., & BäcK, M. (2011). Upregulation of the 5-Lipoxygenase Pathway in Human Aortic Valves Correlates With Severity of Stenosis and Leads to Leukotriene-Induced Effects on Valvular Myofibroblasts. *Circulation*, *98*, 1316–1325.
180. Nagy, E., Lei, Y., Martínez-martínez, E., Body, S. C., Schlotter, F., Creager, M., & Aikawa, E. (2017). Interferon- g Released by Activated CD8 D T Lymphocytes Impairs the Calcium Resorption Potential of Osteoclasts in Calci fi ed Human Aortic Valves. *The Am. J. Pathol.*, *187*(6), 1413–1425.
181. Nakano, K., Inaba, H., Nomura, R., Nemoto, H., Takeda, M., Yoshioka, H., & Ooshima, T. (2006). Detection of Cariogenic Streptococcus mutans in Extirpated Heart Valve and Atheromatous Plaque Specimens. *J. Clin. Microbiol.*, *44*(9), 3313–3317.
182. Nanayakkara, G. K., Wang, H., & Yang, X. (2019). Proton leak regulates mitochondrial reactive oxygen species generation in endothelial cell activation and inflammation- A novel concept. *Arch. Biochem. Biophys.*, *662*, 68–74.
183. Narasimhan, M., & Rajasekaran, N. S. (2015). Reductive potential-A savior turns stressor in protein aggregation cardiomyopathy. *Biochim. Biophys. Acta-Mol. Basis Dis.*, *1852*(1), 53–60.
184. Navarro, M.N., de las Heras, M.M., & Mittelbrunn, M. (2021). Nicotinamide adenine dinucleotide metabolism in the immune response, autoimmunity and inflammageing. *Br. J. Pharmacol.* (179), 1839-1856.
185. New, S. E. ., & Aikawa, E. (2011). Molecular insights into early inflammatory stages of arterial and aortic valve calcification. *Circ. Res.*, *108*(11), 1381–1391.
186. Nicholls, D. G., & Ward, M. W. (2000). Mitochondrial membrane potential and neuronal glutamate excitotoxicity : mortality and millivolts. *Trend Neurosci.*, *23*(4), 166–174.
187. Niessner, A., Shin, M. S., Pryshchep, O., Goronzy, J. J., Chaikof, E. L., & Weyand, C. M. (2007). Synergistic Proinflammatory Effects of the Antiviral Ligands in the Atherosclerotic Plaque. *Circulation*, *116*, 2043–2052.
188. Nkomo, V. T., Gardin, J. M., Skelton, T. N., Gottdiener, J. S., Scott, C. G., & Enriquez-Sarano, M. (2006). Burden of valvular heart diseases: a population-based study. *Lancet*, *368*(9540), 1005–1011.
189. Nonaka, K., Kume, N., Urata, Y., Seto, S., Kohno, T., Honda, S., & Kondo, T. (2007). Serum Levels of S-Glutathionylated Proteins as a Risk-Marker for Arteriosclerosis Obliterans. *Circ. J., 71*(January), 100–105.

190. Nsaibia, M. J., Devendran, A., Goubaa, E., Bouitbir, J., Capoulade, R., & Bouchareb, R. (2022). Implication of Lipids in Calcified Aortic Valve Pathogenesis : Why Did Statins Fail ? *J. Clin. Med.*, *11*(3331), 1–13.
191. O'Neil, L. A., & Hardie, D. G. (2013). Metabolism of inflammation limited by AMPK and pseudo-starvation. *Nature*, *493*, 346–355.
192. Owens, D. S., Katz, R., Takasu, J., Kronmal, R., Budoff, M. J., & Brien, K. D. O. (2010). Incidence and Progression of Aortic Valve Calcium in the Multi-Ethnic Study of Atherosclerosis (MESA). *Am. J. Cardiol*, *105*(5), 701–708.
193. Paik, J., Jung, K., Lee, J., Park, J., & Lee, K. (2017). Reactive oxygen species-driven HIF1α triggers accelerated glycolysis in endothelial cells exposed to low oxygen tension ☆. *Nuclear Medicine and Biology*, *45*, 8–14.
194. Palsson-mcdermott, E. M., Curtis, A. M., Goel, G., Lauterbach, M. A. R., Sheedy, F. J., Gleeson, L. E., & Neill, L. A. J. O. (2015). Pyruvate Kinase M2 Regulates Hif-1a Activity and IL-1 b Induction and Is a Critical Determinant of the Warburg Effect in LPS-Activated Macrophages. *Cell metab.*, *21*(1), 65–80.
195. Parra-izquierdo, I., Castaños-mollor, I., López, J., Gómez, C., Román, J. A. S., Crespo, M. S., & García-rodríguez, C. (2018). Calcification Induced by Type I Interferon in Human Aortic Valve Interstitial Cells Is Larger in Males and Blunted by a Janus Kinase Inhibitor. *Arterioescler. Thromb. Vasc. Biol.*, 1–12.
196. Parra-izquierdo, I., Castaños-mollor, I., López, J., Gómez, C., San Roman, J. A., Sanchez-Crespo, M., & García-Rodríguez, C. (2019). Lipopolysaccharide and interferon-γ team up to activate HIF-1α via STAT1 in normoxia and exhibit sex differences in human aortic valve interstitial cells. *Biochim. Biophys. Acta-Mol. Basis Dis.*, *1865*, 2168–2179.
197. Parra-izquierdo, I., Sánchez-Bayuela, T., Castaños-Mollor, I., López, J., Gómez, C., San Román, A. J., & García-Rodríguez, C. (2021). Clinically used JAK inhibitor blunts dsRNA-induced inflammation and calcification in aortic valve interstitial cells. *The FEBS J.*, *10*, 1–15.
198. Parra-Izquierdo, I., Sánchez-Bayuela, T., López, J., Gómez, C., Pérez-Riesgo, E., San Román, J. A., & García Rodríguez, C. (2021). Interferons Are Pro-Inflammatory Cytokines in Sheared-Stressed Human Aortic Valve Endothelial Cells. *Int. J. Mol. Sci.*, *22*(10605), 1–22.
199. Pawade, T. A., Newby, D. E., & Dweck, M. R. (2015). Calcification in aortic stenosis: The skeleton key. *J. Am. Coll. Cardiol.*, *66*(5), 561–577.
200. Pearce, E. L., & Pearce, E. J. (2013). Metabolic Pathways in Immune Cell Activation and Quiescence. *Immunity*, *38*(4), 633–643.
201. Peltier, M., Trojette, F., Sarano, M. E., Grigioni, F., Slama, M. A., & Tribouilloy, C. M. (2003). Relation between cardiovascular risk factors and nonrheumatic severe calcific aortic stenosis among patients with a three-cuspid aortic valve. *Am. J. Cardiol.*, *91*(1), 97–99.
202. Perrotta, I., Moraca, F. M., Sciangula, A., Aquila, S., & Mazzulla, S. (2015). HIF-1 a and VEGF : Immunohistochemical Profile and Possible Function in Human Aortic Valve Stenosis. *Ultrastructural Pathology*, *00*(00), 1–9.
203. Pfleger, J., He, M., & Abdellatif, M. (2015). Mitochondrial complex II is a source of the reserve respiratory capacity that is regulated by metabolic sensors and promotes cell survival. *Cell Death and Dis..*, *6*, 1–14.
204. Piacenza, L., Trujillo, M., & Radi, R. (2019). Reactive species and pathogen antioxidant networks during phagocytosis. *Journal of Experimental Medicine*, *216*(3), 501–516.
205. Plosker, G. L. (2015). Ruxolitinib : A Review of Its Use in Patients with Myelofibrosis. *Drugs*, *15*, 1–12.
206. Pollock JD, Makaryus AN. Physiology, Cardiac Cycle. [Updated 2022 Oct 3]. In: StatPearls [Internet]. Treasure Island (FL): StatPearls Publishing; 2023 Jan-. Available from: https://www.ncbi.nlm.nih.gov/books/NBK459327/.
207. Porras, A. M., Engeland, N. C. A. Van, Marchbanks, E., Mccormack, A., Bouten, C. V. C., Magdi, H., & Masters, K. S. (2017). Robust Generation of Quiescent Porcine Valvular Interstitial Cell. *J. Am. Heart Assoc.*, *6*, 1–14.
208. Prange, K. H. M., Lutgens, E., Winther, M. P. J. De, Baardman, J., Verberk, S. G. S., Prange, K. H. M., & Velden, S. Van Der. (2018). A Defective Pentose Phosphate Pathway Reduces Inflammatory Macrophage Responses during Hypercholesterolemia. *Cell reports*, *25*, 2044–2052.
209. Puckett, D. L., Alquraishi, M., Chowanadisai, W., & Bettaieb, A. (2021). The Role of PKM2 in Metabolic Reprogramming : Insights into the Regulatory Roles of Non-Coding RNAs. *Int. J. Mol. Sci.*, *22*, 1–55.
210. Qiao, Y. (2022). Reactive Oxygen Species in Cardiovascular Calcification : Role of Medicinal Plants. *Front. Pharmacol.*, *13*, 1–6.
211. Raddatz, X. M. A., Madhur, M. S., & Merryman, X. W. D. (2019). Adaptive Immunity in Cardiovascular Disease Adaptive immune cells in calcific aortic valve disease. *Am J Physiol Cell Physiol*, *317*, 141–155.
212. Raineri, I., Epstein, L. B., & Geigy, C. (1995). Superoxide Radical and Iron Modulate Aconitase Activity in Mammalian Cells *. *J. Biol. Chem*, *270*(22), 13399–13405.
213. Rajamannan, N. M., Evans, F. J., Aikawa, E., Grande-Allen, K. J., Demer, L. L., Heistad, D. D., & Otto, C. M. (2011). Calcific Aortic Valve Disease: Not Simply a Degenerative Process. *Circulation*, *124*(16), 1783–1791.
214. Rajamannan, N. M., Subramaniam, M., Rickard, D., Stuart, R., Donovan, J., Springett, M., & Spelsberg, T. (2014). Human aortic valve calcification is associated with an osteoblast phenotype. *Circulation*, *107*(17), 2181–2184.
215. Rasheed, Z., & Haqqi, T. M. (2012). Endoplasmic reticulum stress induces the expression of COX-2 through activation of eIF2 α , p38-MAPK and NF- κ B in advanced glycation end products stimulated human chondrocytes. *BBA - Mol. Cell. Res.*, *1823*(12), 2179–2189.
216. Rattazzi, M., Bertacco, E., Del Vecchio, A., Puato, M., Faggin, E., & Pauletto, P. (2013). Aortic valve calcification in chronic

kidney disease. *Nephrol. Dial. Transplant.*, *28*(12), 2968–2976.
217. Redza-dutordoir, M., & Averill-bates, D. A. (2016). Activation of apoptosis signalling pathways by reactive oxygen species. *BBA - Mol. Cell. Research*, *1863*(12), 2977–2992.
218. Romero, N., Swain, P., Neilson, A., Dranka, B. P., & Ave, H. (2017). Improving Quantification of Cellular Glycolytic Rate Using Agilent Seahorse XF Technology White Paper. *White Paper*.
219. Rutkovskiy, A., Malashicheva, A., Sullivan, G., Bogdanova, M., Kostareva, A., Fiane, A., & Vaage, J. (2017). Valve Interstitial Cells : The Key to Understanding the Pathophysiology. *J. Am. Heart Assoc.*, 1–23.
220. Saleme, B., Gurtu, V., Zhang, Y., Kinnaird, A., Boukouris, A. E., Gopal, K., & Sutendra, G. (2019). Tissue-specific regulation of p53 by PKM2 is redox dependent and provides a therapeutic target for anthracycline-induced cardiotoxicity. *Sci. Transl. Med*, *11*, 1–12.
221. Schafer, F. Q., & Buettner, G. R. (2001). Redox environment of the cell as viewed through the redox state of the glutathione disulfide/glutathione couple. *Free Radic. Biol. Med.*, *30*(11), 1191–1212.
222. Schindler, C., Levy, D. E., & Decker, T. (2007). JAK-STAT Signaling : From Interferons to Cytokines *. *J. Biol. Chem.*, *282*(28), 20059–20063.
223. Schlotter, F., Halu, A., Goto, S., Blaser, M. C., Body, S. C., Lee, L. H., & Aikawa, E. (2018). Spatiotemporal Multi-omics Mapping Generates a Molecular Atlas of the Aortic Valve and Reveals Networks Driving Disease. *Circulation*, *138*(4), 377–393.
224. Seim, G. L., Britt, E. C., John, S. V, Yeo, F. J., Johnson, A. R., Eisenstein, R. S., & Fan, J. (2019). Two-stage metabolic remodelling in macrophages in response to LPS and IFNg stimulatio. *Nat. Met.*, *1*, 731–742.
225. Selig, J. I., Ouwens, D. M., Raschke, S., Thoresen, G. H., Fischer, J. W., Lichtenberg, A., & Barth, M. (2019). Impact of hyperinsulinemia and hyperglycemia on valvular interstitial cells – A link between aortic heart valve degeneration and type 2 diabetes. *BBA- Mol. Bas. Dis.*, *1865*(9), 2526–2537.
226. Semenza, G. L. (2011). HIF-1 : upstream and downstream of cancer metabolism. *Curr. Opin. Genet., Dec*, *20*(1), 1–10.
227. Sengupta, S., Wang, H., Yang, C., Szczesny, B., & Hegde, M. L. (2020). Ligand-induced gene activation is associated with oxidative genome damage whose repair is required for transcription. *PNAS*, *117*(36), 22183–22192.
228. Setten, E., Castagna, A., Nava-sedeño, J. M., Weber, J., Carriero, R., Reppas, A., & Volk, V. (2022). Understanding fibrosis pathogenesis via modeling macrophage- fibroblast interplay in immune-metabolic context. *Nat. Commun.*, *13*, 1–22.
229. Shen, W., Zhou, J., Wang, C., Xu, G., Wu, Y., & Hu, Z. (2017). High mobility group box 1 induces calcifcation of aortic valve interstitial cells via toll-like receptor 4. *Mol. Med. Reports*, *15*(5), 2530–2536.
230. Shi, L., & Tu, B. P. (2015). Acetyl-CoA and the regulation of metabolism: Mechanisms and Consequences. *Curr. Opin. Cell. Biol.*, *33*, 125–131.
231. Shiratori, R., Furuichi, K., Yamaguchi, M., Miyazaki, N., & Aoki, H. (2019). Glycolytic suppression dramatically changes the intracellular metabolic profile of multiple cancer cell lines in a mitochondrial metabolism- dependent manner. *Scientific reports*, *9*(18699), 1–15.
232. Sider, K. L., Blaser, M. C., & Simmons, C. A. (2011). Animal Models of Calcific Aortic Valve Disease. *Int. J. Inflamm. 2011*, 1–18.
233. Silva-Nunes, J.P., Andrieux, P., Brochet, P., Almeida, R. R., Vieira, R. D. S., & Bydlowski, S. P. (2021). Co-Exposure of Cardiomyocytes to IFN- g and TNF- a Induces Mitochondrial Dysfunction and Nitro- Oxidative Stress : Implications for the Pathogenesis of Chronic Chagas Disease Cardiomyopathy. *Front. Immunol.*, *12*(November), 1–19.
234. Singleton, E. B., & Merten, D. F. (1973). An Unusual Syndrome of Widened Medullary Cavities of the Metacarpals and Phalanges , Aortic Calcification and Abnormal Dentition. *Pediatric Radiology*, *7*, 2–7.
235. Smith, E. R., & Hewitson, T. D. (2020). TGF-β 1 is a regulator of the pyruvate dehydrogenase complex in fibroblasts. *Scientific reports*, *10*(17914), 1–14.
236. Song, R., Fullerton, D. A., Ao, L., Zhao, K., & Meng, X. (2017). An epigenetic regulatory loop controls pro-osteogenic activation by TGF- ᴺ 1 or bone morphogenetic protein 2 in human aortic valve interstitial cells. *J. Biol. Chem*, *292*(21), 8657–8666.
237. Spadaccio, C., Mozetic, P., Nappi, F., Nenna, A., Sutherland, F., Trombetta, M., & Rainer, A. (2016). Cells and extracellular matrix interplay in cardiac valve disease: because age matters. *Basic Res. Cardiol.*, *111*(2), 1–22.
238. Sriskanthadevan, S., Jeyaraju, D. V, Chung, T. E., Prabha, S., Xu, W., Skrtic, M., & Schimmer, A. D. (2016). AML cells have low spare reserve capacity in their respiratory chain that renders them susceptible to oxidative metabolic stress. *Blood J.*, *125*(13), 2120–2131.
239. Stincone, A., Prigione, A., Cramer, T., Wamelink, M. M., Campbell, K., Cheung, E., & Ralser, M. (2015). The return of metabolism: biochemistry and physiology of the pentose phosphate pathway. *Biol. Rec. Chamb. Philos Soc.*, *90*(3), 927–963.
240. Sullivan, P. G., Dubé, C., Dorenbos, K., Steward, O., & Baram, T. Z. (2003). Mitochondrial uncoupling protein-2 protects the immature brain from excitotoxic neuronal death. *Ann. Neurol.*, *53*(6), 711–717.
241. Surendran, A., Edel, A., Chandran, M., Bogaert, P., Hassa-Tash, P., Asokan, A. K.,& Ravandi, A. (2020). Metabolomic Signature of Human Aortic Valve Stenosis. *JACC-Basic Transl. Sci*., *5*(12).
242. Tabas, I., Tall, A., & Accili, D. (2010). The Impact of Macrophage Insulin Resistance on Advanced Atherosclerotic Plaque

Progression. *Circ. Res.*, *106*, 58–67.
243. Tannahill, G. M., Curtis, A. M., Adamik, J., Palsson-Mcdermott, E. M., McGettrick, A. F., Goel, G., & O'Neill, L. A. J. (2013). Succinate is an inflammatory signal that induces IL-1β through HIF-1α. *Nature*, *496*(7444), 238–242.
244. Tarbell, J. M., Shi, Z.-D., Dunn, J., & Jo, H. (2014). Fluid Mechanics, Arterial Disease, and Gene Expression. *Annu. Rev. Fluid Mech.*, *46*, 591–614.
245. Tastet, L., Capoulade, R., Clavel, M., Dahou, A., Arsenault, M., Mathieu, P., & Pibarot, P. (2017). Systolic hypertension and progression of aortic valve calcification in patients with aortic stenosis : results from the PROGRESSA study. *Eur. Heart J.*, *18*, 70–78.
246. Taylor, P. M., Allen, S., & Yacoub, M. H. (2000). Phenotypic and functional characterization of interstitial cells from human heart valves, pericardium and skin. *J. Heart Valve Dis.*, *9*(1), 150–158.
247. Tong, X., Zhao, F., & Thompson, C. B. (2009). The molecular determinants of de novo nucleotide biosynthesis in cancer cells. *Curr. Opin. Genet. Dev.*, *19*(1), 32–37.
248. Torre, M., Hwang, D. H., Padera, R. F., Mitchell, R. N., & Vanderlaan, P. A. (2016). Osseous and chondromatous metaplasia in calci fi c aortic valve stenosis. *Cardiovasc. Pathol.*, *25*(1), 18–24.
249. Towler, D. A. (2013). Molecular and cellular aspects of calcific aortic valve disease. *Circ. Res.*, *23*, 198–208.
250. Tu, J. V., Chu, A., Donovan, L. R., Ko, D. T., Booth, G. L., Tu, K., & Stukel, T. A. (2015). The Cardiovascular Health in Ambulatory Care Research Team (CANHEART): Using Big Data to Measure and Improve Cardiovascular Health and Healthcare Services. *Circulation: Cardiovascular Quality and Outcomes*, *8*(2), 204–212.
251. Vahanian, A., Beyersdorf, F., Praz, F., Milojevic, M., Baldus, S., Bauersachs, J., & Wokakowski, W. (2022). Guidelines for the management of valvular heart disease. *Eur. Heart J.*, *43*, 561–632.
252. Vaupel, P., Schmidberger, H., & Mayer, A. (2019). The warburg effect: essential part of metabolic reprogramming and central contributor to cancer progression. *Int. J. Radiat. Biol.*
253. Vazquez, F., Lim, J., Chim, H., Bhalla, K., Girnun, G., Pierce, K., & Puigserver, P. (2013). PGC1 a Expression Defines a Subset of Human Melanoma Tumors with Increased Mitochondrial Capacity and Resistance to Oxidative Stress. *Cancer Cell*, *23*(3), 287–301.
254. Venardos, N., Bennett, D., Weyant, M. J., Reece, B., Meng, X., & Fullerton, D. A. (2015). Matrix Gla Protein Regulates Calcification of the Aortic Valve. *J. Surg. Res.*, *199*(1), 1–6.
255. Vercellino, I., & Sazanov, L. A. (2022). The assembly , regulation and function of the mitochondrial respiratory chain. *Nat. Rev.*, *23*, 141–161.
256. Villa-Bellosta, R., & Hamczyk, M. R. (2015). Isolation and Culture of Aortic Smooth Muscle Cells and In Vitro Calcification Assay. *Methods Mol. Biol.*, *1339*, 119–129.
257. Vogt, C., Yki-jarvinen, H., Iozzo, P., Pipek, R., Pendergrass, M., Koval, J., & Pi, R. (1998). Effects of Insulin on Subcellular Localization of Hexokinase II in Human Skeletal Muscle in Vivo *. *J. Clin. End. Met.*, *83*(1), 230–234.
258. Wada, T., Nakashima, T., Hiroshi, N., & Penninger, J. M. (2006). RANKL-RANK signaling in osteoclastogenesis and bone disease. *Trends in Mol. Med.*, *12*(1), 17–25.
259. Wang, F., Zhang, S., Jeon, R., Vuckovic, I., Jiang, X., Lerman, A., & Herrmann, J. (2018). Interferon Gamma Induces Reversible Metabolic Reprogramming of M1 Macrophages to Sustain Cell Viability and Pro-Inflammatory Activity. *EBioMedicine*, *30*, 303–316.
260. Wang, H., Tibbitt, M. W., Langer, S. J., Leinwand, L. A., & Anseth, K. S. (2013). Hydrogels preserve native phenotypes of valvular fi broblasts through an elasticity-regulated PI3K / AKT pathway. *PNAS*, *110*(48), 19336–17341.
261. Wang, S., Liu, R., Dong, L., & Bi, Y. (2019). Metabolic reprogramming of macrophages during infections and cancer. *Cancer Letters*, *452*(March), 14–22.
262. Wang, S., Yu, H., Gao, J., Chen, J., He, P., Zhong, H., & Zhu, D. (2022). PALMD regulates aortic valve calcification via altered glycolysis and NF-κ B–mediated inflammation. *J Biol. Chem.*, *298*(5), 1–14.
263. Wang, X., Lee, J., Ali, M., Kim, J., & Lacerda, C. M. . (2017). Phenotype Transformation of Aortic Valve Interstitial Cells Due to Applied Shear Stresses Within a Microfluidic Chip. *Ann. Biomed. Eng.*, *45*(10), 2269–2280.
264. Warburg, O., Wind, F., & Negelein, E. (1926). The metabolism of tumours in the body. *J. gen. physiol.*, *8*(6), 519–530.
265. Wei, J., Shimazu, J., Makinistoglu, M. P., Pessin, J. E., Hinoi, E., Wei, J., & Karsenty, G. (2015). Glucose Uptake and Runx2 Synergize to Orchestrate Article Glucose Uptake and Runx2 Synergize to Orchestrate Osteoblast Differentiation and Bone Formation. *Cell*, *161*(7), 1576–1591.
266. Wirrig, E. E., Gomez, M. V., Hinton, R. B., & Yutzey, K. E. (2015). COX2 Inhibition Reduces Aortic Valve Calcification In Vivo. *Transl. Sci.*, *27*, 938–947.
267. Wolf, A. J., Reyes, C. N., Liang, W., Becker, C., Wheeler, M. L., Cho, H. C., & Underhill, D. M. (2017). Hexokinase Is an Innate Immune Receptor for the Detection of Bacterial Peptidoglycan. *Cell, 166*(3), 624–636.
268. Wu, Duojiao, Sanin, D. E., Everts, B., Pearce, E. L., Cella, M., Pearce, E. J., & Patterson, A. (2016). Type 1 Interferons Induce Changes in Core Metabolism that Are Critical for Immune Function. *Immunity*, *44*(6), 1325–1336.
269. Wu, D., & Yotnda, P. (2011). Induction and testing of hypoxia in cell culture. *J. Vis. Exp.*, (54), 4–7.
270. Wu, H., Yang, P., Hu, W., Wang, Y., Lu, Y., Zhang, L., & Li, Z. (2016). Overexpression of PKM2 promotes mitochondrial fusion through attenuated p53 stability. *Oncotarget*, *7*(47), 78069–78082.
271. Wu, K. K. (2023). Extracellular Succinate : A Physiological Messenger and a Pathological Trigger. *Int. J. Mol. Sci.*,

24(11165), 1–18.

272. Wu, Y., Wang, M., Feng, H., Peng, Y., Sun, J., & Qu, X. (2017). Lactate induces osteoblast differentiation by stabilization of HIF-1a. *Mol. Cell Endocrinol., 17(5), 1-9.*
273. Xiao, W., Oldham, W. M., Priolo, C., Pandey, A. K., & Loscalzo, J. (2021). Immunometabolic Endothelial Phenotypes: Integrating Inflammation and Glucose Metabolism. *Circ. Res.*, *129*(1), 9–29.
274. Xiaolu, Li., Yang, Y., Zhang, B., Lin, X., Fu, X., An, Y., & Yu, T. (2022). Lactate metabolism in human health and disease. *Signal Transduct. Target. Ther.*, *7*(305), 1–22.
275. Xie, N., Zhang, L., Gao, W., & Huang, C. (2020). NAD metabolism: pathophysiologic mechanisms and therapeutic potential. *Signal Transduct. Target. Ther.*, *5(227)*, 1-37.
276. Xu, Y., Shen, J., & Ran, Z. (2020). Emerging views of mitophagy in immunity and autoimmune diseases. *Autophagy*, *16*(1), 3–17.
277. Xue, Y., Hilaire, C. S., Hortells, L., Phillippi, J. A., Sant, V., & Sant, S. (2017). Shape-Specific Nanoceria Mitigate Oxidative Stress-Induced Calcification in Primary Human Valvular Interstitial Cell Culture. *Cell. Mol. Bioeng.*, *10*(5), 483–500.
278. Yang, M., Wu, S., Cai, W., Ming, X., Zhou, Y., & Chen, X. (2022). Hypoxia-induced MIF induces dysregulation of lipid metabolism in Hep2 laryngocarcinoma through the IL6/JAK-STAT pathway. *Lipids Health Dis.*, *21*(82), 1–10.
279. Yang, R., Zhu, Y., Wang, Y., Ma, W., Han, X., & Wang, X. (2019). HIF-1a/PDK4/autophagy pathway protects against advanced glycation end-products induced vascular smooth muscle cell calcification. *Biochem. Biophys. Res. Commun.*, (xxxx), 1–7.
280. Yang, W., & Lu, Z. (2013). Regulation and function of pyruvate kinase M2 in cancer. *Cancer Letters*, *339*(2), 153–158.
281. Yang, W., Xia, Y., Hawke, D., Li, X., Liang, J., Xing, D., & Lu, Z. (2012). PKM2 Phosphorylates Histone H3 and Promotes Gene Transcription and Tumorigenesis. *Cell*, *150*(4), 685–696.
282. Yao, C., Wang, R., Wang, Y., Kung, C., Weber, J. D., & Patti, G. J. (2019). Mitochondrial fusion supports increased oxidative phosphorylation during cell proliferation. BMC *Cell Biol.*, *8*, 1–19.
283. Yetkin-arik, B., Vogels, I. M. C., Nowak-sliwinska, P., Weiss, A., Houtkooper, R. H., Noorden, C. J. F. Van, & Schlingemann, R. O. (2019). The role of glycolysis and mitochondrial respiration in the formation and functioning of endothelial tip cells during angiogenesis. *Nature*, *9*(12608), 1–14.
284. Yin, M., & O'Neill, L. A. J. (2021). The role of the electron transport chain in immunity. *FASEB Journal*, *35*(12), 1–13.
285. Yip, C. Y. Y., Chen, J. H., Zhao, R., & Simmons, C. A. (2009). Calcification by valve interstitial cells is regulated by the stiffness of the extracellular matrix. *Arterioscler. Thromb. Vasc. Biol., 29*(6), 936–942.
286. Yousefi, F., Shabaninejad, Z., Vakili, S., Derakhshan, M., & Movahedpour, A. (2020). TGF- β and WNT signaling pathways in cardiac fibrosis : non-coding RNAs come into focus. *Cell Commun. Signal.*, *18*(87), 1–16.
287. Yu, S., & Kim, S. (2010). Endoplasmic reticulum stress (ER-stress) by 2-deoxy- D -glucose (2DG) reduces cyclooxygenase-2 (COX-2) expression and N-glycosylation and induces a loss of COX-2 activity via a Src kinase-dependent pathway in rabbit articular chondrocytes. *Experimental and Mol. Med.*, *42*(11), 777–786.
288. Yutzey, K. E., Demer, L. L., Body, S. C., Huggins, G. S., Towler, D. A., Giachelli, C. M., & Aikawa, E. (2014). Calcific Aortic Valve Disease: A Consensus Summary From the Alliance of Investigators on Calcific Aortic Valve Disease. *Ateriosclerosis. Thromb. Vasc. Biol.*, *34*, 2387–2393.
289. Zeng, Q., Song, R., Fullerton, D. A., Ao, L., Zhai, Y., Li, S., & Ballak, D. B. (2016). Interleukin-37 suppresses the osteogenic responses of human aortic valve interstitial cells in vitro and alleviates valve lesions in mice. *PNAS*, *114*(7), 1631–1636.
290. Zhan, Q., Song, R., Zeng, Q., Yao, Q., Ao, L., Xu, D., & Fullerton, D. A. (2015). Activation of TLR3 Induces Osteogenic Responses in Human Aortic Valve Interstitial Cells through the NF- κB. *Int. J. Biol Sci., 11(4), 482-493*.
291. Zhang, X. J., Jiang, D. S., & Li, H. (2015). The interferon regulatory factors as novel potential targets in the treatment of cardiovascular diseases. *Br. J. Pharmacol.*, *172*(23), 5457–5476.
292. Zhao, F., Mancuso, A., Bui, T. V, Tong, X., Gruber, J. J., Swider, C. R., & Thompson, C. B. (2010). Imatinib-resistance associated with BCR-ABL upregulation is dependent on HIF-1α-induced metabolic reprogramming. *Oncogene*, *29*(20), 2962–2972.
293. Zhong, G., Su, S., Li, J., Zhao, H., Hu, D., Chen, J., & Zeng, Q. (2023). Activation of Piezo1 promotes osteogenic differentiation of aortic valve interstitial cell through YAP-dependent glutaminolysis. *Sci. Adv*, *9*, 1–20.
294. Zhou, T., Han, D., Liu, J., Shi, J., Zhu, P., Wang, Y., & Dong, N. (2019). Factors influencing osteogenic differentiation of human aortic valve interstitial cells. *J. Thorac. Cardiovasc. Surg.*, *161*(2), e163–e185.
295. Zhu, A. S., Mustafa, T., Connell, J. P., & Grande-allen, K. J. (2021). Tumor necrosis factor alpha and interleukin 1 beta suppress myofibroblast activation via nuclear factor kappa B signaling in 3D-cultured mitral valve interstitial cells. *Acta Biomater.*, *9*(40), 1–10
296. Zhu, D., Zeng, Q., Zheng, Y., Hua, J., & Xu, D. (2015). A case-control study on risk factors of calcific aortic valve disease in a Chinese population. *J. Am. Coll. Cardiol.*, *66*(16), C216–C217.
297. Zhu, Y., Ji, J., Wang, X., Sun, X., Li, M., Wei, Q., & Liu, N. (2023). Periostin promotes arterial calcification through PPARg-related glucose metabolism reprogramming. *Am. J. Physiol. Heart. Circ. Physiol.*, *320*, 2222–2239.
298. Zhu, Y., Qiong, X., Xue, H., Sun, J., Yang, R., Qi, W., & Liu, F. (2020). Lactate accelerates vascular calcification through NR4A1 - regulated mitochondrial fission and BNIP3 - related mitophagy. *Apoptosis*, *25*(5), 321–340.

ANNEX 1-PEER-REVIEWED RESEARCH PAPERS

1. Parra-izquierdo, I*., Sánchez-Bayuela, T*., Castaños-Mollor, I., López, J., Gómez, C., San Román, A. J., Sánchez Crespo, M., García-Rodríguez, C. (2021). **Clinically used JAK inhibitor blunts dsRNA-induced inflammation and calcification in aortic valve interstitial cells**. *The FEBS Journal*, *10*, 1–15. https://doi.org/10.1111/febs.16026

   *Parra-Izquierdo, I., & Sánchez-Bayuela, T., equal contribution

2. Parra-Izquierdo, I., Sánchez-Bayuela, T., López, J., Gómez, C., Pérez-Riesgo, E., San Román, J. A., Sánchez-Crespo, M., Magdi H, Yacoub., Chester, Adrian H., García Rodríguez, C. (2021). Interferons Are Pro-Inflammatory Cytokines in Sheared-Stressed Human Aortic Valve Endothelial Cells. *International Journal of Molecular Sciences*, *22*(10605), 1–22. https:// doi: 10.3390/ijms221910605